Studying the canonical and non-canonical functions of Hsp90 in *Plasmodium falciparum* chromatin biology

A thesis Submitted to University of Hyderabad for the award Doctor of Philosophy in Biochemistry

By Wahida Tabassum 15LBPH06



Department of Biochemistry
School of Life Sciences
University of Hyderabad
Hyderabad-500046
Telangana, India

December 2021



University of Hyderabad Hyderabad -500046, India

Certificate

This is to certify that this thesis entitled "Studying the canonical and non-canonical functions of Hsp90 in *Plasmodium falciparum* chromatin biology" submitted by Miss Wahida Tabassum bearing registration number 15LBPH06 in partial fulfilment of the requirement for the award of Doctor of Philosophy in the Department of Biochemistry, School of Life Sciences, is a bonafide work carried out by her under my supervision and guidance.

This thesis is free from plagiarism and has not been submitted previously in part or in full to this University or any other University or Institution for the award of any degree or diploma.

Part of this thesis has been:

- A. Published in the following journal:
 - Wahida Tabassum, Priyanka Singh, Niranjan Suthram, Sunanda Bhattacharyya, Mrinal Kanti Bhattacharyya. Synergistic action between PfHsp90 inhibitor and PfRad51 inhibitor induces elevated DNA damage sensitivity in the malaria parasite, Antimicrobial Agents and Chemotherapy, (2021), 65 (9), doi: 10.1128/AAC.00457-21
 - Wahida Tabassum, Sunanda Bhattacharyya, Shalu M Varunan, Mrinal Kanti Bhattacharyya. Febrile temperature causes transcriptional down-regulation of *Plasmodium falciparum* Sirtuins through Hsp90 dependent epigenetic modification, Molecular Microbiology, (2021), 155(5), doi: 10.1111/mmi.14692.
- B. Presented in the following conferences:
 - Wahida Tabassum, Sunanda Bhattacharyya and Mrinal Kanti Bhattacharyya. Impact of febrile temperature on *Plasmodium* virulence gene expression. Oral presentation in Bioquest on Cellular Homeostasis: from the Basics to Translational Research, 2019, held at University of Hyderabad, Hyderabad.
 - Wahida Tabassum, Sunanda Bhattacharyya and Mrinal Kanti Bhattacharyya. Exposure to heat breaks the silence: implications into *Plasmodium* virulence gene expression. Oral presentation in International Symposium on Malaria Biology and 29th National Congress of Parasitology on Basic and Applied Aspects, 2018, held at University of Hyderabad, Hyderabad.
 - Wahida Tabassum, Pratap Vydyam, Sunanda Bhattacharyya and Mrinal Kanti Bhattacharyya. Extreme makeover at the chromosomal ends of malaria parasites: a consequence of genomic plasticity. Poster presentation in Indo French conference, 2017, held at IISC, Bangalore.

Wahida Tabassum, Shalu M. Varunan, Sunanda Bhattacharyya and Mrinal Kanti Bhattacharyya. Heat induced transcriptional down-regulation of Plasmodium Sirtuins: implications into antigenic variation. Poster presentation in Malaria conference, 2016, held at Nirma University, Ahmedabad.

Further the student has passed the following courses towards fulfilment of coursework requirement for Ph.D.

Course code	Name	Credits	Pass/Fail
BC 801	Analytical Techniques	. 4	Passed
BC 802	Research ethics, Data analysis and Biostatistics	3	Passed
BC 803	Lab seminar and Records	5	Passed

Dr. MRINAL KANTI BHATTACHARYYA PhD Head, Dept. of Biochemistry

PROFESSOR

PROFESSOR

PROFESSOR

DEPARTMENT OF BIOCHEMISTRY

DEPARTMENT OF LIFE SCIENCES

CCHOOL OF LIFE SCIENCES EPARTMENT OF BIOCHEMISTR' SCHOOL OF LIFE SCIENCES UNIVERSITY OF HYDERABAD HYDERABAD-500046, INDIA.

HYDERABAD-500 046.

School of the Sciences University of Hyderabad Hyderabad-500 046.



University of Hyderabad Hyderabad -500046, India

Declaration

I, Wahida Tabassum, hereby declare that this thesis entitled "Studying the canonical and non-canonical functions of Hsp90 in *Plasmodium falciparum* chromatin biology" submitted by me under the guidance and supervision of **Prof. Mrinal Kanti Bhattacharyya**, is an original and independent research work. I also declare that it has not been submitted previously in part or in full to this University or any other University or Institution for the award of any degree or diploma.

Date: 13/12/2021

Signature of the Student

Mahida Taleassum

Signature of the Supervisor

(Prof. Mrinal Kanti Bhattacharyya)

RINAL KANTI BHATTACHARYYA PhD

PROFESSOR

DEPARTMENT OF BIOCHEMISTRY SCHOOL OF LIFE SCIENCES UNIVERSITY OF HYDERABAD HYDERABAD-500046, INDIA.

i١

Acknowledgments

With the divine grace of Almighty, it's the time for thesis submission. The process of earning a doctorate and writing thesis, is a long and arduous which is outcome of collective efforts of several people. Words put on paper are mere ink marks, but when they have purpose, there exists a thought behind them. I too have purpose to express my gratitude towards several individuals for their faith, encouragement, support and contribution for the completion of this thesis.

On the very outset of this report, I would like to extend my sincere and heartfelt gratitude towards my supervisor Prof. Mrinal Kanti Bhattacharyya for providing me the great opportunity of working under his guidance and introducing me to the world of Malaria research. I thank you sir, for all your teaching, advice, support and wisdom throughout this project, from inception to completion, as well as for your incredible patience in working with me for past six years. It was only due to your valuable guidance, cheerful enthusiasm and ever friendly nature that I was able to complete my thesis work. Your art of simplifying things also played an instrumental role in this accomplishment.

I am grateful to my Doctoral committee members Dr. Sunanda Bhattacharyya and Prof. Kota Arun Kumar for their critical suggestions and insightful comments regarding my work and presentations. I am also indebted to them for extending their lab facilities for me.

I would also take this opportunity to thank Sunanda Ma'am for being an inspiration and always encouraging to do the best.

I am obliged to the Head of the Biochemistry department. Prof Krishnaveni Mishra, and the former Heads. Prof. Mrinal Kanti Bhattacharyya and Prof. N Shiva Kumar for maintaining the departmental facilities

I am extremly thankful to the Dean of School of Life Sciences, Prof. S Dayananda, and the former Deans, Prof KVA Ramiah, Prof. P Reddanna and Prof. WNV Prasad for the school research facilities.

I am ineffably indebted to Dr. Santosh R Kanade for extending his lab facility and his lab members Kiran and Mouboni for assisting me there.

I heartily thank all my teachers starting from kinder garden to post graduations for imparting great deal of knowledge and skills all throughout.

I extend my sincere thanks to Mr. Prabhu, Mr. Chary and all other non-teaching staffs of Department of Biochemistry for their administrative help and cooperation.

I thank profusely all the teaching and non-teaching staffs of School of Life Sciences for their timely help.

I owe deep sense of gratitude to the staffs of Health Centre. University of Hyderabad for withdrawing the blood for me, required for the parasite culture.

I highly acknowledge UGC for providing me the fellowship for five years of my Ph.D tenure. I also thank the funding agencies CSIR, DBT, DST-SERB for funding the lab and DST-71ST, UGC-SAP for funding the department.

During my journey of Ph.D. I was fortunate to have great lab members who provided numerous assistance whenever required and caring friends who were like my family in Hyderabad and part of my every celebration as well my sorrow, without them this journey would have not been that easy and joyful. I thank each one of you from core of my heart. Dr. Shalu, Dr. Nabi, Dr. Sugith, Dr. Shymashree, Dr. Swati, Dr Suresh, Dr. Nidhi, Dr. Tanvi, Dr. Pratap, Dr. Niranjan, Dr Purna Chandra, Payal, Dr. Shephali, Nupur, Priyanka, Khushboo, Abhilasha, Tanishka, Pooja, Jyoti, Akansha, Deepak, Pankaj, Shiraj, Ramji, Sayan and Renu.

I also extend my thanks to all the previous and present M.Sc. Project students of the Bhattacharyya laboratory for their help and cooperation.

I am deeply grateful to Mr. Ramesh for his invaluable assistance in the laboratory.

I really feel very privileged and fortunate to have a loving family who are forever my pillars of support. I extend my deep sense of reverence and gratitude towards my parents Mr. Nizamuddin Ansari and Mrs. Shakila Bano, my brothers Mr. Mustafa Kamal and Mr. Mohasin Kamal for always believing me. I am highly obliged to them for their never ending support and encouragement throughout my Ph.D. tenure without which this achievement would have not been possible.

Wahida....

Table of contents

Contents	Page No.
List of figures	xiii
List of tables	XV
Abbreviations	xvi
Chapter 1: Introduction	
1.1 Malaria	2
1.2 Obstacles in curbing malaria	2
1.2.1 The complex life cycle of the malaria parasite	3
1.2.2 Growing insecticide resistance in the mosquitoes.	5
1.2.3 Increasing drug resistance in the parasites	5
1.2.4 Antigenic variation and immune evasion	6
1.3 Molecular mechanism of antigenic variation in <i>P. falciparum</i>	7
1.4 Malaria biology: a goldmine for discovering novel drug targets	9
1.5 Double strand break repair pathway a lucrative target	11
1.6 Plasmodium biology and heat shock response	12
1.7 Heat shock protein 90 (Hsp90) in model organisms	14
1.7.1 Heat shock protein 90 in model organisms: the canonical functions	17
1.7.2 Heat shock protein 90 in model organisms: the non-canonical roles	21

1.8 Plasmodium Heat shock protein 90	22
1.9 Plasmodium Hsp90 as an antimalarial drug target	23
1.10 Significance of the study	24
1.11 Objectives of the study	26
1.12 Aims of the study	27
Chapter 2: Materials and methods	
2.1 Recombinant DNA techniques	
2.1.1 Bacterial Competent cell preparation	29
2.1.2 Bacterial Transformation	29
2.1.3 Plasmid DNA isolation by alkaline lysis method	30
2.1.4. Recombinant protein expression	31
2.2 Yeast methods	
2.2.1 Yeast competent cell preparation	31
2.2.2 Yeast Transformation	32
2.2.3 Protein isolation by TCA method	32
2.2.4. Yeast-two-hybrid analysis	33
2.3 Methods in <i>Plasmodium falciparum</i> experiments	
2.3.1 Washing of RBCs	34
2.3.2 Thawing of the parasites from liquid nitrogen	34
2.3.3 Maintenance of the parasite culture	35

2.3.4 Synchronisation of the parasites by sorbitol method	36
2.3.5 Freezing of the parasite culture	36
2.3.6 MG132 treatment	36
2.3.7 Harvesting of the parasites by saponin lysis	37
2.3.8 Genomic DNA isolation from the parasites	37
2.3.9 Protein preparation from the parasites	38
2.3.10 RNA isolation from the parasites	38
2.3.11 cDNA preparation	39
2.4 Real time PCR.	39
2.5 MMS sensitivity assay	39
2.6 PCR-based method to quantify DNA damage	40
2.7 Chromatin Immunoprecipitation	40
2.8 FAIRE	44
2.9 Co-immunoprecitation	45
2.10 Western blotting	46
Chapter 3: The canonical functions of Hsp90 in <i>Plasmodium</i> biology	
3.1 Introduction	54
3.2 Results	
3.2.1 Physical interaction between PfHsp90 and PfRad51	56
3.2.2 Chemical inhibition of Hsp90 function induces proteasomal degradation of	59
PfRad51	

3.2.3 Genetic loss of Hsp90 function induces depletion of PfRad51	62
3.2.4 Abrogation of the UV-induced DNA repair activity of PfRad51 under	64
Hsp90- inhibitory condition	
3.2.5 Hsp90 inhibition sensitizes <i>P. falciparum</i> to MMS-induced DNA damage	67
3.3 Discussions	70
Chapter 4: The non-canonical functions of Hsp90 in <i>Plasmodium</i> biolog	gy
4.1 Introduction	72
4.2 Results	
4.2.1 Expression of PfSir2A and antibody generation	74
4.2.2 Brief exposure to elevated temperature results in down-regulation of	76
PfSIR2 protein at the mid-ring stage	
4.2.3 Exposure to heat shock leads to transcriptional down-regulation of <i>PfSIR2A</i>	78
and PfSIR2B specifically at mid-ring stage	
4.2.4 Reduction in recruitment of PfSir2A at the <i>var</i> promoter Ups A	80
upon heat shock	
4.2.5 Brief exposure to elevated temperature results in de-repression of multiple	82
sub-telomeric var genes	
4.2.6 Heat-shock leads to heterochromatinization of chromatin at <i>PfSIR2 UAS</i>	88
4.2.7 Heat induced recruitment of H3K9me3 is responsible for repression of	90
PfSIR2 transcription	

4.2.8 Heat shock leads to overexpression of PfHsp90 at ring stage	92
4.2.9 Heat induced down-regulation of <i>PfSIR2</i> transcription is dependent on	94
Hsp90 activity	
4.2.10 Hsp90 inhibition prevents compaction of SIR2 promoter on heat shock	97
4.2.11 Hsp90 inhibition prevents heat induced enrichment of H3K9me3 at	99
PfSIR2 promoter proximal regions	
4.2.12 Occupancy of PfHsp90 at the upstream regions of PfSIR2A and	101
PfSIR2B genes	
4.3 Discussions	104
Chapter 5: Discussions	107
References	117
Appendix	
Synopsis	133
 Publications 	144

List of figures

Figure	Page No.
1.1: Life cycle of the malaria parasite <i>P.falciparum</i> involving mosquito	4
and human host	
1.2: PfSir2A and PfSir2B control different sets of <i>var</i> genes	10
1.3: Parasite encounters various temperature variation during its life cycle involving	13
two hosts	
1.4: Hsp90 is a specialised chaperone and provide maturation to only a subset of	15
client proteins	
1.5: Diverse functions of Hsp90	16
1.6: The chaperone cycle of Hsp90 in maturation of the client protein	19
1.7: Fate of the client protein on Hsp90 inhibition	20
3.1: Yeast-two-hybrid analysis demonstrating physical interaction between	57
PfRad51 and PfHsp90	
3.2: Co-immunoprecipitation experiment demonstrating physical interaction	58
between PfRad51 and PfHsp90	
3.3: Treatment with 17-AAG induces depletion of PfRad51	60
3.4: 17-AAG induces proteasomal degradation of PfRad51	61
3.5: Temperature sensitive yHsp90 mutant induces depletion of PfRad51 at	63
the non-permissive temperature	
3.6: Abrogation of the UV-induced DNA repair activity of PfRad51 under	66
Hsp90 inhibitory condition	
3.7: Hsp90 inhibition sensitizes <i>P. falciparum</i> to MMS induced DNA damage	69
4.1: Expression of recombinant PfSir2A and specificity check of anti-PfSir2 antibod	ly 75

4.2: Heat induced down-regulation of PfSir2A protein is specific to the	77
mid-ring stage	
4.3: Exposure to heat shock leads to transcriptional down-regulation of <i>PfSIR2A</i>	79
and PfSIR2B specifically at the mid-ring stage	
4.4: Reduction in recruitment of PfSir2A at the <i>var</i> promoter Ups A upon heat shock	81
4.5: De-repression of <i>var</i> genes upon heat shock	83
4.6: Heat-shock lead to heterochromatinization of chromatin at <i>PfSIR2 UAS</i>	89
4.7: Heat induced recruitment of H3K9me3 is responsible for repression of	91
PfSIR2 transcription	
4.8: Heat shock leads to overexpression of PfHsp90 at ring stage	93
4.9: Heat induced down-regulation of <i>PfSIR2</i> transcription is dependent on	96
Hsp90 activity	
4.10: Hsp90 inhibition prevents compaction of SIR2 promoter on heat shock	98
4.11: Hsp90 inhibition prevents heat induced enrichment of H3K9me3 at	100
PfSIR2 promoter proximal regions	
4.12: Occupancy of PfHsp90 at the upstream regions of <i>PfSIR2A</i> and <i>PfSIR2B</i> genes	102
5.1: Model depicting the reduction in activity of PfRad51 upon Hsp90 inhibition	109
5.2: Model depicting the alteration at <i>PfSIR2</i> landscape upon heat shock	111

List of tables

Table	Page No.
2.1: List of the primers used in the study	48
2.2: List of yeast strains used in the study	52
4.1: Fold change in the expression of <i>var</i> genes upon heat shock	85

Abbreviations

Ade Adenine

Amp Ampere

cDNA Complementary DNA

Da Dalton

DEPC Diethyl pyrocarbonate

DMSO Dimethyl sulphoxide

DNA Deoxyribonucleic acid

DNase Deoxyribonuclease

DSB Double strand break

DTT Dithiothreitol

EDTA Ethylene diamine tetra acetic acid

FAIRE Formaldehyde Assisted Isolation of Regulatory Elements

HR Homologous Recombination

IgG Immunoglobin G

iRBC infectefed RBC

kDa Kilo Dalton

LB Luria-bertani broth

Leu Leucine

LiOAC Lithium Acetate

M Molar

mg Milli gram

mM Milli molar

MMS Methyl Methane Sulphate

ml Milli liter

NaCl Sodium Chloride

NaOAc Sodium Acetate

NaOH Sodium hydroxide

ng nano gram

OD Optical Density

ORF Open reading frame

PAGE Polyacrylamide gel electrophoresis

PBS Phosphate buffered saline

PCIA Phenyl Chloroform Isoamyl alcohol

PCR Polymerase chain reaction

PEG Polyethylene glycol

PMSF Phenyl-methane-sulphonyl-fluoride

PVDF Poly vinylidene Fluoride

Q-PCR Quantitative PCR

RBC Red Blood Cell

RNA Ribonucleic acid

RNase Ribonuclease

rpm rotation per minute

RPMI Roswell park memorial institute medium

RT Room temperature

RT-PCR Reverse transcriptase - polymerase chain reaction

SC Synthetic complete

SDS Sodium dodecyl sulfate

SDS-PAGE Sodium dodecyl sulfate Poly acryl amide gel electrophoresis

ssDNA Single strand DNA (Salmon sperm DNA)

TBE Tris Borate EDTA

TCA Trichloroacetic acid

TE Tris EDTA

TRP Tryptophan

Ura Uracil

μg Microgram

μl Microliter

WHO World health organisation

YPD Yeast extract dextrose

17AAG 17-demethoxygeldanamycin

Chapter-1 Introduction

1.1 Malaria

Malaria is one of the most ancient and deadliest infectious diseases. It still possesses a threat to mankind as half of the world population lives in the endemic regions and are at risk of malaria. According to the WHO report, in 2020 there were 241 million cases recorded worldwide, accounting for 6,27,000 deaths (1). Malaria is prevalent in more than 100 countries and territories of Africa, south Asia, southern and central parts of America, Middle East and Oceania. The causative agent of malaria is a protozoan parasite *Plasmodium*. The five species responsible for the manifestation of disease in human are P. falciparum, P. vivax, P. malariae, P. ovale, and P. knowlesi. P. falciparum is the deadliest among all the species, also causes the cerebral malaria and is responsible for maximum number of deaths due to malaria. The transmission of disease occurs through bite of the infected female Anopheles mosquitoes. A sub population is at greater risk of succumbing to the disease which includes children under age of 5 years, pregnant women, patients with HIV and immune compromised migrants. The initial symptoms of the disease include fever, chills, headache, vomiting and diarrhoea. If not treated, severity of the disease can increase and might lead to other complications like severe anaemia, respiratory distress, multiple organ failure, seizures, coma and death. The alarming scenario is that till date, there is no potent and commercial vaccine available and the emergence and spread of drug resistance in the parasites.

1.2. Obstacles in curbing malaria

Effort for controlling and curbing malaria have been made since ages, but still malaria continues to be one the major health problems. The factors which are major roadblocks in eradicating the disease include complex life cycle of the parasite, growing insecticide resistance

in vector mosquitoes, increasing drug resistance in the parasites and the most important is the ability of the parasites to elicit antigenic variation.

1.2.1 The complex life cycle of the malaria parasite

The parasite *Plasmodium* requires two hosts to complete its life cycle, making its biology difficult to understand, thereby making the task of curbing malaria difficult. The asexual cycle occurs in a human host while the sexual development of the parasite takes in the mosquito. When an infected mosquito bites the human host, it injects parasites in the form of sporozoites. These sporozoites migrate to the liver and infects the hepatocyte. Within the hepatocytes, exoerythrocytic schizogony occurs which leads to the formation of merozoites. These merozoites are released in the blood stream and invade the RBC. The parasites then undergo asexual development that comprises of ring, trophozoites and schizonts stages. The formed schizonts ruptures to release 16-32 merozoites and these merozoites can further infect new RBC. This intra- erythrocytic stage is responsible for the manifestation of the clinical symptoms as the rupture of schizonts and lysis of the RBC induces fever and chills in the human host. Some of the merozoites differentiates to form the male and the female gametocytes. These gametocytes are taken up by the mosquito during its blood meal and further sexual development takes place in the mosquito. The male and female gamete fuses to form zygote that develops into ookinite, which further matures to form oocysts. The oocysts rupture to release the sporozoites which migrate to the salivary gland and can be injected to human on mosquito bite.

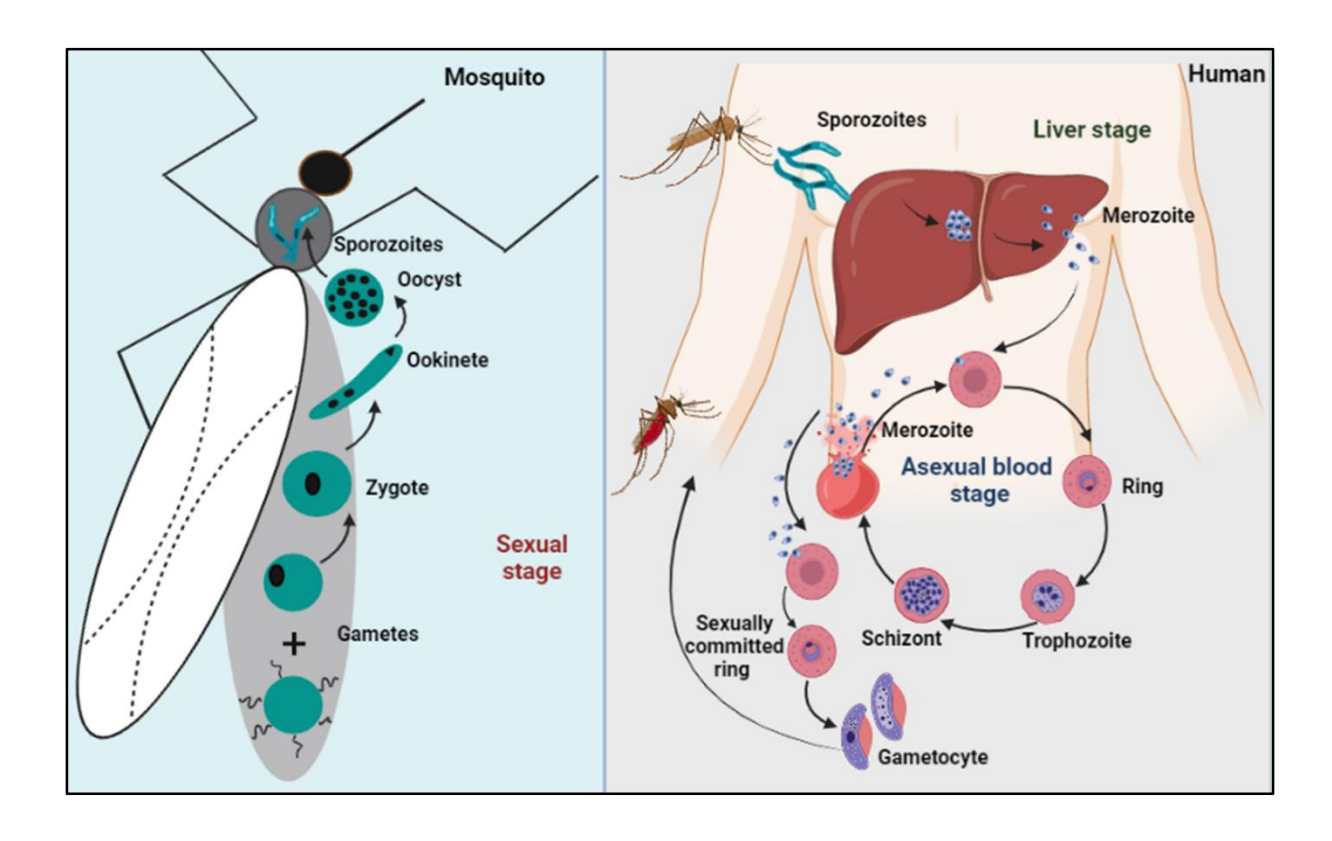


Figure 1.1: Life cycle of the malaria parasite *P. falciparum* involving mosquito and human host.

1.2.2 Growing insecticide resistance in the mosquitoes

Global endeavours to combat the malarial burden by using the integrated approach of consolidated measure of vector control mechanism involving use of long-lasting insecticidal nets (LLINs) and indoor residual spraying (IRS) with early diagnosis, greater access to improved antimalarial drugs has led to remarkable reduction in malarial cases and mortality in Africa by 42% and 66% respectively. This has also helped to reduce burden of malaria in various endemic regions. The insecticides currently used to control the vector of malaria are organochlorines, organophosphates, carbamates and pyrethroids. But there are reports of the emergence and spread of insecticide resistance in the majority of the malaria vectors, compromising the credibility of efficient malarial control strategy (2-4).

1.2.3 Increasing drug resistance in the parasites

Emergence of drug resistance in the parasites to most of known anti-malarial drugs is the greatest menace. This has proved to be a huge set back in the disease management and is responsible for the resurgence of the disease leading to increase in mortality and morbidity related to malaria. The parasites have developed resistance to several antimalarial drug, which includes chloroquine sulphadoxinepyrimethamine, amodiaquine, mefloquine, and quinine. Currently, most effective drug available is artemisinin and artemisinin based combination therapy is widely being used for the treatment. Increase in drug resistance to amodiaquine has also been observed in the parasite in eastern Africa which has resulted reduction in effectiveness of combination therapy of artesunate and amadiaquine. Unfortunately, resistance in *P. falciparum* to artisunate have also been reported in Thai-Cambodian border (5, 6).

1.2.4 Antigenic variation and immune evasion

The most important reason for failure in curbing malaria is due to the ability of the parasite to elicit antigenic variation. Antigenic variation is the strategy by which parasite evade the host immune response by the mono allelic expression of its virulence gene and also by employing its switching (7-10).

As parasite requires human RBC for replication, it is essential for the parasite to evade host immune response for its survival and proliferation. When merozoites infects the RBC, the parasite undergo a series of biochemical and morphological changes, it also induces modification in structure of the RBC and exports several proteins to the surface of the RBC which aid the parasites in establishing the infection. The RBC infected by *P. falciparum* on its surface display erythrocyte membrane protein 1 (PfEMP1), repetitive interspersed family (RIFIN) and sub-telomeric variable open reading frame (STEVOR) proteins. RIFIN and STEVOR are the minor epitopes and human immune response is majorly generated against the PfEMP1, which is encoded by a family of var gene (11). There around 59 copies of var gene present per haploid genome of the parasite and out of these only one PfEMP1 protein is found to be expressed at surface of the infected RBC at trophozoite and schizont stage. As PfEMP1 is recognised by the human immune system as immunogenic target, body generate antibody against the displayed antigen, for augmenting the process of opsonisation and thereby clearance of the infected RBC. But the parasite is able to escape this immune attack of the host as it has ability of switching the expression of the var gene, evades the recognition by antibody and thus parasite is able to maintain the infection via clonal antigenic variation. The parasite is able to switch the expression of var gene at rate of 2% per cycle which enable it to generate new clone with different antigenic PfEMP1 (12-14).

Another mechanism adopted by the parasite to evade the host immune response is sequestration. RBC infected by *P. falciparum* undergo modification and there is an increase in the rigidity of the erythrocyte. The erythrocyte with increased rigidity can be recognised as abnormal cell and cleared from the circulation through splenic filtration, but parasite is able to escape this immune response of the host also, as PfEMP1 displayed on the surface of infected RBC allows it adhere to endothelial tissue and sequester into the microvasculature of different organs. The parasite *P. falciparum* of stage trophozoite and schizonts are not present in the blood circulation, rather found sequestered in the microvasculature of several tissues (15) whereas the gametocyte stage (I-IV) are found sequestered in organs like spleen and bone marrow (16-18). Additionally parasite infected RBC forms rosette with uninfected RBC and also auto agglutinate with infected RBC bridging through platelets to escape the splenic filtration (19-21).

1.3 Molecular mechanism of antigenic variation in P. falciparum

var genes are the key determinant of antigenic variation in the parasites encoding Erythrocyte Membrane Protein 1 (PfEmp1), which is found to be decorated on the surface of infected RBC (22). In natural isolates of *P. falciparum* the number of var genes varies from 45 to 90 (23). In the reference genome of *P. falciparum* 3D7 strain. The 59 var genes present per haploid genome of the parasite, are found to be distributed on 13 out of 14 chromosomes (24). Most of them are localised at sub-telomeric regions, whereas 24 of them are present at internal chromosomal loci (24). The var genes have been classified into four subgroups based on the sequence similarity of their 5'promoter regions: Ups A, Ups B, Ups C, and Ups E (25). Hybrid promoter BA and BC have also been reported (26). Ups C comprises of var genes that are localised at central chromosomal locus, UpsB consists of var genes that are either subtelomeric

and transcribed away from the telomere or chromosome central in tandem arrays with other UpsB or Ups C *var* genes. Ups A and Ups E- type *var* genes are subtelomeric but transcribed towards the telomere in the opposite direction to the Ups B *var* gene (24, 25). The expression of *var* genes occur in mutual exclusive fashion and are expressed differentially in different developmental stages. Out of the 59 *var* genes, only one of the *var* gene is transcriptionally expressed at ring stage, whereas at trophozoite and schizonts stage, single PfEmp1is found on the surface of infected RBC (27, 28). Certain studies based on RT PCR analysis of the *var* transcripts, suggests that all *var* genes are expressed during the ring stage and only one is found to be expressed at trophozoite stage (10, 29), however, through northern blot analysis full length transcripts were only found to be expressed at ring stage (29, 30). Another study indicates that transcription of only one dominant *var* gene as functional mRNA occurs at ring stage whereas the all other *var* gene are transcribed as truncated transcripts (31).

The transcriptional activation of only one *var* gene and silencing of the all others are reported to be mediated by epigenetic regulation. The 5' end of the active *var* gene is found to be associated with activation epigenetic marks H3K4me2, H3K3me3, H3K9ac. The histone variant H2A.Z known to increase the transcriptional activity (32) is found incorporated around the transcription start site of active *var* gene in the ring stage and removed in the later stages (33). The promoter of the silent *var* genes are marked by heterochromatin marks H3K9me3 and HP1 protein (34). Heterochromatin is confined in the nuclear periphery and silent *var* genes are also found in the region pertaining to the heterochromatin (35, 36). A report indicates that DNA helicase RecQ1, play role in maintaining the clonal expression of the *var* gene by maintaining its location at active transcription site in peri nucleus and allowing the decrease of heterochromatin mark H3K9me3 from its promoter (37). PfSir2, the known histone deacetylase

has been reported to localize within the telomeric clusters in the nuclear periphery and promoters of the *var* genes. PfSir2, has been implicated to play important role in regulating the expression of *var* genes and is involved in the silencing of the *var* genes by promoting hypoacetylation of upstream of the *var* genes which in turn favours the deposition of H3K9me3 heterochromatin mark (35, 36). There are two paralogue of *SIR2* present in *P. falciparum* i.e., *PfSIR2A* and *PfSIR2B*. Studies suggest that knock out of *PfSIR2A* leads to de-repression of *var* gene under the control of Ups A, Ups E, and Ups C whereas *var* genes under the control of Ups B are found to be highly up-regulated when *PfSIR2B* is disrupted (26).

1.4 Malaria biology: a goldmine for discovering novel drug targets

The malarial parasite *P. falciparum* possesses exceptionally unique biology with strikingly different genome. It has most AT rich genome sequenced till date and out of 5268 predicted protein product, 2/3 of its protein are indigenous (specific) to the parasite (24). Additionally parasite harbours distinct organelle apicoplast which is absent in the higher eukaryotes. Several metabolic pathways have been reported which are exclusive to the parasite and are different from the pathways known to operate in its human host. These features extends several parasite specific targets which can be exploited for the drug therapy.

The degradation of haemoglobin is the primary requisite of the parasite as it is the source of amino acid pool essential for its growth. The major haemoglobin degradation takes place in specialised organelle food vacuole, this degradation pathway offers several promising antimalarial targets. Free heme is produced as a by-product of haemoglobin digestion, which is known to be toxic for the parasite and need to be detoxified. The pathways dedicated for its removal can also serve as potent target for antimalarial (38). Apicoplast is a crucial organelle for the parasite as various parasite specific metabolic pathway like synthesis of fatty acid, isoprenoid precursor and heme biosynthesis occur in it (39). These pathways are essential

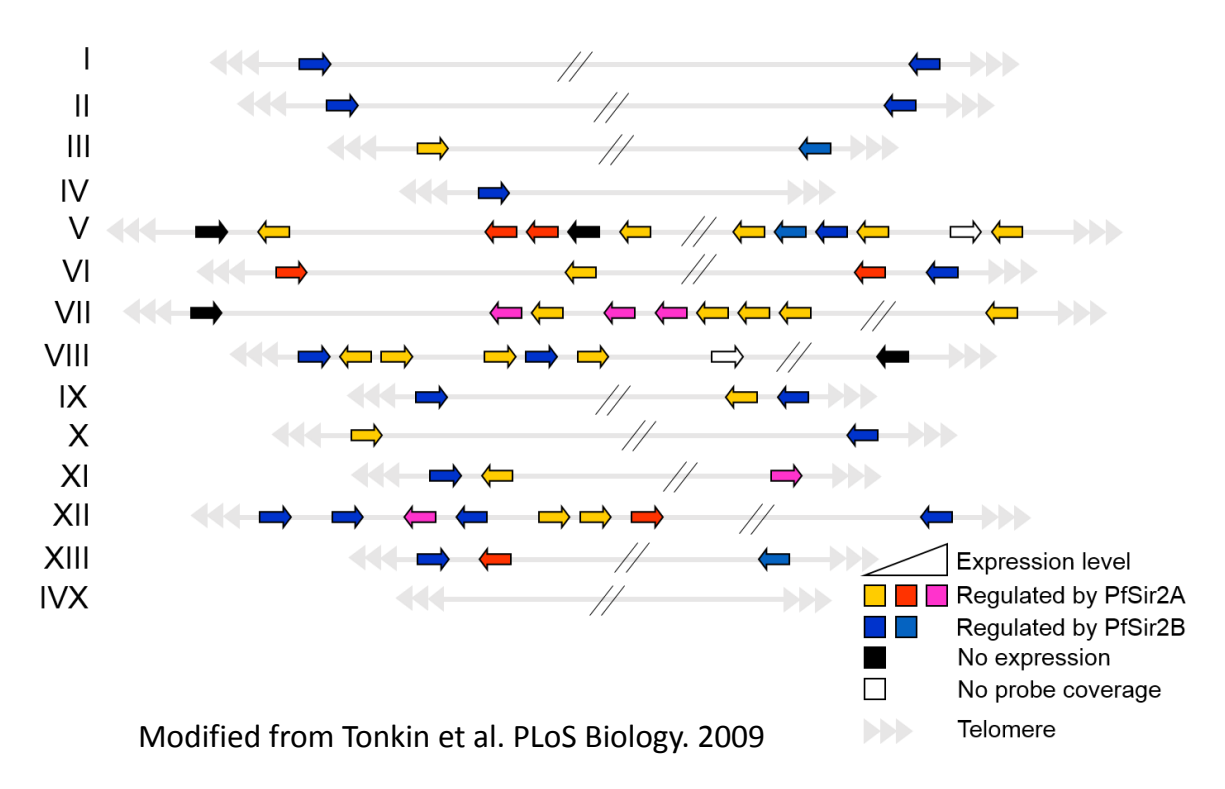


Figure 1.2: PfSir2A and PfSir2B control different sets of var genes.

for the parasite survival but does not operate in the human host, so can serve as promising targets (40-42). Although apicoplast has its own genome, but various nuclear encoded proteins are required in apicoplast and need to be transported, so pathway operating for the trafficking of these proteins can also serve as an excellent drug target (38, 43). Additionally, several essential metabolic pathways like shikimate pathway, methionine synthesis pathway, glycolytic pathway and Purine biosynthesis pathway occur in cytoplasm and either parasite specific or employ structurally different enzyme from host (38), thus offering the advantage of usage of enzymes involved in it as drug targets. Mitochondria are another vital organelle for the parasite survival and are involved protein synthesis and electron transport chain. As there exists molecular and functional difference in mitochondria of parasite and its human counterpart and therefore organelle accounts for promising antimalarial drug target (44). Numerous other pathways like transport, DNA repair, membrane biosynthesis, protein synthesis, autophagy and players like kinases and tubulin with parasite specific, unique aspects can also be exploited for the development of antimalarial chemotherapy (38).

1.5 Double strand break repair pathway a lucrative target

The prime requisite of any organism for survival is the maintenance of genome integrity. The most detrimental form of DNA damage is double strand beak (DSB). Parasite during its life cycle are under constant assault of the genotoxic stress due to the various cellular processes like haemoglobin degradation and generation of free radicals, error in replication, immune response of the host. These genotoxic insults are responsible for the generation of DSB in the parasite genome. As single unrepaired DSB confers lethality to the unicellular organism hence parasite for its viability need to repair it (45). Thus the players of DSB repair pathway have the potential of promising drug target.

1.6 Plasmodium biology and heat shock response

Malaria is associated with cyclical fever. So the *Plasmodium* during its life cycle encounters periodic cycle of heat shock which is reported to coincide with the rupture of schizonts (46). There is variation in the episode of cyclical fever among different species of *Plasmodium*, which depend on the duration of erythrocytic cycle. In the case of *P. falciparum* it is 48 hours. In vitro studies performed on *P. falciparum* culture, suggests that elevated temperature has an adverse impact on the growth of the parasite culture. As observed, when the asynchronous culture was grown at 41°C for 2, 8 and 16 hours, there was reduction in survival of the parasite by 23%, 66% and 100% respectively (47). However, recurrent fever has been reported to accelerate the parasite growth rather than hinder, as study indicates that there was no reduction in growth when parasites were subjected to two heat shock episodes separated by the recovery period of 10 hours at 37°C (48). It is also observed that heat shock leads to synchronisation of intra-erythrocytic stages of the *P. falciparum* parasites (49). From all these studies it is speculated that the parasite has acquired mechanism to deal with the heat shock experienced during the malaria fever and also elevated temperature might be serving as communication signal to the parasite to maintain the synchrony.

It is observed that exposure of parasite to the febrile temperature induces formation of pyknotic and hypo-segmented schizonts i.e., the crisis form of the parasite and TUNEL positive parasite was detected by the TUNEL assay. This indicates that the killing of the parasite on exposure to heat shock is mediated by apoptosis (50).

In a study aimed to elucidate the molecular alteration induced in the parasite on exposure to febrile temperature. Microarray analysis was conducted on the asynchronous parasite grown at 37°C and exposed to heat shock at 41°C. Transcriptional up-regulation two molecular

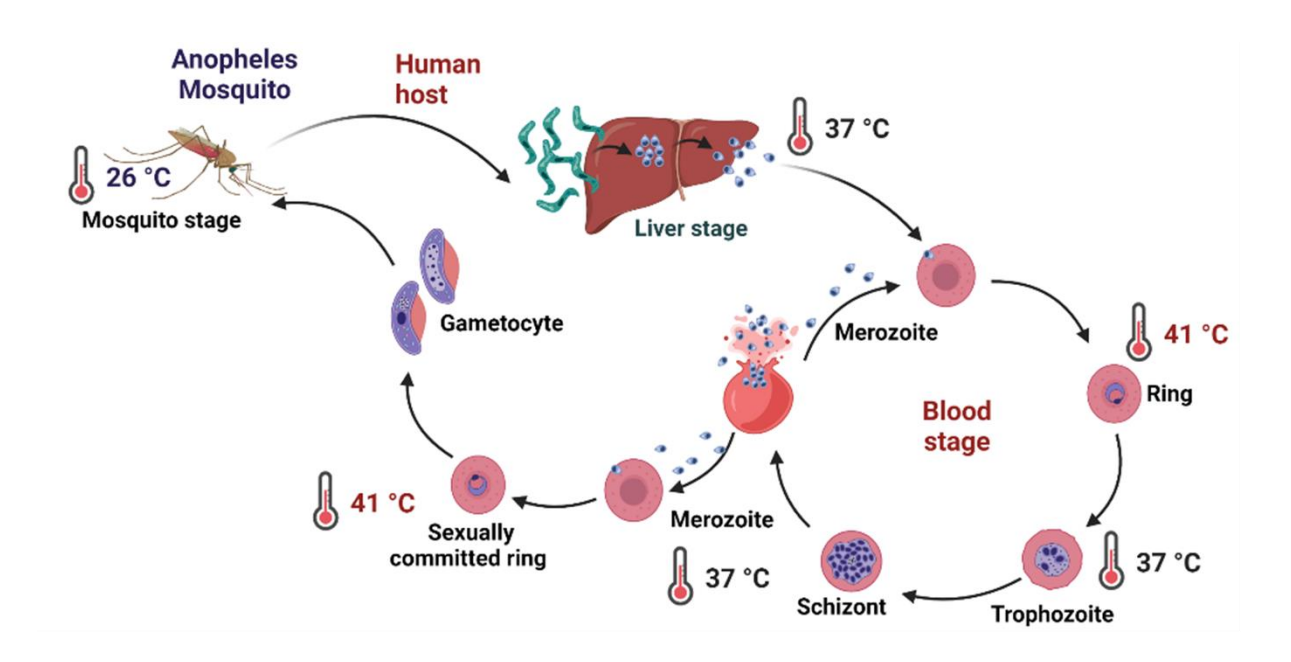


Figure 1.3: Parasite encounters various temperature variation during its life cycle involving two hosts.

chaperones *HSP90* and *HSP70* along with nine other DNA J domain proteins which are the reported co-chaperones of Hsp70 indicating that these proteins might be playing role in heat shock mediated response. Additionally, it was observed that exposure to febrile temperature, slowed down the process of protein degradation, replication, translation, as genes involved in the process were down regulated. Also, there was induction in transcriptional expression of five *var* gene responsible for encoding the PfEMP1 and surprisingly *PfSIR2A*, the epigenetic regulator of *var* gene, involved in its silencing was found be transcriptionally up regulated (47). This reveals that malarial fever augments the cytoadherence of the parasite by altering the expression of antigenic variants.

1.7 Heat shock protein 90 (Hsp90) in model organisms

Cells are under the constant assaults of environmental and endogenous stress, which might induce alteration in the state of proteins by modulating its folding and thereby having detrimental effect on their function. To counter the effect of the stress, cell expresses various sets of stress proteins and among them one of the important proteins is molecular chaperones. Molecular chaperones play critical role in ensuring the integrity of the cells by maintaining the protein homeostasis and preventing aggregation and misfolding of the proteins. One prominent group involved in this adaptive process is Heat shock proteins (51-53). Hsp40 and Hsp70 complex are involved in the folding of the nascent polypeptides. A specialised group of chaperone Hsp90, is known to be involved in folding of a of partially folded proteins which require additional folding for their stability and functional maturity (54). Hsp90 is known to be one of highly conserved chaperonic protein in eukaryotes. It plays critical role in several cellular processes which includes replication, transcription, translation, telomere maintenance, apoptosis, cell cycle progression, signal transduction and DNA repair (55-57). Hsp90 is found

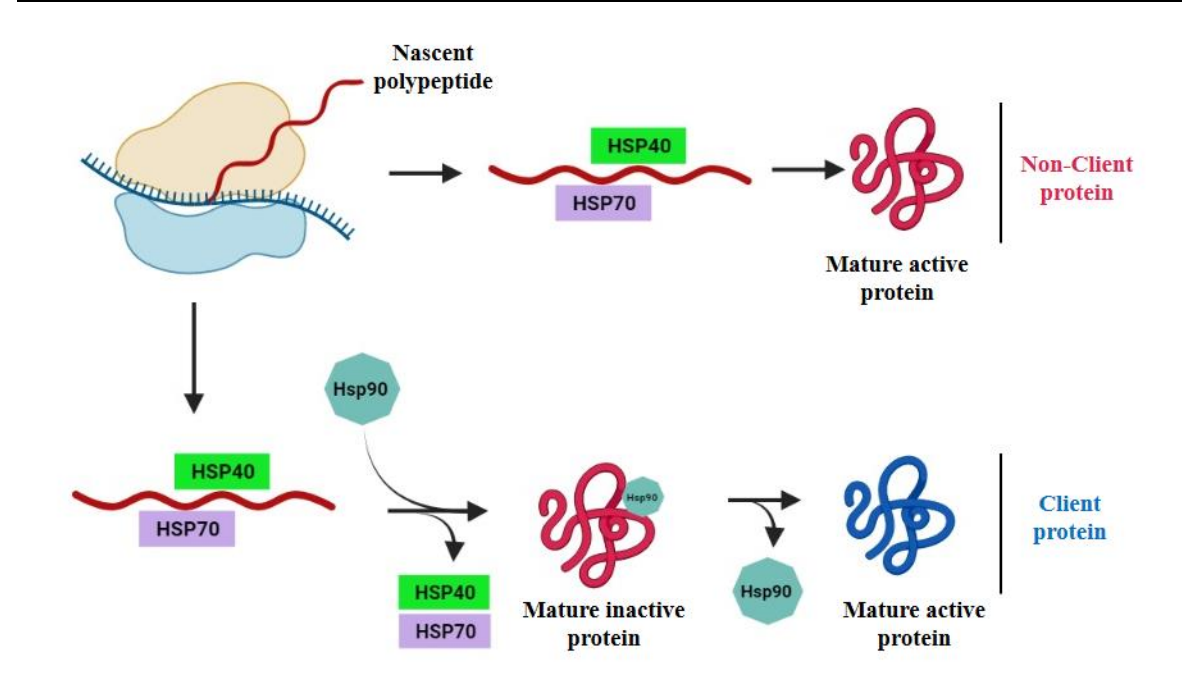


Figure 1.4: Hsp90 is a specialised chaperone and provide maturation to only a subset of client proteins.

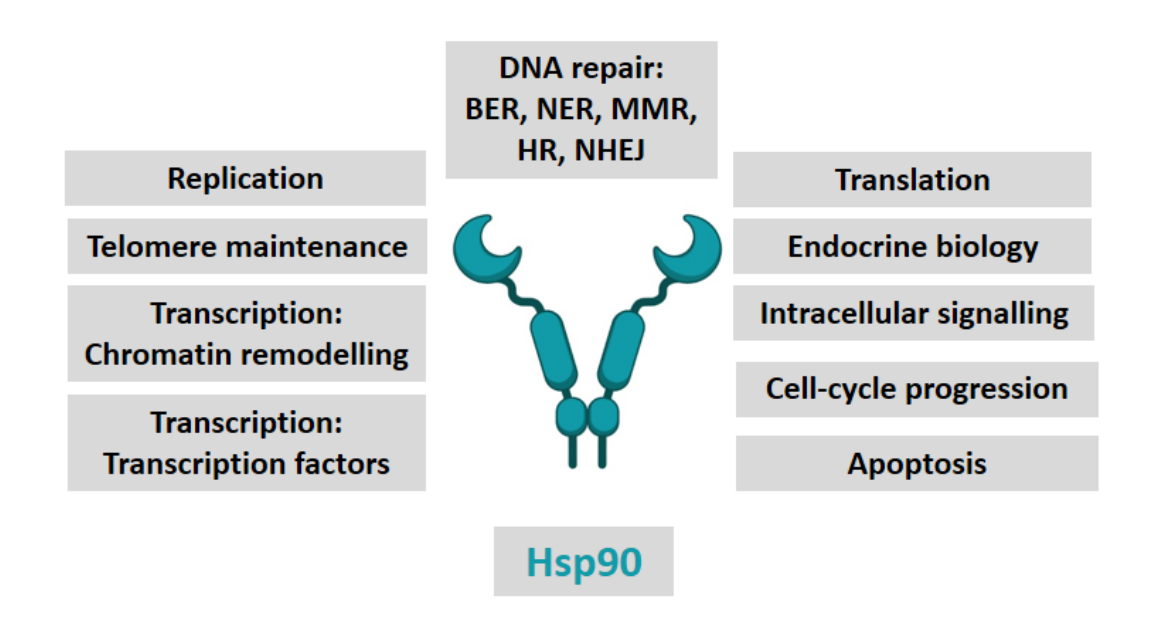


Figure 1.5: Diverse functions of Hsp90.

to be localised in cytosol, ER, mitochondria, Chloroplast and nucleoplasm. Most of the eubacteria harbours one copy of Hsp90 but due to the gene duplication, eukaryotes have two isoform of Hsp90 in the cytosol. One form is constitutively expressed in the cell while the other is the inducible form, the expression of which is induced upon stress (58, 59).

There exits basic, structural similarity between the members of Hsp90 family. Hsp90 exists as dimer and comprises of three sub-domains: N terminal domain which consists of the ATP binding site known as Bergerate fold. The middle domain has been predicted to be the site of binding of the client proteins and linked to the N terminal domain by charged linker region. C terminal domain aid in the dimerization and consists of conserved MEEVD motif which allow binding of the co-chaperones. The chaperonic action relies on its ATPase activity (59).

1.7.1 Heat shock protein 90 in model organisms: the canonical functions

Hsp90 being a cytosolic chaperone play prime role in maturation of its client proteins, which require additional folding for their stability and functioning under normal and stressful condition. Under stress the expression of Hsp90 is increased from 2% to 10% of the cellular protein, and thereby it prevents aggregation of misfolded proteins (60). Hsp90 is able to regulate the folding, assembly and functional maturity of its various client proteins by the concerted action of protein partners, imunophilins and cochaperones which includes Hsp40, Hsp70, Hip, Hop, Cdc37, p23 and several others. These act in precise and dynamic fashion and facilitates Hsp90 to form a functional super chaperone complex and thereby aid it in performing the diverse role in various cellular processes. The nascent polypeptide formed or the misfolded protein is bound by Hsp40/Hsp70/ADP complex to prevent its aggregation and this complex is further bound by Hsp70-interacting protein (HIP) or Bcl2 for its stabilization and exchange of ADP to ATP. Hsp90 binds to its client protein bound by the HSP70 complex and its interaction

with Hsp70 is aided by HOP/Sti1 (Hsp90-Hsp70 organising protein). After loading of the client protein to Hsp90, several other co-chaperone and immunophilns bind the Hsp90 complex, leading to the formation of functional heteroprotein complex and the release of the Hsp70, Hip and Hop. Further ATP binds at the NTD of Hsp90 in the complex and induces conformational change which switches Hsp90 from open state to the closed state. This is followed by ATP hydrolysis and folding of the client protein by Hsp90 assisted by binding and action of other co-chaperones. The folded protein along with the co-chaperones are then released (55). When Hsp90 is inhibited, its client protein losses its stability and either aggregate or are degraded by the proteasomal pathway (61).

The prominent clients of Hsp90 are transcription factors including steroid hormone receptors, signalling kinases and DNA repair proteins (62, 63). Hsp90 enables the cell to withstand the stress as it has the ability to modulate the expression of several genes as various transcription factors are its clients. HIF1α, ATF3, p53, NF-κB, STATs, and Bcl-6 are some of the TFs which are the clients of Hsp90 (60). Thus, by ensuring the stability and functional maturity of the transcription factor, Hsp90 is able to govern several biological pathways and thereby plays crucial role in the advancement of numerous diseases. Hsp90 is also involved in conferring conformational stability to the steroid hormone receptors like estrogen receptor, glucocorticoid receptor, progesterone receptor and facilitates high affinity hormone binding state (60, 62). It is instrumental in the process of signal transduction, as kinases such as eIF-2, Cdk4, Raf-1, Mek, Wee1, EGFR, B-raf, and SRC rely on Hsp90 for their maturity and functional activity (62). Hsp90 also plays crucial role in the DNA repair pathway of homologous recombination (HR) as it regulates the recruitment of HR machinery on the damaged site. MRN complex, BRACA2, FANCA, Rad51, Blm known to be involved in the HR mediated DNA repair pathway are stabilised and maintained at functionally active state by Hsp90 (63-67).

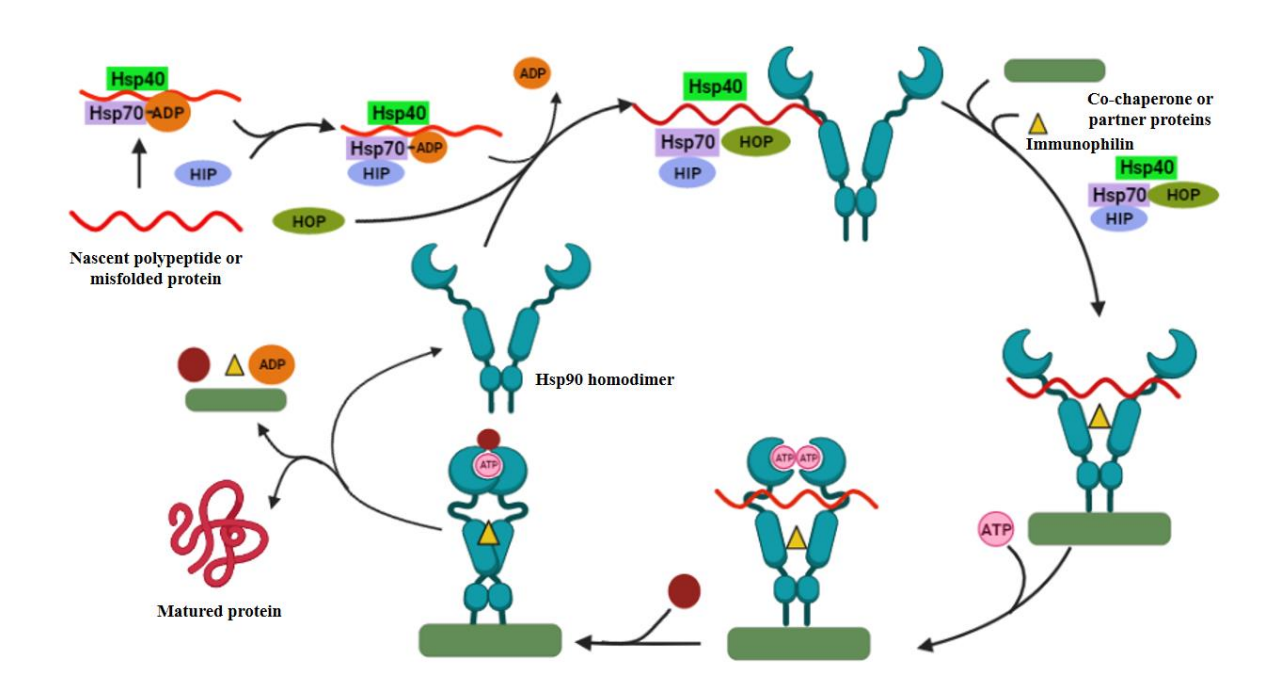


Figure 1.6: The chaperone cycle of Hsp90 in maturation of the client protein.

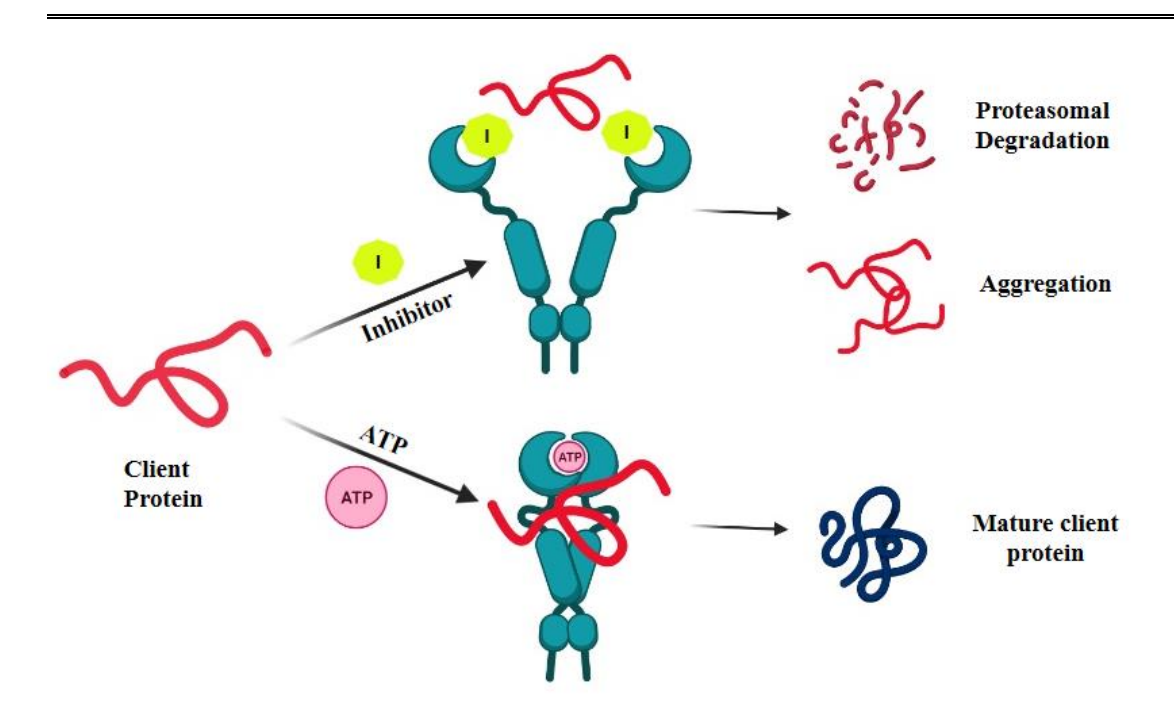


Figure 1.7: Fate of the client protein on Hsp90 inhibition.

In *S. cerevisiae*, loss of function of Hsp90 ortholog leads to decrease in expression of Rad51 and Rad52 and reduction in foci formation of Rad51 thereby renders cells more sensitive towards DNA damaging agents MMS and UV rays (65).

1.7.2 Heat shock protein 90 in model organisms: the non-canonical roles

Hsp90 apart from performing its classical chaperoning function also executes its non-canonical nuclear roles to perform moonlighting functions which includes nuclear import, assembly and disassembly of protein complexes on the chromatin and chromatin remodelling (60).

Hsp90 has been reported to interact with several chromatin modifiers, for instance Hsp90 on interaction with SMYD3, a histone methyl transferase, augments its activity and thereby aid in the progression of colorectal-, liver- and breast cancer (68-70). In S. cerevisiae overexpression of Hsp90 leads to transcriptional repression of an epigenetic eraser SIR2 (histone deacetylase) and leads to decrease in its abundance (71). Reports suggest that in *Drosophila melanogaster*, Hsp90 associates with a chromatin modifier complex TrithoraxG and in turn regulates the development of Drosophila. Inhibition of Hsp90 results in depletion of trithorax which leads to reduction in active chromatin at several gene loci (72). Additionally, genome wide ChIP analysis indicated that Hsp90 is associated with the transcription start site of at least 50% of the genes in Drosophila genome and thereby play a global role in transcriptional regulation (73). Hsp90 also assists in nucleosome eviction from the promoters and loss of function of Hsp90 in yeast halts transcriptional activation of GAL1 due to detention of the nucleosome (74). Hsp90 is also known to remove several other proteins from the promoters as observed it dictates the removal of the steroid hormone receptor from the nuclear locus (60). Hsp90 also governs the DNA protein interaction at the telomere of the eukaryotes. In yeast, Hsp90 has been reported to be involved in the removal of the primary capping complex (CST) present at. the chromosome end to provide access to the telomerase for the extension the DNA ends.

Moreover Hsp90 stimulates the telomerase activity of DNA binding and nucleotide addition, as reported mutation in Hsp90 leads to shortening of the telomere (63).

1.8 Plasmodium Heat shock protein 90

PfHsp90 is expressed in all the three blood stages of the parasite and account for 2% of the proteome of the parasite (75). Four paralogs of PfHsp90 are encoded by the parasites genome. PF3D7_0708400 (PF07_0029) is the inducible form of Hsp90 and is present in the cytoplasm. PF3D7_1443900 (PF14_0417) is the cytosolic constitutive Hsp90 (76), although certain report suggests its presence in the apicoplast (77). PF3D7_1222300 (PFL1070c) is reported to be confined in the ER and PF3D7_1118200 (PF11_0188) is known to localise in the mitochondria (76). The cytosolic inducible PfHsp90 is found to be quite similar to the canonical Hsp90 ortholog and is reported to have 64% amino acid sequence identity with its human Hsp90. It shares basic domain similarity with Hsp90 found in other organisms and comprises three similar domains: N-terminal domain, Middle domain, and C-terminal ending with MEEVD motif and a charge linker domain connecting the NTD and the MD. Interestingly PfHsp90 possesses longer charge linker region with more negative charge compared to the human and yeast counterparts (77).

As it is evident that parasite during course of its life cycle experiences heat shock i.e., during the transition from mosquito to human and when the human host experiences fever. In order to withstand these temperature variations and episodes of heat shock, parasite need to have robust chaperone protein control system for proper folding of the protein and to prevent aggregation and misfolding of the protein. Among them one potent chaperone is Hsp90, which is known to be induced upon the heat shock and known to play role in the manifestation of the infection in its human host and governs the stage switch or play role in the transition of the stage (48, 78). Hsp90 in model organism has been reported to provide stability and maturation

to variety of its clients, but the clients of this chaperone in *Plasmodium* biology are yet to be identified. Additionally, none of its nuclear functions have been reported till date in the protozoan parasite.

1.9 Plasmodium Hsp90 as an antimalarial drug target

As PfHsp90 is found to be expressed in intra-erythrocytic stage of the parasite which is induced upon stress and is essential for the survival of the parasite (79, 80). Although PfHsp90 is 70% identical to the HsHsp90, still it possesses the potential of serving as an excellent chemotherapeutic target as PfHsp90 harbours a unique long charged acidic linker region and slightly varied binding pocket due to amino acid substitution which leads to more constricted and the hydrophobic end of the binding pocket (81, 82). Various inhibitors of Hsp90 like Geldanamycin, Radicicol, 17AAG, 17-DMAG, has been reported to inhibit the in vitro growth of *Plasmodium* culture (83, 84). Additionally, 17AAG is known to inhibit the activity of purified protein (85). Reports depict that PfHsp90 has more binding affinity towards GA than HsHsp90 and has more efficient ATPase activity as compared to other Hsp90 counterpart (85). Complementation assay performed in yeast revealed that yeast strain harbouring PfHsp90 is hyper-sensitive to Hsp90 inhibition- mediated growth arrest (86). Thus, this small difference in PfHsp90 from its human ortholog, would allow to design drugs that can specifically inhibit PfHsp90. Geldanamycin has been reported to show synergism with anti-malarial drug chloroquine against the asexual stage of the parasite and also acts synergistically with cyclosporine A (inhibitor of calcineurin) in anti plasmodial activity (80, 87, 88). Inhibitors of Altogether, this suggest that PfHsp90 can serve as a potent antimalarial target and using inhibitors of Hsp90 in combination therapy with anti-malarial drugs would be an excellent approach to curb malaria.

1.10 Significance of the study

Malarial parasite *Plasmodium* possesses very unique biology and resides in two hosts which are very unlike each other. One is the invertebrate mosquito while the other is the vertebrate human host. The body temperature of the two hosts are quite different. Thus, the parasite on transition from mosquito to human host encounters temperature variation of 10° C. Additionally parasite also encounters the febrile temperature when human host undergoes episodes of fever. The specialised molecular chaperone Hsp90 is reported to play very crucial role in maintaining the protein homeostasis when parasites are under the temperature stress. Hsp90 enables the parasite withstand the stress by preventing the aggregation of the misfolded proteins and by aiding in various other process. In this study, we have established PfRad51, the chief player of the HR pathway for the DNA repair as the client of PfHsp90. Here we uncover the canonical role of PfHsp90 in the client maturation of PfRad51 and its role in governing the DSB repair pathway in the parasites. We demonstrate that PfRad51 interacts with PfHsp90 and on inhibition of PfHsp90, PfRad51 undergo proteasomal degradation resulting in the abrogation of its DNA repair activity. It suggests new drug combination therapy, which can be used to tackle malaria. Additionally, it can be used as a model to get further insights of the Hsp90 chaperone cycle. Apart from this we have also probed into the non-canonical function of PfHsp90 in transcriptional regulation of the epigenetic eraser PfSIR2. We found that the master epigenetic regulator of virulence gene in Plasmodium, namely PfSir2, is itself regulated transcriptionally by epigenetic modification. Here we show that Hsp90, a molecular chaperone that modulates chromatin states in other eukaryotes, is the key link between environmental heat stress and chromatin modification in this parasite. Our study reveals that PfSIR2 is transcriptionally down-regulated upon exposure of the parasite to heat shock. This down regulation was found

to be mediated by PfHsp90 via epigenetic modifications. Additionally, it is observed that exposure to febrile temperature modulates the expression of virulence genes which could impact chronicity of malaria infection. Thus, understanding the molecular mechanism underlying *PfSIR2* gene regulation might offer novel intervention strategies for curbing malaria.

1.11 Objectives of the study

Emergence of drug resistance in the malaria parasites against the variety of first line drugs and unavailability any potent vaccine are the causes for greater morbidity due to malaria. So there is a need to develop new drugs and identify new drug targets to win the war against malaria. Thereby current situation is compelling us to understand the parasite biology for identification of new drug targets. Hsp90 is the molecular chaperone which is essential for the parasite survival, and inhibition of PfHsp90 halts the in vitro growth of the parasite. Additionally, inhibitors of PfHsp90 have been reported to show synergism with the anti-malarial drugs and thus indicates that PfHsp90 can serve as excellent drug target. In the model organism, Hsp90 drives several cellular processes by providing functional maturity to its client protein and by executing its non-canonical nuclear functions. However, in *Plasmodium* clients of Hsp90 are still unidentified and none of its non-canonical function has been elucidated. In this study, we have investigated the clientship of PfHsp90 which is its canonical function and also explored its non-canonical nuclear functions in regulating the transcriptional repression of *PfSIR2* upon heat shock.

1.12 Aims of the study

To decipher the canonical functions of PfHsp90 in Plasmodium biology

In this regard, we aimed to determine whether PfRad51 is a client of PfHsp90 and studied the following aspects

- 1) Physical interaction of PfRad51 and PfHsp90
- 2) Effect of PfHsp90 inhibition on the steady state of PfRad51
- 3) Effect of PfHsp90 inhibition on DSB repair function of PfRad51
- To explore the non-canonical functions PfHsp90 in *Plasmodium* biology

In this regard we aimed to probe in role of PfHsp90 in epigenetic regulation of *PfSIR2* transcription and studied the following aspects

- 1) Effect of heat-shock on *PfSIR2* expression and activity
- 2) Identification of heat induced alterations in chromatin landscape of *PfSIR2*
 - A. Study of chromatin state
 - B. Identification of the altered epigenetic mark(s)
- 3) Role of PfHsp90 in altering the chromatin state of PfSIR2 upon heat shock
 - A. Inhibition of PfHsp90
 - I. Effect on PfSIR2 transcription
 - II. Effect on chromatin state
 - III. Effect on epigenetic mark(s)
 - B. Association of PfHsp90 at PfSIR2 promoter-proximal region

Chapter-2 Materials and methods

2.1 Recombinant DNA techniques

2.1.1 Bacterial competent cell preparation

The primary inoculum of the bacterial culture was given using a single colony of the bacteria in LB media with appropriate antibiotic. The culture was allowed to grow overnight at 37°C, 200 rpm. 1 % Secondary culture was set with the primary culture on next day in 40 ml LB media with appropriate antibiotic and was grown in the similar condition till the O.D reaches 0.5. Further the cells were harvested by centrifuging the bacterial culture at 8000rpm, 4°C for 8 minutes. The cell pellet obtained was gently re-suspended in ice- cold 12.5ml calcium chloride (0.1M) and the suspension was then centrifuged again at 8000rpm, 4°C for 8 minutes. The supernatant was discarded and the cell pellet was again re-suspended gently in ice- cold 12.5ml calcium chloride (0.1M). The cell suspension was incubated on ice for 4 hours. After the incubation, the cells were harvested by centrifugation at 8000rpm, 4°C for 8 minutes. The bacterial pellet was then very gently re-suspended in 1.07 ml of ice- cold calcium chloride (0.1M) and 170 μl of glycerol. The prepared bacterial competent cells (100 μl) were aliquot in pre chilled micro-centrifuge tubes. For storage, the cells were frozen in liquid nitrogen and kept at -80°C.

2.1.2 Bacterial transformation

The bacterial competent cells stored at -80°C, was allowed to thaw on ice. The plasmid DNA (20-25ng) was then added to the cells and incubated on ice for 30 min. Depending upon the cell type, the cells were subjected to heat shock at 42 °C for various time periods: TOP10 cells for 30sec and the expression cells for 90 sec. The cells were immediately incubated on ice for 2 minutes after the heat shock. LB broth (900 µl) was further added to the cells and allowed

to grow at 37°C, 200 rpm for 1 hour. The cells were then centrifuged at top speed for 2 min and most of the supernatant was discarded. The cell pellet was re-suspended in the remaining media and was plated on LB plate with appropriate antibiotics followed by incubation at 37°C for 12 -16 hours.

2.1.3 Plasmid DNA isolation by alkaline lysis method

The bacterial inoculum was given in 5 ml of LB broth containing appropriate antibiotics using a single bacterial colony harbouring the plasmid of interest and was grown overnight 37°C, 200 rpm. The bacterial cells were harvested by centrifuging the culture at 4500 rpm for 10 minutes. The cell pellet was re-suspended in 200 µl of solution 1 (Tris 25 mM pH 8.0, EDTA 10 mM pH 8.0) and transferred to micro-centrifuge tube. Then 200 µl of solution 2 (NaOH 0.2 M, SDS 1%) was added to the cell suspension and vigorous mixing was performed by inverting the tubes several times for the cell lysis. Two hundred microliter of solution 3 (NaOAc 3M, pH 5.2) was then added to the suspension and the tube was inverted 4-5 times for mixing, followed by incubation on ice for 5 minutes with intermittent mixing. The sample was further centrifuged at 1200 rpm for 10 minutes, RT to separate the white precipitate formed. The supernatant obtained is transferred to fresh micro-centrifuge tube and 400 µl of absolute ethanol was added followed by incubation at -20 °C for 45 minutes. After the incubation, the sample was centrifuged at 12000, 4°C for 30 min for DNA precipitation. The pellet obtained was washed with 70 % ethanol by centrifugation at 12000 rpm for 5 minutes. The supernatant was then discarded and the pellet was air dried. The pellet was further re-suspended in 50 µl of 1X TE (10 mM Tris pH 8.0, EDTA 1 mM pH 8.0) and 5 µl of RNase (10mg/ml) was added to it and incubated at 37 °C for 30 minutes. 1X TE was added to the sample to make its volume to 400µl and then 400 µl of PCIA (Phenol: Chloroform: Isoamyl alcohol=25:24:1) was added.

The sample was vortexed for 3 minutes for mixing and then centrifuged at 14.5 rpm, RT for 10 minutes. The aqueous layer formed was transferred into fresh micro-centrifuge tube avoiding the interface and the organic layer. Then 1/10th volume of solution 3 and 2.2 volume of absolute ethanol was added to it and incubated at -80 °C for 1 hour. The sample was then centrifuged at 12000, 4° C for 30 minutes and the pellet obtained was subjected to washing with 500 μ l of 70 % ethanol by centrifugation at 12000 rpm for 5 minutes. The pellet was then air dried and re-suspended in 30 μ l of 1 X TE.

2.1.4. Recombinant protein expression

Induction of recombinant protein *PfSIR2A*- GST was performed as described previously (89). *PfSIR2A* cloned in bacterial expression vector pGEX-6p2 vector was transformed in bacterial expression strain BL21 codon plus and primary inoculum was given in LB containing ampicillin from these transformed bacterial cell. The primary culture was grown overnight at 37 °C, 200rpm. Next day secondary inoculum was given using 1% of the primary culture and grown at 37 °C, 200rpm till the OD₆₀₀ reached 0.6. For induction, 0.4 mM isopropyl-β-thiogalactopyranoside (IPTG, sigma) was added to the culture and incubated at 22 °C for 10 hours. The bacterial pellet was collected and re-suspended in 1X laemmli buffer. The induced recombinant protein was visualised by SDS- PAGE

2.2 Yeast methods

2.2.1 Yeast competent cell preparation

Primary inoculum for the yeast culture was given with a single colony of required strain in 5ml of appropriate medium and was grown overnight at 30°C, 200 rpm. OD_{600} of the primary culture was determined next day and secondary inoculum was given in 40 ml of appropriate medium using the formula: Volume of inoculum = (Final volume of secondary culture \times 0.5

OD) / (Initial OD \times 2²). The secondary culture was grown at 30°C, 200 rpm till the OD₆₀₀ reaches 0.6 - 0.8. The cells were harvested by centrifugation at 3500 rpm, 4°C for 5 minutes. To remove the media, the cell pellet was washed by re-suspending in 10 ml sterilized Milli-Q water followed by centrifugation at 3500 rpm, 4°C for 5 minutes. For making the cells competent, cell pellet was re-suspended in 300 μ l of Lithium solution (1X TE, 1X LiOAc).

2.2.2 Yeast Transformation

DNA sample (0.5-1 µg) was mixed with 10µg of the carrier DNA (salmon sperm DNA) in a micro-centrifuge tube and 200 µl of the competent cells were added to it. Then, 1.2 ml of PEG solution (for 10 ml, 1 ml of 10X LiOAc, 1 ml of 10X TE, 8 ml of 50% PEG2000 solution) was added to it and the cells were allowed to grow at 30°C, 200 rpm for 30 minutes. The cell were then subjected to heat shock at 42°C for 15 minutes followed by incubation on ice for 2 minutes. The cells were then harvested by centrifugation at top speed for 10 seconds, the pellet obtained was re-suspended in 100 µl of 1X TE buffer and plated on appropriate plates followed by the incubation at 30°C till the transformant colonies were observed.

2.2.3 Protein isolation by TCA method

Primary inoculum was given with a single colony of the required yeast strain in 5 ml of appropriate growth medium and was grown overnight at 30°C. The temperature sensitive iG170Dhsp82 strain was grown at 25°C. Secondary inoculum was given next day in 20 ml of growth medium with the primary culture using the formula: Volume of inoculum = (Final volume of secondary culture \times 0.5 OD) / (Initial OD \times 2²). The secondary culture was grown till the OD₆₀₀ reaches 0.5. After that the culture was divided in two parts , one part of the culture was grown at 25°C for 4 hours while the other part was grown at 37 °C for 16 hours. The cells

equivalent to 10 OD were harvested by centrifugation at 3500 rpm, 4° C for 5 minutes. The cell pellet obtained was re-suspended in 500 ml sterilized Milli-Q water and transferred to 2 ml centrifuge tube. At this point, the cells were either stored at -80°C or were right away used for the protein isolation. For protein isolation, cells are initially washed by re-suspending it in 500 μ l of 20% TCA and then centrifuged at 12000rpm, 4° C for 5 minutes. The cell pellet was then re-suspended in 200 μ l of 20% TCA and glass bead was added. The sample was vortexed for 10 minutes and placed on ice for 5 minutes rest. This step was repeated 2 more times. The supernatant was collected and transferred to fresh microfuge tube when glass beads settled. The remaining glass bead and cell mixture was washed with 200 μ l of 5% TCA by mixing thoroughly and then supernatant was collected after settling of the glass beads. This steps was repeated till the supernatant obtained after washing of glass beads became clear. The supernatant collected was centrifuged at 3000 rpm, RT for 10 minutes. The supernatant was then discarded and the precipitate was re-suspended in 90 μ l 1X SDS-PAGE loading buffer. 10 μ l of 1M DTT and 50 μ l of 1 M Tris pH 8.8 were added to the sample and was then boiled for 5 minutes and spun at top speed for 5 minutes.

2.2.4. Yeast-two-hybrid analysis

PJ694a yeast strain was used for the Y2H analysis. To determine the interaction between PfHsp90 and PfRad51, *PfHSP90* was cloned in pGBDUC1 and fused to the binding domain while *PfRAD51* was cloned in pGADC1 to fuse with the activation domain. Both the plamsids were transformed in the PJ694a strain and the transformants were selected on double drop out plate Sc-Leu-Ura. The interaction between Pf Hsp90 and PfRad51 was confirmed by the growth on triple dropout plates Sc-Leu-Ura-His and Sc-Leu-Ura-Ade. Growth on Sc-Leu-Ura-His depicts weak interaction while growth on Sc-Leu-Ura-Ade suggests strong interaction. The

possibility of the self-activation of the reporter gene was ruled out by screening the interaction PfHsp90 and PfRad51 with empty prey and empty bait vector. Additionally to ascertain the specificity of the interaction, *PfACTIN* was cloned in the pGADC1 and screened for its interaction with PfHsp90. For the comparative growth analysis of the control and test strains, spotting analysis was performed in which serially diluted strains were spotted on the double and triple drop out plates. The plates were incubated in 30°C and further observed for growth.

2.3 Methods in *Plasmodium falciparum* experiments

2.3.1 Washing of RBCs

The collected blood (10 ml) was taken in 15ml centrifuge tube and was spun at 15000 rpm for 15 minutes. The upper yellow serum layer obtained along with the white buffy layer was removed with the Pasteur pipette. The volume of RBC obtained was monitored and then equal volume of incomplete medium was added to it and mixed gently. The blood was then centrifuged at 3000 rpm for 15 minutes. The supernatant was aspirated and washing of RBC pellet was repeated twice with the incomplete medium. To obtain 50% haematocrit, the washed RBC pellet was mixed gently with equal volume of incomplete medium. The tube was marked and stored at 4°C.

2.3.2 Thawing of the parasites from liquid nitrogen

A cryovial of the frozen parasites was taken out from the liquid nitrogen tank and was thawed by partially dipping the vial in 37°C pre-warmed water for 2- 3 minutes. In order to avoid contamination, vial was bathed with 70 % alcohol and wiped. The thawed parasite culture was transferred into 50ml centrifuge tube and solution - I (0.2 ml of solution- I /1 ml of parasite culture) was added with gentle shaking maintaining the drop rate one drop per second. The

culture was then left undisturbed for 5 minutes. Further, 10ml of solution – II (1.6% NaCl) per 1ml of thawed parasites was added in similar drop wise manner. The sample was centrifuged at 1000 rpm for 10 minutes at room temperature and supernatant was aspirated using the Pasteur pipette. The tube was gently tapped to loosen the pellet and then 10 ml of solution – III (0.9% NaCl, 0.2% Glucose) per 1ml of thawed parasites was added to the pellet in similar drop wise manner with gentle mixing. The sample was centrifuged 1000 rpm for 10 minutes and supernatant was removed using the Pasteur pipette. The obtained pellet was re-suspended in 3 ml of complete medium and 0.2 ml of washed blood was added to it and then the culture was transferred to culture plate and kept in the incubator.

2.3.3 Maintenance of the parasite culture

In vitro culture of *P. falciparum* was maintained at haematocrit of 5%, 37 °C by candle jar method in RPMI media supplemented with 1% albumax and 0.005% hypoxanthine. The medium of the culture was changed every day under aseptic condition. RBC in the culture tend to settle at bottom of the culture plate, the used medium was aspirated from top with the help of Pasteur pipette carefully without disturbing the bottom cellular layer and then required volume of pre-warmed complete medium was added to the culture. The culture plate was gently shaken for mixing the culture. The culture plate was then placed in the candle jar in the incubator, candle was lit and lid of the jar was closed with small opening. When the candle extinguished, the lid was completely closed. The parasitemia of the culture was regularly monitored through Giemsa stained smear made from the culture. Subculture was performed when the parasitemia of the culture reached 2%. For sub-culturing 0.5 ml of the culture, 0.5 ml of RBC (50 % haematocrit) and 4ml of pre-warmed complete media was added to the new well and mixed gently.

2.3.4 Synchronisation of the parasites by sorbitol method

The parasite culture consisting of mostly ring stage was taken in 15ml centrifuge tube and centrifuged at 3000 rpm at room temperature for 10 minutes. The supernatant was aspirated using the Pasteur pipette and the pellet was re-suspended in twice the pellet volume of pre-warmed 5% sorbitol. The culture tube was incubated at 37 °C for 15 minutes with intermittent shaking. Incomplete RPMI 1640 medium was added to the culture for diluting the sorbitol and was then centrifuged 3000 rpm at room temperature for 10 minutes. The supernatant was removed and the pellet was washed with incomplete RPMI 1640 medium 3 more times. After washing, the pellet was re-suspended in appropriate volume of the pre-warmed complete medium and then placed back in the culture plate. The culture plate was then kept back in the incubator.

2.3.5 Freezing of the parasite culture

For freezing, 10 ml of ring stage parasite culture with 4-6% parasitemia was taken in 50 ml centrifuge tube and spun at 2500 rpm, RT for 10 min. The supernatant was aspirated with Pasteur pipette and freezing solution equal to pellet volume was added with a speed of 1 drop/second. The sample was left undisturbed for 5 minutes. Then 1.3 volume of freezing solution was added tin drop wise manner. Then, 1ml of the culture was transferred to each cryo-vial and placed in iso-propanol bath at -20 °C for one day. Next day, the frozen culture was transferred to liquid nitrogen tank

2.3.6 MG132 treatment

Synchronous ring stage culture was treated with 133 nM MG132 for 12 h, then culture was removed from MG132 containing medium and was grown in complete medium till late and trophozoite/ early schizont stage. Parasites were then harvested and total protein was extracted

and used for western blot analysis.

2.3.7 Harvesting of the parasites by saponin lysis

The parasite culture was transferred to a centrifuge tube and centrifuged at 3000 rpm, room temperature for 10 minutes. The supernatant was aspirated and double the volume of pellet 0.15% saponin was added. The sample was vortexed for mixing and then incubated at 37 °C water bath for 15 minutes with intermittent mixing. Five volume of cold 1X PBS was added to the sample to dilute the concentration of saponin and then centrifuged at 5000rpm, 4°C for 10 minutes. Supernatant was removed along with the top layer of ghost RBC. The parasite pellet obtained was washed with cold 1X PBS 3 times or till reddish colour disappear. The parasite pellet was then stored at -80°C till further use.

2.3.8 Genomic DNA isolation from the parasites

Ten millilitre of the parasite culture was harvested by saponin lysis. The obtained pellet was re- suspended in 75 μl of Milli-Q water and 25 μl of lysis buffer (10mM Tris HCl pH-8, 20 mM EDTA pH-8, 0.5% SDS 0.1mg proteinase K) and vortexed for 1 minute for mixing. The sample was then incubated in 37°C water bath for 3 hours with intermittent mixing every 30 minutes. 350 μl of Milli-Q water and 400 μl of PCIA solution was added to the sample after incubation and vortexed for 3 minutes. The sample was then centrifuged at top speed RT for 15 minutes. The aqueous layer obtained was transferred to fresh microfuge tube and 50 μl of RNase (10mg/ml) was added. The RNase treatment was performed for 30 minutes and then the PCIA extraction was repeated. 2.2 volume of 100% ethanol and 1/3 volume of solution III was to the aqueous layer was collected and the sample was incubated in -80 °C overnight for the DNA precipitation. The sample was centrifuged next day at 12000 rpm, 4°C for 30 minutes, the supernatant was discarded and the pellet obtained was washed with 70 % ethanol 12000 rpm, 4°C for 5 minutes. The obtained pellet was air dried and then re-suspended in 1X TE.

buffer and the quality of the genomic DNA was assessed by running it on the agarose gel.

2.3.9 Protein preparation from the parasites

The parasite pellet obtained after saponin lysis from 10-15 ml of the culture was re-suspended in 1X laemmli buffer (63 mM Tris-HCl – pH6.8, 10% glycerol, 0.005% Bromophenol blue, 0.1% 2- Mercaptoethanol). The sample was boiled in boiling water bath for 10 minutes and then centrifuged at 8000 rpm for 8 minutes. The protein quality was checked on SDS-PAGE.

2.3.10 RNA isolation from the parasites

Total RNA was isolated following the protocol described elsewhere (90). Ten milliliters of synchronised culture was centrifuged at 1800 rpm for 3 minutes and supernatant was removed. Pre-warmed TRIzol was added to the pellet. For ring stage 10 pellet volume and for trophozoite and schizont 20 pellet volume of TRIzol was used. The sample was shaken to dissolve the clumps and then incubated at 37°C for 5 minutes. The sample was vortexed for 3 minutes after adding 0.2 TRIzol volume of chloroform and then allowed to stand for 3 minutes. To extract the aqueous layer, the sample was centrifuged at 4500 rpm, 4°C for 30 minutes. The aqueous layer obtained was transferred to new microfuge tube, 0.5 TRIzol volume of 2-propanol was added and then incubated overnight at 4°C. Next day, the sample was spun at 14000 rpm, 4°C for 30 minutes. One milliliter of 75 % ethanol was added to the pellet and mixed. The sample was pooled in single tube if multiple tube were used and centrifuged at 14000 rpm, 4°C for 30 minutes. The pellet obtained was air dried for 5 minutes and re-suspended in 30 µl nuclease free water. The quality of RNA was assessed by running it in FA agarose gel.

2.3.11 cDNA preparation

The concentration of isolated RNA was measured by spectroscopic analysis using JASCO spectrophotometer EMC-709. Five microgram of total RNA was subjected to DNase (Fermentas) treatment in order to remove the genomic DNA contamination. PCR analysis was performed without cDNA preparation (– RT) to confirm the complete removal of genomic DNA prior to cDNA synthesis. For cDNA synthesis, 1 µg of RNA was reverse transcribed with oligo dT primer (Sigma) using Omniscript reverse transcriptase. The synthesized cDNA was further subjected to PCR analysis.

2.4 Real time PCR.

Applied Biosystems 7500 Fast Real Time PCR system was used for the Real time analysis. 10 μ l of reaction mixture was prepared which comprised of 0.5 μ l of the forward and reverse primers (concentration 10 pmole / μ l) each, 5 μ l of SYBR premix (Takara), 2 μ l of Milli Q water and 2 μ l of the template. The fold change was calculated using $\Delta\Delta$ CT method.

The mean values (±SEM) from three independent experiments were plotted using Graph Pad Prism 6 software.

2.5 MMS sensitivity assay

Synchronous ring stage parasites were treated with different concentrations of 17AAG (170 nM to 850 nM) or Radiciciol (1.5 μ M) and grown till late trophozoite/ early schizont stage. Pretreated parasite (1% parasitemia) was then subjected to MMS treatment (0.001%, 0.005% and 0.1%) for 2 hours. Further 3 times washing with RPMI was performed in order to remove the MMS. Then the parasites were allowed to grow for 48 hours in the presence of the respective concentrations of 17AAG or Radicicol. The parasitemia was monitored by the Giemsa-stained smear.

The percent survivability was calculated using the following equation:

% Survivability = (% parasitemia in the absence of MMS/ % parasitemia in the presence of MMS) x 100.

2.6 PCR-based method to quantify DNA damage

To monitor the repair kinetics of damaged nuclear DNA, ring stage culture with parasitemia 6% was pre-treated with 17AAG (1.7 μM), with B02 (1 μM) or with Atovaquone (0.3 nM). DNA damage was induced at early trophozoite stage through UV exposure at 100 J/m². Further, the cultures were maintained in the presence of the respective inhibitors for 24 hours. Parasites were harvested for genomic DNA isolation before the damage (UT), just after the damage (0 h), at 12 h and at 24 h. PCR for long-range (7200 bp) and short range (269 bp) fragment were performed from equal amount isolated genomic DNA for each time point using the primer-sets mentioned in table 2.1. Quantification of the PCR product was performed using SYBR green I dye, and the fluorescence readings of the long-range PCR products were normalized by the reading obtained from the short-range PCR product. The amount of damaged DNA at any given time point was deduced from the following equation: damaged DNA = 1- (fluorescence intensity of the long PCR product/ fluorescence intensity of the short PCR product × 26.76), where the factor 26.76 represents the ratio of the sizes of the two amplicons. The amount of damaged DNA from the UV-untreated sample was considered as 0% and the zero-hour sample was considered as 100%. The amount of residual damaged DNA at each time point was plotted using GraphPad Prism 6 software.

2.7 Chromatin Immunoprecipitation

The crosslinking of the parasites for ChIP was performed as described previously (91). Hundred millilitre of synchronised ring stage cultures treated under different conditions were harvested and lysed by saponin treatment. The liberated parasites were washed with pre-

warmed 1X PBS 3-4 times till the lysed RBC was removed. The harvested parasite pellet was re-suspended in 3.65 ml of pre-warmed 1X PBS. Then 50µl of 37% formaldehyde (final concentration 0.5%) was added to it and incubated on rocker for 10 minutes at RT for the crosslinking. For stopping the reaction, 300µl of 1.67 M glycine (in PBS) was added and the parasites were incubated on ice for 5 minutes. The parasites were then centrifuged at 4000g RT for 5 minutes. The supernatant was removed and parasite pellet was washed with ice-cold PBS. The obtained parasite pellet after centrifugation was frozen in liquid nitrogen and stored in -80°C or used for the further processing. The cross-linked parasites were thawed on ice if frozen. The parasites were then re-suspended in 2ml of cold lysis buffer (10mM HEPES pH7.9, 10mM KCl, 0.1mM EDTA pH8, 0.1mM EGTA pH8, 1mM DTT, protease inhibitor) and incubated on ice for 1 hour with intermittent mixing. Nonidet -40 was added to final concentration of 0.25% and the re-suspended parasites were transferred to the pre chilled dounce homogenizer and 200 strokes were given for the lysis of the parasites. The lysate was transferred to 1.5 ml microfuge tube, 1ml in each and then centrifuged for 10 minutes at 14000 rpm, 4°C. The supernatant was discarded and the pellet in each tube were re-suspended in 125 ul of SDS lysis buffer (1% SDS, 10mM EDTA pH8, 50mM Tris HCl pH8 supplemented with PI, PMSF and DTT). The DNA was then sheared using Elma water bath sonicator, sonication of the chromatin solution was performed for 6 sessions (10 sec burst and 5 min rest) at 37 hz frequency. The chromatin solution were pooled in single tube and was 10 fold diluted by adding 2250 µl of chromatin dilution buffer (0.01% SDS, 1.1% tritonX100, 1.2 mM EDTA, 16.7 mM Tris HCl pH8, 150mM NaCl, PI and PMSF). The chromatin shearing was monitored by running the chromatin solution on the agarose gel. For the pre cleaning of the chromatin solution, 190 µl of equilibrated protein A agarose beads with the equilibration buffer (0.1%) BSA, 0.1% Na azide, 1X TE) was added to it and incubated on rocker, 4°C for 2 hours. The

protein A agarose beads were removed by spinning the chromatin solution at 2500 rpm, 4°C for 10 seconds. The supernatant was transferred to fresh tube and for each immunoprecipitation 400μl and for input 250μl of chromatin solution were used. For immunoprecipitation, 10 μl of antibodies against H3K9me3 (Millipore Sigma), H3K36me2 (Abcam), Hsp90 (Sigma), PfSir2A (generated in this study) and IgG were added to the chromatin solution and incubated on rocker, 4°C for overnight. Next day 45μl of equilibrated protein A agarose beads were added to the chromatin solution containing the respective antibodies and incubated on rocker, 4°C for 2 hours. The samples were then centrifuged at 7000 rpm for 10 seconds. The supernatant obtained was stored at -20°C and was used as IP supernatant samples. The bound beads were then subjected to washing on rocker 4°C for 5 minutes with 1ml of each the following cold buffers. The wash buffers were discarded after each wash by centrifuging the sample at 7000 rpm for 10 seconds

- 1- Low salt immune complex wash buffer 0.1% SDS, 1% Triton X100, 2mM EDTA, 20mM Tris HCl pH8, 150mM NaCl.
- 2- High salt immune complex wash buffer 0.1% SDS, 1% Triton X100, 2mM EDTA, 20mM Tris HCl pH8, 500 mM NaCl
- 3- LiCl immune complex wash buffer 0.25M LiCl, 1% NP-40, 1% Deoxycolate, 1mM EDTA, 10mM Tris HCl pH8.
- 4- TE 10mM Tris HCl pH8 and 1mM EDTA.

After washing, 500µl of TE was added to the beads, mixed gently and transferred into fresh microfuge tube, again 500µl of TE was added to the old tube mixed gently and transferred into new microfuge tube. Further, spinning of the samples were performed as before and for elution of the immune complexes freshly prepared 250µl of SDS/ NaHCO3 (1% SDS, 0.1M NaHCO3)

buffer was added to the beads, mixed by vortexing and was incubated on rocker 4°C for 15 minutes. The samples were spun and the supernatant was transferred into fresh microfuge tube and the elution step was repeated once more with the beads. The sample were again spun and the supernatant was collected and combined with supernatant obtain in the previous elution step. The obtained supernatant was once again spun to remove any residual beads and transferred in fresh microfuge tube.

For reverse HCHO crosslinking, 20µl of 5M NaCl was added to the eluted immune complexes (pellet fraction), 2.5µl to 300µl of IP supernatant fraction and 10µl to the input. The samples were mixed by vortexing, subjected to short spin and then incubated at 65°C for 5 hours. Further, samples were spun briefly and then transferred into new tube. 2.2 volume of absolute ethanol was added to it and then kept for precipitation at -20°C for overnight.

Next day, samples were centrifuged at 12000 rpm, 4°C for 30 minutes and the pellet was washed with 70 % ethanol for 5 minutes. The pellet was then air dried for about 5 minutes and re-suspended in 100µl of TE followed by incubation on ice for 10 minutes. Further 25µl of 5X proteinase K buffer (50mM Tris HCl pH8, 25mM EDTA, 1.25% SDS) and 1.5µl of proteinase K (20mg/ml) was added to the sample, mixed and incubated at 42°C for 2 hours. After incubation, 175µl of TE was added to the IP pellet fraction and 275µl of TE to the input and the IP supernatant fraction. Equal volume of PCIA (phenol: chloroform: Isoamyl alcohol -25:24:1) was added to the samples, mixed by vortexing for 3 minutes and then centrifuge at the top speed, RT for 10 minutes. The obtained aqueous layer is then transferred to fresh microfuge tube. The organic extraction step is repeated for the input and the IP supernatant fraction once more. 5µg of glycogen, 1/10 volume of 3M sodium acetate and 2.2 volume of absolute ethanol was added to the samples and kept for precipitation at -20°C for overnight.

The samples were spun at 12000 rpm, 4°C for 30 minutes and the pellet was washed with 70 % ethanol for 5 minutes. The pellet was air dried and IP pellet fraction was re-suspended in 150µl of TE, input in 250 µl of TE and IP supernatant fraction in 300µl of TE. The DNA obtained was analysed through PCR and the primer sets used for amplifying various chromosomal loci are listed in table 2.1

2.8 FAIRE

The procedure for FAIRE was performed as previously described (92, 93). Synchronised 30 ml of mid-ring stage P. falciparum in vitro cultures were centrifuged to remove the media and re-suspended in 30 ml of 1X PBS. For crosslinking, culture was treated with 37% formaldehyde (final concentration 1%) and incubated at room temperature on an orbital shaker at 80 rpm, for 20 min. Formaldehyde was quenched by treatment with 2.5 M glycine (final concentration 125 mM) and incubated at room temperature on an orbital shaker at the 80 rpm for 10 min. Further cultures were spun at 3000 rpm for 10 min. Pellet obtained was washed with ice cold PBS containing 2 mM PMSF for three times. Washed pellet was frozen under liquid nitrogen and stored in -80°C or proceeded for DNA extraction. For reference sample, 10 ml of mid-ring stage un-cross-linked cultures were used. Pellets were thawed if stored in -80°C and then resuspended in lysis buffer (25 mM Tris-HCl at pH7.8, 1 mM EDTA, 0.25% [v/v] IGEPAL CA-630, complete mini EDTA-free protease inhibitor cocktail (Roche, Basel, Switzerland), 20mM N-ethylmaleimide). One millilitre of lysis buffer was used per 0.4 g of pellet. The lysate was further sonicated for 6 sessions in Elma water bath sonicator (10 sec burst and 5 min rest on ice) followed by centrifugation at 16,000 g for 20 min at 4°C. For isolation of DNA, the supernatant was treated with equal volume of Phenol-Chloroform-Isoamyl alcohol (25:24:1) and DNA precipitation was performed from the aqueous layer obtained by adding 2 volume of 100 % ethanol, 1/10 volume of 3M sodium acetate and 1μl glycogen, followed by incubation at -20 °C. Next day, the sample was then centrifuged at 12000, 4°C for 30 minutes and the pellet obtained was subjected to washing with 500 μl of 70 % ethanol by centrifugation at 12000 rpm for 5 minutes. The pellet was then air dried and re-suspended in 1X TE. The obtained DNA was analysed through PCR using the primer sets listed in table 2.1

2.9 Co-immunoprecitation

CoIP was performed using Pierce Crosslink Immunoprecipitation Kit (Thermo Scientific) following the manufacture's protocol with slight modification. 50 µl of Pierce Protein A/G Plus Agarose bead was taken in the screw cap column and washed twice with 1X coupling buffer. The supernatant was discarded and then antibody solution (25µl anti-PfRad51 antibody and 125µl of 1X coupling buffer) was added to the column. The column was incubated on a rotator for 2 hours at room temperature. The column was then placed into collection tube and centrifuged. The resin was initially washed with 100 µl of 1X coupling buffer and then twice with 300µl of 1X coupling buffer. Then the bound antibody to bead was cross-linked using DSS solution on the rotator at RT for 90 minutes. After that, column was centrifuged to remove the DSS solution. 50µl of elution buffer was added to column and centrifuged. To quench the crosslinking, beads were washed twice with 100µl of elution buffer followed by washing twice with 200µl of IP Lysis/ wash buffer. Beads were re-suspended in IP lysis buffer and stored at 4°C. Parasites released after saponin treatment from 80 ml schizont stage culture with parasitemia 8%, were re-suspended in 700µl of IP lysis buffer and incubated on ice for 30 minutes with intermittent mixing. The lysate was separated from the cell debris by centrifugation at 13000g, 4°C for 10 minutes. 80µl of Control agarose resin was taken in new

with 100μl of coupling buffer. For pre- cleaning, 600μl of the lysate was added to the column with control agarose resin and incubated on rotator at 4°C for 60 minutes. The antibody bound beads were centrifuged to remove the buffer. Further pre-cleaned lysate was added to the antibody bound beads and incubated on the rotator at 4°C for overnight. Next day, the column was placed in a collection tube and flow through was collected and stored as supernatant fraction. Beads were then subjected to washing thrice with 200μl of wash buffers and once with 100μl of 1X conditioning buffer. Next for elution of the bound antigen, the column containing the beads was placed in collection tube containing 5μl of Tris-HCl pH 9.5 and 10μl of elution buffer was added followed by centrifugation. Further 50μl of elution buffer was added to the column and incubated for 5 minutes at RT. The tube was centrifuged and flow through was collected as IP fraction. The lysate (input), supernatant fraction and IP fraction was mixed with the sample buffer, boiled and then subjected to western blot analysis. All the centrifugation of the beads was carried out at 2000g, 4°C for 60 seconds. The lysis buffer; wash buffer; conditioning buffer; and the elution buffer used was provided in the kit.

2.10 Western blotting

The appropriate amount of protein was separated on 12 % SDS polyacrylamide gel and transferred to Polyvinylidene difluoride (PVDF) membrane pre-treated with methanol for 30sec, double distilled water for 2 minutes and 1X semi-dry transfer buffer (5.86 gm Glycine, 11.64Tris base, 0.75 gm SDS dissolved in final volume of water 1600ml with added 400 ml of methanol) for 5 minutes. The transfer was performed at 250mA for 80 minutes. The blocking of the membrane was then performed on rocker for 2 hours at room temperature using blocking buffer (5% skimmed milk in 1X TBST). The blot was then incubated in primary antibody

overnight at 4°C under rocking condition. The primary antibody anti-PfSir2A raised in rabbit was used at 1:10,000 dilutions. Anti-PfRad51 (raised in rabbit), anti-Actin, anti-ScActin, anti-Hsp90 (all raised in mouse) were used at 1:5000 dilutions. Next day blot was initially washed thrice at room temperature under rocking condition with large volume of 1X TBST(0.2M Tris base, 9% sodium chloride, pH 7.6, 0.1% Tween 20) for 1minute. Blot was then subjected to 1X TBST wash thrice for 15 minutes each with 1 minute, internment wash of water. After washing, blot was incubated in secondary antibody at room temperature under rocking condition for 2 hours. HRP conjugated anti-rabbit and anti-mouse secondary antibodies (Promega) were used at 1:10,000 dilutions. Further, washing of the blot was performed in similar manner. The signal for the protein was detected using enhanced chemiluminescence kit (Pierce) in Bio-rad Chemi-doc system. Quantification of the band intensity was performed using Image J software and the graph was plotted using GraphPad Prism 6 software.

Table 2.1: List of the primers used in the study

Gene name and	Primer
purpose	
PfHSP90 Gene	OMKB 469 FP TCAGGA TCCATGTCAACGGAAACATTCGC
amplification	
	OMKB 470 RP TCAGTCGACATCCTTTAGTCAACTTCTTCC
PfACTIN Gene	OMKB 766 FP
amplification	TCAGGATCCATGGGAGAAGAAGATGTTCAAG
	OMKB 767 RP
	TCAGTCGACAATTTAGAAACATTTTCTGTGGAC
Long range PCR	OMKB463
Repair kinetics	FPTCAGTCGACATGTTGAATGATATGAATGATAAAAAAG
	OMKB464 RP
	TCAGTCGACTCAACCTATGTAACCTTTACACTTC
Short range PCR	OSB94 FP CTGTAACACATAATAGATCCGAC
Repair kinetics	OSB95 RP TTAACCATCGTTATCATCATTATTTC
SIR2A(A0): qRT PCR	OMKB 244 FP GTAATTGGCACATCGTCTACTG
and ChIP	OMKB 245 RP TATATATGTGCGTGTGAGCTAC
SIR2B(B0): qRT PCR	OMKB 246 FP AAATACCAAAATATGTAAAGCCAC
and ChIP	OMKB 247 RP TTACATAATTTAGGATCCAATAAGG
UPSB: ChIP	OMKB 419 FP TATTACAGGATATGTCATATATATAT
	OMKB 420 RP AAATACGAAAATACATACATATAAAA
UPSA: ChIP	OMKB 445 FP ATGGATACATATTATAGATAATAGAG
	OMKB 446 RP TTTCTATACCAAAGGTTTGCC
Cox3: FAIRE	OSB 177 FP GCT TCT GAT ATT ATG ATA GAT AAC
	OMKB 418 RP TTACGGCACATTATCTCACCG
ARP UPS: FAIRE and	OMKB 409 FP GAAAACAAAGTTCTATTTATCATC
ChIP	OMKB 410 RP TCTTACGTATGCTTGGGGTC
SIR2A _{UPS} (A1) : ChIP	OMKB 407 FP TAAACTTAACACTTGTGTACTG
and FAIRE	OMKB 261 RP
	GCTATGCATTTATTTTAATCTTAACAAATTATG
SIR2B UPS (B1) :ChIP	OMKB 408 FP AATGTGTATACCTCCTAAATG
and FAIRE	OMKB 259 RP
	CTATGCATTAATATGTTATTGATAAATAAATGTG
SIR2A _{UPS} (A2) : ChIP	OMKB 721 FP ATATTTCTTCTTCCTGATTAAC
	OMKB 722 RP CGAAAAGACCTTCTAATTCG
SIR2B _{UPS} (B2) :ChIP	OMKB 727 FP ATATGTTTCTTTTTTATATAAG
	OMKB 728 RP AATGATGAAATAAGTAATTTTATTG
SIR2A UPS(A3): ChIP	OMKB 719 FP TTGTATTGATATTTCTCTTCATATTC
	OMKB 720 RP TTTCAATGTGCATAGAAAATTAAATG
SIR2B _{UPS} (B3):ChIP	OMKB 725FP TGTATAAAGTTCAATATGAAAAAG
	OMKB 726 RP AGATCTTGTATAACATATATAATC
SIR2A _{UPS} (A4) : ChIP	OMKB 717 FP TGAATGTTAATAAAAGTATAATA
, ,	OMKB 718 RP TTATTATATAGTTATTCTTTTCATC
SIR2B UPS (B4) :ChIP	OMKB 723 FP ACAATATACGCAATGAAGGTTAG
, ,	OMKB 724 RP CTGACTTAATAATATGAATATTTCG

var PF3D7_0400400	OMKB280 FP ATATGGGAAGGGATGCTCTG
qRT PCR	OMKB281 RP TGAACCATCGAAGGAATTGA
var PF3D7_0800200	OMKB564 FP GGTGTCAAGGCAGCTAATGA
qRT PCR	OMKB565 RP TATGTCCTGCGCTATTTTGC
var PF3D7_0937600	OMKB705 FP CGTAAAACATGGTGGGATGA
qRT PCR	OMKB706 RP GGCCCATTCAGTTAACCATC
var PF3D7_1100200	OMKB580 FP GACGGCTACCACAGAGACAA
qRT PCR	OMKB580 TF GACGGCTACCACAGAGACAA OMKB581 RP GTCATCATCGTCTTCGTTT
var PF3D7_1150400	OMKB282 FP TGCTGAAGACCAAATTGAGC
qRT PCR	OMKB283 RP TTGTTGTGGTGGTTGTTGTG
var PF3D7_1300300	OMKB240 FP CACAGGTATGGGAAGCAATG
qRT PCR	
	OMKB241 RP CCATACAGCGTGACTACAGAAGA
var PF3D7_0100100	OMKB544 FP TGCGCTGATAACTCACAACA
qRT PCR	OMKB545 RP AGGGGGAATA GGATTA GGA
var PF3D7_0115700	OMKB546 FP AACCCCCAATACCATTACGA
qRT PCR	OMKB547 RP TTCCCCACTCATGTAACCAA
var PF3D7_0200100	OMKB548 FP ATGTGCGCTACAAGAAGCTG
qRT PCR	OMKB549 RP TTGATCTCCCCATTCAGTCA
var PF3D7_0223500	OMKB550 FP CAATTTTGGGTGTGGAATCA
qRT PCR	OMKB551 RP CACTGGCCACCAAGTGTATC
var PF3D7_0324900	OMKB234 FP CAATCTGCGGCAATAGAGAC
qRT PCR	OMKB235 RP CCACTGTTGAGGGGTTTTCT
var PF3D7_0300100	OMKB234 FP CAATCTGCGGCAATAGAGAC
qRT PCR	OMKB235 RP CCACTGTTGAGGGGTTTTCT
var PF3D7_0400100	OMKB683 FP GACGACGATGAAGACGAAGA
qRT PCR	OMKB684 RP AGATCTCCGCATTTCCAATC
var PF3D7_0426000	OMKB552 FP TGACGACTCCTCAGACGAAG
qRT PCR	OMKB553 RP CTCCACTGACGGATCTGTTG
var PF3D7_0500100	OMKB554 FP GAAGCTGGTGGTACTGACGA
qRT PCR	OMKB555 RP TATTTTCCCACCAGGAGGAG
var PF3D7_0632800	OMKB558 FP GACAAATACGGCGACTACGA
qRT PCR	OMKB559 RP TGTTTCACCCCATTCTTCAA
var PF3D7_0733000	OMKB453 FP TGACGACGATAAATGGGAAA
qRT PCR	OMKB448 RP TTCTTTTGGAGCAGGGAGTT
var PF3D7_0800100	OMKB562 FP GTCGTGGAAAAACGAAAGGT
qRT PCR	OMKB563 RP TATCTATCCAGGGCCCAAAG
var PF3D7_0937800	OMKB572 FP CACACGTGGACCTCAAGAAC
qRT PCR	OMKB573 RP AAAACCGATGCCAATACTCC
var PF3D7_1000100	OMKB574 FP GACGAGGAGTCGGAAAAGAC
qRT PCR	OMKB575 RP TGGACAGGCTTGTTTGAGAG
var PF3D7_1041300	OMKB576 FP GTGCACCAAAAGAAGCTCAA
qRT PCR	OMKB577 RP ACAAAACTCCTCTGCCCATT
var PF3D7_1100100	OMKB578 FP GAGGCTTATGGGAAACCAGA
qRT PCR	OMKB579 RP AGGCAGTCTTTGGCATCTTT
var PF3D7_1200100	OMKB286 FP CGGAGGAGGAAAAACAAGAG
qRT PCR	OMKB287 RP TGCCGTATTTGAGACCACAT

var PF3D7_1219300	OMKB586 FP GACGCCTGCACTCTCAAATA
qRT PCR	OMKB587 RP TTGGAGAGCACCACCATTTA
var PF3D7_1240400	OMKB677 FP AAAGCCACTAGCGAGGGTAA
qRT PCR	OMKB678 RP TGTTTTTGCCCACTCCTGTA
var PF3D7 1255200	OMKB284 FP GGCACGAAGTTTTGCAGATA
qRT PCR	OMKB285 RP TTTGTGCGTCTTTCTTCGTC
var PF3D7_1300100	OMKB588 FP ACAAAGGAACGTCCATCTCC
qRT PCR	OMKB589 RP GCCAATACTCCACATGATCG
var PF3D7_1373500	OMKB242 FP CGGAATTAGTTGCCTTCACA
qRT PCR	OMKB243 RP CATTGGCCACCAAGTGTATC
var PF3D7_0412400	OMKB447 FP ACCGCCCATCTAGTGATAG
qRT PCR	OMKB458 RP CACTTGGTGATGTGTTCA
var PF3D7_0412700	OMKB449 FP TAAAAGACGCCAACAGATGC
qRT PCR	OMKB450 RP TCATCGTCTTCGTCTC
var PF3D7_0412900	OMKB681 FP ACTTTCTGGTGGGGAATCAG
qRT PCR	OMKB682 RP TTCACCGCCACTTACTTCAG
var PF3D7_0420700	OMKB451 FP AGAGGGTTATGGGAATGCAG
qRT PCR	OMKB45111 AGAGGGTTATGGGAATTCCTT OMKB452 RP GCATTCTTTGGCAATTCCTT
var PF3D7_0420900	OMKB452 RF GCATTCTTTGGCAATTCCTT OMKB451 FP AGAGGGTTATGGGAATGCAG
qRT PCR	OMKB45111 AGAGGGTTATGGGAATGCAG OMKB452 RP GCATTCTTTGGCAATTCCTT
var PF3D7_0421300	OMKB685 FP TGCAACGAAACATTAGCACA
qRT PCR	OMKB686 RP AGCAGGGGATGATGCTTTAC
var PF3D7_0617400	OMKB556 FP ATTTGTCGCACATGAAGGAA
qRT PCR	OMKB557 RP AACTTCGTGCCAATGCTGTA
var PF3D7_0711700	OMKB691 FP CAATTTTCCGACGCTTGTA
qRT PCR	OMKB692 RP CACATATAGCGCCGTCCTTA
var PF3D7_0712000	OMKB697 FP GTTGAGTCTGCGGCAATAGA
qRT PCR	OMKB698 RP CTGGGGTTTGTTCAACACTG
var PF3D7_0712600	OMKB701 FP CGTGGTAGTGAAGCACCATC
qRT PCR	OMKB702 RP CCCACCTTCTTGTGGTTTCT
var PF3D7_0712900	OMKB699 FP CACACATGTCCACCACAAGA
qRT PCR	OMKB700 RP ACCCTTCTGTGGTGTCTTCC
var PF3D7_1240600	OMKB679 FP CATCCATTACGCAGGATACG
qRT PCR	OMKB680 RP AAATAGGGTGGGCGTAACAC
var PF3D7_1200600	OMKB584 FP TGGTGATGGTACTGCTGGAT
qRT PCR	OMKB585 RP TTTATTTTCGGCAGCATTTG
var PF3D7_0632500	OMKB558 FP ATGTGTGCGAGAAGGTGAAG
qRT PCR	OMKB559 RP TGCCTTCTAGGTGGCATACA
var PF3D7_0600200	OMKB236 FP TGGAAAGAACATGGACCTGA
qRT PCR	OMKB237 RP TTCCTCGAGGGAAGAATCAC
var PF3D7_0800300	OMKB566 FP TTTGGGATGACACCAAGAAA
qRT PCR	OMKB567 RP GTCGCTTGATGAAGGAGTCA
var PF3D7_1200400	OMKB582 FP TCGATTATGTGCCGCAGTAT
qRT PCR	OMKB583 RP TTCCCGTACAATCGTATCCA
var PF3D7_0413100	OMKB681 FP ACTTTCTGGTGGGGAATCAG
qRT PCR	OMKB682 RP TTCACCGCCACTTACTTCAG

OMKB236 FP ACCAAGTGGTGACAAAGCAG
OMKB237 RP GGGTGGCACACAAACACTAC
OMKB695 FP ACCAAATGGTGACTTGCTCA
OMKB696 RP TTTTCATCGACGGATGATGT
OMKB693 FP GCGACGCTCAAAAACATTTA
OMKB694 RP TCATCCAACGCAATCTTTGT
OMKB560 FP ACGTGGTGGAGACGTAAACA
OMKB561 RP CCTTTGTTGTTGCCACTTTG
OMKB568 FP TTTGTCCGGAAGACGATACA
OMKB569 RP ATCTGGGGCAGAATTACCAC
OMKB707 FP TGCAAGGGTGCTAATGGTAA
OMKB708 RP CCTGCATTTTGACATTCGTC
OMKB288 FP TGCAAACCACCAGAAGAAAG
OMKB289 RP GTTCTCCGTGTTGTCCTCCT
OMKB675 FP AGCAAAATCCGAAGCAGAAT
OMKB676 RP CCCACAGATCTTTTCCTCGT
OMKB592 FP AAGTAGCAGGTCATCGTGGTT
OMKB593 RP TTCGGCACATTCTTCCATAA

Table 2.2: List of yeast strains used in the study

Strain	Genotype
PJ69-4A	MATa trpl-901 leu2-3, 112 ura3-52 his3-200 ga14D ga180D
	LYS2::GAL1-HIS3 GAL2-ADE2 met2::GAL7-lacZ
iG170Dhsp82	MATa
	can1-100 ade2-1 his3-11, 15 leu2-3, 112 trp1-1 ura3-1
	hsp82::LEU2 hsc82::LEU2 HIS3::HSP82G170D
W303a	MATa leu2-3, 112 his3-11, 15 ade2-1, trp1, ura3-1
TAY1	MATacan1-100 ade2-1 his3-11, 15 leu2-3, 112 trp1-1 ura3-1
	hsp82::LEU2 hsc82::LEU2 HIS3::HSP82G170D pTA
	PfRAD51:TRP1
TAY2	MATa leu2-3, 112 his3-11, 15 ade2-1, trp1, ura3-1 pTA
	PfRAD51:TRP1

Chapter-3
The canonical
functions of Hsp90 in
Plasmodium biology

3.1 Introduction

Heat shock protein 90 (Hsp90) is an evolutionary conserved molecular chaperone that regulates the conformation and stability of a specific group of proteins, known as its clients (94) and hence governs several cellular processes (55-57). It is one of the most active players involved in stress response of cell by maintaining the protein homeostasis.

Parasite during its life cycle encounters various endogenous and environmental genotoxic agents which are responsible for extensive DNA damage. Most lethal among them are double strand break (DSB) and parasite being an unicellular organism needs to repair it for its survival (45). The classical Non-homologous end joining pathway (NHEJ) is absent and homologous recombination (HR) pathway is the predominant pathway which operates in P. falciparum to mend the DSB (95). As reported previously the deficiency of HR cannot be compensated by any other pathway (96). This underlines the importance of targeting the exclusive DSB repair HR pathway. The Plasmodium recombinase, PfRad51 which has been identified and characterised, has been reported to execute a pivotal role in HR repair pathway of homology search and strand exchange (97-99). Small molecule inhibitor, B02 has been reported to bind PfRad51 and prevent the homomerisation of PfRad51 molecules and thereby inhibits its ATPase and strand exchange activity (100). Additionally, it was noted that *P. falciparum* in vitro culture on treatment with B02 becomes more susceptible to methyl methanesulfonate (MMS), as B02 treatment leads to significant reduction in MMS-induced Rad51 nuclear foci formation and hence increases accumulation of unrepaired DNA in the parasites (100). A report also suggests that mice infected with a mutant Plasmodium berghei strain harbouring a dominant negative mutant allele of rad51 (Pfrad51:K143R), exhibits remarkable reduction in parasite burden (96) reinforcing the essentiality of Rad51. It was also observed that the loss of Rad51 activity could not be compensated by other DSB repair pathways (96).

Hsp90 is reported to act as an important regulator of the DNA damage response pathway as well as the DNA break repair pathway. Hsp90 inhibitors are found to show synergistic antitumor activities with DNA-damaging agents (101). Multiple components of the DSB repair pathways have been described as the clients of Hsp90 (102). In budding yeast, Rad51 acts as a client of yHsp90 (65) and dynamic interaction between yRad51 and yHsp90 is crucial for the DNA damage-induced nuclear function of yRad51 (103). Whether the abundance and activity of PfRad51 are regulated by the PfHsp90 chaperone system was unexplored. With this we were curious to investigate whether PfRad51 is a client of PfHsp90 and whether Rad51 mediated HR repair pathway is regulated by PfHsp90.We hypothesize that if PfRad51 comes under PfHsp90 clientele group, then PfRad51 must interact with PfHsp90. Also the stability of PfRad51 protein and its function should be compromised upon PfHsp90 inactivation and thus PfHsp90 should control the PfRad51-mediated HR pathway in response to DSBs at the *Plasmodium* chromosomes. The following questions have been addressed here: first, whether PfRad51 physically interact with PfHsp90? Second, whether PfRad51 is depleted upon Hsp90 inhibition? Third, whether DSB repair function of PfRad51 is lost upon inhibition of PfHsp90? This study provides insights into the interaction of PfRad51 with PfHsp90 and effect of PfHsp90 inhibition on the stability and function of PfRad51.

3.2. Results

3.2.1 Physical interaction between PfHsp90 and PfRad51:

To test the hypothesis that PfRad51 is the client of PfHsp90, we first intended to study their physical interaction. To monitor the physical interaction between PfRad51 and PfHsp90 Yeast -two- hybrid analysis was performed. Two yeast expression vectors, one harbouring PfHsp90 fused to the Gal4 DNA binding domain (bait) and another harbouring PfRad51 fused to the Gal4 activation domain (prey) were generated. The yeast strain PJ69-4A, which allows scoring both weak and strong interactions by the measurement of *HIS3* and *ADE2* reporter genes activities, respectively was used. It was found that the yeast strain carrying both the vectors was able activate the *HIS3* as well as the *ADE2* reporter genes and thereby was able to grow on both the triple drop out plates SC-leu-ura-his and SC-leu-ura-ade. This indicated a strong physical association between PfHsp90 and PfRad51 (Fig. 3.1). Yeast strains harbouring empty bait and empty prey vectors were used as the negative control and no growth for these strain were observed in either of the triple drop out plates. The *PfACTIN* gene was cloned in the prey vector and scored for its interaction with PfHsp90. It served as an additional negative control as no growth was observed in both the triple drop out plate and hence no interaction was found between PfHsp90 and PfActin (Fig. 3.1).

To further confirm the interaction between PfRad51 and PfHsp90, co-immunoprecipitation experiment was performed using the parasite lysate. Anti Rad51 antibody was used for the pull-down. Western blot analysis performed with the CoIP fractions revealed that PfHsp90 was co-immunoprecipitated with PfRad51 (Fig. 3.2). A protein extract of the same culture pulled down with pre-immune IgG was used as a negative control and PfHsp90 was not observed to be co-immunoprecipitated. Thus, the data presented here demonstrate a specific interaction between PfHsp90 and PfRad51 in the parasite.

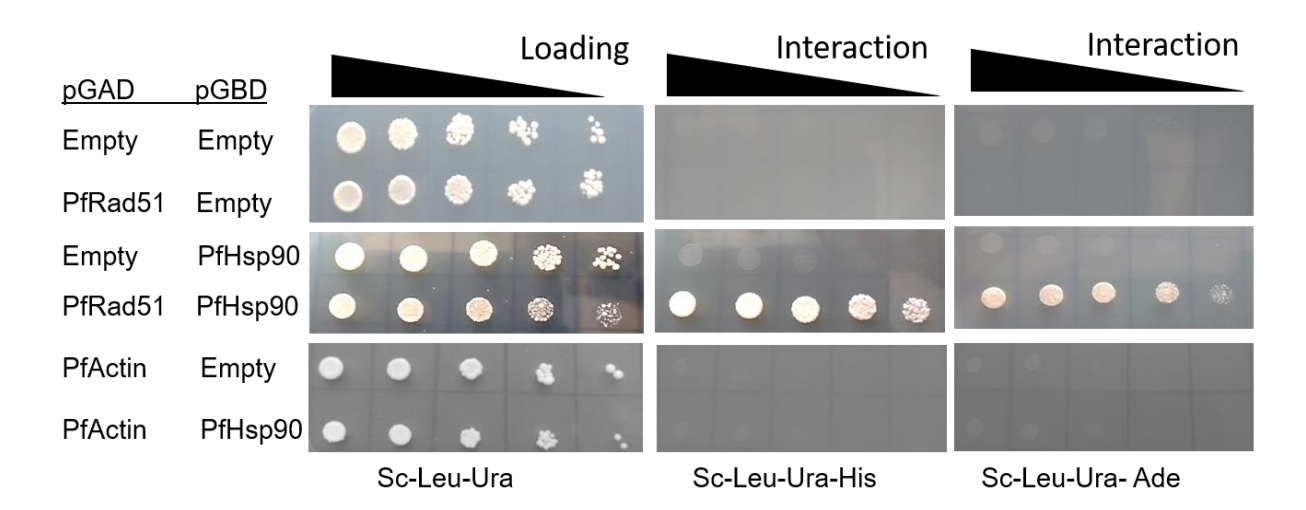


Figure 3.1: Yeast-two-hybrid analysis demonstrating physical interaction between PfRad51 and PfHsp90. The interaction of PfRad51 and PfHsp90 was confirmed by yeast two-hybrid assay. *PfRAD51* or *PfACTIN* genes were cloned in pGADC1 vector and was fused to GAL4 activation domain (GAL4-AD) while *PfHSP90* gene was cloned in pGBDUC1 vector and fused to GAL4 DNA binding domain (GAL4-BD). Yeast strain PJ69-4A with *ADE2* and *HIS3* as reporter genes was used for the interaction studies. For spotting, the cells were grown till OD₆₀₀ 0.5, further were 10-fold serially diluted and spotted onto plate lacking leucine and uracil to check for the presence of the bait and the prey plasmids. The interaction was checked by spotting onto triple dropout plates lacking leucine, uracil, histidine or leucine, uracil, adenine. Each assay was repeated three times.

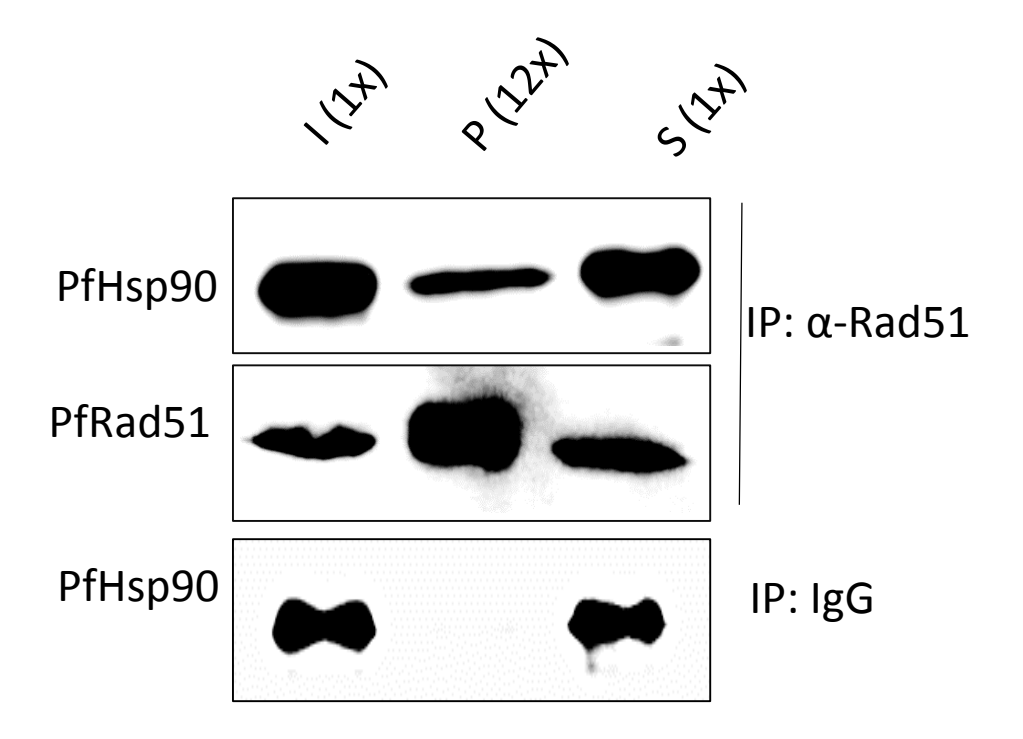


Figure 3.2: Co-immunoprecipitation experiment demonstrating physical interaction between PfRad51 and PfHsp90. A representative western blot analysis out of three independent experiments depicting the co-immunoprecipitation of PfRad51 and PfHsp90 from the parasite lysate. Anti-PfRad51 and IgG antibodies were used for the immunoprecipitation. Probing was performed with anti-PfRad51 and anti-PfHsp90 antibodies. The lanes are I- input, P- IP pellet fraction, S- supernatant. The pellet fraction was loaded 12-times more (12X) than the input or supernatant fraction (1X).

3.2.2 Chemical inhibition of Hsp90 function induces proteasomal degradation of PfRad51:

To decipher whether PfRad51 is dependent on PfHsp90 for its stability, the steady-state level of PfRad51 was measured in the Hsp90 inhibitory condition i.e., in the presence of 17-AAG. To elucidate this, ring stage-specific parasites were treated with increasing doses of 17-AAG (425nM to1.7mM). As the half-maximal inhibitory concentration (IC₅₀) of 17-AAG was determined to be 510 nM, a sub-IC₅₀ concentration was chosen as the starting dose. The treated cultures were harvested at the late trophozoite/early schizont stage. Ideally, when Hsp90 is inhibited, its client proteins tend to undergo depletion. Through western blot analysis, a dose-dependent depletion of PfRad51 protein was observed (Fig. 3.3A). The levels of PfRad51 were quantified in untreated and 17-AAG-treated samples which indicated that there was 15%, 26%, and 87% reductions in the level of PfRad51 in the presence of 425 nM, 850 nM, and 1.7mM 17-AAG, respectively (Fig. 3.3B).

Reports suggest that when Hsp90 is inhibited, its clients undergo proteasomal degradation (61), so we were keen to know whether PfRad51 undergo proteasomal degradation upon PfHsp90 inhibition. In order to investigate this, ring stage parasite culture was taken and divided in three parts, one part was left untreated, which served as a control, second part was treated only with 17AAG, while third part was treated with both 17AAG and proteasome inhibitor MG132. The parasites were harvested at the late trophozoite/early schizont stage and total proteins were isolated. Western blot analysis performed with isolated proteins indicated that the 17-AAG-induced reduction in PfRad51 was reversed in the presence of the proteasome inhibitor MG132 (Fig. 3.4A and B). This suggests that PfHsp90 protects PfRad51 from degradation via a proteasomal pathway.

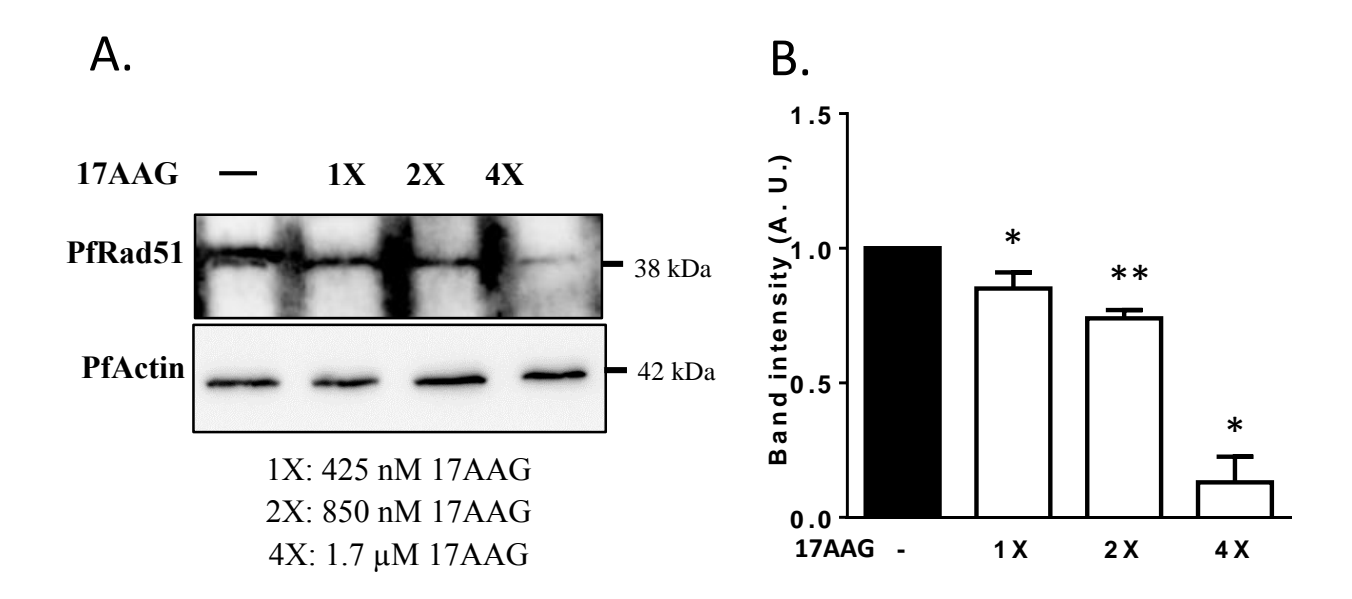


Figure 3.3: Treatment with 17-AAG induces depletion of PfRad51. (A) Western blot analysis showing steady-state level of PfRad51 protein, performed with total protein isolated from untreated parasites and parasites treated with three different concentrations of 17-AAG (as indicated). Actin was used as the loading control. (B) Graph was plotted from the quantification of band intensities, depicting lower abundance of PfRad51 upon 17-AAG treatments. Error bar indicates the SEM obtained from four individual experiments. The P value was calculated using the two tailed t-test (* means P value < 0.05; ** means P value < 0.01).

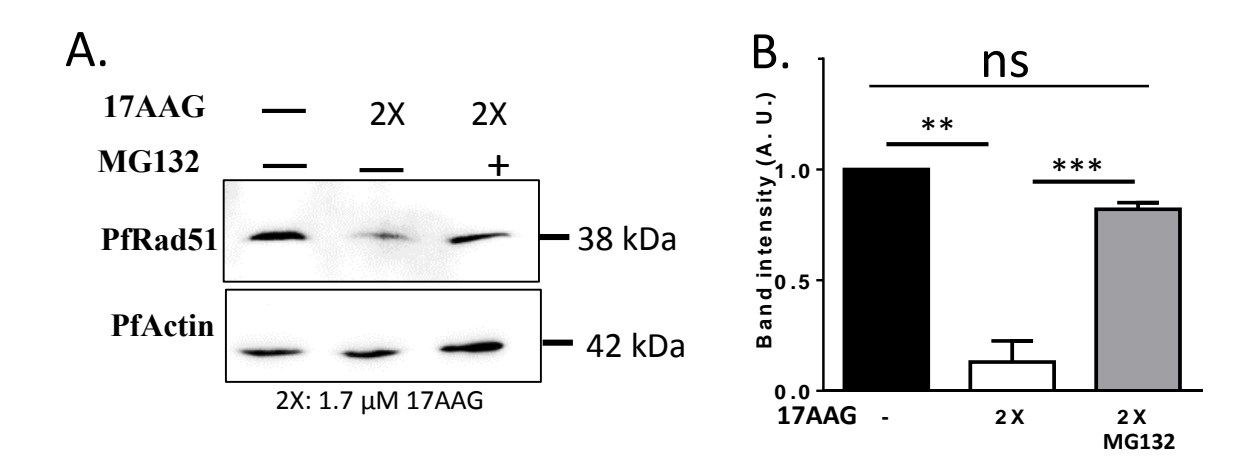


Figure 3.4: 17-AAG induces proteasomal degradation of PfRad51. (A) Western blot analysis depicting PfRad51 protein level, performed with total protein isolated from untreated, 17-AAG treated (1.7 μ M), and 17-AAG (1.7 μ M) plus MG132 (133 nM) treated parasites. Actin was used as the loading control. (B) Graph was plotted from the value of band intensities obtained from three independent experiments with error bar indicating the SEM. The *P* value was calculated using the two tailed t-test (** means *P* value < 0.01; *** means *P* value < 0.001).

3.2.3 Genetic loss of Hsp90 function induces depletion of PfRad51:

To further support our conclusion that Hsp90 activity is required for the PfRad51stability, we employed a yeast surrogate system to conduct genetic analysis. PfRad51 was expressed in a temperature-sensitive yeast strain, iG170Dhsp82 (104), which harbours non-functional Saccharomyces cerevisiae Hsp90a (ScHsp90a), when the strain is grown at the restrictive temperature of 37°C. The steady state level of PfRad51 was compared using the total protein isolated from the yeast culture grown at restrictive temperature (37°C) and permissive temperature (25°C). Although yeast Hsp90a shares 74% sequence similarity and only 57% sequence identity with PfHsp90, western blot analysis indicates that, it can provide stability to PfRad51, as evident from the steady-state level of PfRad51, when the strain was grown at a permissive temperature (25°C). However, a significant reduction in the stability of PfRad51 was observed under the non-permissive condition (37°C), where ScHsp90a was non-functional (Fig. 3.5A and B). To rule out the possibility that the reduction in the PfRad51 level was not a temperature effect, PfRad51 was expressed in a wild-type yeast strain (W303a), and proteins were extracted after growing the strain at two different temperatures, as used earlier. Through western blot analysis, no noticeable difference was observed in the stability of PfRad51 at 25°C and 37°C (Fig. 3.5A). Together, these data establish that Hsp90 provides stability to the PfRad51 protein.

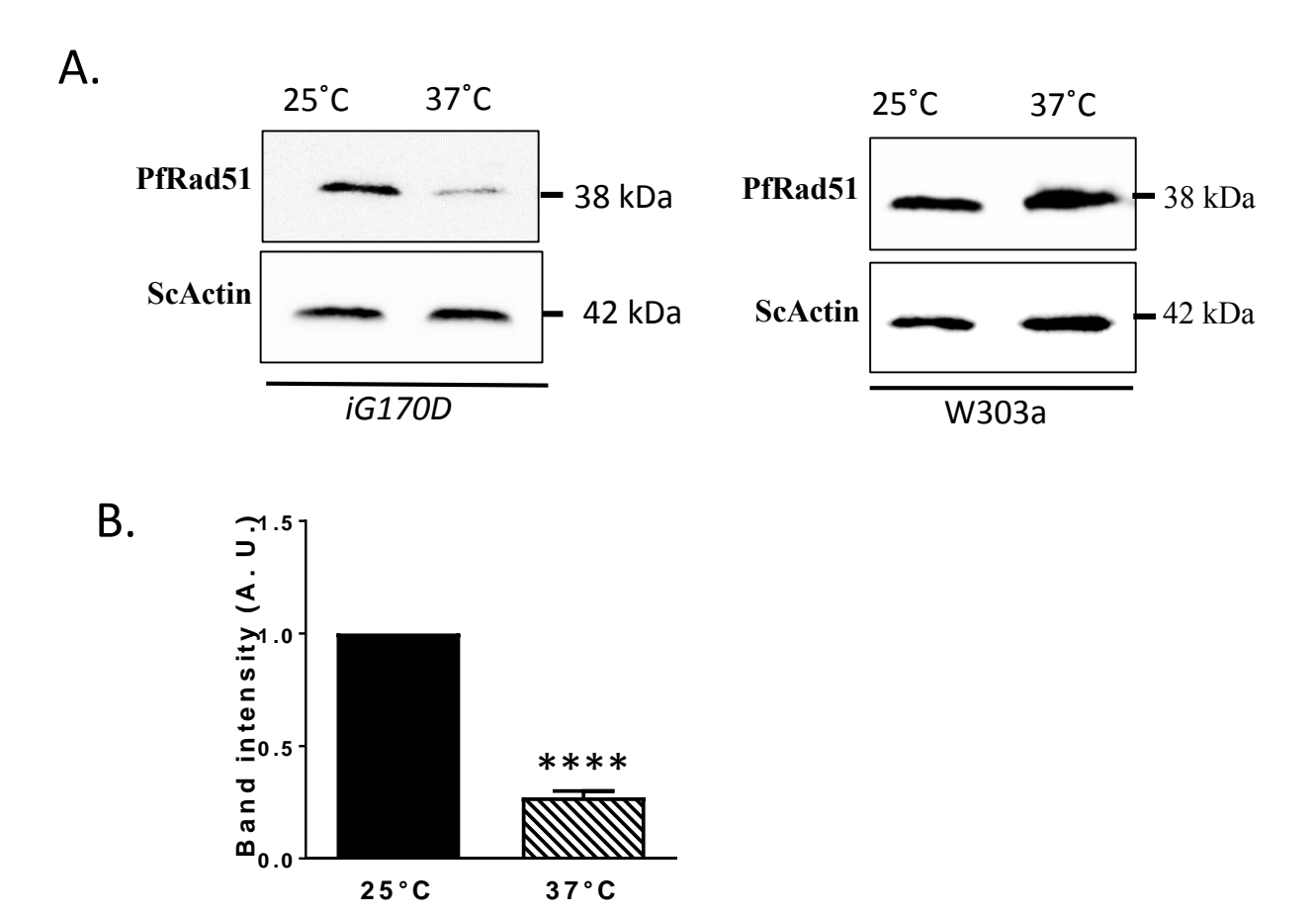


Figure 3.5: Temperature sensitive yHsp90 mutant induces depletion of PfRad51 at the non-permissive temperature. Western blot analysis showing the PfRad51 level performed with total protein isolated from, yeast temperature sensitive strain of Hsp90, iG170Dhsp82 harbouring PfRad51 plasmid (left panel), grown at permissive temperature 25°C and restrictive temperature 37°C, or from wild-type yeast strain W303a harbouring PfRad51 plasmid (right panel). ScActin was used as the loading control. The molecular weight of the respective proteins is marked on the right side of each gel. (F) Graph was plotted from the value of band intensities obtained from three independent experiments with error bar indicating the SEM. The P value was calculated using the two tailed t-test (**** means P value <0.0001).

3.2.4 Abrogation of the UV-induced DNA repair activity of PfRad51 under Hsp90-inhibitory condition:

The physical interaction between PfHsp90 and PfRad51 and dependence of PfRad51 on Hsp90 for its stability prompted us to investigate the effect of the PfHsp90 inhibitor on PfRad51 DNA repair activity. We reasoned that if PfRad51 is a client of PfHsp90, there must be lost of function of PfRad51 in PfHsp90 inhibitory condition. To investigate the effect of inhibition of PfHsp90 on PfRad51-dependent DNA repair activity, the effect of 17-AAG on the repair kinetics of the damaged *Plasmodium* genome upon UV irradiation was monitored. UV-C irradiation produces reactive oxygen species, which result in the formation of DSBs at the chromosomes (105, 106). In response to UV- induced DNA damage, Rad51 is localized to the damaged chromatin and forms foci, which are a hallmark for the HR-mediated DNA repair pathway (100, 107). Thus, UV sensitivity is an indirect measure of the HR-mediated DSB repair efficiency of the cells. Here, we have developed a direct measure of the repair of UVinduced DNA damage. To this end, P. falciparum in vitro cultures were exposed to UV doses (100 J/m2) to induce genome-wide DNA double-strand breaks and then allowed to recover. Kinetics of DSB repair were followed using a highly sensitive PCR based DNA repair assay (108). The assay is based on the fact that if the DNA is intact, there will be amplification of the short range amplicon (269bp) using the primer set FP and RP1 as well as the long range amplicon (7200bp) with the primer pair FP and RP2. However, if the DNA is damaged, amplicon of short fragment will be obtained whereas amplicon of the longer fragment will not be obtained. It is assumed that the amplification of long fragment will occur when the DNA is repaired, as there is a greater probability for the longer segment of the genome to harbour the UV induced break. Lesser the amplification of the longer fragment greater is the damaged and unrepaired DNA.

The amplification of short fragment will occur irrespective of the fact, whether DNA is damaged or repaired, as the likelihood of DNA damage within the short segment of DNA is very less and hence can be used for normalisation of the DNA (Figure 3.6A). It was previously established in our laboratory that trophozoite stage-specific parasites, once subjected to the UV doses, require 24 h for complete repair of the damaged DNA (108). This repair activity is directly linked to the active PfRad51 protein levels in the parasite. Under conditions in which the parasites were pre-treated with B02, a complete loss of DNA repair activity was observed even after 24 h after UV irradiation (Fig. 3.6B). So to determine the effect of PfHsp90 inhibition on the DNA repair activity of PfRad51, the DNA repair kinetics of the parasite genome in the presence of 17-AAG were measured and compared to the repair kinetics of the untreated parasites. It was observed that parasites pre-incubated with 17-AAG, once subjected to UV irradiation, behaved similar to the B02-treated parasites, i.e., there was no reduction in the residual damaged DNA by 12 h, or even at the end of a 24-h recovery period (Fig. 3.6B). An unrelated chemical, atoyaquone, was used as a negative control for this experiment. Atovaquone-pretreated parasites exhibited similar repair kinetics to those of the untreated parasites, i.e., 70% repair was achieved at the end of 12 h, and 100% repair was seen after 24 h. These data indicate that, similarly to the recombinase inhibitor B02, the PfHsp90 inhibitor 17-AAG blocks the repair of UV irradiation-induced DNA damage in the parasite.

A. PCR based DNA repair assay system



Damaged Nuclear DNA

Undamaged Nuclear DNA

FP & RP1: 269 bp amplicon

FP & RP2: 7200 bp amplicon

FP & RP1: 269 bp amplicon

FP & RP2: No amplicon

B. Repair kinetics of UV- damaged DNA

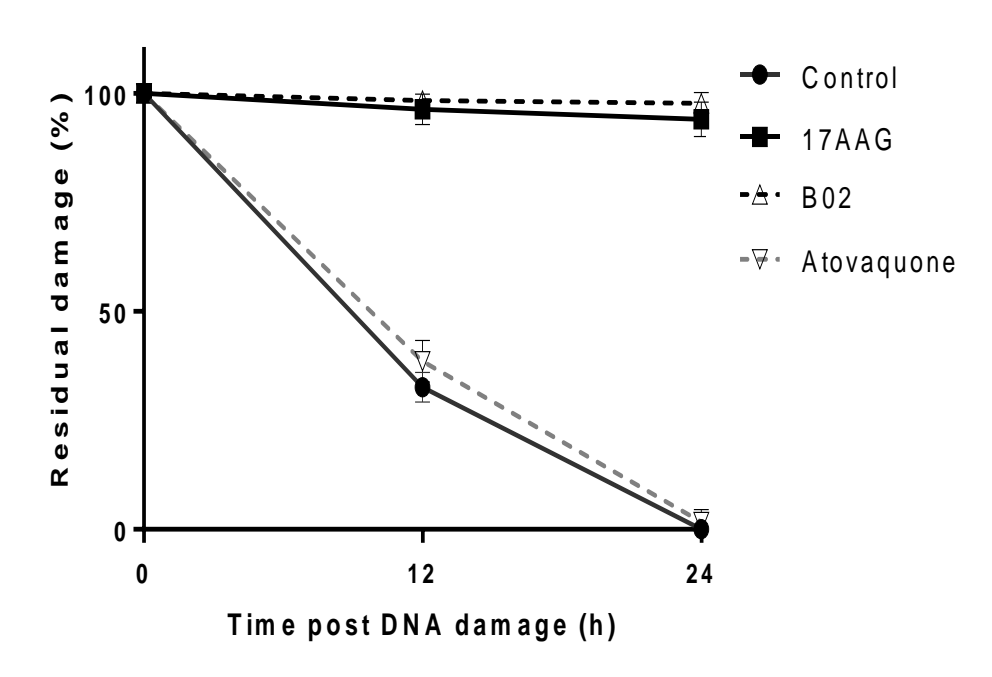


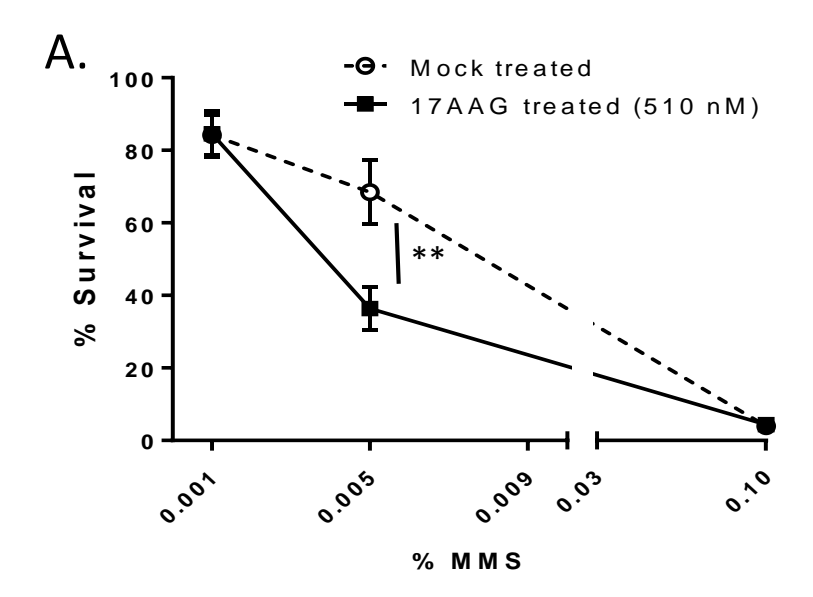
Figure 3.6: Abrogation of the UV-induced DNA repair activity of PfRad51 under Hsp90 inhibitory condition. (A) Schematic representation of the principle of DNA repair assay. The relative position of the primer pair for the long and short range amplicon used in the assay. (B) At the trophozoite stage, 17-AAG (1.7 μ M), B02 (1 μ M), and Atovaquone (0.3 nM) pretreated and mock-treated cultures were UV irradiated at 100 J/m². Post UV treatment, cultures were maintained in the respective drug for 24 hours, along with this the mock treated culture was maintained in complete medium lacking any drug. Genomic DNA was isolated from the harvested parasite at the indicated time points: before UV damage, after 0 hour, 12 hours and 24 hours post damage. The mean values \pm SEM from three independent experiments are plotted.

3.2.5 Hsp90 inhibition sensitizes *P. falciparum* to MMS-induced DNA damage:

To further elucidate the role of PfHsp90 in the PfRad51-mediated DSB repair pathway, the effects of 17-AAG on MMS-induced cytotoxicity was studied. MMS is known to promote DSB by creating stalled replication fork (109). In response to MMS induced DNA damage, Rad51 is localized to the damaged DNA and forms foci, the requisite for HR mediated DNA repair pathway. Thus, MMS sensitivity also serves as an indirect measure of the HR mediated DSB repair efficiency of the cells.

So, to monitor the effect of Hsp90 inhibition on DSB repair efficiency of the cells, parasite culture pre-treated with 17-AAG were subjected to three different doses of MMS for 2 h and then subsequently returned to growth in a medium containing 17-AAG. As a control, parasite culture which was not treated with 17-AAG (mock-treated) was taken. The parasitemia of the MMS-treated and the untreated parasites were measured to determine the survivability upon MMS treatment. It was found that for the mock-treated parasites, the survivability was around 85% upon 0.001% MMS treatment, considering the survivability of MMS-untreated cultures to be 100%. No significant difference in the survivability was observed for the 17-AAG pretreated cultures when exposed to 0.001% MMS. However, a significant 2-fold reduction in survivability was observed between the mock-treated and the 17-AAG-treated cultures when both were subjected to 0.005% MMS treatment. At a much higher dose of MMS (0.1%), both mock-treated and 17-AAG pre-treated cultures showed extreme MMS sensitivity, and thus any difference in survivability was indistinguishable (Fig. 3.7A). As at 0.005% MMS concentration, a measurable difference in the survivability was observed, so this concentration of MMS was used for further studies. In order to ascertain the specificity of PfHsp90 inhibition by 17-AAG, the parasites were treated with various doses of 17-AAG to investigate whether

the sensitivity of the parasites increases in a dose-dependent manner. Our study shows that increasing doses of 17-AAG cause increased MMS sensitivity in a dose-dependent manner (Fig. 3.7B). In order to establish our conclusion, another established inhibitor of PfHsp90, namely, radicicol, was used in the assay. The parasite culture was treated with 1.5 mM radicicol, as it was observed previously that treatment with higher concentrations of this drug results in the arrestation of the parasite culture at the schizont stage (84). It was observed that the parasites pre-treated with radicicol manifest about 30% reduction in parasite survival upon MMS treatment compared to that of the mock-treated parasites (Fig. 3.7B). Since MMS-induced DNA damage, if unrepaired, could be lethal for the parasites, the efficiency of the repair process can be assayed as a function of parasite viability. Thus, our study suggests that the impact of PfHsp90 inhibition on the DSB repair machinery of the parasite is severe.



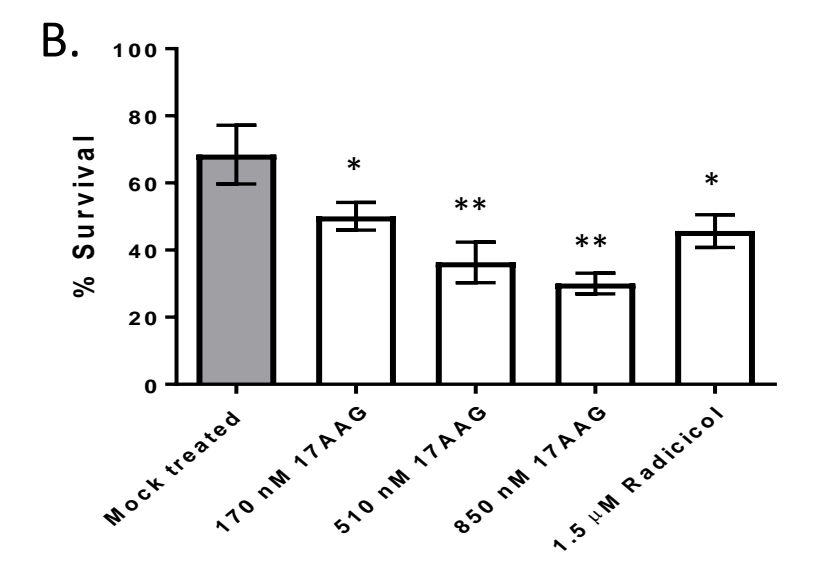


Figure 3.7: Hsp90 inhibition sensitizes P. falciparum to MMS induced DNA damage. (A) Return to growth assays were performed to determine the sensitivity of mock treated and 17-AAG treated 3D7 parasites at different concentration of MMS (as indicated on the X-axis). Graph depicts the percent survival of parasites after 48-hour return-to-growth post MMS treatment. Each data point indicates mean value \pm SD from three independent experiments. (B) Return to growth assay performed to determine the MMS sensitivity of 3D7 parasites treated with different doses of 17-AAG and Radicicol compared to mock treated parasite. Graph depicts the mean percent survival (\pm SD) after 48 hours post MMS treatment (0.005%) from four experiments. The P value was calculated using the two tailed t-test (* means P value < 0.05; ** means P value < 0.01).

3.3 Discussions

In this chapter, through yeast two hybrid assay and co-immunoprecipitation, the interaction of PfRad51 and PfHsp90 was established. The proteasomal degradation of PfRad51 in the presence of Hsp90 inhibitor 17AAG, indicated the requirement of PfHsp90 activity for maintaining the steady state of PfRad51. Dependence of PfRad51 on Hsp90 for its stability was also verified using the yeast surrogate system. The DNA repair activity of PfRad51 was also found to be compromised on PfHsp90 inhibition. The parasites were unable to repair the UV irradiation induced damaged DNA in the presence of 17AAG, as activity of PfRad51 was abrogated. Additionally, inhibition of Hsp90 rendered parasites more sensitive to DNA damaging agent MMS. Altogether, this study establishes PfRad51 as a bonafied client of PfHsp90 and illustrates the canonical function of PfHsp90 in regulating DNA repair pathway in the protozoan parasites.

Chapter-A The non-canonical functions of Hsp90 in Plasmodium biology

4.1 Introduction

Hsp90 in spite of being a cytoplasmic chaperone, has been reported to mark its presence in the nucleus by executing its non-canonical functions. Additionally, Hsp90 has been found to be associated with the chromosomes at the promoter-proximal regions in higher organisms and modulate the gene expression (70, 72).

Chronicity of malaria caused by *Plasmodium falciparum* is maintained by antigenic variation which is the outcome of mutually exclusive expression of *var* genes encoding PfEMP1. This selective mode of *var* gene expression, its switching and thereby exhibition of only one particular PfEMP1 at the surface of infected RBC enable the parasite to bypass the immune response of the host and prolong the infection (7-10, 22). The silencing of entire repertoire of *var* gene except one has been reported to be mediated by the epigenetic modifier *Plasmodium* Sirtuins (PfSir2A and PfSir2B) (35). PfSir2 being a histone deacetylase is recruited at *var* promoter and is involved in the deacetylation of H3K9 thereby allowing the methyl transferase to deposit the silencing marks (110). Thus, PfSir2 aids the parasite to maintain its virulence.

In model organism, budding yeast *S. cereviaiae*, expression of Hsp90 is induced at higher temperature and its non -canonical function is also found to be modulated by the change in temperature. As reported, heat shock results in down regulation of *ScSIR2* expression, in turn there is loss of telomere silencing. ScHsp90 is able to dictates the expression of *ScSIR2* by governing the steady state level of transcription factor (Cup9) and its recruitment at *SIR2* promoter (71, 111). Till date, the chromosomal occupancy of Hsp90 or its role in modulating chromatin dynamics has not been reported in any protozoan parasites. In *P. falciparum* four paralogues of the *HSP90* genes have been identified (24). However, any direct or indirect roles of PfHsp90 in transcriptional regulation has not been established yet.

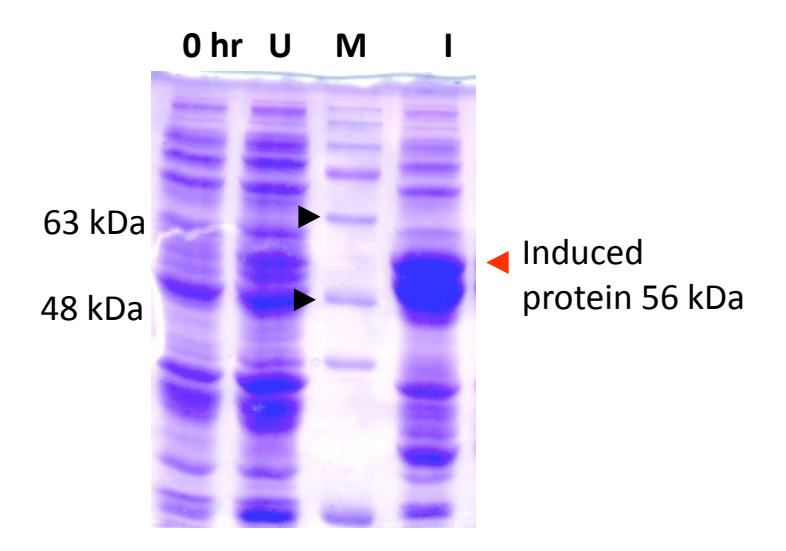
Recurrent fever is the hallmark of malaria, and the parasite encounters heat shock when the human host experiences the fever. It is the ring stage of the parasite that is exposed to the higher temperature as the rupture of schizont is accompanied by release of haemozoin and glycosylphosphatidylinositol (GPI), responsible for the fever in the host (46, 112). PfHsp90 has also been reported to be induced, when *P.falciparum* in vitro culture is subjected to higher temperature (47). Interestingly, certain report suggests that multiple var transcript are observed at the ring stage whereas at other stage only one of the var transcript is found to be expressed (10, 29). This prompted us to investigate whether febrile temperature modulates the activity Hsp90 and whether PfSIR2 transcription is also a function of temperature in the protozoan parasite. We hypothesized that, as exposure of the parasite to heat shock leads to over expression of Hsp90 and if PfSIR 2 expression is dictated by the non-cannonical function of PfHsp90, expression of PfSIR2 must also be altered upon heat treatment. The following questions have been addressed here: First, whether PfSIR2 expression is altered in response to higher temperature? Second, whether *PfSIR2* expression is guided by altered chromatin state? Third, whether PfHsp90 plays any role in altering the chromatin state? In this study, we have explored the mechanism of *PfSIR2A* and *PfSIR2B* gene expression in response to heat shock. Interestingly, we found that upon heat shock, PfSIR2A and PfSIR2B are down-regulated in a mid-ring stage specific manner and concomitantly majority of var genes are also de-repressed. Further, our work shows that heat shock leads to increased occupancy of trimethylated-H3K9 at both SIR2_{UAS} causing heterochromatinization of this locus. We have further established that such process is directly dependent on PfHsp90 activity at the promoter proximal region of PfSIR2A and PfSIR2B. Thus, this work depicts that an environmental cue, such as heat shock, amends *PfSIR2A* and *PfSIR2B* gene expression via Hsp90 dependent epigenetic modifications.

4.2 Results

4.2.1 Expression of PfSir2A and antibody generation:

For generation of antibody against PfSir2A, the gene *PfSIR2A* cloned in expression vector pGEX-6p2 was expressed in BL21 DE3* bacterial strain. The induction of protein was performed using 0.4 mM IPTG at 20 °C for 10 hours (89) (Fig 4.1A). The expressed protein was used for antibody generation. The specificity of the antibody was checked by Western blot analysis using parasite lysate. The antibody detected a specific band of molecular weight 30 kDa corresponding to PfSir2A but did not recognise PfSir2B protein, whose molecular weight is around 143 kDa (Fig.4.1B). The specificity of this antibody was ascertained by the absence of a similar band on a blot probed with the pre-immune sera.

A.



В.

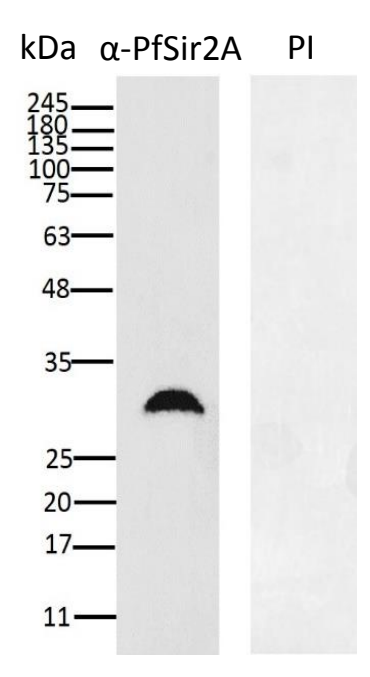


Figure 4.1: Expression of recombinant PfSir2A and specificity check of anti-PfSir2 antibody. (A) SDS-PAGE analysis showing expression of recombinant protein PfSir2A, Lanes: 0h- before induction, U-un-induced, M-marker, I- induced. (B)Western blot analysis performed with total parasite proteins to depict the specificity of anti- PfSir2A antibody versus the pre-immune sera. The position of molecular marker is indicated on the left.

4.2.2 Brief exposure to elevated temperature results in down-regulation of *PfSIR2* protein at the mid-ring stage:

Changes in the environment often leads to changes in gene transcription through epigenetic modifications of chromatins (113, 114). Since the epigenetic erasers PfSir2A and PfSir2B have been implicated to play crucial roles in parasite physiology by virtue of regulating the virulence gene expression, we sought to explore whether the steady-state levels of these two proteins are altered due to exposure to febrile temperatures. To address this, we took synchronous parasite cultures of early-ring, mid-ring, trophozoite and schizont stages and divided each stage specific culture in two parts: one part was subjected to heat shock at 41°C for two hours, while the other part was grown at normal condition (37°C). Western blot analysis was performed with the total protein isolated from parasites grown under these conditions. PfSir2A antibody raised in this study was used to detect the steady state level of PfSir2A on Western blot, whereas PfActin was used as a loading control (Fig. 4.2A). Due to the lack of a PfSir2B antibody, the steady state level of this protein could not be measured. We observed 2.2-fold reduction in the steady state level of PfSir2A protein upon heat treatment at the mid-ring stage (Fig. 4.2B). No such reduction of PfSir2A protein was observed if heat treatment was given at the early-ring, trophozoite or schizont stages.

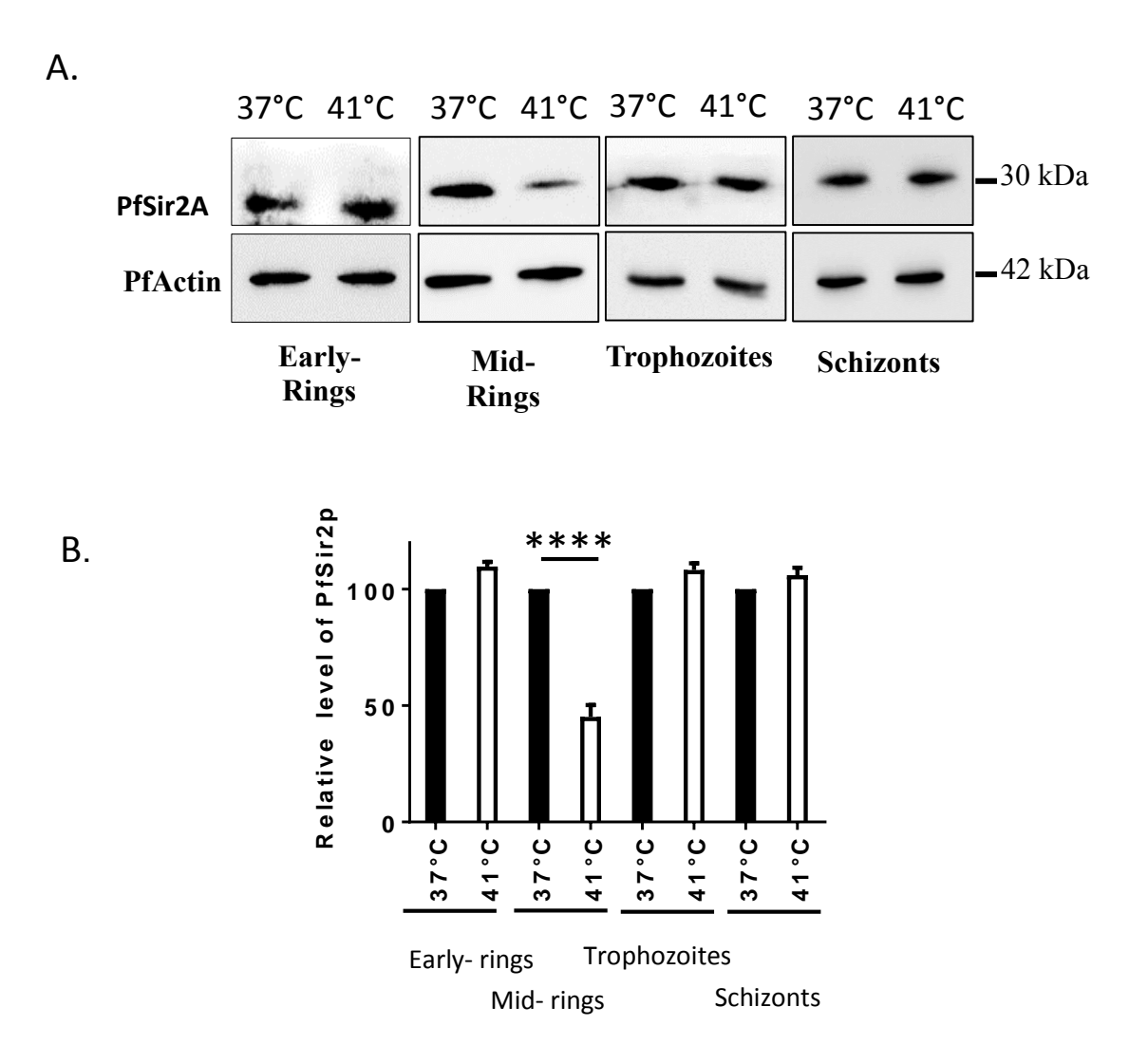


Figure 4.2: Heat induced down-regulation of PfSir2A protein is specific to the mid-ring stage. (A) Western blot analysis of PfSir2A expression performed with total protein isolated from parasites of different stages grown under normal condition (37°C) and heat-treated condition (41°C). PfActin was used as a loading control. (B) Quantification of band intensities shows a lower abundance of PfSir2A upon heat shock at the mid-ring stage. Error bar indicates the SEM obtained from three individual experiments. Asterisks indicate values significantly different from the control, as follows: ****, P<0.0001. The abbreviation h.p.i stands for hours post infection of RBC with merozoite.

4.2.3 Exposure to heat shock leads to transcriptional down-regulation of *PfSIR2A* and *PfSIR2B* specifically at mid-ring stage:

In order to investigate whether the less abundance of PfSir2 protein upon heat shock is due to any down-regulation at the transcriptional level, real-time RT-PCR analysis was performed with RNA isolated from control and heat-treated parasites and the expression of *PfSIR2A* and *PfSIR2B* were then analysed. Rivetingly it was observed that there is almost 8 fold down regulation in transcripts of both *PfSIR2A* and *PfSIR2B* upon heat shock (Fig. 4.3A,B) and this down regulation was specific to the mid-ring stage (8-12 hours post invasion). In the case of trophozoite or schizont stages slight increase in the level of mRNA was observed in the heat treated parasites. While no alteration in the transcript level at the very early-ring stage (0-4 hours post invasion) was witnessed.

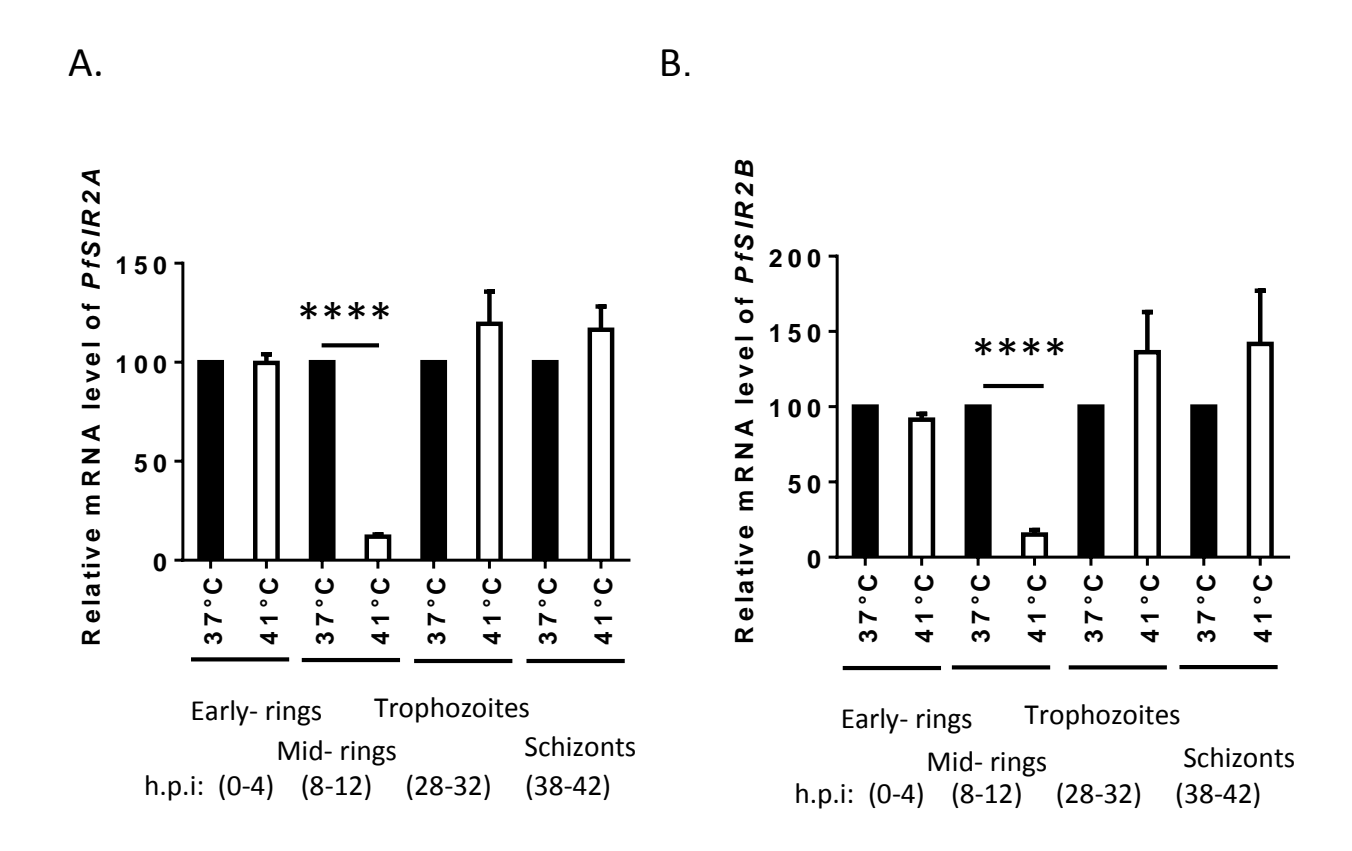


Figure 4.3: Exposure to heat shock leads to transcriptional down-regulation of *PfSIR2A* **and** *PfSIR2B* **specifically at the mid-ring stage.** (A) Real time RT PCR analysis showing mRNA levels of *PfSIR2A* at the four different stages of parasites in control 37°C and heat-treated conditions. (B) Real time RT PCR showing mRNA levels of *PfSIR2B* at four different stages of parasites in control and heat-treated conditions. The RT qPCR results are representative of three independent experiments, error bar indicates the SEM and *SERYL-tRNA SYNTHETASE* was used as the normalising control. Asterisks indicate values significantly different from the control, as follows: ****, *P*<0.0001.

4.2.4 Reduction in recruitment of PfSir2A at the *var* promoter Ups A upon heat shock:

As it was evident that exposure to heat shock, induces transcriptional down-regulation of PfSIR2 which in turn leads to lower abundance of PfSir2 protein. We were further keen in investigating whether lower abundance of PfSir2 under heat-treated condition results in lower occupancy of this protein at the var promoter leading to de-repression of var genes. To this end, chromatin-immuno-precipitation (ChIP) analysis using anti-PfSir2A antibody was performed and the occupancy of PfSir2A at two var promoters: Ups A and Ups B were investigated. The primer set used is listed in Table 2.1. For amplification of Ups A we have used a primer set that would amplify two Ups A sequences (PF3D7_0400400; PF3D7_1300300). For Ups B (PF3D7_10_v3:1650432.1650766) amplification we have used a previously used primer set (115). The ChIP analysis indicated that only Ups A is associated with PfSir2A protein (Fig. 4.4A,B). The ChIP performed with IgG antibody acted as a negative control. Lack of PfSir2A recruitment at the Ups B locus also acted as an internal negative control, emphasising the specificity of the anti-PfSir2A antibody. This finding corroborates well with previous finding that PfSir2A regulates Ups A type var genes and PfSir2B regulates Ups B type var genes (26). As expected, upon heat shock there was almost 3 fold reduced occupancy of PfSir2A at the Ups A loci.

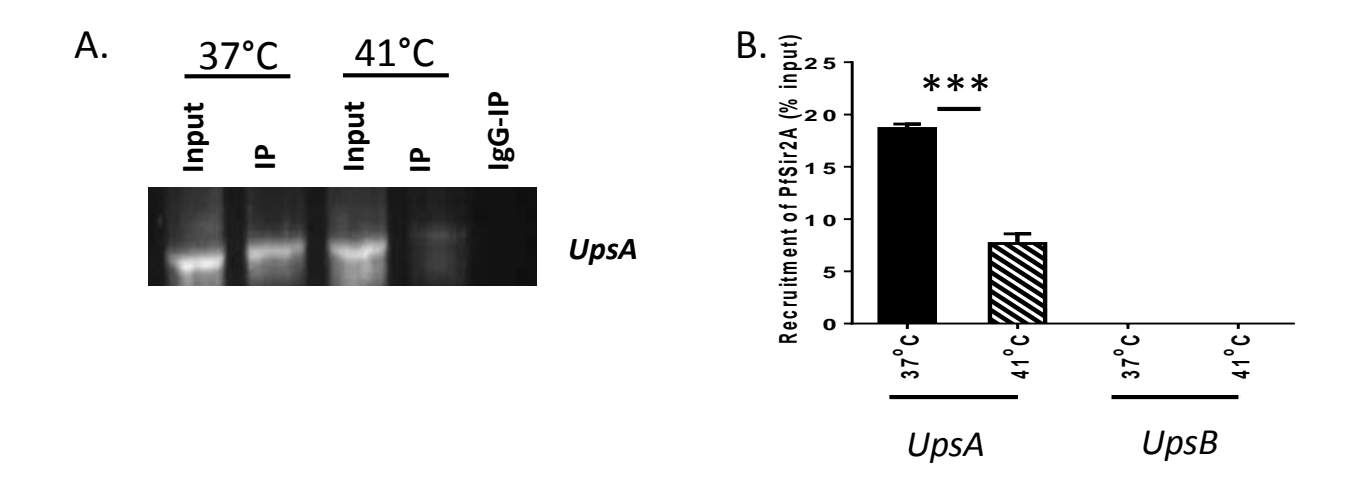
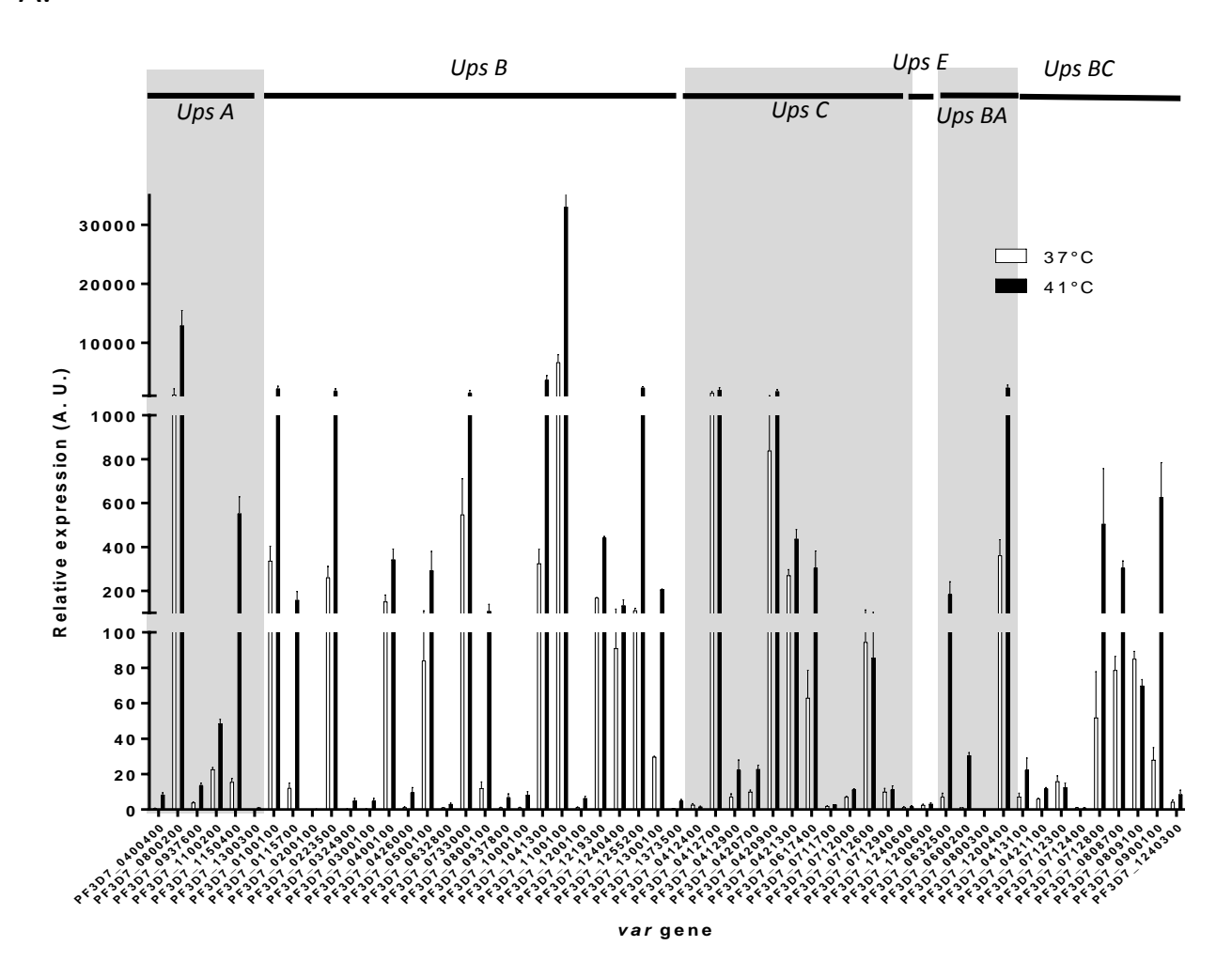


Figure 4.4: Reduction in recruitment of PfSir2A at the var promoter Ups A upon heat shock. (A) ChIP assay was performed using mid-ring stage parasites grown under normal and heat-treated conditions. Anti PfSir2A antibody was used for precipitations. Input and immunoprecipitated DNA were amplified by PCR with primers specific to two Ups A (PF3D7 0400400; PF3D7_1300300) sequences and Ups В (PF3D7 10 v3: 1650432.1650766). Gel picture depicts enrichment of PfSir2A at Ups A, lane1: Input (37°C), lane2: Sir2A IP (37°C) 3: Input (41°C), lane4: Sir2A IP (41°C), lane5: IgG IP. (F) Graph was plotted from the value of band intensities obtained from three independent experiments with error bar indicating the SEM. Asterisks indicate values significantly different from the control, as follows ***, *P*<0.001.

4.2.5 Brief exposure to elevated temperature results in de-repression of multiple subtelomeric *var* genes:

In P. falciparum 3D7 strain PfSir2A and PfSir2B have been implicated as the negative regulators of sub-telomeric var gene expressions (26). However, for FCR3 or NF54 strains such strong negative correlation could not be established (116). Thus, we were interested in finding out whether heat-shock induced down-regulation of PfSir2A and PfSir2B correlates with the de-repression of sub-telomeric var genes in P. falciparum 3D7 strain. To investigate this, the synchronous parasites from the mid-ring stage of P. falciparum in vitro culture was exposed to heat treatment and analysed the level of var transcripts by q-RT-PCR using the primer sets developed earlier (117) and is listed in the Table 2.1. These var genes belong to the different promoter types such as Ups A, Ups B, Ups C, Ups E types and hybrid promoters Ups BA, and Ups BC. In this study, any pseudo-var or var-like sequences have not been included. For the analysis *in vitro* grown parasite population which are expected to express the *var* genes randomly have been used, instead of taking pan-selected or drug-selected parasites where expression of a single var gene in the entire population is artificially induced. The majority of the var genes were observed to be up-regulated irrespective of their chromosomal locations (Fig.4.5A). Fourteen var genes exhibited more than 9-fold up-regulation in their expression, eighteen var genes were up-regulated more than 3-fold but less than 9-fold, twelve var genes depicted less than 3-fold but more than 1.5-fold up-regulation, and the remaining var genes showed less than 1.5-fold change in their expression upon heat shock (Fig 4.5B, Table 4.1). These observations suggest that indeed environmental cue, such as temperature plays crucial role in governing activity of PfSir2 and thereby the expression of var genes in P. falciparum 3D7 strain and such regulation was found to correlate well with the steady-state level of the prominent epigenetic modifier PfSir2 protein.

A.



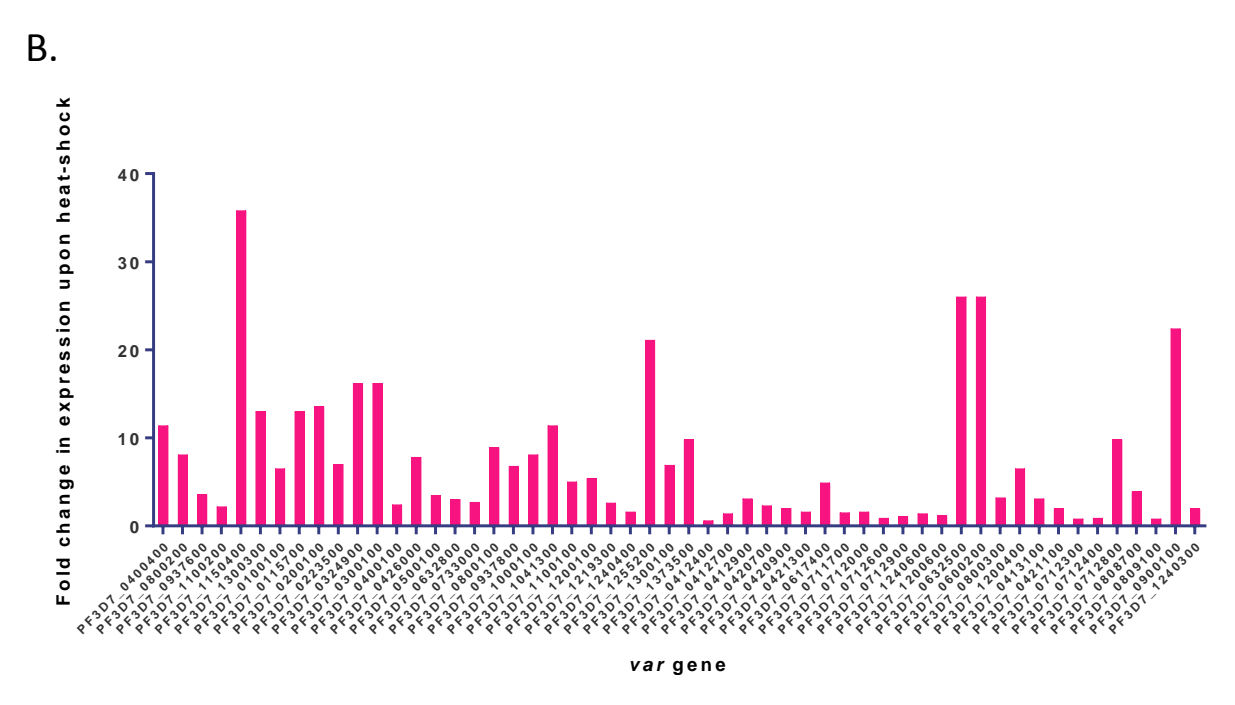


Figure 4.5: De-repression of *var* **genes upon heat shock.** (A) The graph depicting the abundance of *var* transcripts with respect to *SERYL-tRNA SYNTHETASE* at normal condition (37°C) and upon heat shock at 41°C at mid-ring stage, quantified through real time RT PCR. The qPCR results are representative of three independent experiments with data indicating the mean± SEM. The corresponding *UPS* type of each var gene is also marked (B) Graph indicating the fold change in expression of *var* gene upon heat treatment at 41°C at mid-ring stage, determined through real time RT PCR. The Gene ID of each *var* gene is written on the X-axis.

Table 4.1: Fold change in the expression of var genes upon heat shock.

No.	Gene ID	Fold change in expression
1	PF3D7_0400400	11.4
2	PF3D7_0800200	8.1
3	PF3D7_0937600	3.6
4	PF3D7_1100200	2.2
5	PF3D7_1150400	35.8
6	PF3D7_1300300	13
7	PF3D7_0100100	6.5
8	PF3D7_0115700	13
9	PF3D7_0200100	13.6
10	PF3D7_0223500	7
11	PF3D7_0324900	16.2
12	PF3D7_0300100	16.2
13	PF3D7_0400100	2.4
14	PF3D7_0426000	7.8
15	PF3D7_0500100	3.5
16	PF3D7_0632800	3
17	PF3D7_0733000	2.7
18	PF3D7_0800100	8.9
19	PF3D7_0937800	6.8
20	PF3D7_1000100	8.1
21	PF3D7_1041300	11.4
22	PF3D7_1100100	5

23	PF3D7_1200100	5.4
24	PF3D7_1219300	2.6
25	PF3D7_1240400	1.6
26	PF3D7_1255200	21.1
27	PF3D7_1300100	6.9
28	PF3D7_1373500	9.8
29	PF3D7_0412400	0.6
30	PF3D7_0412700	1.4
31	PF3D7_0412900	3.1
32	PF3D7_0420700	2.3
33	PF3D7_0420900	2
34	PF3D7_0421300	1.6
35	PF3D7_0617400	4.9
36	PF3D7_0711700	1.5
37	PF3D7_0712000	1.6
38	PF3D7_0712600	0.9
39	PF3D7_0712900	1.1
40	PF3D7_1240600	1.4
41	PF3D7_1200600	1.2
42	PF3D7_0632500	26

26
3.2
6.5
3.1
2
0.8
0.9
9.8
3.9
0.8
22.4
2

4.2.6 Heat-shock leads to heterochromatinization of chromatin at PfSIR2 UAS:

In order to get mechanistic insights into the heat induced down-regulation of PfSIR2A and PfSIR2B expression, the chromatin status of the upstream sequence of PfSIR2A (SIR2A_{UPS}) and PfSIR2B (SIR2B_{UPS}) genes before and after heat-treatment were investigated. Since the promoter or the transcription start site (TSS) are not defined for PfSIR2A or PfSIR2B, region of 300 bp sequence up-stream of the translation start site (ATG) for both the genes were used for the analysis. To this end, FAIRE (Formaldehyde Assisted Isolation of Regulatory Elements) technique, where the enrichment of FAIRE DNA represents the nucleosome-free state and the absence of FAIRE DNA represents the nucleosome-occupied state of the locus under investigation (92, 93) was performed. Upon heat treatment a significant shift from the nucleosome-free state to the nucleosome-occupied state of both SIR2A_{UPS} and SIR2B_{UPS} loci (Fig. 4.6A) was observed. The mitochondrial gene *COX3* acted as a normalising control as the mitochondrial genome is not associated with histones. Quantitative PCR analysis revealed 2.1fold and 1.5-fold increase in the chromatin compaction at the SIR2A_{UPS} locus and SIR2B_{UPS} locus, respectively (Fig. 4.6B). Thus, this result reveals that the heterochromatinization of the upstream regions of the PfSIR2 genes are responsible for the down regulation of PfSIR2 expression. As a negative control, the promoter region of *PfARP* gene was also analysed as it is abundantly expressed at the ring stage. The analysis indicated that there was no change in the chromatin compaction before or after the heat-treatment at this locus (Fig. 4.5A). Thus, the promoter region of *PfARP* acted as a control for the FAIRE experiments emphasizing that the compaction of the *PfSIR2A* and *PfSIR2B* up-stream regions upon heat treatment are specific.

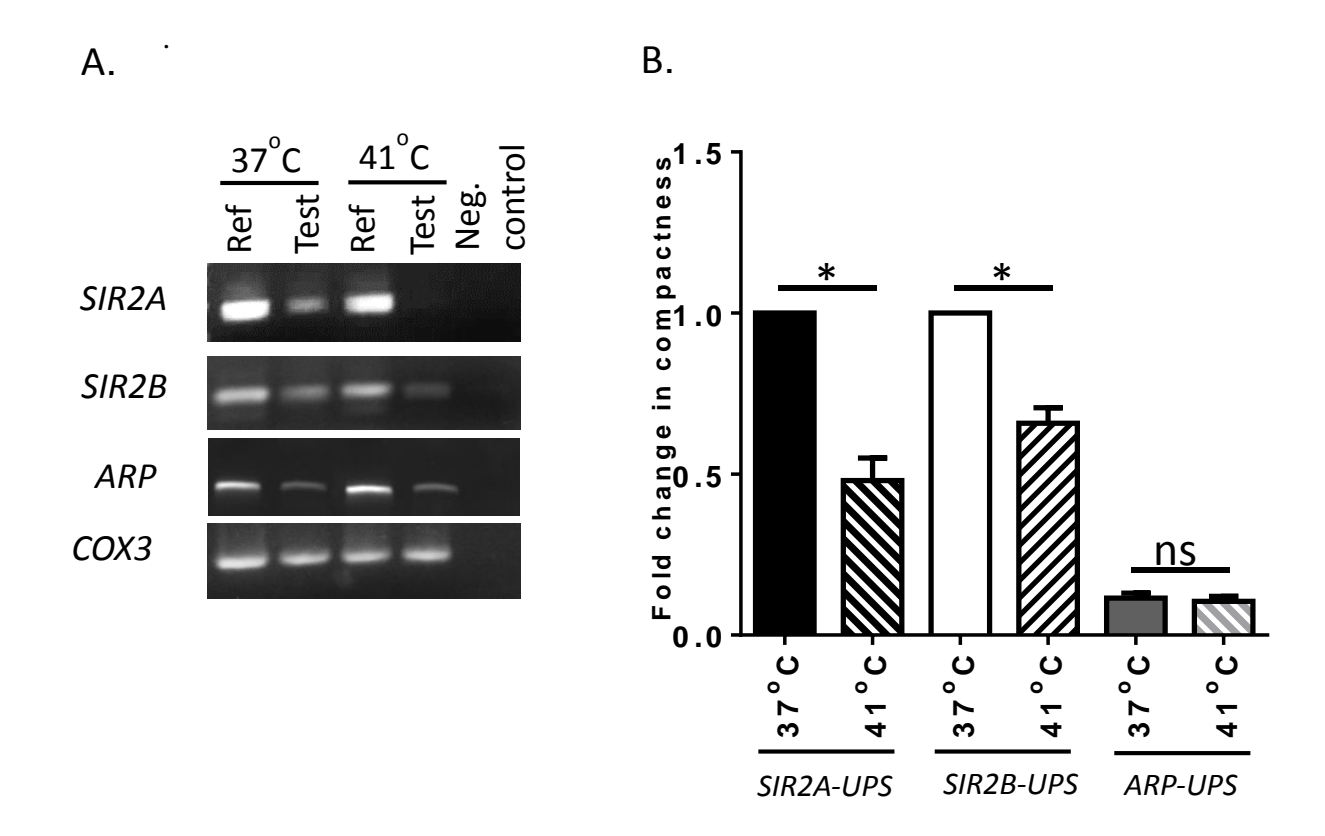


Figure 4.6: Heat-shock lead to heterochromatinization of chromatin at *PfSIR2 UAS*. (A) FAIRE was performed using mid-ring stage parasites grown at normal condition and heat-treated condition to determine the change in chromatin compactness at $SIR2_{UPS}$ upon heat shock. Lane 1- 37°C reference, lane 2- 37°C test, lane 3- 41°C reference, and lane 4- 41°C test, lane 5- no template control. Semi-quantitative PCR was performed using DNA obtained through FAIRE and total DNA as reference DNA as templates. *COX3* was used for normalisation and *ARP* acted as a negative control for the assay. (B) Real time PCR was performed to quantify the change in DNA abundance of nucleosome free DNA upon heat shock. *UPS* stands for up-stream sequences. The mean values \pm SEM from three independent experiments are plotted Asterisk indicates values significantly different from the control as follows *, *P*< 0.05; ns, non-significant.

4.2.7 Heat induced recruitment of H3K9me3 is responsible for repression of *PfSIR2* transcription:

As it was elucidated that heat-shock lead to tightening of chromatin structure at PfSIR2 promoter, we wanted to decipher the epigenetic marks associated with such heterochromatinization of the PfSIR2A and PfSIR2B promoter proximal regions. To unravel this, ChIP analysis with synchronous mid-ring stage parasite cultures grown at 37°C (control sample) or at 41°C (heat treated sample) using anti-H3K9me3, anti-H3K36me2, and preimmune IgG antibodies were performed. These antibodies used have been well established in detecting specific modifications on *Plasmodium* histones (118, 119). A dramatic increase in the recruitment of H3K9me3 was observed at both SIR2A_{UPS} and SIR2B_{UPS loci} upon heat-shock. Any recruitment of H3K36me2 at the SIR2A_{UPS} or SIR2B_{UPS} loci before and after heat treatment was not detected (Fig. 4.7A). The different recruitment patterns of the two repressor marks emphasize the specificity of the findings. ChIP experiment with IgG acted as a negative control. No recruitment was observed at the control locus ARP. As var-loci are known to be associated with H3K9me3, var-Ups A was used as a positive control for ChIP analysis. Quantitative PCR analysis with ChIP DNA revealed that upon heat treatment there were almost 13 folds and 6 folds increased recruitment of H3K9me3 at the SIR2A_{UPS} and SIR2B_{UPS}, respectively (Fig. 4.7B). These results suggest that the trimethylation of H3K9 is responsible for the heat induced heterochromatinization of *PfSIR2* promoter proximal region leading to the down-regulation of PfSIR2 transcription. The recruitment of H3K9me3 at the var-UPS A loci was found to be little less upon heat-treatment. However, such reduction was not statistically significant

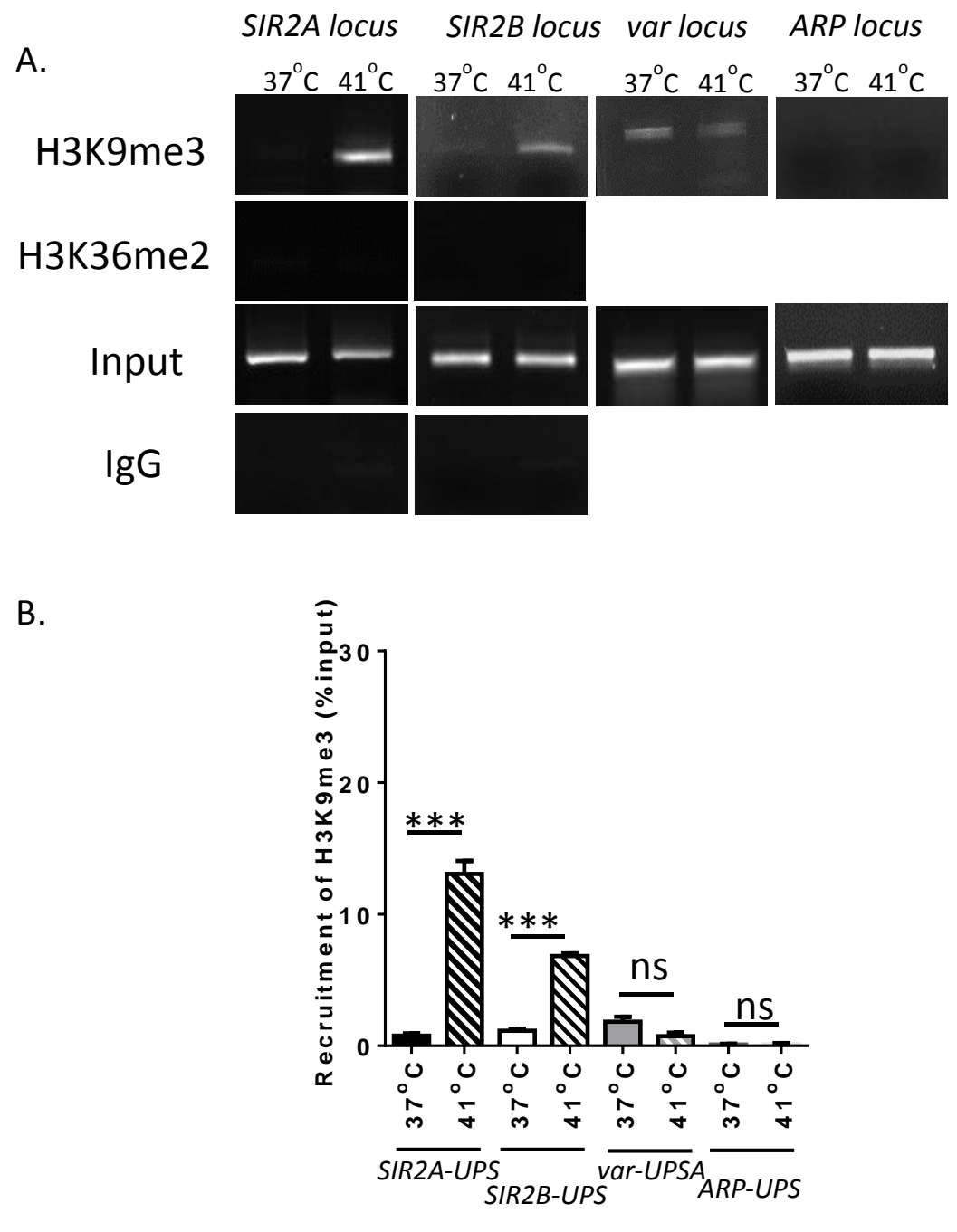


Figure 4.7: Heat induced recruitment of H3K9me3 is responsible for repression of PfSIR2 transcription. ChIP assay was performed using mid-ring stage parasites grown under normal condition (37°C) and parasite that were subjected to heat shock (41°C). Anti- H3K9me3 and IgG antibodies were used for immune-precipitation. (A) Semi quantitative PCR was performed with the input and immune-precipitated DNA with primers specific to $SIR2A_{UPS}$ and $SIR2B_{UPS}$ and also of ARP_{UPS} which served as negative control and var_{UPS} that acted as the positive control. (D) Quantitative PCR from three different ChIP assay were performed and mean density± SEM are plotted. Asterisk indicates value significantly different from the control, as follows ***, P<0.001; ns, non-significant.

4.2.8 Heat shock leads to overexpression of PfHsp90 at ring stage:

As the molecular chaperone PfHsp90 was found to be induced when asynchronous cultures of *P. falciparum* were exposed to heat-treatment (47) and Hsp90 orthologues are known to play regulatory roles during transcription of several genes in a variety of organisms (60, 120), we sought to investigate whether the stage specific down-regulations of *PfSIR2A* and *PfSIR2B* genes are mediated by PfHsp90. To address this, we were interested to first investigate whether PfHsp90 is induced in highly synchronous parasites belonging only to the ring stage upon heat-shock. There are four paralogues of Hsp90 in *P. falciparum* genome having IDs as following: PF3D7_0708400; PF3D7_1222300, PF3D7_1118200; and PF3D7_1443900. Out of these, the gene product of PF3D7_0708400 (old ID: PF07_0029) is known to be recognised by the anti-Hsp90 antibody used in this study (80). Western blot analysis reveals that indeed there was around 2.5 fold induction of PfHsp90 upon heat-treatment (Fig. 4.8 A, B). PfActin was used as a loading control.

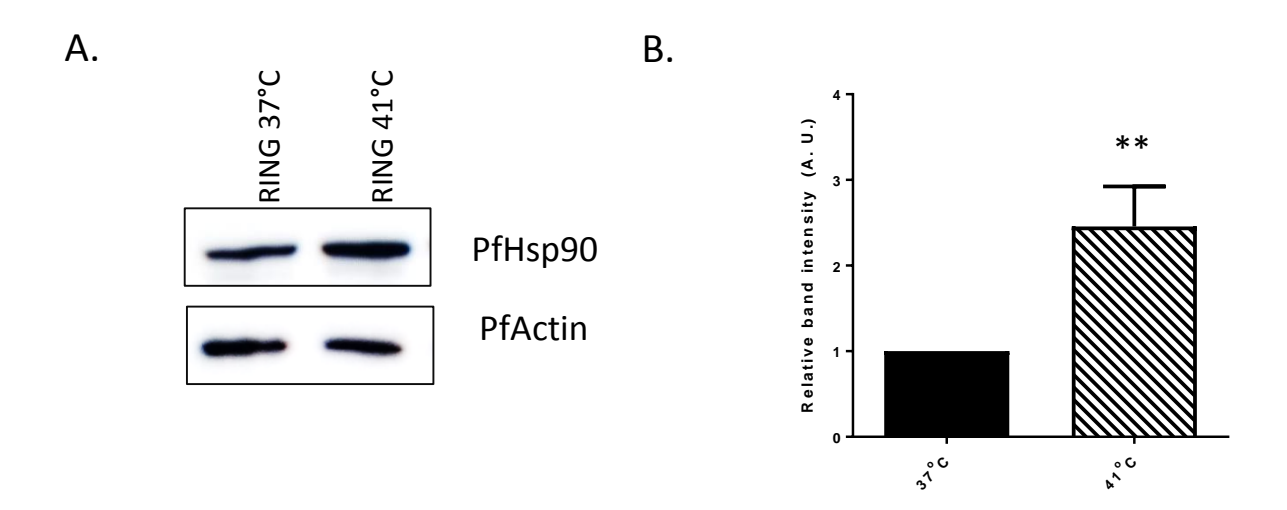


Figure 4.8: Heat shock leads to overexpression of PfHsp90 at ring stage. (A) Western blot analysis showing PfHsp90 is over expressed in heat shock treated ring stage parasites. (B) Graph plotted with the values of band intensity quantified from three different set of experiments Data was normalised against PfActin and mean density \pm SEM were plotted Asterisk indicates value significantly different from the control, as follows **, P < 0.01.

4.2.9 Heat induced down-regulation of *PfSIR2* transcription is dependent on Hsp90 activity:

In order to investigate whether PfHsp90 activity is required for transcriptional down-regulation of PfSIR2A and PfSIR2B, a potent chemical inhibitor of Hsp90, 17AAG was used for the analysis. To this end in vitro cultures of P. falciparum were treated with 170 nM 17AAG (1x) to inactivate PfHsp90 according to the previously established protocol (84). Synchronous parasite cultures of mid-ring stage were divided in four parts: two such cultures were grown at normal condition at 37°C with or without 17AAG treatment, while the other two cultures were subjected to heat treatment with and without 17AAG treatments. Real-time RT-PCR analysis on RNA isolated from the aforementioned four groups of parasites revealed that the heat induced down regulation of PfSIR2A and PfSIR2B transcripts do not take place in cultures that were treated with 17AAG (Fig.4.9A). In order to ascertain the specificity of this finding that 17AAG mediated inhibition of PfHsp90 is responsible for the reversal of the heat-induced transcriptional down-regulation of PfSIR2A and PfSIR2B genes a dose-dependent study was performed: where in a parallel experiment the cultures were treated with half the concentration of 17AAG (85 nM = 0.5x). With this a significant reversal of the phenotype, albeit to a lesser extent was observed (Fig. 4.9 A). Additionally, an experiment was performed where the parasite cultures were not pre-incubated with 17AAG and instead 17AAG (1x) was added at the onset of the 2-hour heat-treatment. A partial reversal of the phenotype, which was significant for PfSIR2B but not for PfSIR2A was found (Fig. 4.9 A). Besides Geldanamycin and its derivatives, such as 17AAG, there is another unrelated chemical inhibitor, namely Radicicol, available that is found to be effective against PfHsp90 (86). We sought to investigate if treatment with Radicicol also can exert a similar effect on the heat-induced down regulation of PfSIR2A and PfSIR2B transcription. To this end, parasite cultures were treated with 1.5 μM Radicicol as it was observed earlier that higher concentrations of the drug results in the arrestation of the culture at the schizont stage (84). Parasites pre-treated with Radicicol were subjected to heat-treatment for 2 hours at the mid-ring stage and were evaluated for the level of *PfSIR2A* and *PfSIR2B* transcripts. Parallel cultures maintained at 37°C with or without Radicicol treatment were also evaluated. It was observed that heat-induced transcriptional down-regulation of both the genes do not take place if the cultures are treated with Radicicol (Fig. 4.9B). These experiments clearly demonstrate that heat induced down-regulation of *PfSIR2A* and *PfSIR2B* expression is dependent on PfHsp90.

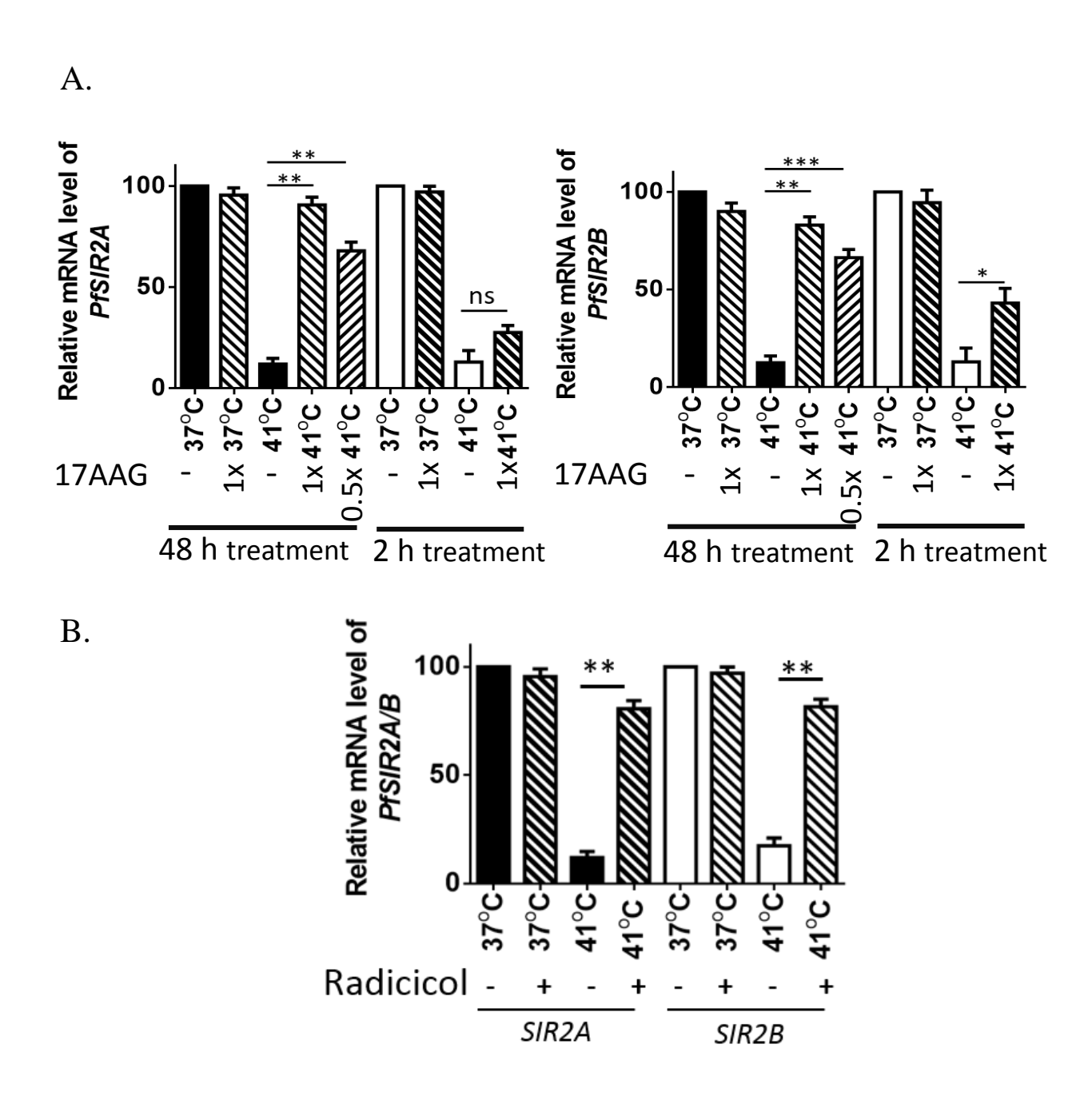


Figure 4.9: Heat induced down-regulation of PfSIR2 transcription is dependent on Hsp90 activity. (A) Real time RT-PCR were performed to quantify the relative abundance of PfSIR2A and PfSIR2B transcripts in 17AAG treated and untreated mid-ring stage parasites grown under normal and heat-treated conditions. Transcript levels were normalised by the housekeeping genes SERYL-tRNA SYNTHETASE transcript. The mean values \pm SEM from three independent experiments are plotted. (B) Real time RT-PCR were performed to quantify the relative abundance of PfSIR2A and PfSIR2B transcripts in Radicicol treated and untreated mid-ring stage parasites grown under normal and heat-treated conditions. Transcript levels were normalised by SERYL-tRNA SYNTHETASE transcript. The real time plot is indicative of three independent experiments \pm SEM. Asterisks indicate values significantly different from the control, as follows***, P<0.001***, P<0.01.

4.2.10 Hsp90 inhibition prevents compaction of SIR2 promoter on heat shock:

As heat-induced transcriptional down-regulation of *PfSIR2* genes was found to be associated with the heterochromatinization of *PfSIR2_{UPS}*, we were curious to find out whether treatment with 17AAG or Radicicol prevent the heat-induced compaction of the local chromatin. To this end parasite cultures were treated with 17AAG or Radicicol and FAIRE analysis was performed with mid- ring stage parasite culture to determine the chromatin status at *PfSIR2* locus under conditions with and without heat treatment. It was indeed observed that there is no reduction in the abundance of nucleosome free DNA of *PfSIR2A_{UPS}* and *PfSIR2B_{UPS}* loci upon heat-shock when the cultures were treated with 17AAG or Radicicol (Fig. 4.10 A, B). *PfCOX3* was used as normalising control. This suggests that Hsp90 activity is required for heat-induced heterochromatinization of *PfSIR2A* and *PfSIR2B* promoter proximal regions.

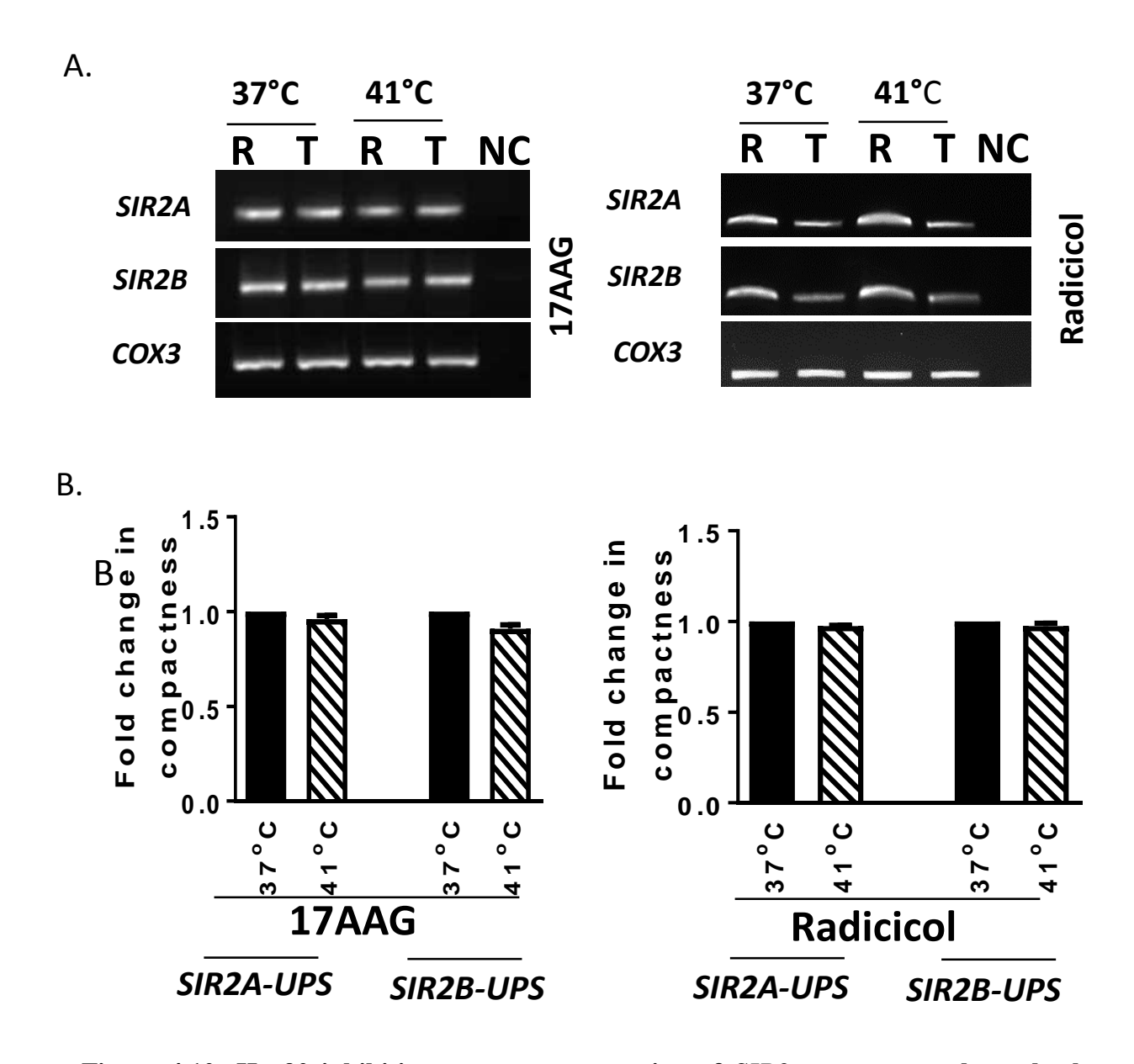


Figure 4.10: Hsp90 inhibition prevents compaction of *SIR2* promoter on heat shock. FAIRE was performed to determine the chromatin compactness at *PfSIR2A* and *PfSIR2B* loci in 17AAG or Radicicol treated mid-ring stage parasite grown at 37°C and at 41°C. (A) Semi-quantitative PCR was performed using DNA obtained through FAIRE and reference DNA as templates. *COX3* was used for normalisation Lane 1- 37°C reference (R), lane 2- 37°C test (T), lane 3- 41°C reference ®, lane 4- 41°C test (T), lane 5- no template control (NC). (B) Quantitative PCR was performed with the FAIRE DNA to quantify the change in DNA abundance of nucleosome free DNA. Mean value± SEM were plotted. *UPS* stands for upstream sequences.

4.2.11 Hsp90 inhibition prevents heat induced enrichment of H3K9me3 at *PfSIR2* promoter proximal regions:

In order to test that the failure in establishing the heterochromatic state is owing to a defect in the recruitment of H3K9me3 under Hsp90 inhibitory condition, ChIP experiments with the control and heat-treated mid-ring stage parasite cultures in the presence or absence of 17AAG were performed. Anti-H3K9me3, and pre-immune IgG antibodies were used for the assay. Interestingly, a complete abolishment of H3K9me3 recruitment in 17AAG treated samples (Fig. 4.11A, B) was noted. This indicates that PfHsp90 activity is required for the heat-induced epigenetic modification of the chromatin present at the *PfSIR2A* and *PfSIR2B* promoter proximal regions.

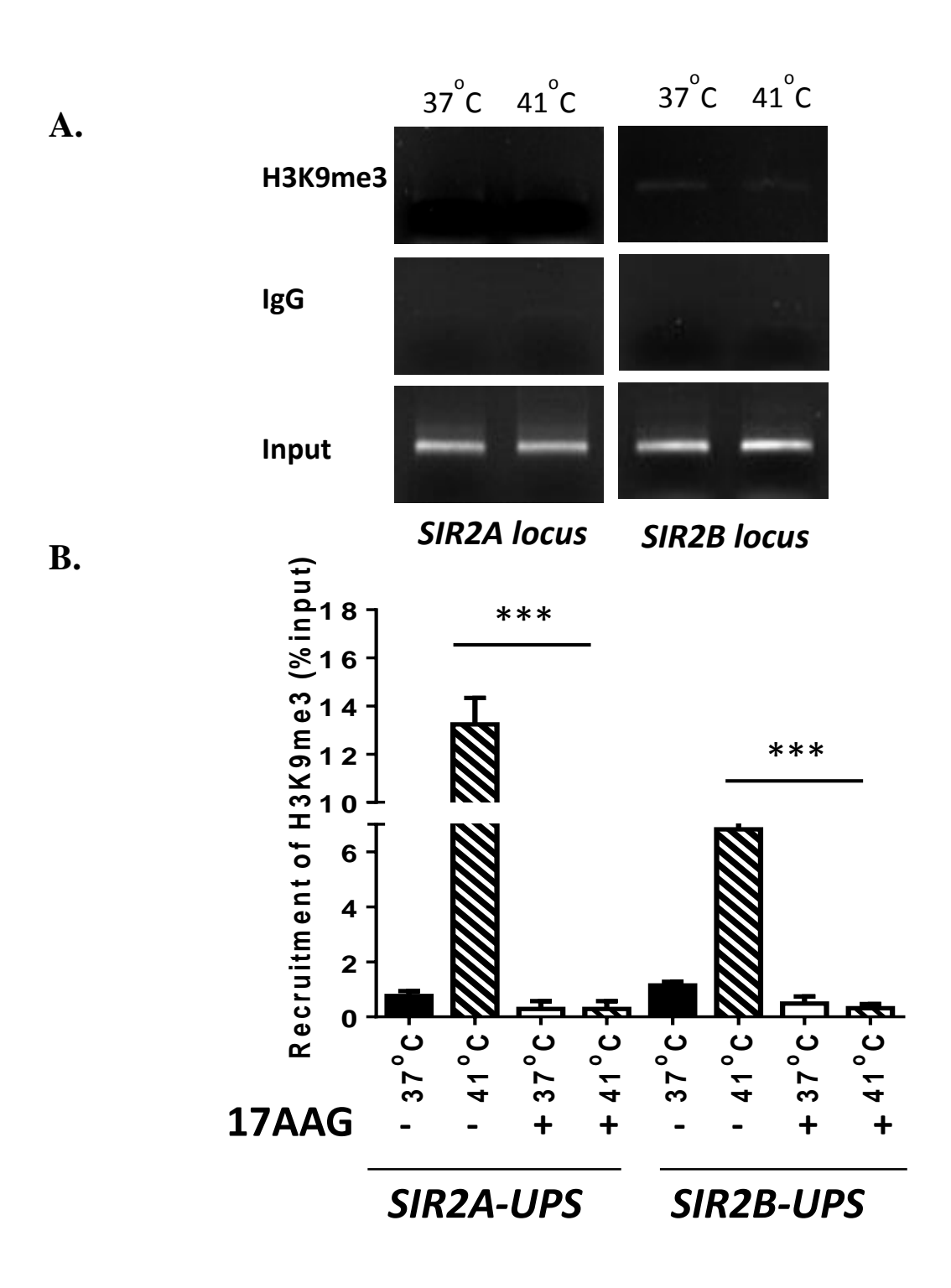
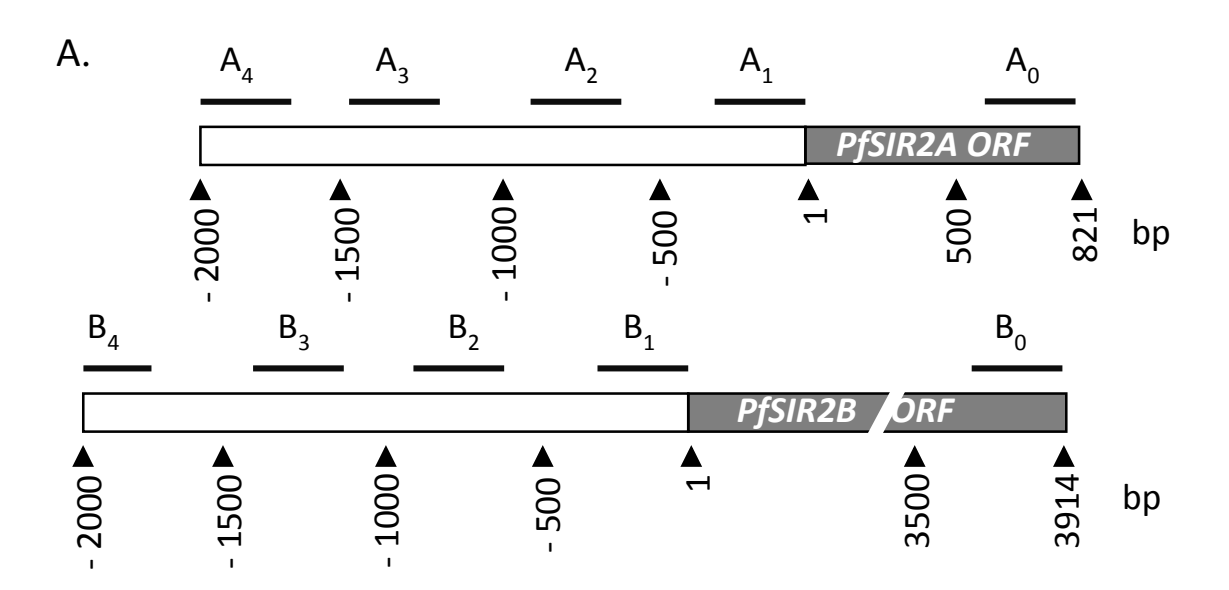
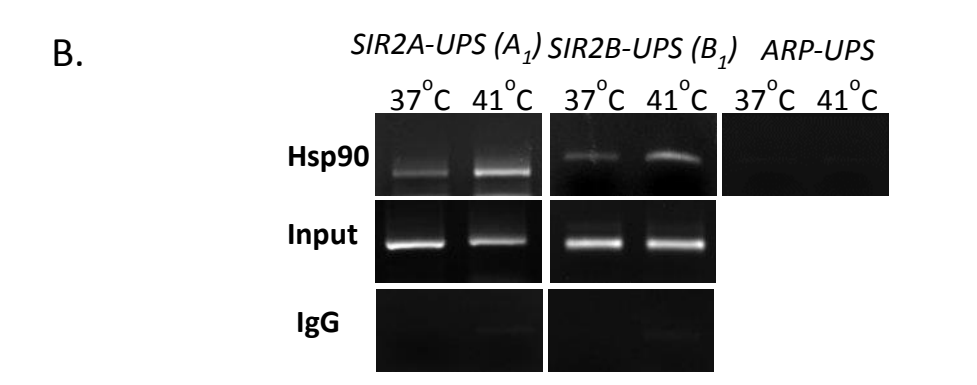


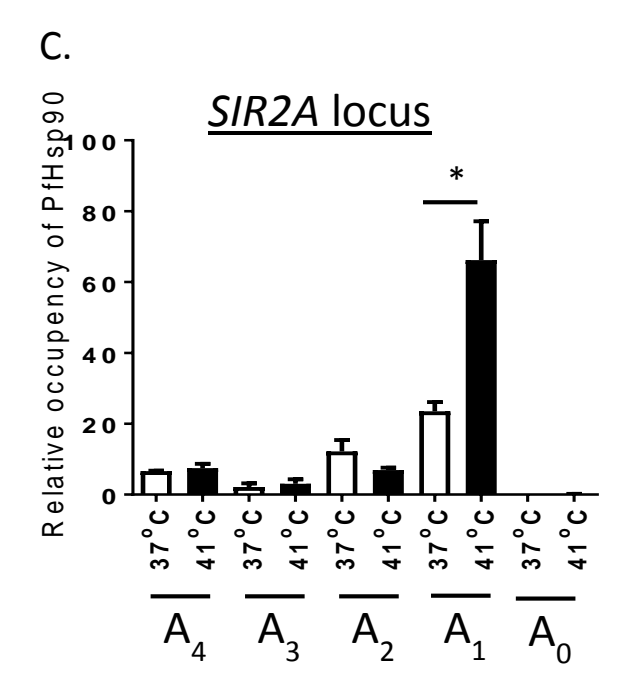
Figure 4.11: Hsp90 inhibition prevents heat induced enrichment of H3K9me3 at PfSIR2 promoter proximal regions. ChIP assay was performed with 17AAG treated mid-ring parasites grown under normal and heat-treated conditions. The antibodies used are marked on the left side. (A) Input and immunoprecipitated DNA were amplified by PCR with primers specific to $SIR2A_{UPS}$, $SIR2B_{UPS}$ and ARP_{UPS} , which served as a negative control. (B) Quantitative PCR from three different ChIP experiments were performed the Input and immunoprecipitated DNA and mean density \pm SEM are plotted. Asterisk indicates values significantly different from the control as follows: ***, P<0.001.

4.2.12 Occupancy of PfHsp90 at the upstream regions of PfSIR2A and PfSIR2B genes:

As it was established that PfHsp90 modulates the epigenetic mark and chromatin state of PfSIR2 promoter upon heat shock. We were keen to investigate whether PfHsp90 plays any direct role in PfSIR2A and PfSIR2B down-regulation. ChIP experiment using anti-Hsp90 antibody was performed to investigate its recruitment at PfSIR2_{UAS}. Five probes for each gene (PfSIR2A and PfSIR2B) were used to map the recruitment zones. Four probes were used to scan the upstream region (UPS) and one probe was within the ORF (Fig. 4.12A). Under heat treated condition it was observed that, there is increased recruitment of PfHsp90 at the immediate upstream sequences of PfSIR2 genes (A1/B1 regions). No recruitment was observed at control ARP locus (Fig. 4.12B). Quantitative analysis of the ChIP DNA from the heat treated samples revealed 2.8 folds and 2.2 folds more occupancy of PfHsp90 at PfSIR2AUPS (A1) and $PfSIR2B_{UPS}(B_1)$ loci, respectively (Fig. 4.12C). Further upstream regions (A₂ to A₄ or B₂ to B₄) were not found to be associated with PfHsp90 protein and hence acted as internal negative controls for this experiment. PfHsp90 occupancy was not observed within the ORF of any of the genes (A₀ or B₀ regions). Thus, this indicates that not only the recruitment of PfHsp90 at the immediately upstream region of PfSIR2 genes is very specific, but also its increased recruitment upon heat shock is very significant. The results from these experiments are suggestive of a direct non-canonical role of PfHsp90 in modulating PfSIR2A and PfSIR2B transcription.







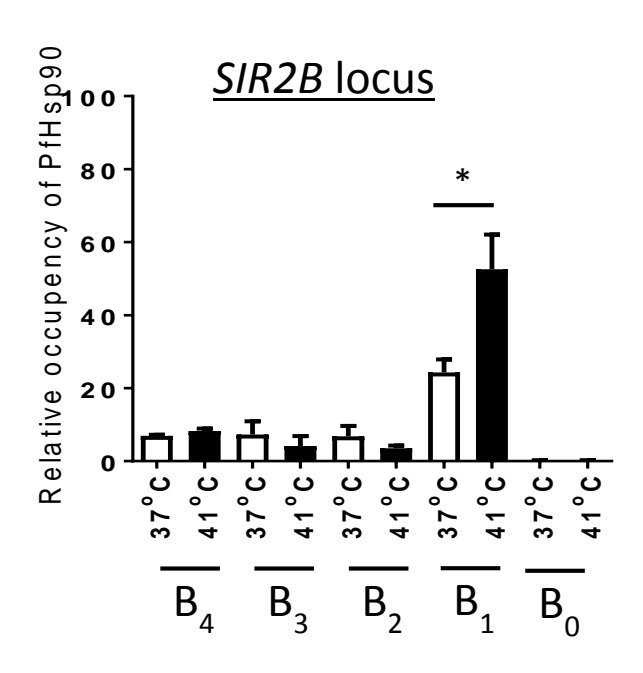


Figure 4.12: Occupancy of PfHsp90 at the upstream regions of PfSIR2A and PfSIR2B genes. (A) Schematic representation of PfSIR2A and PfSIR2B gene loci. Positions of PCR amplicons using ChIP DNA as template are marked as A_0 to A_4 and B_0 to B_4 . (B) ChIP assay was performed using parasites grown under normal or heat-treated conditions to determine the recruitment of PfHsp90 at $PfSIR2A_{UPS}$ and $PfSIR2B_{UPS}$. Antibodies used are marked on the left side. Input and immunoprecipitated DNA were amplified by PCR with primers specific to A_1 region, B_1 region, and ARP_{UPS} , which served as a negative control. (C) Recruitment of PfHsp90 at different regions of the PfSIR2A and PfSIR2B gene loci. Quantitative PCR of three different ChIP experiments were performed and the mean density \pm SEM are plotted. Asterisks indicate values significantly different from the control, as follows *, P < 0.05.

4.3 Discussions

In this chapter, it has been established that the cellular abundance of PfSir2 is subjected to the change in temperature in a developmentally regulated manner. PfSIR2A and PfSIR2B were found to be transcriptionally down-regulated specifically at the mid-ring stage in response to febrile temperature. Chip analysis also revealed reduced enrichment of PfSir2A at UpsA, the var promoter upon heat shock as a result de-repression of majority of var gene expression was observed. FAIRE analysis depicted that heat shock leads to shift of PfSIR2 promoter from nucleosome free state to heterochromatic state. Chip analysis further indicated that the heterochromatinization of PfSIR2 promoter occur due to deposition of repression epigenetic mark H3K9me3 on exposure to heat shock. Interestingly, it was deciphered that the heat induced transcriptional down-regulation of PfSIR2 and hence its reduced activity is mediated by PfHsp90. As it was observed that brief exposure to heat-shock leads to the induction of PfHsp90 protein in the mid-ring stage parasite and inhibition of PfHsp90 by its potent inhibitor 17AAG and Radicicol prevented the heat induced transcriptional repression of *PfSIR2*. Additionally it was also established that inhibition of PfHsp90 prevents the heat induced deposition of the epigenetic mark H3K9me3 on PfSIR2 promoter and hence its heterochromatinization. It was further validated by ChIP analysis that, upon heat treatment greater abundance of PfHsp90 results in greater chromosomal occupancy of this protein at the immediate promoter proximal regions of PfSIR2A and PfSIR2B genes, where PfHsp90 helps in recruiting H3K9me3 and thereby confer heterochromatic state. This leads to the downregulation of *PfSIR2* transcription. As a result, the steady-state level of PfSir2 also goes down, leading to its reduced occupancy at the corresponding var promoters that eventually causes the de-repression of var genes. Interestingly, as heat induced down-regulation of PfSIR2 transcription was found to be specific to the mid-ring stage, it is noteworthy to mention that

during an in vivo infection in human host, it is the ring stage parasites which are exposed to febrile temperature.

Thus, this study altogether provides insight on the non-canonical function of PfHsp90 and establishes its moonlighting role in the transcriptional regulation of *PfSIR2*. Additionally, this study provides a link between environmental cue, epigenetics and malaria pathogenesis.

Chapter-5 Discussions

5.1 Discussions

This study unravels the essential canonical and non-canonical roles of PfHsp90 in the *Plasmodium* biology. It provides insights into the chaperoning activity of PfHsp90 in rendering stability to PfRad51. Additionally, this study also uncovers the moonlighting role of PfHsp90 in regulating the expression of epigenetic eraser *PfSIR2* in response to an environmental cue such as temperature.

In the first part of the study, the canonical function of PfHsp90 in terms of providing stability to its client has been explored. This work provides evidence that PfRad51 acts as a direct client of PfHsp90. It was observed that PfHsp90 interacts with PfRad51 both under in vivo and in vitro conditions. The nature and the extent of 17-AAG-mediated inhibition of the repair of UV-induced damage in the parasite genome was positively correlated with the inhibitory effect of B02, a potent inhibitor of recombinase PfRad51. Most importantly, it was noted that treatment of 17-AAG resulted in the depletion of PfRad51 by accelerating the proteasomal degradation of the protein. The essentiality of PfHsp90 in *Plasmodium* biology has been rightfully advocated previously (121-124). However, no client of PfHsp90 that is important in parasite biology has been identified earlier. To our knowledge, this is the first report that identifies a bona fide client of PfHsp90. As PfRad51 and its mutants can be easily expressed and purified using bacterial expression systems (96), this now allows biochemical investigation of the PfHsp90 chaperone cycle and the involvements of its co-chaperones, using PfRad51 as a model client protein.

The malaria parasites during their intraerythrocytic life cycle encounter extraordinarily high levels of genotoxic stresses that cause various modifications of DNA bases, single-stranded

DNA (ssDNA) breaks, and most deleterious of all, DNA DSBs in the haploid chromosomes. As the unrepaired DSBs lead to the death of the unicellular parasite *Plasmodium falciparum* (45), targeting its DSB repair pathway is a promising option. It has been previously demonstrated that PfRad51 plays an indispensable function in the parasite's biology under DNA damage conditions (96). None of the components of the non-homologous end-joining pathway is found in the parasite genome. Besides, some of the proteins involved in homologous recombination, namely Rad52 and BRCA1, are also not annotated in the *Plasmodium* genome. Thus, PfRad51 has emerged as one of the major targets for blocking HR-mediated DSB repair in this parasite. Previously, B02 has been established as a specific inhibitor of PfRad51, but its IC50 was found to be in the micro molar range (3 to 8mM) (100). While lead optimization could be a strategy for increasing the potency of the chemical derivatives of B02, regulating the cellular abundance of the target protein, i.e., PfRad51, could also, in principle, reduce the IC50 of native B02. As our study indicates that treatment with the PfHsp90 inhibitor induces the proteasomal degradation of PfRad51, and we speculate that, this would lead to decrease in the IC₅₀ of B02. In a subsequent work it was observed that B02 and 17-AAG acted synergistically and the IC₅₀ of B02 was reduced more than 250 folds in the presence of Hsp90 inhibitor (125). Thus, this result serves as a proof of concept that the regulation of the abundance or activity of PfRad51 could be key to increasing the effectiveness of the recombinase inhibitors (Fig 5.1). This will now stimulate research on the identification of the negative modulators of *Plasmodium* homologous recombination machinery. The highly synergistic interaction between B02 and 17-AAG indicates that these two target proteins may also act in a non-epistatic manner. Our finding shows that inhibition of PfHsp90 and PfRad51 together causes a profound effect on parasite survivability and raises the possibility that PfHsp90 might control other DNA repair pathways as well. In humans, Hsp90 has been found

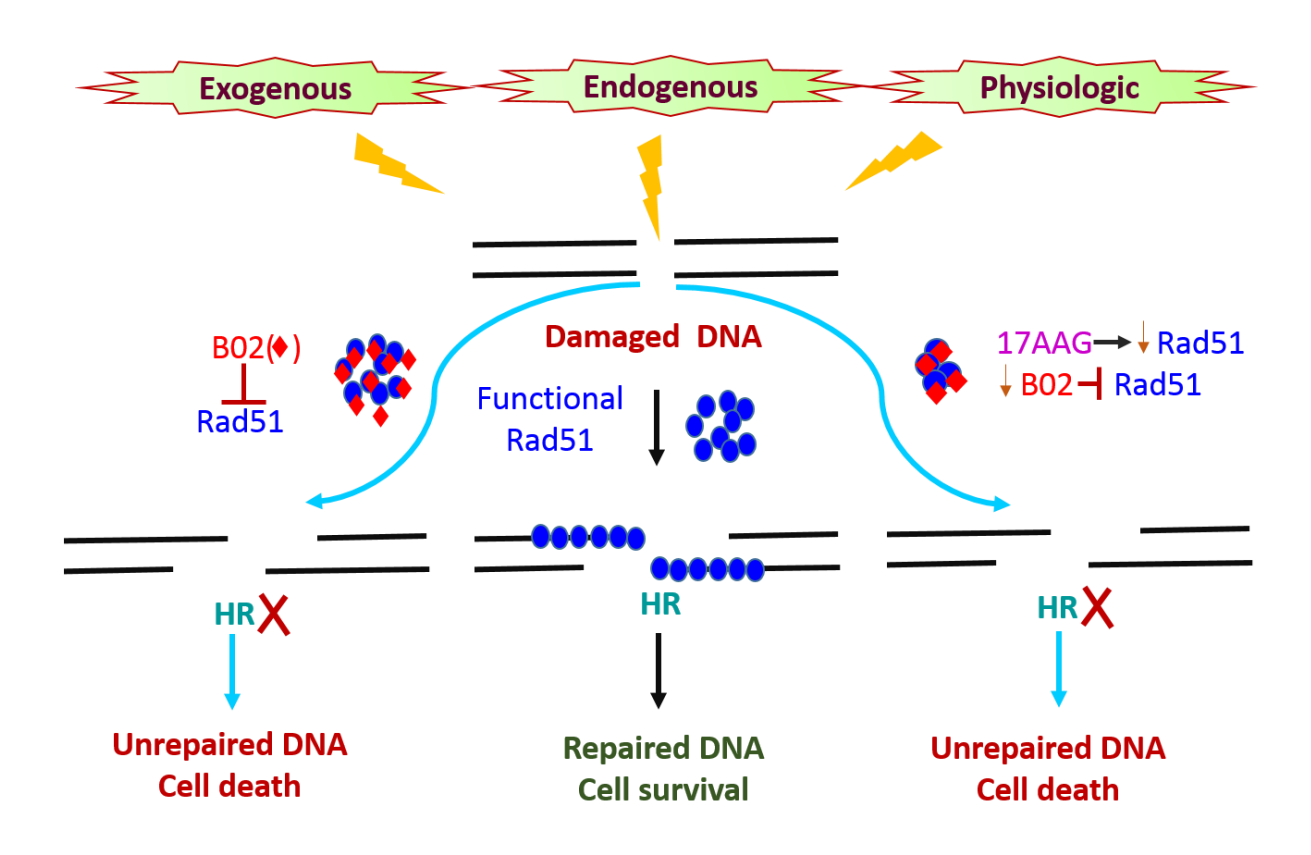


Figure 5.1: Model depicting the reduction in activity of PfRad51 upon Hsp90 inhibition.

to regulate DNA damage response (DDR), as well as the base excision repair (BER), the nucleotide excision repair (NER), and the mismatch repair (MMR) pathways by providing clientship to some of the major proteins involved in these pathways (102). In the budding yeast, it was observed that ScHsp90 modulates the DDR pathway by regulating a DNA repair signalling kinase, Rad53 (126). In malaria parasites, the long-patch BER pathway has been identified previously (127). Recently, in silico analyses have identified almost all components of NER (128) and MMR (129) pathways in the *Plasmodium* genome. However, it is still not known whether the enzymes involved in these pathways are regulated via the PfHsp90 chaperone system, which can be explored.

The second part of the study, deciphers a non-canonical function of PfHsp90 in negatively regulating the expression of *Plasmodium* sirtuins, The Sirtuin paralogues from *P. falciparum*, namely PfSir2A and PfSir2B have been implicated to play pivotal roles in negatively regulating *var* gene expression (26). Additionally, expression of *var* genes has been correlated with the changes in environment, especially temperature (47). Here, we report for the first time that the expressions of these two epigenetic modifiers are also subjected to the change in temperature. We report that a brief exposure to heat-shock leads to the induction of PfHsp90 protein. Greater abundance of PfHsp90 results in greater chromosomal occupancy of this protein at the upstream regulatory regions of *PfSIR2A* and *PfSIR2B* genes, where PfHsp90 brings about changes in the associated chromatin structure, from the nucleosome-free state to the heterochromatic state and thereby repressing the expression of *PfSIR2A* and *PfSIR2B* genes. As a result, the steady-state level of PfSir2 goes down, leading to less occupancy at the corresponding *var* promoters that eventually leads to the de-repression of *var* genes (Fig 5.2). Interestingly, such down-regulation of *PfSIR2* genes was found to be specific to the ring stage.

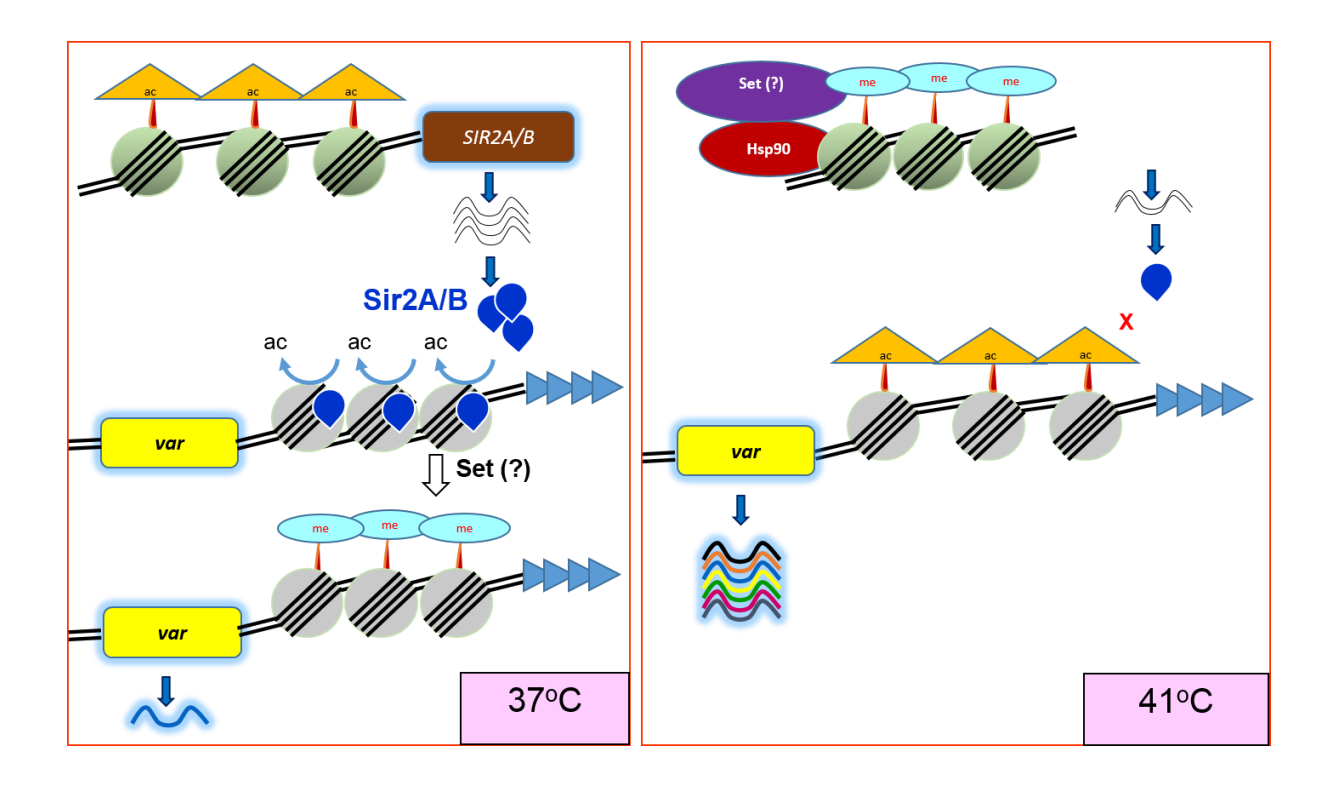


Figure 5.2: Model depicting the alteration at *PfSIR2* landscape upon heat shock.

It is possible that there is an innate transcriptional wiring that sets in transcriptionally repressed state for the sub-telomeric genes during trophozoite and schizont stages which is relaxed to some extent in the ring stage allowing de-repression of multiple sub-telomeric genes and such de-repression is more pronounced upon exposure to heat-shock. At this point it is noteworthy to mention that during an in vivo infection in human host the ring stage parasites are exposed to febrile temperature. Thus, it is not unlikely that the parasites at the ring stage are equipped with a multicomponent machinery that would sense the rise in temperature; transduce such signal to the chromatin and finally regulate the expression of the stress-induced genes. It is very tempting to speculate that a coordinated action of the components of such machinery would give the parasite an opportunity to break the tightly controlled mutually exclusive mode of var gene expression and allow the high-level expression of multiple var genes at the ring stage under febrile condition. Thus, leaving the parasite with multiple alternatives to choose from during switching for one var gene to another, which will eventually impact the chronicity of infection. Interestingly two of the three var genes found to be highly de-repressed in our study, were also reported to be highly de-repressed in sir2 knockout parasites (26). Thus, it could be possible that the effect of lower abundance of PfSir2 is more pronounced on certain var genes, while there is a general effect on all the sub-telomeric var genes. Currently, we do not have any mechanistic insights into this.

Contrary to our finding on *PfSIR2A* and *PfSIR2B* down-regulation, an earlier study reported up-regulation of *PfSIR2A* transcription upon heat-shock (47). Although the heat-treatment protocols were the same between our study and the previous study, the difference was that we have used highly synchronous mid-ring stage culture for our experiment and in the previous study asynchronous parasite cultures were used. In order to investigate whether the difference stems from the use of cultures belonging to different developmental stages of the parasites, in

our study we have tested the effect of heat-shock on four different asexual stages of the parasite life cycle. We observed transcriptional down-regulation of *PfSIR2A* and *PfSIR2B* transcripts at elevated temperatures only with highly synchronous mid-ring stage culture. Such down-regulation was observed neither at more advanced stages not at the very early-ring stage of the *in vitro* cultures. Interestingly, at the trophozoite or schizont stages moderate up-regulations of *PfSIR2A* and *PfSIR2B* were observed instead. This observation underscores the fact that heat induced transcriptional down regulation of *PfSIR2A* and *PfSIR2B* is tightly controlled in a developmental stage specific manner.

It is unlikely that the difference in the transcription profile between the treated and control cultures is due to any delay in the parasite development owing to the treatment, because in our study RNA was isolated from the cultures immediately after the brief exposure to heat stress while both the untreated and treated cultures were still in the mid-ring stage.

With highly synchronous early to mid-ring stage culture we observed transcriptional down-regulation of *PfSIR2* transcripts at elevated temperatures, especially at 41°C. Such down-regulation was not observed at more advanced stages of the in vitro cultures. Interestingly, at the trophozoite or schizont stages moderate up-regulations of *PfSIR2* were observed instead. This observation underscores the fact that heat induced transcriptional down regulation of *PfSIR2* is tightly controlled in a developmental stage specific manner. This observation probably explains why heat induced transcriptional up-regulation of *PfSIR2* was observed with asynchronous *P. falciparum* cultures while *var* transcription remained de-repressed (47). These findings corroborate with an earlier report demonstrating slight increase in *PfSIR2* transcripts from parasites isolated from patients with temperatures above 37.5°C. The same study also correlated *PfSIR2* expression with lactate levels in the patient and with severity of malaria (130). Thus, the regulation of *PfSIR2* gene appears to be dependent on several environmental

factors. Our study dissects out the contribution of one of the major factor, temperature and establishes the link between environment, epigenetics and malaria pathogenesis. We observed that the down-regulation of PfSIR2 upon heat-shock is specific to the mid-ring stage, although PfHsp90 is not only present in all the asexual blood stages but is also up-regulated upon heat treatment. Currently, we do not know why PfHsp90 mediated transcription repression of PfSIR2 does not take place in all the stages. It could be possible that Hsp90 mediates transcriptional down-regulation of *PfSIR2* via one of the histone-methyl-transferase (HMT) proteins as our results reveal that there is more occupancy of H3K9me3 at the *PfSIR2* upstream regions. In P. falciparum there are ten HMT proteins (named as SET 1 to SET 10)(131). It is reasonable to propose that one or more of these Set proteins are engaged with PfHsp90 and such interaction could be ring stage specific. It could also be possible that the expression or heat-shock induced up-regulation of the client Set protein is ring stage specific. In mammalian cell it has been observed that a HMT protein (SMYD3) physically interacts with Hsp90 (69, 70). Future experimentation would be required to establish any such interaction in P. falciparum. In a previous study, it was established that in budding yeast S. cereviaiae Hsp90 acts as a repressor of ScSIR2 expression, down-regulating its expression upon heat stress. To that end a transcription factor, Cup9 was identified whose steady state level and recruitment at SIR2 promoter is controlled by Hsp90 activity (71). In fact, a number of transcription factors have been found to be the clients of Hsp90 in a variety of organisms (60). In *Plasmodium* not many TFs are identified and no association of any of the TFs with PfHsp90 has been established yet. However, the possibility of a ring stage specific TF regulating PfSIR2 expression upon heat stress cannot be ruled out.

It is widely accepted in the field that in *P. falciparum* gene regulation happens through epigenetic modifications on histones. The relative occupancy of the activation marks and

repression marks co-ordinately brings out the heterochromatic or euchromatic states and thus control gene expression (119). Genome-wide studies have revealed that H3K9me3 modifications are associated with repressed sub-telomeric var genes and H3K36me2 modification is found around the transcriptionally silent genes that are located at internal chromosomal sites (34, 119, 132). Our findings that the involvement of H3K9me3 in repression of non-sub-telomeric PfSIR2 genes, suggests that such binary distribution of repressor marks may not always be the case. Another possibility is that H3K36me2 might be the general repressor mark under normal situation and under heat stress condition H3K9me3 may play an important role. A comparative genome wide ChIP-seq analyses with H3K9me3 or H3K36me2 antibodies under normal and heat stressed condition would be useful to test such hypothesis. Hsp90, initially discovered as a cytoplasmic chaperone, is found to play several functions at the nucleus, particularly at the chromatin (68, 70-73, 111, 120). Although chromosomal occupancy of Hsp90 or its role in modulating chromatin dynamics, which is its non-canonical function, has not been reported in any of the protozoan parasites. It is noteworthy that Hsp90 itself is not a DNA binding protein. Thus its occupancy at various DNA elements must be via interactions with other DNA binding proteins. At this point the identity of such DNA binding protein(s) remains elusive. Nonetheless, this is the first report that demonstrates a noncanonical function of Hsp90 in *Plasmodium* biology and provides evidence not only for its recruitment at the PfSIR2 promoter-proximal region but also its probable action as a transcriptional repressor. Other components of such repressor complex that along with PfHsp90 are involved in transcriptional repression are yet to be identified in this parasite. Taken together, the two components of this study establish the chaperoning function and the moonlighting function of Hsp90 in *Plasmodium* biology. Our data provides evidence for its canonical function in providing stability to its client protein PfRad51. Hence, our findings open up new avenues of research to target both the DNA repair machinery and the Hsp90 chaperone system for arresting parasite growth and suggest new drug combination therapy for malaria treatment. This work also reports the non-canonical function of PfHsp90 in transcriptional regulation of the chromatin modifier *PfSIR2*. Since PfSir2A &B play key roles in the silencing of the *var* genes and ensures mono-allelic expression of the virulence genes, insufficient amount of Sir2 protein is likely to de-repress the *var* genes and thereby, results in the non-mutually exclusive expression of multiple *var* genes at the same time. This would express a large number, if not the entire *var* repertoire to the host immune-system and limits the parasite's ability of immune evasion through antigenic variation. Thus, understanding the molecular mechanism underlying *PfSIR2* gene regulation might offer novel targets and intervention strategies for limiting antigenic variation and vaccine development to curb malaria. In conclusion, this work unravels two important functions of PfHsp90 in *Plasmodium* chromatin biology- in maintain genome integrity, and in regulating genome expression. Both of these crucial processes of parasite biology can be exploited to develop novel strategies to tackle malaria.

References



- 1. https://www.who.int/news-room/fact-sheets/detail/malaria. 2021.
- 2. Kokwaro G. 2009. Ongoing challenges in the management of malaria. Malar J 8 Suppl 1:S2.
- Killeen GF, Masalu JP, Chinula D, Fotakis EA, Kavishe DR, Malone D, Okumu F. 2017.
 Control of Malaria Vector Mosquitoes by Insecticide-Treated Combinations of Window
 Screens and Eave Baffles. Emerg Infect Dis 23:782-789.
- 4. https://www.malariaconsortium.org/media-downloads/19/Insecticides%20Fact%20Sheet.
- Miotto O, Almagro-Garcia J, Manske M, Macinnis B, Campino S, Rockett KA, Amaratunga C, Lim P, Suon S, Sreng S, Anderson JM, Duong S, Nguon C, Chuor CM, Saunders D, Se Y, Lon C, Fukuda MM, Amenga-Etego L, Hodgson AV, Asoala V, Imwong M, Takala-Harrison S, Nosten F, Su XZ, Ringwald P, Ariey F, Dolecek C, Hien TT, Boni MF, Thai CQ, Amambua-Ngwa A, Conway DJ, Djimdé AA, Doumbo OK, Zongo I, Ouedraogo JB, Alcock D, Drury E, Auburn S, Koch O, Sanders M, Hubbart C, Maslen G, Ruano-Rubio V, Jyothi D, Miles A, O'Brien J, Gamble C, Oyola SO, et al. 2013. Multiple populations of artemisinin-resistant Plasmodium falciparum in Cambodia. Nat Genet 45:648-55.
- 6. Dondorp AM, Nosten F, Yi P, Das D, Phyo AP, Tarning J, Lwin KM, Ariey F, Hanpithakpong W, Lee SJ, Ringwald P, Silamut K, Imwong M, Chotivanich K, Lim P, Herdman T, An SS, Yeung S, Singhasivanon P, Day NP, Lindegardh N, Socheat D, White NJ. 2009. Artemisinin resistance in Plasmodium falciparum malaria. N Engl J Med 361:455-67.
- 7. Su XZ, Heatwole VM, Wertheimer SP, Guinet F, Herrfeldt JA, Peterson DS, Ravetch JA, Wellems TE. 1995. The large diverse gene family var encodes proteins involved in cytoadherence and antigenic variation of Plasmodium falciparum-infected erythrocytes. Cell 82:89-100.
- 8. Smith JD, Chitnis CE, Craig AG, Roberts DJ, Hudson-Taylor DE, Peterson DS, Pinches R, Newbold CI, Miller LH. 1995. Switches in expression of Plasmodium falciparum var genes correlate with changes in antigenic and cytoadherent phenotypes of infected erythrocytes. Cell 82:101-10.



- Baruch DI, Pasloske BL, Singh HB, Bi X, Ma XC, Feldman M, Taraschi TF, Howard RJ. 1995.
 Cloning the P. falciparum gene encoding PfEMP1, a malarial variant antigen and adherence receptor on the surface of parasitized human erythrocytes. Cell 82:77-87.
- Scherf A, Hernandez-Rivas R, Buffet P, Bottius E, Benatar C, Pouvelle B, Gysin J, Lanzer M.
 1998. Antigenic variation in malaria: in situ switching, relaxed and mutually exclusive transcription of var genes during intra-erythrocytic development in Plasmodium falciparum.
 Embo j 17:5418-26.
- 11. Chan JA, Howell KB, Reiling L, Ataide R, Mackintosh CL, Fowkes FJ, Petter M, Chesson JM, Langer C, Warimwe GM, Duffy MF, Rogerson SJ, Bull PC, Cowman AF, Marsh K, Beeson JG. 2012. Targets of antibodies against Plasmodium falciparum-infected erythrocytes in malaria immunity. J Clin Invest 122:3227-38.
- 12. Bull PC, Lowe BS, Kortok M, Molyneux CS, Newbold CI, Marsh K. 1998. Parasite antigens on the infected red cell surface are targets for naturally acquired immunity to malaria. Nat Med 4:358-60.
- Ofori MF, Dodoo D, Staalsoe T, Kurtzhals JA, Koram K, Theander TG, Akanmori BD, Hviid
 L. 2002. Malaria-induced acquisition of antibodies to Plasmodium falciparum variant surface
 antigens. Infect Immun 70:2982-8.
- 14. Rénia L, Goh YS. 2016. Malaria Parasites: The Great Escape. Front Immunol 7:463.
- 15. Miller LH, Baruch DI, Marsh K, Doumbo OK. 2002. The pathogenic basis of malaria. Nature 415:673-9.
- Smalley ME, Abdalla S, Brown J. 1981. The distribution of Plasmodium falciparum in the peripheral blood and bone marrow of Gambian children. Trans R Soc Trop Med Hyg 75:103-5.
- 17. Farfour E, Charlotte F, Settegrana C, Miyara M, Buffet P. 2012. The extravascular compartment of the bone marrow: a niche for Plasmodium falciparum gametocyte maturation?

 Malar J 11:285.



- 18. Joice R, Nilsson SK, Montgomery J, Dankwa S, Egan E, Morahan B, Seydel KB, Bertuccini L, Alano P, Williamson KC, Duraisingh MT, Taylor TE, Milner DA, Marti M. 2014. Plasmodium falciparum transmission stages accumulate in the human bone marrow. Sci Transl Med 6:244re5.
- Carlson J, Helmby H, Hill AV, Brewster D, Greenwood BM, Wahlgren M. 1990. Human cerebral malaria: association with erythrocyte rosetting and lack of anti-rosetting antibodies. Lancet 336:1457-60.
- 20. Rowe JA, Moulds JM, Newbold CI, Miller LH. 1997. P. falciparum rosetting mediated by a parasite-variant erythrocyte membrane protein and complement-receptor 1. Nature 388:292-5.
- 21. Roberts DJ, Pain A, Kai O, Kortok M, Marsh K. 2000. Autoagglutination of malaria-infected red blood cells and malaria severity. Lancet 355:1427-8.
- 22. Miller LH, Good MF, Milon G. 1994. Malaria pathogenesis. Science 264:1878-83.
- 23. Otto TD, Böhme U, Sanders M, Reid A, Bruske EI, Duffy CW, Bull PC, Pearson RD, Abdi A, Dimonte S, Stewart LB, Campino S, Kekre M, Hamilton WL, Claessens A, Volkman SK, Ndiaye D, Amambua-Ngwa A, Diakite M, Fairhurst RM, Conway DJ, Franck M, Newbold CI, Berriman M. 2018. Long read assemblies of geographically dispersed Plasmodium falciparum isolates reveal highly structured subtelomeres. Wellcome Open Res 3:52.
- 24. Gardner MJ, Hall N, Fung E, White O, Berriman M, Hyman RW, Carlton JM, Pain A, Nelson KE, Bowman S, Paulsen IT, James K, Eisen JA, Rutherford K, Salzberg SL, Craig A, Kyes S, Chan MS, Nene V, Shallom SJ, Suh B, Peterson J, Angiuoli S, Pertea M, Allen J, Selengut J, Haft D, Mather MW, Vaidya AB, Martin DM, Fairlamb AH, Fraunholz MJ, Roos DS, Ralph SA, McFadden GI, Cummings LM, Subramanian GM, Mungall C, Venter JC, Carucci DJ, Hoffman SL, Newbold C, Davis RW, Fraser CM, Barrell B. 2002. Genome sequence of the human malaria parasite Plasmodium falciparum. Nature 419:498-511.
- 25. Kraemer SM, Kyes SA, Aggarwal G, Springer AL, Nelson SO, Christodoulou Z, Smith LM, Wang W, Levin E, Newbold CI, Myler PJ, Smith JD. 2007. Patterns of gene recombination



- shape var gene repertoires in Plasmodium falciparum: comparisons of geographically diverse isolates.

 BMC Genomics 8:45.
- 26. Tonkin CJ, Carret CK, Duraisingh MT, Voss TS, Ralph SA, Hommel M, Duffy MF, Silva LM, Scherf A, Ivens A, Speed TP, Beeson JG, Cowman AF. 2009. Sir2 paralogues cooperate to regulate virulence genes and antigenic variation in Plasmodium falciparum. PLoS Biol 7:e84
- 27. Kyes S, Christodoulou Z, Pinches R, Kriek N, Horrocks P, Newbold C. 2007. Plasmodium falciparum var gene expression is developmentally controlled at the level of RNA polymerase II-mediated transcription initiation. Mol Microbiol 63:1237-47.
- 28. Gardner JP, Pinches RA, Roberts DJ, Newbold CI. 1996. Variant antigens and endothelial receptor adhesion in Plasmodium falciparum. Proc Natl Acad Sci U S A 93:3503-8.
- Chen Q, Fernandez V, Sundström A, Schlichtherle M, Datta S, Hagblom P, Wahlgren M. 1998.
 Developmental selection of var gene expression in Plasmodium falciparum. Nature 394:392-5.
- Kyes S, Pinches R, Newbold C. 2000. A simple RNA analysis method shows var and rif multigene family expression patterns in Plasmodium falciparum. Mol Biochem Parasitol 105:311-5.
- 31. Taylor HM, Kyes SA, Harris D, Kriek N, Newbold CI. 2000. A study of var gene transcription in vitro using universal var gene primers. Mol Biochem Parasitol 105:13-23.
- 32. Bártfai R, Hoeijmakers WA, Salcedo-Amaya AM, Smits AH, Janssen-Megens E, Kaan A, Treeck M, Gilberger TW, Françoijs KJ, Stunnenberg HG. 2010. H2A.Z demarcates intergenic regions of the plasmodium falciparum epigenome that are dynamically marked by H3K9ac and H3K4me3. PLoS Pathog 6:e1001223.
- 33. Petter M, Lee CC, Byrne TJ, Boysen KE, Volz J, Ralph SA, Cowman AF, Brown GV, Duffy MF. 2011. Expression of P. falciparum var genes involves exchange of the histone variant H2A.Z at the promoter. PLoS Pathog 7:e1001292.
- 34. Lopez-Rubio JJ, Gontijo AM, Nunes MC, Issar N, Hernandez Rivas R, Scherf A. 2007. 5' flanking region of var genes nucleate histone modification patterns linked to phenotypic inheritance of virulence traits in malaria parasites. Mol Microbiol 66:1296-305.



- 35. Duraisingh MT, Voss TS, Marty AJ, Duffy MF, Good RT, Thompson JK, Freitas-Junior LH, Scherf A, Crabb BS, Cowman AF. 2005. Heterochromatin silencing and locus repositioning linked to regulation of virulence genes in Plasmodium falciparum. Cell 121:13-24.
- 36. Freitas-Junior LH, Hernandez-Rivas R, Ralph SA, Montiel-Condado D, Ruvalcaba-Salazar OK, Rojas-Meza AP, Mâncio-Silva L, Leal-Silvestre RJ, Gontijo AM, Shorte S, Scherf A. 2005. Telomeric heterochromatin propagation and histone acetylation control mutually exclusive expression of antigenic variation genes in malaria parasites. Cell 121:25-36
- 37. Li Z, Yin S, Sun M, Cheng X, Wei J, Gilbert N, Miao J, Cui L, Huang Z, Dai X, Jiang L. 2019.
 DNA helicase RecQ1 regulates mutually exclusive expression of virulence genes in Plasmodium falciparum via heterochromatin alteration. Proc Natl Acad Sci U S A 116:3177-3182.
- 38. Kumar S, Bhardwaj TR, Prasad DN, Singh RK. 2018. Drug targets for resistant malaria: Historic to future perspectives. Biomed Pharmacother 104:8-27.
- 39. Lim L, McFadden GI. 2010. The evolution, metabolism and functions of the apicoplast. Philos Trans R Soc Lond B Biol Sci 365:749-63.
- 40. Roos DS, Crawford MJ, Donald RG, Fraunholz M, Harb OS, He CY, Kissinger JC, Shaw MK, Striepen B. 2002. Mining the Plasmodium genome database to define organellar function: what does the apicoplast do? Philos Trans R Soc Lond B Biol Sci 357:35-46.
- 41. Limenitakis J, Soldati-Favre D. 2011. Functional genetics in Apicomplexa: potentials and limits. FEBS Lett 585:1579-88.
- 42. Ralph SA, D'Ombrain MC, McFadden GI. 2001. The apicoplast as an antimalarial drug target.

 Drug Resist Updat 4:145-51.
- 43. Foth BJ, Ralph SA, Tonkin CJ, Struck NS, Fraunholz M, Roos DS, Cowman AF, McFadden GI. 2003. Dissecting apicoplast targeting in the malaria parasite Plasmodium falciparum. Science 299:705-8.
- 44. Goodman CD, Buchanan HD, McFadden GI. 2017. Is the Mitochondrion a Good Malaria Drug
 Target? Trends Parasitol 33:185-193.



- 45. Frankenberg-Schwager M. 1990. Induction, repair and biological relevance of radiation-induced DNA lesions in eukaryotic cells. Radiat Environ Biophys 29:273-92.
- 46. Golgi C. 1886. Sull'infezione malarica. Arch Sci Med (Torino) 10: 109-134.
- 47. Oakley MS, Kumar S, Anantharaman V, Zheng H, Mahajan B, Haynes JD, Moch JK, Fairhurst R, McCutchan TF, Aravind L. 2007. Molecular factors and biochemical pathways induced by febrile temperature in intraerythrocytic Plasmodium falciparum parasites. Infect Immun 75:2012-25.
- 48. Pavithra SR, Banumathy G, Joy O, Singh V, Tatu U. 2004. Recurrent fever promotes Plasmodium falciparum development in human erythrocytes. J Biol Chem 279:46692-9.
- 49. Kwiatkowski D. 1989. Febrile temperatures can synchronize the growth of Plasmodium falciparum in vitro. J Exp Med 169:357-61.
- 50. Oakley MS, Gerald N, McCutchan TF, Aravind L, Kumar S. 2011. Clinical and molecular aspects of malaria fever. Trends Parasitol 27:442-9.
- Karagöz GE, Rüdiger SG. 2015. Hsp90 interaction with clients. Trends Biochem Sci 40:117 25.
- 52. Jego G, Hazoumé A, Seigneuric R, Garrido C. 2013. Targeting heat shock proteins in cancer.

 Cancer Lett 332:275-85.
- 53. Calderwood SK, Repasky EA, Neckers L, Hightower LE. 2019. The IXth CSSI international symposium on heat shock proteins in biology and medicine: stress responses in health and disease: Alexandria Old Town, Alexandria, Virginia, November 10-13, 2018. Cell Stress Chaperones 24:1-6.
- 54. Picard D. 2002. Heat-shock protein 90, a chaperone for folding and regulation. Cell Mol Life Sci 59:1640-8.
- 55. Hoter A, El-Sabban ME, Naim HY. 2018. The HSP90 Family: Structure, Regulation, Function, and Implications in Health and Disease. Int J Mol Sci 19.
- 56. Dubrez L, Causse S, Borges Bonan N, Dumétier B, Garrido C. 2020. Heat-shock proteins: chaperoning DNA repair. Oncogene 39:516-529.



- 57. Schopf FH, Biebl MM, Buchner J. 2017. The HSP90 chaperone machinery. Nat Rev Mol Cell Biol 18:345-360.
- 58. Gupta RS. 1995. Phylogenetic analysis of the 90 kD heat shock family of protein sequences and an examination of the relationship among animals, plants, and fungi species. Mol Biol Evol 12:1063-73.
- Biebl MM, Buchner J. 2019. Structure, Function, and Regulation of the Hsp90 Machinery. Cold
 Spring Harb Perspect Biol 11.
- 60. Khurana N, Bhattacharyya S. 2015. Hsp90, the concertmaster: tuning transcription. Front Oncol 5:100.
- 61. Theodoraki MA, Caplan AJ. 2012. Quality control and fate determination of Hsp90 client proteins. Biochim Biophys Acta 1823:683-8.
- Mayer MP, Bukau B. 1999. Molecular chaperones: the busy life of Hsp90. Curr Biol 9:R322-5.
- 63. Gvozdenov Z, Kolhe J, Freeman BC. 2019. The Nuclear and DNA-Associated Molecular Chaperone Network. Cold Spring Harb Perspect Biol 11.
- 64. Cheng AN, Fan CC, Lo YK, Kuo CL, Wang HC, Lien IH, Lin SY, Chen CH, Jiang SS, Chang IS, Juan HF, Lyu PC, Lee AY. 2017. Cdc7-Dbf4-mediated phosphorylation of HSP90-S164 stabilizes HSP90-HCLK2-MRN complex to enhance ATR/ATM signaling that overcomes replication stress in cancer. Sci Rep 7:17024.
- 65. Suhane T, Laskar S, Advani S, Roy N, Varunan S, Bhattacharyya D, Bhattacharyya S, Bhattacharyya MK. 2015. Both the charged linker region and ATPase domain of Hsp90 are essential for Rad51-dependent DNA repair. Eukaryot Cell 14:64-77.
- 66. Oda T, Hayano T, Miyaso H, Takahashi N, Yamashita T. 2007. Hsp90 regulates the Fanconi anemia DNA damage response pathway. Blood 109:5016-26.
- 67. Bhattacharyya S, Keirsey J, Russell B, Kavecansky J, Lillard-Wetherell K, Tahmaseb K, Turchi JJ, Groden J. 2009. Telomerase-associated protein 1, HSP90, and topoisomerase IIalpha



- associate directly with the BLM helicase in immortalized cells using ALT and modulate its helicase activity using telomeric DNA substrates. J Biol Chem 284:14966-77.
- 68. Hamamoto R, Silva FP, Tsuge M, Nishidate T, Katagiri T, Nakamura Y, Furukawa Y. 2006. Enhanced SMYD3 expression is essential for the growth of breast cancer cells. Cancer Sci 97:113-8.
- 69. Hamamoto R, Furukawa Y, Morita M, Iimura Y, Silva FP, Li M, Yagyu R, Nakamura Y. 2004. SMYD3 encodes a histone methyltransferase involved in the proliferation of cancer cells. Nat Cell Biol 6:731-40.
- 70. Brown MA, Foreman K, Harriss J, Das C, Zhu L, Edwards M, Shaaban S, Tucker H. 2015. C-terminal domain of SMYD3 serves as a unique HSP90-regulated motif in oncogenesis. Oncotarget 6:4005-19.
- 71. Laskar S, K S, Bhattacharyya MK, Nair AS, Dhar P, Bhattacharyya S. 2015. Heat stress-induced Cup9-dependent transcriptional regulation of SIR2. Mol Cell Biol 35:437-50.
- 72. Tariq M, Nussbaumer U, Chen Y, Beisel C, Paro R. 2009. Trithorax requires Hsp90 for maintenance of active chromatin at sites of gene expression. Proc Natl Acad Sci U S A 106:1157-62.
- 73. Sawarkar R, Sievers C, Paro R. 2012. Hsp90 globally targets paused RNA polymerase to regulate gene expression in response to environmental stimuli. Cell 149:807-18.
- 74. Floer M, Bryant GO, Ptashne M. 2008. HSP90/70 chaperones are required for rapid nucleosome removal upon induction of the GAL genes of yeast. Proc Natl Acad Sci U S A 105:2975-80.
- 75. Daniyan MO, Przyborski JM, Shonhai A. 2019. Partners in Mischief: Functional Networks of Heat Shock Proteins of Plasmodium falciparum and Their Influence on Parasite Virulence. Biomolecules 9.
- 76. Shahinas D, Folefoc A, Pillai DR. 2013. Targeting Plasmodium falciparum Hsp90: Towards Reversing Antimalarial Resistance. Pathogens 2:33-54.



- 77. Stofberg ML, Caillet C, de Villiers M, Zininga T. 2021. Inhibitors of the Plasmodium falciparum Hsp90 towards Selective Antimalarial Drug Design: The Past, Present and Future. Cells 10.
- 78. Shonhai A. 2010. Plasmodial heat shock proteins: targets for chemotherapy. FEMS Immunol Med Microbiol 58:61-74.
- 79. Banumathy G, Singh V, Pavithra SR, Tatu U. 2003. Heat shock protein 90 function is essential for Plasmodium falciparum growth in human erythrocytes. J Biol Chem 278:18336-45.
- 80. Kumar R, Musiyenko A, Barik S. 2003. The heat shock protein 90 of Plasmodium falciparum and antimalarial activity of its inhibitor, geldanamycin. Malar J 2:30.
- 81. Kumar R, Pavithra SR, Tatu U. 2007. Three-dimensional structure of heat shock protein 90 from Plasmodium falciparum: molecular modelling approach to rational drug design against malaria. J Biosci 32:531-6.
- 82. Corbett KD, Berger JM. 2010. Structure of the ATP-binding domain of Plasmodium falciparum Hsp90. Proteins 78:2738-44.
- 83. Murillo-Solano C, Dong C, Sanchez CG, Pizarro JC. 2017. Identification and characterization of the antiplasmodial activity of Hsp90 inhibitors. Malar J 16:292.
- 84. Chalapareddy S, Bhattacharyya MK, Mishra S, Bhattacharyya S. 2014. Radicicol confers midschizont arrest by inhibiting mitochondrial replication in Plasmodium falciparum. Antimicrob Agents Chemother 58:4341-52.
- 85. Pallavi R, Roy N, Nageshan RK, Talukdar P, Pavithra SR, Reddy R, Venketesh S, Kumar R, Gupta AK, Singh RK, Yadav SC, Tatu U. 2010. Heat shock protein 90 as a drug target against protozoan infections: biochemical characterization of HSP90 from Plasmodium falciparum and Trypanosoma evansi and evaluation of its inhibitor as a candidate drug. J Biol Chem 285:37964-75.
- 86. Wider D, Péli-Gulli MP, Briand PA, Tatu U, Picard D. 2009. The complementation of yeast with human or Plasmodium falciparum Hsp90 confers differential inhibitor sensitivities. Mol Biochem Parasitol 164:147-52.



- 87. Kumar R, Musiyenko A, Barik S. 2005. Plasmodium falciparum calcineurin and its association with heat shock protein 90: mechanisms for the antimalarial activity of cyclosporin A and synergism with geldanamycin. Mol Biochem Parasitol 141:29-37.
- 88. Milan D, Griffith J, Su M, Price ER, McKeon F. 1994. The latch region of calcineurin B is involved in both immunosuppressant-immunophilin complex docking and phosphatase activation. Cell 79:437-47.
- 89. Prusty D, Mehra P, Srivastava S, Shivange AV, Gupta A, Roy N, Dhar SK. 2008. Nicotinamide inhibits Plasmodium falciparum Sir2 activity in vitro and parasite growth. FEMS Microbiol Lett 282:266-72.
- 90. Kirsten Moll AK, Arthur Scherf and Mats Wahlgren. 2013. METHODS IN MALARIA RESEARCH, 6 ed.
- 91. Bozdech Z, Mok S, Gupta AP. 2013. DNA microarray-based genome-wide analyses of Plasmodium parasites. Methods Mol Biol 923:189-211.
- 92. Giresi PG, Lieb JD. 2009. Isolation of active regulatory elements from eukaryotic chromatin using FAIRE (Formaldehyde Assisted Isolation of Regulatory Elements). Methods 48:233-9.
- 93. Ponts N, Harris EY, Prudhomme J, Wick I, Eckhardt-Ludka C, Hicks GR, Hardiman G, Lonardi S, Le Roch KG. 2010. Nucleosome landscape and control of transcription in the human malaria parasite. Genome Res 20:228-38.
- 94. Whitesell L, Lindquist SL. 2005. HSP90 and the chaperoning of cancer. Nat Rev Cancer 5:761-72.
- 95. Lee AH, Symington LS, Fidock DA. 2014. DNA repair mechanisms and their biological roles in the malaria parasite Plasmodium falciparum. Microbiol Mol Biol Rev 78:469-86.
- 96. Roy N, Bhattacharyya S, Chakrabarty S, Laskar S, Babu SM, Bhattacharyya MK. 2014.
 Dominant negative mutant of Plasmodium Rad51 causes reduced parasite burden in host by abrogating DNA double-strand break repair. Mol Microbiol 94:353-66.
- 97. Namsaraev E, Berg P. 1997. Characterization of strand exchange activity of yeast Rad51 protein. Mol Cell Biol 17:5359-68.



- 98. Bhattacharyya MK, Kumar N. 2003. Identification and molecular characterisation of DNA damaging agent induced expression of Plasmodium falciparum recombination protein PfRad51. Int J Parasitol 33:1385-92.
- 99. Bhattacharyya MK, Bhattacharyya nee Deb S, Jayabalasingham B, Kumar N. 2005. Characterization of kinetics of DNA strand-exchange and ATP hydrolysis activities of recombinant PfRad51, a Plasmodium falciparum recombinase. Mol Biochem Parasitol 139:33-9
- 100. Vydyam P, Dutta D, Sutram N, Bhattacharyya S, Bhattacharyya MK. 2019. A small-molecule inhibitor of the DNA recombinase Rad51 from Plasmodium falciparum synergizes with the antimalarial drugs artemisinin and chloroquine. J Biol Chem 294:8171-8183.
- 101. Bagatell R, Beliakoff J, David CL, Marron MT, Whitesell L. 2005. Hsp90 inhibitors deplete key anti-apoptotic proteins in pediatric solid tumor cells and demonstrate synergistic anticancer activity with cisplatin. Int J Cancer 113:179-88.
- 102. Pennisi R, Ascenzi P, di Masi A. 2016. Correction: Pennisi, R., et al. Hsp90: A New Player in DNA Repair? Biomolecules 2015, 5, 2589-2618. Biomolecules 6.
- 103. Suhane T, Bindumadhavan V, Fangaria N, Nair AS, Tabassum W, Muley P, Bhattacharyya MK, Bhattacharyya S. 2019. Glu-108 in Saccharomyces cerevisiae Rad51 Is Critical for DNA Damage-Induced Nuclear Function. mSphere 4.
- 104. Nathan DF, Lindquist S. 1995. Mutational analysis of Hsp90 function: interactions with a steroid receptor and a protein kinase. Mol Cell Biol 15:3917-25.
- 105. Wiseman H, Halliwell B. 1996. Damage to DNA by reactive oxygen and nitrogen species: role in inflammatory disease and progression to cancer. Biochem J 313 (Pt 1):17-29.
- 106. Cadet J, Sage E, Douki T. 2005. Ultraviolet radiation-mediated damage to cellular DNA. Mutat Res 571:3-17.
- 107. Tashiro S, Walter J, Shinohara A, Kamada N, Cremer T. 2000. Rad51 accumulation at sites of DNA damage and in postreplicative chromatin. J Cell Biol 150:283-91.



- 108. Suthram N, Padhi S, Jha P, Bhattacharyya S, Bulusu G, Roy A, Bhattacharyya MK. 2020.
 Elucidation of DNA Repair Function of PfBlm and Potentiation of Artemisinin Action by a
 Small-Molecule Inhibitor of RecQ Helicase. mSphere 5.
- 109. Constant JF, O'Connor TR, Lhomme J, Laval J. 1988. 9-[(10-(aden-9-yl)-4,8-diazadecyl)amino]-6-chloro-2-methoxy-acridine incises DNA at apurinic sites. Nucleic Acids Res 16:2691-703.
- 110. Figueiredo L, Scherf A. 2005. Plasmodium telomeres and telomerase: the usual actors in an unusual scenario. Chromosome Res 13:517-24.
- 111. Laskar S, Bhattacharyya MK, Shankar R, Bhattacharyya S. 2011. HSP90 controls SIR2 mediated gene silencing. PLoS One 6:e23406.
- 112. Francis SE, Sullivan DJ, Jr., Goldberg DE. 1997. Hemoglobin metabolism in the malaria parasite Plasmodium falciparum. Annu Rev Microbiol 51:97-123.
- 113. Lobo I. 2008. Environmental Influences on Gene Expression. Nature Education 1(1):39.
- 114. Vinci MC. 2012. Sensing the Environment: Epigenetic Regulation of Gene Expression. Journal of Physical Chemistry & Biophysics S3:001.
- 115. Deshmukh AS, Srivastava S, Herrmann S, Gupta A, Mitra P, Gilberger TW, Dhar SK. 2012. The role of N-terminus of Plasmodium falciparum ORC1 in telomeric localization and var gene silencing. Nucleic Acids Res 40:5313-31.
- 116. Merrick CJ, Jiang RH, Skillman KM, Samarakoon U, Moore RM, Dzikowski R, Ferdig MT, Duraisingh MT. 2015. Functional analysis of sirtuin genes in multiple Plasmodium falciparum strains. PLoS One 10:e0118865.
- 117. Salanti A, Staalsoe T, Lavstsen T, Jensen AT, Sowa MP, Arnot DE, Hviid L, Theander TG.
 2003. Selective upregulation of a single distinctly structured var gene in chondroitin sulphate
 A-adhering Plasmodium falciparum involved in pregnancy-associated malaria. Mol Microbiol 49:179-91.



- 118. Kafsack BF, Rovira-Graells N, Clark TG, Bancells C, Crowley VM, Campino SG, Williams AE, Drought LG, Kwiatkowski DP, Baker DA, Cortés A, Llinás M. 2014. A transcriptional switch underlies commitment to sexual development in malaria parasites. Nature 507:248-52.
- 119. Karmodiya K, Pradhan SJ, Joshi B, Jangid R, Reddy PC, Galande S. 2015. A comprehensive epigenome map of Plasmodium falciparum reveals unique mechanisms of transcriptional regulation and identifies H3K36me2 as a global mark of gene suppression. Epigenetics Chromatin 8:32.
- 120. Sawarkar R, Paro R. 2013. Hsp90@chromatin.nucleus: an emerging hub of a networker. Trends

 Cell Biol 23:193-201.
- 121. Seraphim TV, Chakafana G, Shonhai A, Houry WA. 2019. Plasmodium falciparum R2TP complex: driver of parasite Hsp90 function. Biophys Rev 11:1007-1015.
- 122. Bayih AG, Pillai DR. 2014. Mouse studies on inhibitors of Plasmodium falciparum Hsp90: progress and challenges. Parasitology 141:1216-22.
- 123. Chua CS, Low H, Sim TS. 2014. Co-chaperones of Hsp90 in Plasmodium falciparum and their concerted roles in cellular regulation. Parasitology 141:1177-91
- 124. Ramdhave AS, Patel D, Ramya I, Nandave M, Kharkar PS. 2013. Targeting heat shock protein 90 for malaria. Mini Rev Med Chem 13:1903-20.
- 125. Tabassum W, Singh P, Suthram N, Bhattacharyya S, Bhattacharyya MK. 2021. Synergistic Action between PfHsp90 Inhibitor and PfRad51 Inhibitor Induces Elevated DNA Damage Sensitivity in the Malaria Parasite. Antimicrob Agents Chemother 65:e0045721.
- 126. Khurana N, Laskar S, Bhattacharyya MK, Bhattacharyya S. 2016. Hsp90 induces increased genomic instability toward DNA-damaging agents by tuning down RAD53 transcription. Mol Biol Cell 27:2463-78.
- 127. Haltiwanger BM, Matsumoto Y, Nicolas E, Dianov GL, Bohr VA, Taraschi TF. 2000. DNA base excision repair in human malaria parasites is predominantly by a long-patch pathway. Biochemistry 39:763-72.



- 128. Tajedin L, Anwar M, Gupta D, Tuteja R. 2015. Comparative insight into nucleotide excision repair components of Plasmodium falciparum. DNA Repair (Amst) 28:60-72.
- 129. Tarique M, Ahmad M, Chauhan M, Tuteja R. 2017. Genome Wide In silico Analysis of the Mismatch Repair Components of Plasmodium falciparum and Their Comparison with Human Host. Front Microbiol 8:130.
- 130. Merrick CJ, Huttenhower C, Buckee C, Amambua-Ngwa A, Gomez-Escobar N, Walther M, Conway DJ, Duraisingh MT. 2012. Epigenetic dysregulation of virulence gene expression in severe Plasmodium falciparum malaria. J Infect Dis 205:1593-600.
- 131. Chen PB, Ding S, Zanghì G, Soulard V, DiMaggio PA, Fuchter MJ, Mecheri S, Mazier D, Scherf A, Malmquist NA. 2016. Plasmodium falciparum PfSET7: enzymatic characterization and cellular localization of a novel protein methyltransferase in sporozoite, liver and erythrocytic stage parasites. Sci Rep 6:21802.
- 132. Chookajorn T, Dzikowski R, Frank M, Li F, Jiwani AZ, Hartl DL, Deitsch KW. 2007. Epigenetic memory at malaria virulence genes. Proc Natl Acad Sci U S A 104:899-902.

Appendix



Synopsis

Malaria caused by the protozoan parasite, *Plasmodium* continues to be one of the most life threatening disease responsible for millions of death every year. Among the five species known to infect humans, *P.falciparum* is responsible for the most severe form of malaria. It is spread by bite of infected female anopheles mosquito. Complex life cycle of the parasite, its ability to exhibit the antigenic variation, emergence of drug resistance in the parasite to the known antimalarial drugs, lack of any potent vaccine and increasing insecticide resistance in the mosquitoes are the hurdles in curbing malaria. The ability of the parasite to elicit the phenomenon of antigenic variation and evade host immune response has made eradication of malaria difficult. Antigenic variation is the strategy by which parasite exhibits mono-allelic expression of the virulence (var) gene. The ability of parasite to express only one var gene at a particular time out of 59 copy present and to switch its expression, enables the parasite to evade the host immune response (1-4). The expression of var gene is known to be regulated by the histone deacetylase PfSir2. The two paralogues of PfSir2 reported in *Plasmodium* biology are PfSir2A and PfSir2B (5). The RBC infected by the parasite possess a knob like structure, PfEmp1 molecule (encoded by var gene) on its surface which enables it to cling to the endothelial lining of the blood vessels and escape the splenic filtration (6). So there is a dire need to understand and explore *Plasmodium* biology in order to identify more of new drug targets.

Plasmodium during course of life cycle experiences various temperature variations and also encounters heat shock when the human host experiences fever. Several proteins responds to heat shock to combat this stress and majority among them are chaperons. Prominent among them are cytosolic chaperons. Hsp40/70 are known to be involved in folding of the nascent



peptide while Hsp90 serves as a specialised chaperon and provides additional folding to a subset of proteins (clients) required for their stability and functioning (7). This highlights the essentiality of Hsp90 in *Plasmodium* biology. In model organisms, Hsp90 has been reported to perform diverse functions (8, 9). Hsp90 interacts with its client proteins to provide it maturation, which is its canonical function. Also, it interacts with its non-client proteins to execute its non-canonical nuclear function of regulating assembly and dis-assembly of protein complexes, nuclear import and chromatin remodelling (10). In *Plasmodium* several inhibitors of Hsp90, such as Geldanamycin, 17AAG, 17-DMAG, Radicicol, has been identified which inhibit the in vitro growth of the parasite (11, 12). 17AAG has also been reported to inhibit the function of purified Hsp90 (13). In *Plasmodium* biology none of the Hsp90 clients have been identified, nor has any of its non-canonical functions reported. In this study we aimed to study the clientship of PfHsp90 and explore its nuclear functions with a view of targeting the chaperon machinery to curb malaria.

Majority of Hsp90 clients are signalling kinases, transcription factors, and DNA repair proteins (10, 14-16). In *Plasmodium* biology signalling kinases which has been identified are very poorly conserved and there is a paucity of transcription factors (17). As DNA repair proteins has been identified and very well characterised (18-22), so we started our quest to discover the first client of PfHsp90 with DNA repair proteins. HR pathway is the predominant repair pathway and its loss can cannot be compensated by any other pathway, inhibition of Rad51 by small molecule inhibitor B02 leads to abrogation of repair of the *Plasmodium* genome (18, 19, 21, 23). The DNA repair protein Rad51 in model organism yeast has been reported to be client of Hsp90 (15) and its ortholog in *Plasmodium* has been characterised (18, 19). So in first part of my study, I was interested in investigating whether PfRad51 is a client of PfHsp90. To this end, three objectives were framed: First, whether PfRad51 interacts with PfHsp90? Second,



whether PfRad51 is depleted upon inhibition of PfHsp90? Third, whether DSB repair function of PfRad51 is lost upon inhibition of PfHsp90. To investigate whether PfRad51 interacts with PfHsp90, yeast two hybrid analysis was performed. For which *PfHSP90* was cloned in bait vector and *PfRAD51* in prey vector and transformed in yeast strain PJ694a. Their interaction was scored in SC- Leu- Ura- His and SC- Leu- Ura- Ade plates. It was observed that yeast strain harbouring both PfRad51 and PfHsp90 was able to activate both the reporter genes, HIS and ADE suggesting strong interaction. Further, CoIP was performed to ascertain the interaction using the parasite lysate. Anti Rad51 antibody was used for pull down and PfHsp90 was also found to be co-immunoprecipitated, confirming the interaction of PfHsp90 and PfRad51. The next objective was to study the effect of PfHsp90 inhibition upon the steady state of PfRad51. To investigate this the parasite culture was treated with different concentrations of 17AAG. Ideally, when Hsp90 is inhibited its client proteins tend to undergo depletion and through western blot analysis similar result was observed, with increasing concentration of 17AAG treatment to the parasite culture there was dose dependent depletion of PfRad51. Reports suggest that when Hsp90 is inhibited its clients undergo proteasomal degradation (24). In order to investigate whether PfRad51 undergo proteasomal degradation upon PfHsp90 inhibition, the parasite culture was treated with MG132 (inhibitor of proteasomal degradation pathway) along with 17AAG. Through western blot analysis it was observed that PfRad51 level were restored upon PfHsp90 inhibition in the presence of MG132. This suggest that upon PfHsp90 inhibition i.e., on treatment with 17AAG, PfRad51 undergo proteasomal degradation and activity of PfHsp90 is required for the stability of PfRad51. To further support this finding PfRad51 was expressed in yeast temperature sensitive strain of Hsp90, iG170D hsp82 and the steady state of PfRad51was then compared when yeast culture were grown under permissive and restrictive temperatures. It was observed that PfRad51 is stable when the yeast strain is



grown at permissive temperature 25°C but it loses its stability when the yeast strain was grown at restrictive temperature of 37°C. This further strengthen the finding that inhibition of Hsp90 leads to loss of stability of PfRad51. The third objective was to probe into the effect of PfHsp90 inhibition on DNA repair activity of PfRad51. So to monitor this, the effect of 17AAG on the repair kinetics of the damaged *Plasmodium* genome upon UV irradiation was analysed. To investigate this, P. falciparum in-vitro culture was exposed to UV (100/m²) to induce genome wide DNA damage and allowed for recovery and then kinetics DSB repair was monitored using highly sensitive PCR based DNA repair Assay. Previous reports from our laboratory suggest that parasite exposed to UV irradiation require 24 hours to repair the damage and this repair is hindered if Rad51is inhibited by B02 (22). Similarly, in this study it was observed that parasite were unable to repair its damaged DNA in 24 hours when treated with 17AAG on UV exposure. This indicated that the DNA repair activity of PfRad51is abrogated upon PfHsp90 inhibition by 17AAG. We were also curious to investigate the effect PfHsp90 inhibition on MMS induced DNA repair activity of PfRad51. To monitor this, the effect of 17AAG treatment on MMS induced cytotoxicity was determined. For this, parasite pre-treated with 17AAG and mock treated parasite were subjected to MMS and return to growth assay was performed. It was observed that there is two-fold reduction in survival of 17AAG pre-treated parasite on MMS exposure. To further ascertain the finding, dose dependent assay was performed and pre-treated the parasite with different concentration of 17AAG and also with another inhibitor of Hsp90, Radicicol and was then subjected to MMS treatment. It was noted that the increased dose of 17AAG treatment lead to increased MMS sensitivity in dose dependent manner and 30% reduction in parasite survival was observed for Radicicol treated parasite when compared to mock treated parasite. This indicates that PfHsp90 inhibition sensitizes P. falciparum to MMS induced DNA damage. As it was observed that PfRad51 and PfHsp90 interacts and inhibition



of Hsp90 leads proteasomal degradation of PfRad51, in turn abrogates its DNA repair activity. Thus it can be concluded that PfRad51 is client of PfHsp90. Implication of the study is that if PfHsp90 is inhibited by 17AAG, PfRad51 is depleted and less of Rad51 is available in the cell. So if one want to completely halt the process of HR pathway of DNA repair by inhibiting PfRad51, less of PfRad51 inhibitor will be required for the inhibition and lead to reduction in its lethal concentration.

Second part of my study was to explore the non-canonical functions of Hsp90, specifically probe into role of PfHsp90 in epigenetic regulation of *PfSIR2* transcription. In model organisms report suggests that PfHsp90 in spite of being cytoplasmic chaperon, is also present in the nucleus and perform various functions, including the regulation of assembly and dis-assembly of several chromatin modifiers (10, 25-29). In *Plasmodium*, it has been observed that the expression of var genes are regulated by heat shock (30) and PfSir2 is involved in its silencing. Also in yeast, Hsp90 has been reported to regulate heat induced down regulation of ScSir2 by modulating the transcription factor Cup9 (29). Thus it would be a great idea to explore the noncanonical function of PfHsp90 in transcription of PfSIR2. So I was curious to study whether expression of PfSIR2 is regulated by PfHsp90 and framed three objectives: First, whether PfSIR2 expression is altered in response to higher temperature? Second, whether PfSIR2 expression is guided by altered chromatin state? Third, whether PfHsp90 plays any role in altering the chromatin state? As Hsp90 has been reported to be induced by higher temperature and in model organism it has been observed that non-canonical function of Hsp90 is modulated by high temperature so the first objective was to explore whether PfSIR2 expression is a function of temperature. For this purpose PfSir2 antibody was required, so recombinant PfSIR2A was expressed and was used for antibody production. In order to investigate the effect of heat shock on *PfSIR2* expression, the different stages of parasite culture were subjected to a



higher temperature of 41 °C for two hours. The western blot analysis revealed that heat shock leads to decrease in abundance of PfSir2A protein specifically at mid ring stage by 2.2 fold, whereas it remain unaltered at other stages. Due to lack of PfSirB antibody, the impact of heat shock on Sir2B protein levels could not be monitored. Real time RT PCR analysis indicated, down-regulation in transcription of PfSIR2A and PfSIR2B both specifically at mid ring stage by 8 fold upon heat shock. As it was observed that heat shock leads to altered expression of PfSIR2A/B and PfSir2A is known to be recruited at UpsA promoter, it was further interesting to investigate whether heat shock have impact on PfSir2A recruitment at var promoter. ChIP analysis was performed and it was noted that there is 3 fold reduced recruitment of PfSir2A on var promoter UpsA upon heat shock. We were also curious to explore the effect of heat shock on the activity of PfSir2A/B. As PfSir2 is known to regulate the expression of var gene so as a read out the effect heat shock on expression of var genes was investigated. Real time RT PCR analysis indicated that majority of var gene get up-regulated upon heat shock confirming the effect of heat shock on activity of PfSir2A/B. In *Plasmodium* gene regulation is majorly governed by epigenetic modification (17, 31), so the next objective was to determine the alteration occurring in the chromatin landscape of *PfSIR2A/B* promoter upon heat shock, which is responsible for its altered expression. To monitor this, an experiment named as Formaldehyde Assisted Isolation of Regulatory Element (FAIRE) was performed. It was discovered that upon heat shock there is reduction in abundance of nucleosome free DNA of both PfSIR2A/B locus which suggested that heat shock leads to compactness of the PfSIR2A/B promoter. Next, we were curious to know what exact epigenetic modification occur at PfSIR2A/B which leads to its compactness. To probe into this, ChIP was performed with known repressor marks in *Plasmodium* biology, H3K9me3 and H3K36me2 (32-34). ChIP analysis depicted that there is increase in enrichment of H3K9me3 on PfSIR2A/B promoter region upon



heat shock. The next objective was to decipher whether heat induced down-regulation of PfSIR2A/B is mediated by PfHsp90 activity. To elucidate this, aim was to inhibit Hsp90 and determine its effect on heat induced transcriptional down-regulation of PfSIR2A/B, alteration in chromatin landscape and epigenetic modification of PfSIR2A/B promoter. In order to investigate the role of PfHsp90 in transcriptional regulation of PfSIR2A/B, mid ring stage parasite culture was treated with 17AAG to inhibit PfHsp90 and the effect of heat shock was then determined. Real time RT PCR analysis indicated that the heat induced transcription down- regulation of PfSIR2A/B does not take place when PfHsp90 is inhibited. To ascertain specificity of the finding dose dependent study was conducted and 0.5X concentration of 17AAG treatment was used and also in a set of experiment, treatment of 17AAG was given for short duration. In both the cases, partial reversal of the phenotype was noted. Inhibition of Hsp90 by another inhibitor Radicicol also prevented the transcriptional down-regulation of PfSIR2A/B upon heat shock. Thus the data suggests that heat induced transcriptional downregulation of PfSIR2A/B is mediated by PfHsp90. Further we were keen to know whether inhibition of PfHsp90 prevents the heat induced compaction of PfSIR2A/B promoter. To investigate this, FAIRE was performed after inhibiting PfHsp90 by 17AAG and Radicicol individually in different set of experiments. In both set of experiments it was observed that there is no reduction in abundance of nucleosome free DNA of PfSIR2A/B locus upon heat shock, which indicates that PfHsp90 activity is required for heat induced compaction of PfSIR2A/B promoter. ChIP analysis was also performed after inhibiting PfHsp90 by 17AAG to determine whether activity of PfHsp90 is required for heat induced epigenetic modification of PfSIR2A/B promoter. It revealed that there is complete abolishment of enrichment of H3K9me3 upon heat shock on *PfSIR2A/B* promoter suggesting the requirement of PfHsp90 activity for the process. Lastly, we were keen to investigate whether PfHsp90 play direct role



in heat induced down-regulation of *PfSIR2A/B* and is itself recruited to *PfSIR2A/B* promoter. To monitor this, ChIP analysis was performed and observed that the recruitment of PfHsp90 at immediate upstream *PfSIR2A/B* gene is increased upon heat shock. Thus, we could establish the non- canonical moonlighting function of the specialised chaperon PfHsp90 in gene regulation of the chromatin eraser *PfSIR2A/B*. Implication of this study is that if we could artificially perturb the Sir2/ Hsp90 axis. There might be abrogation of antigenic variation in the parasite, multiple *var* gene will be expressed and parasite will not be able to evade the host immune response.

Through First part of the study, I was able to establish PfRad51 as the first client of PfHsp90 and it can be used as model for further research to understand *Plasmodium* Hsp90 chaperone cycle involving its co-chaperones. The findings of the study also opens new avenue on regulation of homologous regulation and suggests new drug combination therapy to curb malaria. Second part of the study impart light on the non-canonical function of PfHsp90. It provides link between environment, epigenetics and malaria pathogenesis which can be further explored to identify new drug targets. It highlights that novel strategy aimed at regulating PfSir2 activity may limit antigenic variation and help in vaccine development.



References

- 1. Su XZ, Heatwole VM, Wertheimer SP, Guinet F, Herrfeldt JA, Peterson DS, Ravetch JA, Wellems TE. 1995. The large diverse gene family var encodes proteins involved in cytoadherence and antigenic variation of Plasmodium falciparum-infected erythrocytes. Cell 82:89-100.
- 2. Smith JD, Chitnis CE, Craig AG, Roberts DJ, Hudson-Taylor DE, Peterson DS, Pinches R, Newbold CI, Miller LH. 1995. Switches in expression of Plasmodium falciparum var genes correlate with changes in antigenic and cytoadherent phenotypes of infected erythrocytes. Cell 82:101-10.
- 3. Baruch DI, Pasloske BL, Singh HB, Bi X, Ma XC, Feldman M, Taraschi TF, Howard RJ. 1995. Cloning the P. falciparum gene encoding PfEMP1, a malarial variant antigen and adherence receptor on the surface of parasitized human erythrocytes. Cell 82:77-87.
- 4. Scherf A, Hernandez-Rivas R, Buffet P, Bottius E, Benatar C, Pouvelle B, Gysin J, Lanzer M. 1998. Antigenic variation in malaria: in situ switching, relaxed and mutually exclusive transcription of var genes during intra-erythrocytic development in Plasmodium falciparum. Embo j 17:5418-26.
- 5. Tonkin CJ, Carret CK, Duraisingh MT, Voss TS, Ralph SA, Hommel M, Duffy MF, Silva LM, Scherf A, Ivens A, Speed TP, Beeson JG, Cowman AF. 2009. Sir2 paralogues cooperate to regulate virulence genes and antigenic variation in Plasmodium falciparum. PLoS Biol 7:e84.
- 6. Miller LH, Good MF, Milon G. 1994. Malaria pathogenesis. Science 264:1878-83.
- 7. Picard D. 2002. Heat-shock protein 90, a chaperone for folding and regulation. Cell Mol Life Sci 59:1640-8.
- 8. Hoter A, El-Sabban ME, Naim HY. 2018. The HSP90 Family: Structure, Regulation, Function, and Implications in Health and Disease. Int J Mol Sci 19.
- 9. Backe SJ, Sager RA, Woodford MR, Makedon AM, Mollapour M. 2020. Post-translational modifications of Hsp90 and translating the chaperone code. J Biol Chem 295:11099-11117.
- 10. Khurana N, Bhattacharyya S. 2015. Hsp90, the concertmaster: tuning transcription. Front Oncol 5:100.
- 11. Murillo-Solano C, Dong C, Sanchez CG, Pizarro JC. 2017. Identification and characterization of the antiplasmodial activity of Hsp90 inhibitors. Malar J 16:292.
- 12. Chalapareddy S, Bhattacharyya MK, Mishra S, Bhattacharyya S. 2014. Radicicol confers midschizont arrest by inhibiting mitochondrial replication in Plasmodium falciparum. Antimicrob Agents Chemother 58:4341-52.



- 13. Pallavi R, Roy N, Nageshan RK, Talukdar P, Pavithra SR, Reddy R, Venketesh S, Kumar R, Gupta AK, Singh RK, Yadav SC, Tatu U. 2010. Heat shock protein 90 as a drug target against protozoan infections: biochemical characterization of HSP90 from Plasmodium falciparum and Trypanosoma evansi and evaluation of its inhibitor as a candidate drug. J Biol Chem 285:37964-75.
- 14. Pennisi R, Ascenzi P, di Masi A. 2016. Correction: Pennisi, R., et al. Hsp90: A New Player in DNA Repair? Biomolecules 2015, 5, 2589-2618. Biomolecules 6.
- 15. Suhane T, Laskar S, Advani S, Roy N, Varunan S, Bhattacharyya D, Bhattacharyya S, Bhattacharyya MK. 2015. Both the charged linker region and ATPase domain of Hsp90 are essential for Rad51-dependent DNA repair. Eukaryot Cell 14:64-77.
- 16. Khurana N, Laskar S, Bhattacharyya MK, Bhattacharyya S. 2016. Hsp90 induces increased genomic instability toward DNA-damaging agents by tuning down RAD53 transcription. Mol Biol Cell 27:2463-78.
- 17. Iyer LM, Anantharaman V, Wolf MY, Aravind L. 2008. Comparative genomics of transcription factors and chromatin proteins in parasitic protists and other eukaryotes. Int J Parasitol 38:1-31.
- 18. Bhattacharyya MK, Kumar N. 2003. Identification and molecular characterisation of DNA damaging agent induced expression of Plasmodium falciparum recombination protein PfRad51. Int J Parasitol 33:1385-92.
- Bhattacharyya MK, Bhattacharyya nee Deb S, Jayabalasingham B, Kumar N. 2005.
 Characterization of kinetics of DNA strand-exchange and ATP hydrolysis activities of recombinant PfRad51, a Plasmodium falciparum recombinase. Mol Biochem Parasitol 139:33-9.
- Badugu SB, Nabi SA, Vaidyam P, Laskar S, Bhattacharyya S, Bhattacharyya MK. 2015.
 Identification of Plasmodium falciparum DNA Repair Protein Mre11 with an Evolutionarily Conserved Nuclease Function. PLoS One 10:e0125358.
- 21. Vydyam P, Dutta D, Sutram N, Bhattacharyya S, Bhattacharyya MK. 2019. A small-molecule inhibitor of the DNA recombinase Rad51 from Plasmodium falciparum synergizes with the antimalarial drugs artemisinin and chloroquine. J Biol Chem 294:8171-8183.
- 22. Suthram N, Padhi S, Jha P, Bhattacharyya S, Bulusu G, Roy A, Bhattacharyya MK. 2020. Elucidation of DNA Repair Function of PfBlm and Potentiation of Artemisinin Action by a Small-Molecule Inhibitor of RecQ Helicase. mSphere 5.
- 23. Roy N, Bhattacharyya S, Chakrabarty S, Laskar S, Babu SM, Bhattacharyya MK. 2014. Dominant negative mutant of Plasmodium Rad51 causes reduced parasite burden in host by abrogating DNA double-strand break repair. Mol Microbiol 94:353-66.



- 24. Theodoraki MA, Caplan AJ. 2012. Quality control and fate determination of Hsp90 client proteins. Biochim Biophys Acta 1823:683-8.
- 25. Sawarkar R, Paro R. 2013. Hsp90@chromatin.nucleus: an emerging hub of a networker. Trends Cell Biol 23:193-201.
- 26. Brown MA, Foreman K, Harriss J, Das C, Zhu L, Edwards M, Shaaban S, Tucker H. 2015. Cterminal domain of SMYD3 serves as a unique HSP90-regulated motif in oncogenesis. Oncotarget 6:4005-19.
- 27. Tariq M, Nussbaumer U, Chen Y, Beisel C, Paro R. 2009. Trithorax requires Hsp90 for maintenance of active chromatin at sites of gene expression. Proc Natl Acad Sci U S A 106:1157-62.
- 28. Laskar S, Bhattacharyya MK, Shankar R, Bhattacharyya S. 2011. HSP90 controls SIR2 mediated gene silencing. PLoS One 6:e23406.
- 29. Laskar S, K S, Bhattacharyya MK, Nair AS, Dhar P, Bhattacharyya S. 2015. Heat stress-induced Cup9-dependent transcriptional regulation of SIR2. Mol Cell Biol 35:437-50.
- 30. Oakley MS, Kumar S, Anantharaman V, Zheng H, Mahajan B, Haynes JD, Moch JK, Fairhurst R, McCutchan TF, Aravind L. 2007. Molecular factors and biochemical pathways induced by febrile temperature in intraerythrocytic Plasmodium falciparum parasites. Infect Immun 75:2012-25.
- 31. Hakimi MA, Deitsch KW. 2007. Epigenetics in Apicomplexa: control of gene expression during cell cycle progression, differentiation and antigenic variation. Curr Opin Microbiol 10:357-62.
- 32. Chookajorn T, Dzikowski R, Frank M, Li F, Jiwani AZ, Hartl DL, Deitsch KW. 2007. Epigenetic memory at malaria virulence genes. Proc Natl Acad Sci U S A 104:899-902.
- 33. Lopez-Rubio JJ, Gontijo AM, Nunes MC, Issar N, Hernandez Rivas R, Scherf A. 2007. 5' flanking region of var genes nucleate histone modification patterns linked to phenotypic inheritance of virulence traits in malaria parasites. Mol Microbiol 66:1296-305.
- 34. Karmodiya K, Pradhan SJ, Joshi B, Jangid R, Reddy PC, Galande S. 2015. A comprehensive epigenome map of Plasmodium falciparum reveals unique mechanisms of transcriptional regulation and identifies H3K36me2 as a global mark of gene suppression. Epigenetics Chromatin 8:32.

Publications





Synergistic Action between PfHsp90 Inhibitor and PfRad51 Inhibitor Induces Elevated DNA Damage Sensitivity in the Malaria Parasite

Wahida Tabassum, a Priyanka Singh, b Niranjan Suthram, a Sunanda Bhattacharyya, b D Mrinal Kanti Bhattacharyya

^aDepartment of Biochemistry, School of Life Sciences, University of Hyderabad, Hyderabad, India

ABSTRACT The DNA recombinase Rad51 from the human malaria parasite Plasmodium falciparum has emerged as a potential drug target due to its central role in the homologous recombination (HR)-mediated double-strand break (DSB) repair pathway. Inhibition of the ATPase and strand exchange activity of P. falciparum Rad51 (PfRad51) by a smallmolecule inhibitor, B02 [3-(phenylmethyl)-2-[(1E)-2-(3-pyridinyl)ethenyl]-4(3H)-quinazolinone], renders the parasite more sensitive to genotoxic agents. Here, we investigated whether the inhibition of the molecular chaperone PfHsp90 potentiates the antimalarial action of B02. We found that the PfHsp90 inhibitor 17-AAG [17-(allylamino)-17-demethoxygeldanamycin] exhibits strong synergism with B02 in both drug-sensitive (strain 3D7) and multidrug-resistant (strain Dd2) P. falciparum parasites. 17-AAG causes a greater than 200-fold decrease in the half-maximal inhibitory concentration (IC₅₀) of B02 in 3D7 parasites. Our results provide mechanistic insights into such profound synergism between 17-AAG and B02. We report that PfHsp90 physically interacts with PfRad51 and promotes the UV irradiation-induced DNA repair activity of PfRad51 by controlling its stability. We find that 17-AAG reduces PfRad51 protein levels by accelerating proteasomal degradation. Consequently, PfHsp90 inhibition renders the parasites more susceptible to the potent DNA-damaging agent methyl methanesulfonate (MMS) in a dose-dependent manner. Thus, our study provides a rationale for targeting PfHsp90 along with the recombinase PfRad51 for controlling malaria propagation.

KEYWORDS *Plasmodium* DNA repair, PfHsp90, PfRad51, 17-AAG, B02, synergy between 17-AAG and B02

he genetic material of *Plasmodium falciparum* is exposed to various endogenous and environmental genotoxic agents throughout its life cycle. The intraerythrocytic parasites degrade hemoglobin, thereby releasing heme, which is further oxidized from ferrous (Fe²⁺) to ferric (Fe³⁺). During this process, reactive oxygen species are generated, which are harmful DNA-damaging agents (1). Out of various types of damage, double-strand breaks (DSBs) in the chromosome are the most deleterious to the cell if left unrepaired. The apparent loss of the classical nonhomologous end joining (C-NHEJ)-mediated DSB repair pathway in the malaria parasites underlines the importance of targeting the homologous recombination (HR) pathway, as this is the exclusive DSB repair machinery (2). The Rad51 recombinase executes an important step in the HRmediated DSB repair pathway. It searches for the homologous template and catalyzes the DNA strand exchange reaction, which is the pivotal step in the HR pathway (3). The Plasmodium recombinase P. falciparum Rad51 (PfRad51) has been previously identified (4) and biochemically characterized (5). Recently, we presented evidence that a small molecule, B02, binds to P. falciparum recombinase Rad51 (6). Upon binding to PfRad51, B02 inhibits ATP hydrolysis activity, DNA strand exchange activity, and the homodimerization

Citation Tabassum W, Singh P, Suthram N, Bhattacharyya S, Bhattacharyya MK. 2021. Synergistic action between PfHsp90 inhibitor and PfRad51 inhibitor induces elevated DNA damage sensitivity in the malaria parasite. Antimicrob Agents Chemother 65:e00457-21. https://doi.org/10.1128/AAC.00457-21.

Copyright © 2021 American Society for Microbiology. All Rights Reserved.

Address correspondence to Sunanda Bhattacharyya, sdeb70@gmail.com, or Mrinal Kanti Bhattacharyya, mrinal00lanirm@gmail.com.

Received 6 March 2021

Returned for modification 7 April 2021

Accepted 19 May 2021

Accepted manuscript posted online

7 June 2021

Published 17 August 2021

Department of Biotechnology and Bioinformatics, School of Life Sciences, University of Hyderabad, Hyderabad, India

Downloaded from https://journals.asm.org/journal/aac on 17 August 2021 by 14.139.69.175

of PfRad51. Plasmodium cultures treated with B02 were found to be more susceptible to methyl methanesulfonate (MMS), as B02 treatment significantly reduced MMS-induced Rad51 nuclear focus formation and hence increased accumulation of unrepaired DNA in the parasites. Earlier, we demonstrated that mice infected with a mutant Plasmodium berghei strain harboring a dominant negative mutant allele of rad51 (Pfrad51:K143R), showed significantly reduced parasite burden (7), reinforcing the essentiality of Rad51. It was also observed that the loss of Rad51 activity could not be compensated by other DSB repair pathways (7).

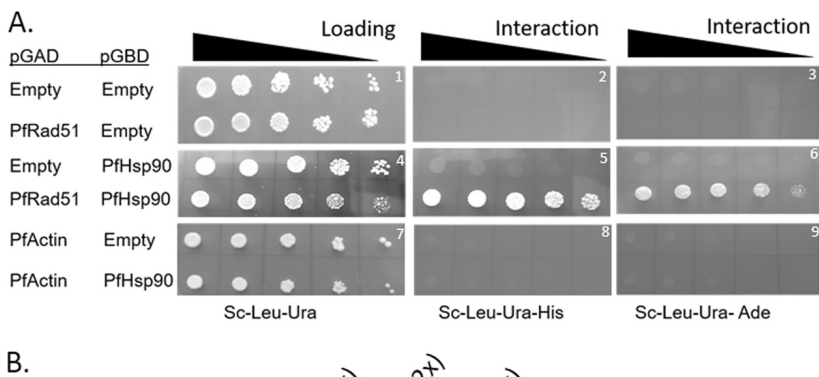
In addition to inducing cyclobutene pyrimidine dimers between the two adjacent thymidine residues, which are primarily repaired by the nucleotide excision repair (NER) pathway, UV-C irradiation also produces reactive oxygen species, which result in the formation of DSBs at the chromosomes (8, 9). Similarly, MMS alkylates the bases of DNA, produces an adduct that blocks DNA polymerase (10), and eventually generates stalled replication forks, which in turn promote DSBs in the chromosomes (11). It was observed that HR-deficient cells are more sensitive than the NHEJ0-deficient cells to MMS-induced DNA damage (12). In response to UV- and MMS-induced DNA damage, Rad51 is localized to the damaged chromatin and forms foci, which are a hallmark for the HR-mediated DNA repair pathway (6, 13). Thus, UV and MMS sensitivity are indirect measures of the HR-mediated DSB repair efficiency of the cells.

Heat shock protein 90 (Hsp90) is an evolutionary conserved molecular chaperone that regulates the conformation and stability of a specific group of proteins, known as its clients (14). The Hsp90 N-terminal domain has a characteristic pocket known as the Bergerat fold, in which ATP binds (15). The function of Hsp90 was found to be dependent on its ability to hydrolyze ATP (16). 17-AAG (an analog of geldenamycin) and radicicol bind specifically to the ATP binding site of Hsp90 and thereby inhibit its function (17, 18). Although a number of chemical inhibitors of Hsp90 have been identified that exhibit antiplasmodial activity (19, 20), 17-AAG is the only chemical whose inhibitory activity has been verified on purified PfHsp90 protein (21). Similarly, using a yeastbased assay system, it was found that radicicol inhibits the function of PfHsp90 (22).

In recent years, Hsp90 is found to act as an important regulator of the DNA damage response, as well as the DNA break repair pathway. Hsp90 inhibitors were found to show synergistic antitumor activities with DNA-damaging agents (23). Multiple components of the DSB repair pathways have been described as the clients of Hsp90 (24). In budding yeast, Rad51 acts as a client of yHsp90 (25) and dynamic interaction between yRad51 and yHsp90 is crucial for the DNA damage-induced nuclear function of yRad51 (26). Whether the abundance and activity of PfRad51 are regulated by the PfHsp90 chaperone system is currently unknown. We hypothesize that if PfHsp90 is engaged with PfRad51, then PfHsp90 also should control the PfRad51-mediated HR pathway in response to DSBs at the Plasmodium chromosomes. The following two questions are addressed here: first, whether PfHsp90 controls the DSB repair pathway in the malaria parasites, and second, whether a small-molecule inhibitor of PfHsp90 could potentiate the action of B02. We provide evidence that PfHsp90 promotes the stability of PfRad51. Furthermore, we show that PfHsp90 inhibition causes the accumulation of UV-induced DNA damage in the parasite and sensitizes it to MMS. Also, PfHsp90 and PfRad51 inhibitors show profound synergistic interaction in both drug-sensitive and drug-resistant parasites. Thus, our study has opened a new avenue to target the malaria parasite, which should be explored more in the future.

RESULTS

Physical interaction between PfHsp90 and PfRad51. To test our hypothesis regarding whether PfHsp90 controls the Rad51-dependent DNA repair pathway, we first studied their physical interaction. We generated two yeast expression vectors, one harboring PfHsp90 fused to the Gal4 DNA binding domain (bait) and another harboring PfRad51 fused to the Gal4 activation domain (prey). We used the PJ69-4A strain, which allows scoring both weak and strong interactions by the measurement of HIS3



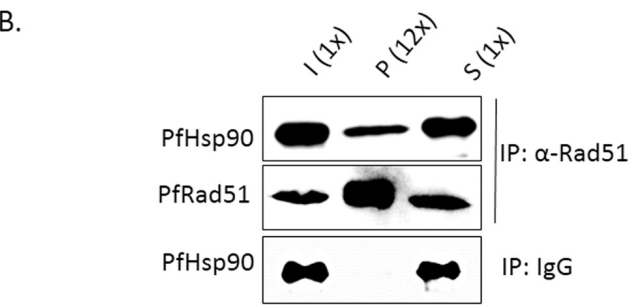


FIG 1 Physical interaction between PfRad51 and PfHsp90. (A) The interaction of PfRad51 and PfHsp90 was confirmed by yeast two-hybrid assay. PfRAD51 or PfACTIN genes were cloned in pGADC1 vector and fused to the GAL4 activation domain (GAL4-AD), while the PfHSP90 gene was cloned in pGBDUC1 vector and fused to the GAL4 DNA binding domain (GAL4-BD). Yeast strain PJ69-4A with ADE2 and HIS3 as reporter genes was used for the interaction studies. For spotting, the cells were grown until an optical density at 600 nm (OD $_{600}$) of 0.5 and then were 10-fold serially diluted and spotted onto a plate lacking leucine and uracil to check for the presence of the bait and the prey plasmids. The interaction was checked by spotting onto triple-dropout plates lacking either leucine, uracil, and histidine or leucine, uracil, and adenine. Each assay was repeated at least three times. (B) Representative Western blot analysis out of three independent experiments depicting the coimmunoprecipitation of PfRad51 and PfHsp90 from the parasite lysate. Anti-PfRad51 and IgG antibodies were used for the immunoprecipitation. Probing was performed with anti-PfRad51 and nati-PfHsp90 antibodies. Lanes are as follows: I, input; P, immunoprecipitation (IP) pellet fraction; S, supernatant. The pellet fraction was loaded $1\times$, and the input and supernatant fractions were loaded $1\times$.

or *ADE2* reporter genes activities, respectively. It was found that the yeast strain carrying both the vectors can activate both the *HIS3* and the *ADE2* reporter genes, indicating a strong physical association between PfHsp90 and PfRad51 (Fig. 1A, subpanel 4). Yeast strains harboring empty bait and empty prey vectors were used as the negative control for these yeast two-hybrid experiments. The *PfACTIN* gene cloned in the prey vector was used as an additional negative control, as no interaction was observed between PfHsp90 and PfActin (Fig. 1A, subpanel 6). In order to investigate any such interaction between PfRad51 and PfHsp90 proteins within the parasite itself, we performed a coimmunoprecipitation experiment. PfHsp90 was coimmunoprecipitated with PfRad51 in *P. falciparum* 3D7 *in vitro* cultures (Fig. 1B). A protein extract of the same culture pulled down with preimmune IgG was used as a negative control. Thus, the data presented here demonstrate a specific interaction between PfHsp90 and PfRad51 in the parasite.

Abrogation of the UV-induced DNA repair activity of PfRad51 under Hsp90-inhibitory condition. The physical interaction between PfHsp90 and PfRad51 prompted us to investigate the effect of the PfHsp90 inhibitor on PfRad51 DNA repair activity. We reasoned that if PfHsp90 is a positive regulator of PfRad51, then PfHsp90 inhibition would have a negative effect on PfRad51 function; however, if PfHsp90 is a negative regulator of PfRad51, then inhibition of PfHsp90 would promote PfRad51 activity. To investigate the effect of PfHsp90 on PfRad51-dependent DNA repair activity, we studied the effect of 17-AAG on the repair kinetics of the damaged *Plasmodium* genome upon UV irradiation. To this end, *P. falciparum in vitro* cultures were exposed to

Repair kinetics of UV-damaged genome

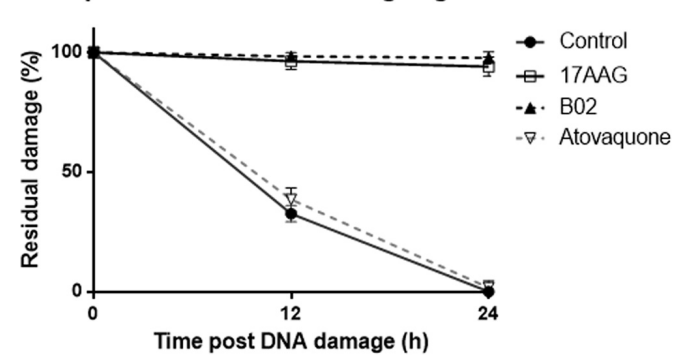


FIG 2 Abrogation of the UV-induced DNA repair activity of PfRad51 under Hsp90-inhibitory conditions. At the trophozoite stage, 17-AAG (1.7 μ M), B02 (1 μ M), and atovaquone (0.3 nM) pretreated and mock-treated cultures were UV-irradiated at 100 J/m². After UV treatment, cultures were maintained in the respective drug for 24 h; along with this, the mock-treated culture was maintained in complete medium lacking any drug. Genomic DNA was isolated from the harvested parasites at the indicated time points, namely, before UV damage and at 0 h, 12 h, and 24 h postdamage. The mean value \pm standard error of the mean (SEM) from three independent experiments is plotted.

UV doses (100 J/m²) to induce genome-wide DNA double-strand breaks and then allowed to recover. Kinetics of DSB repair were followed using a highly sensitive PCRbased DNA repair assay (27). It was previously established in our laboratory that trophozoite stage-specific parasites, once subjected to the UV doses, require 24 h for complete repair of the damaged DNA (27). This repair activity is directly linked to the active PfRad51 protein levels in the parasite. Under conditions in which the parasites were pretreated with B02, a complete loss of DNA repair activity was observed even after 24 h after UV irradiation (Fig. 2). The DNA repair kinetics of the parasite genome in the presence of 17-AAG were measured and compared to the repair kinetics of the untreated parasites. It was observed that parasites preincubated with 17-AAG, once subjected to UV irradiation, behaved similar to the B02-treated parasites, i.e., there was no reduction in the residual damaged DNA by 12 h, or even at the end of a 24-h recovery period (Fig. 2). An unrelated chemical, atovaquone, was used as a negative control for this experiment. Atovaquone-pretreated parasites show similar repair kinetics to those of the untreated parasites, i.e., 70% repair was achieved at the end of 12 h, and 100% repair was seen after 24 h. These data indicate that, similarly to the recombinase inhibitor B02, the PfHsp90 inhibitor 17-AAG blocks the repair of UV irradiation-induced DNA damage in the parasite.

17-AAG induces proteasomal degradation of PfRad51. To understand the biochemical basis of 17-AAG-induced suppression of DNA repair activity in UV-treated parasites, the steady-state level of PfRad51 was measured in the presence of 17-AAG. Ring stage-specific parasites were treated with increasing doses of 17-AAG (425 nM to $1.7 \,\mu$ M). As the half-maximal inhibitory concentration (IC₅₀) of 17-AAG was determined to be 510 nM in our study, a sub-IC $_{50}$ concentration was chosen as the starting dose. The treated cultures were harvested at the late trophozoite/early schizont stage. A dose-dependent depletion of PfRad51 protein was observed (Fig. 3A). These experiments were performed four times, and the levels of PfRad51 were quantified in untreated and 17-AAG-treated samples. Our data show 15%, 26%, and 87% reductions in the level of PfRad51 in the presence of 425 nM, 850 nM, and 1.7 μ M 17-AAG, respectively (Fig. 3B). It was observed that the 17-AAG-induced reduction in PfRad51 was reversed in the presence of the proteasome inhibitor MG132 (Fig. 3C and D). This suggests that PfHsp90 protects PfRad51 from degradation via a proteasomal pathway. To further support our conclusion, PfRad51 was expressed in a temperature-sensitive yeast strain, iG170Dhsp82 (28), which harbors nonfunctional Saccharomyces cerevisiae

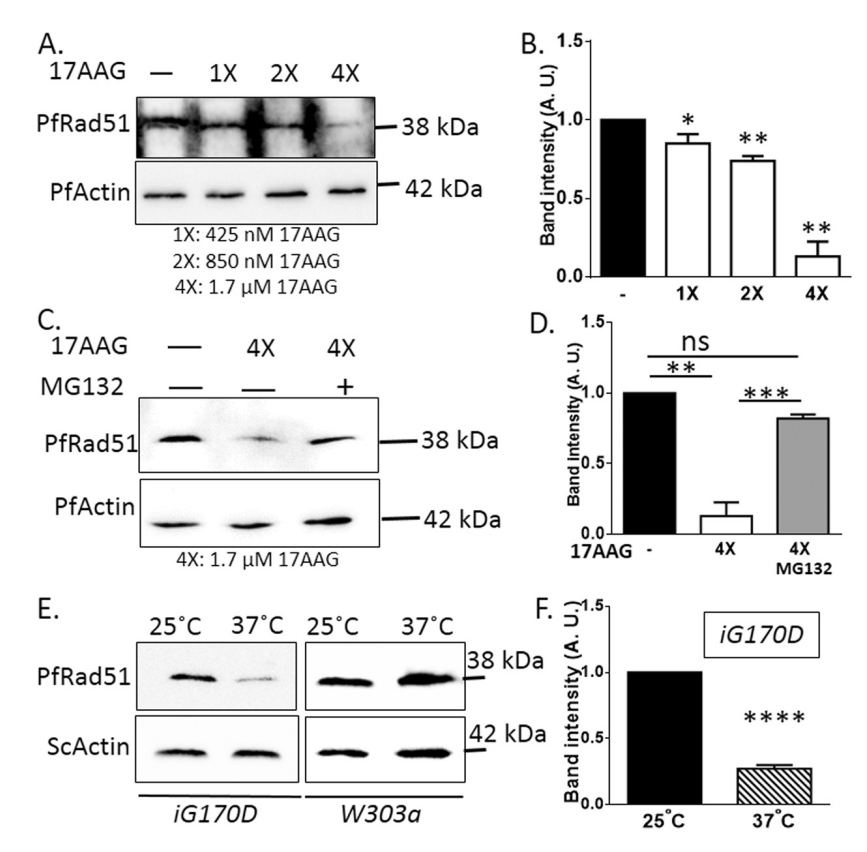


FIG 3 17-AAG induces proteasomal degradation of PfRad51. (A) Western blot analysis showing steady-state level of PfRad51 protein, performed with total protein isolated from untreated parasites and parasites treated with three different concentrations of 17-AAG (as indicated). Actin was used as the loading control. (B) The graph was plotted from the quantification of band intensities, depicting lower abundance of PfRad51 upon 17-AAG treatments. Error bar indicates the SEM obtained from four individual experiments. (C) Western blot analysis depicting PfRad51 protein level, performed with total protein isolated from untreated, 17-AAG-treated (1.7 μ M), and 17-AAG (1.7 μ M) plus MG132 (133 nM)-treated parasites. Actin was used as the loading control. (D) The graph was plotted from the values of band intensities obtained from three independent experiments, with error bar indicating the SEM. (E) Western blot analysis showing the PfRad51 level, performed with total protein isolated from the temperature-sensitive yeast strain iG170Dhsp82 harboring the PfRad51 plasmid (left), grown at a permissive temperature of 25°C and a restrictive temperature of 37°C, or from yeast strain W303a harboring the PfRad51 plasmid (right). ScActin was used as the loading control. The molecular weight of the respective proteins is marked on the right side of each gel. (F) Graph was plotted from the value of band intensities obtained from three independent experiments, with error bar indicating the SEM. The P value was calculated using a two-tailed t test (*, P < 0.05; **, P < 0.01; ****, P < 0.001; ****, P < 0.0001; ns, nonsignificant).

Hsp90 α (ScHsp90 α), when the strain was grown at the restrictive temperature of 37°C. Although yeast Hsp90 α shares 74% sequence similarity and only 57% sequence identity with PfHsp90, it can provide stability to PfRad51, as evident from the steady-state level of PfRad51, when the strain was grown at a permissive temperature (25°C) (Fig. 3E). However, a significant reduction in the stability of PfRad51 was observed under the nonpermissive condition (37°C), where ScHsp90 α is nonfunctional (Fig. 3E and F). To rule out the possibility that the reduction in the PfRad51 level is not due to a temperature effect, PfRad51 was expressed in a wild-type yeast strain (W303a), and proteins were extracted after growing the strain at two different temperatures, as used earlier. No noticeable difference was observed in the stability of PfRad51 at 25°C and 37°C (Fig. 3E). Together, our data establish that Hsp90 provides stability to the PfRad51 protein.

Hsp90 inhibition sensitizes *P. falciparum* **to MMS-induced DNA damage.** In our study, we found that PfHsp90 inhibition impairs the stability of PfRad51 in the parasite. Hence, to further elucidate the role of PfHsp90 in the PfRad51-mediated DSB repair

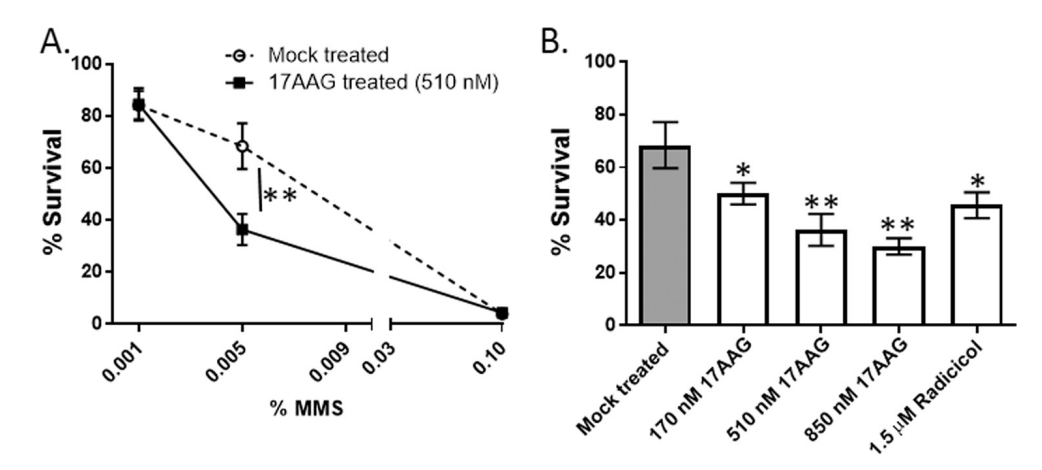


FIG 4 Hsp90 inhibition sensitizes *P. falciparum* to methyl methanesulfonate (MMS)-induced DNA damage. Return-to-growth assays were performed to determine the sensitivity of mock-treated and 17-AAG-treated 3D7 parasites at different concentration of MMS (as indicated on the *x* axis). The graph depicts the percent survival of parasites after a 48-h return to growth after MMS treatment. Each data point indicates mean value \pm standard deviation (SD) from three independent experiments. (B) Return-to-growth assay performed to determine the MMS sensitivity of 3D7 parasites treated with different doses of 17-AAG and radicicol compared to that of mock-treated parasite. Graph depicts the mean percent survival (\pm SD) after 48 h after MMS treatment (0.005%) from four experiments. The *P* value was calculated using a two-tailed *t* test (*, *P* < 0.05; **, *P* < 0.01).

pathway, the effects of 17-AAG on MMS-induced cytotoxicity were studied. Parasites pretreated with 17-AAG were subjected to three different doses of MMS for 2h and then subsequently returned to growth in a medium containing 17-AAG. As a control, parasites which were not treated with 17-AAG (mock-treated) were taken. The parasitemia of the MMS-treated and the untreated parasites was measured to determine the survivability upon MMS treatment. It was found that for the mock-treated parasites, the survivability is around 85% upon 0.001% MMS treatment, considering the survivability of MMS-untreated cultures to be 100%. No significant difference in the survivability was observed for the 17-AAG-pretreated cultures when exposed to 0.001% MMS. However, a significant 2-fold reduction in survivability was observed between the mock-treated and the 17-AAG-treated cultures when both were subjected to 0.005% MMS treatment. At a much higher dose of MMS (0.1%), both mock-treated and 17-AAG pretreated cultures showed extreme MMS sensitivity, and thus any difference in survivability was indistinguishable (Fig. 4A). A 0.005% MMS concentration, a measurable difference in the survivability was observed, so this concentration of MMS was used for further studies. In order to ascertain the specificity of PfHsp90 inhibition by 17-AAG, the parasites were treated with various doses of 17-AAG to investigate whether the sensitivity of the parasites is increased in a dose-dependent manner. Our study shows that increasing doses of 17-AAG cause increased MMS sensitivity in a dose-dependent manner (Fig. 4B). In order to establish our conclusion, another established inhibitor of PfHsp90, namely, radicicol, was used in our assay. The culture was treated with 1.5 μ M radicicol, as it was observed previously that treatment with higher concentrations of this drug results in the arrestation of the parasite culture at the schizont stage (29). It was observed that the parasites pretreated with radicicol manifest about 30% reduction in parasite survival upon MMS treatment compared to that of the mock-treated parasites (Fig. 4B). Since MMS-induced DNA damage, if unrepaired, could be lethal for the parasites, the efficiency of the repair process can be assayed as a function of parasite viability. Thus, our study suggests that the impact of PfHsp90 inhibition on the DSB repair machinery of the parasite is severe.

17-AAG decreases the IC_{50} value of B02 in a synergistic way. We wanted to investigate the interaction between 17-AAG and B02. Since 17-AAG causes proteasomal degradation of PfRad51 and B02 inactivates the PfRad51 function, we predicted that

TABLE 1 Potentiation of B02 action by 17-AAG and vice versa

P. falciparum strain	Combination of drugs	IC_{50} (mean \pm SD [μ M])	Potentiation factor
3D7	B02 (alone)	7.45 ± 0.89	1
	B02 (17-AAG) ^a	0.034 ± 0.0017	219.1
	17-AAG (alone)	0.51 ± 0.0005	1
	17-AAG (B02) ^b	0.039 ± 0.005	13.07
Dd2	B02 (alone)	3.73 ± 0.35	1
	B02 (17-AAG) ^c	0.022 ± 0.004	169.54
	17-AAG (alone)	0.537 ± 0.06	1
	17-AAG (B02) ^d	0.018 ± 0.0017	29.8

^aThe IC₅₀ concentration of 17-AAG in strain 3D7 was used.

the depletion of PfRad51 due to the action of 17-AAG would render the parasites more sensitive to B02 action. The IC₅₀ concentrations of both B02 and 17-AAG were determined in our experimental setup. To this end, synchronous late ring-stage cultures were treated with the respective drugs at different concentrations for 48 h, and the IC₅₀ values were determined in the drug-sensitive strain 3D7 and in the multidrug-resistant strain Dd2. The IC $_{50}$ values of B02 were found to be 7.45 \pm 0.89 $\mu{\rm M}$ and $3.73 \pm 0.35~\mu\text{M}$ for the 3D7 and Dd2 strains, respectively (Table 1). These values are in good agreement with the previously reported values (6). The IC₅₀ value of B02 was also determined by incubating the parasite cultures with different concentrations of B02 in the presence of the IC₅₀ concentration of 17-AAG. It was found that the presence of 17-AAG could reduce the IC₅₀ value of B02 to 34 nM in the 3D7 and to 22 nM in the Dd2 parasites. Thus, the potentiation factor is about 219 in the 3D7 strain. Similarly, the potentiation factor in the Dd2 strain was found to be 169 (Table 1). Thus, 17-AAG treatment greatly potentiates the inhibitory effect of B02 in both drug-sensitive and multidrug-resistant parasite strains. We then sought to investigate whether B02 could also potentiate the antiparasitic action of 17-AAG. To determine this, the parasites were incubated at various doses of 17-AAG in the presence of the IC₅₀ concentration of B02. As different IC₅₀ values of 17-AAG are reported in the literature depending upon the parasitic stages when the treatment is begun and also upon the duration of the treatments (19, 29, 30), we first determined the IC₅₀ of 17-AAG under our experimental conditions. The IC_{50} values of 17-AAG were found to be 510 nM and 537 nM in 3D7 and Dd2 strains, respectively (Table 1). In the presence of IC_{50} concentrations of B02, the IC_{50} value of 17-AAG dropped to 39 nM and 18 nM in 3D7 and Dd2 in vitro cultures, respectively (Table 1). Thus, there was 13- to 30-fold potentiation of 17-AAG by B02. As each of the drugs potentiated the other's action, we wanted to investigate whether the interaction between these two drugs is additive or synergistic in nature. To this end, a fixed-ratio drug combination assay was performed. The mean fractional inhibitory concentration (FIC) values derived from the dose-response curve of each combination were compiled, as shown in Table 2. The sum of FICs was plotted in isobolograms for 3D7 (Fig. 5A) and Dd2 (Fig. 5B) strains. Our study demonstrates profound synergistic interactions between 17-AAG and B02 in both drug-sensitive (3D7) and multidrugresistant (Dd2) parasites.

DISCUSSION

We have provided evidence that PfRad51 acts as a direct client of PfHsp90. First, we found that PfHsp90 interacts with PfRad51 both *in vivo* and *in vitro*. Second, the nature and the extent of 17-AAG-mediated inhibition of the repair of UV-induced damage in the parasite genome positively correlates with the inhibitory effect of B02, a potent inhibitor of recombinase PfRad51. Third, and most importantly, treatment of 17-AAG resulted in the depletion of PfRad51 by accelerating the proteasomal degradation of

 $[^]b$ The IC₅₀ concentration of B02 in strain 3D7 was used.

^cThe IC₅₀ concentration of 17-AAG in strain Dd2 was used.

^dThe IC₅₀ concentration of B02 in strain Dd2 was used.

TABLE 2 FIC values of drug combinations

P. falciparum strain	17AAG:B02	FIC _{17AAG}	FIC _{B02}	∑FIC
3D7	5:0	1	0	1
	4:1	0.39	0.1	0.49
	3:2	0.25	0.2	0.45
	2:1	0.07	0.11	0.18
	1:4	0.03	0.14	0.17
	0:5	0	1	1
Dd2	5:0	1	0	1
	4:1	0.48	0.17	0.65
	3:2	0.22	0.21	0.43
	2:1	0.04	0.08	0.12
	1:4	0.05	0.3	0.35
	0:5	0	1	1

the protein. The essentiality of PfHsp90 in *Plasmodium* biology has been rightfully advocated previously (31–34); however, no client of PfHsp90 that is important in parasite biology has been identified yet. To our knowledge, this is the first report that identifies a *bona fide* client of PfHsp90. Given that PfRad51 and its mutants can be easily expressed and purified using bacterial expression systems (7), this now allows biochemical investigation of the PfHsp90 chaperone cycle and the involvements of its cochaperones, using PfRad51 as a model client protein.

The malaria parasites during their intraerythrocytic life cycle encounter extraordinarily high levels of genotoxic stresses that cause various modifications of DNA bases, single-stranded DNA (ssDNA) breaks, and most deleterious of all, DNA DSBs in the haploid chromosomes. As the unrepaired DSBs lead to the death of the unicellular parasite Plasmodium falciparum, targeting its DSB repair pathway is a promising option. Our previous study demonstrated that PfRad51 plays an indispensable function in the parasite's biology under DNA damage conditions (7). None of the components of the nonhomologous end-joining pathway is found in the parasite genome. Besides, some of the proteins involved in homologous recombination, namely Rad52 and BRCA1, are also not annotated in the Plasmodium genome. Thus, PfRad51 has emerged as one of the major targets for blocking HR-mediated DSB repair in this parasite. Previously, B02 was established as a specific inhibitor of PfRad51, but its IC₅₀ was found to be in the micromolar range (3 to $8 \mu M$) (6). While lead optimization could be a strategy for increasing the potency of the chemical derivatives of B02, regulating the cellular abundance of the target protein, i.e., PfRad51, could also, in principle, reduce the IC₅₀ of native B02. Here, we find that the treatment with the PfHsp90 inhibitor induces the proteasomal degradation of

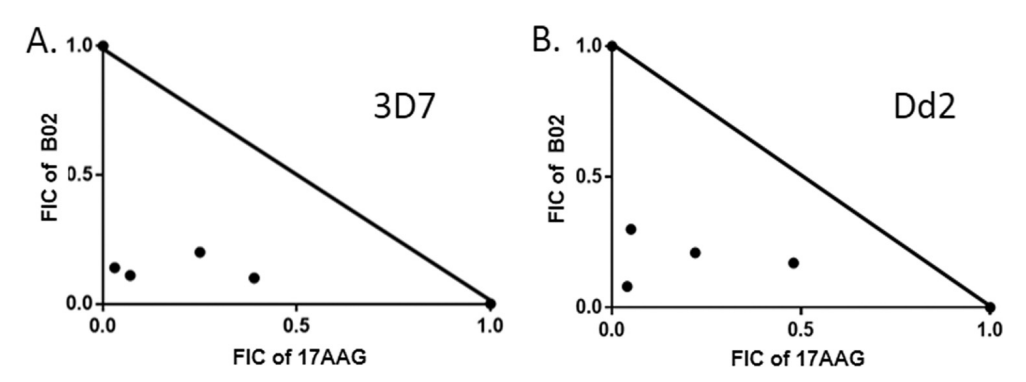


FIG 5 Synergistic interaction between the PfHsp90 inhibitor 17-AAG and the PfRad51 inhibitor B02. Isobolograms of 17-AAG and B02 in the 3D7 (A) and Dd2 (B) strains. Fixed-ratio drug combination assays were performed. Each point represents the mean half-maximal inhibitory concentration (IC_{50}) of the drug combination from three independent experiments. A solid line is drawn between the IC_{50} values of each drug when used alone. FIC, fractional inhibitory concentration.

Downloaded from https://journals.asm.org/journal/aac on 17 August 2021 by 14.139.69.175

PfRad51, resulting in a dramatic decrease in the steady-state level of the target of B02 and thereby reducing the IC_{50} of B02 to the nanomolar range (22 to 34 nM). Thus, this result serves as a proof of concept that the regulation of the abundance or activity of PfRad51 could be key to increasing the effectiveness of the recombinase inhibitors. This will now stimulate research on the identification of the negative modulators of *Plasmodium* homologous recombination machinery.

The highly synergistic interaction between B02 and 17-AAG indicates that these two target proteins may also act in a nonepistatic manner. Our finding showing that inhibition of PfHsp90 and PfRad51 together causes a profound effect on parasite survivability raises the possibility that PfHsp90 might control other DNA repair pathways as well. In humans, Hsp90 has been found to regulate DNA damage response (DDR), as well as the base excision repair (BER), the nucleotide excision repair (NER), and the mismatch repair (MMR) pathways by providing clientship to some of the major proteins involved in these pathways (24). In the budding yeast, it was observed that ScHsp90 modulates the DDR pathway by regulating a DNA repair signaling kinase, Rad53 (35). In malaria parasites, the long-patch BER pathway has been identified previously (36). Recently, *in silico* analyses have identified almost all components of NER (37) and MMR (38) pathways in the *Plasmodium* genome. However, it is still not known whether the enzymes involved in these pathways are regulated via the PfHsp90 chaperone system. Hence, our findings open up new avenues of research to target both the DNA repair machinery and the Hsp90 chaperone system for arresting parasite growth.

MATERIALS AND METHODS

Plasmids. The plasmids pTA:PfRAD51, and pGADC1:PfRad51 have been previously described (7). PfHSP90 was amplified using the forward primer OMKB 469 (TCAGGA TCCATGTCAACGGAAACATTCGC) and the reverse primer OMKB 470 (TCAGTCGAC ATCCTTTAGTCAACTTCTTCC), and PfACTIN was amplified using the forward primer OMKB 766 (TCA GGATCCATGGGAGAAGAAGATGTTCAAG) and the reverse primer OMKB 767 (TCAGTCGACAATTTAGAAACATTTTCTGTGGAC), using P. falciparum 3D7 genomic DNA as the template. PfHSP90 and PfACTIN were cloned in pGBDUC1 vector and pGADC1 vector, respectively, for yeast two-hybrid analysis.

Antibodies used. Anti-PfRad51 was generated in our laboratory (7). The anti-actin antibody (Sigma, St. Louis, MO) recognizes PfActin, as previously described (27). The anti-Hsp90 antibody (Sigma) recognizes PfHsp90 protein, as previously described (39), and the anti-ScActin antibody (Abcam, Cambridge, UK), recognizes ScActin (7). Horseradish peroxidase (HRP)-conjugated anti-rabbit and anti-mouse secondary antibodies (Promega, Madison, WI) were used.

Parasite culture. *P. falciparum* cultures were maintained in RPMI 1640 medium supplemented with 1% AlbuMax (Invitrogen, Carlsbad, CA) and 0.005% hypoxanthine at 5% hematocrit by the candle jar method at 37°C as described previously (40). Synchronization of the parasite culture was performed using 5% sorbitol (Sigma) treatment at the ring stage.

Yeast strains. pTA vector harboring *PfRAD51* was transformed into strains iG170Dhsp82 (*MATa can1-100 ade2-1 his3-11, 15 leu2-3, 112 trp1-1 ura3-1 hsp82::LEU2 hsc82::LEU2 HlS3::HSP82G170D*) (28) and W303a (*MATa leu2-3, 112 his3-11, 15 ade2-1, trp1, ura3-1*) (41) to generate the strains TAY1 and TAY2, respectively. pGADC1 vector harboring *PfRAD51* or *PfACTIN* and pGBUC1 vector harboring *PfHSP90* were transformed into the PJ69-4A strain (*MATa trpl-901 leu2-3, 112 ura3-52 his3-200 ga14*Δ *ga180*Δ *LYS2:: GALI-HIS3 GAL2-ADE2 met2::GAL7-lacZ*) (42) for yeast two-hybrid studies.

Yeast transformation. Yeast transformation was done as described previously (43). The transformed yeast cells with pTA:*PfRAD51* plasmid were selected on synthetic complete medium lacking tryptophan (SC-trp). The transformants with the bait plasmids (pGBDUC1 and its derivatives) were selected on SC medium lacking uracil (SC-ura), and the transformants with the prey plasmids (pGADC1 or PGADC1-PfRad51) were selected on SC medium lacking uracil and leucine (SC-ura-leu).

Yeast two-hybrid analysis. The yeast two-hybrid analysis was done as described previously (43). Briefly, 10-fold serial dilutions of PJ69-4A cells transformed with both bait and prey plasmids were plated on SC medium lacking uracil, leucine, and histidine (SC-ura-leu-his) or SC medium lacking uracil, leucine, and adenine (SC-ura-leu-ade) to score for the expression of the *HIS3* reporter gene or the *ADE2* reporter gene, respectively. As a control, the cells were also plated on the SC-ura-leu double-dropout plates.

Coimmunoprecipitation. Coimmunoprecipitation was performed using the Pierce cross-link immunoprecipitation kit (Thermo Scientific) following the manufacturer's protocol. Briefly, the anti-PfRad51 antibody was coupled to Pierce Protein A/G Plus agarose in a screw-cap column on a rotator. Then, the antibody-bound beads were cross-linked using disuccinimidyl suberate (DSS) solution on the rotator. Washes were performed per the protocol to quench the cross-linking. Parasites released after saponin treatment were lysed using the immunoprecipitation (IP) lysis buffer (0.025 M Tris, 0.15 M NaCl, 0.001 M EDTA, 1% NP-40, and 5% glycerol [pH 7.4]). The lysate was then separated from the cell debris by centrifugation. Protein concentrations of lysates were determined, and 1 mg of lysate was precleaned using the control agarose resin slurry. Then, the precleaned lysate was incubated overnight with antibody-bound

beads. The column was placed in a collection tube, and flowthrough was collected. Antigen-antibodybound beads were then subjected to washes with wash buffers and conditioning buffer. Bound antigen was further eluted using the elution buffer, mixed with the sample buffer, and then subjected to Western blot analysis. The lysis buffer, wash buffer, conditioning buffer, and elution buffer were from the kit.

Western blot analysis. Total extracted protein from the parasite was separated on a 12% SDS polyacrylamide gel, and the Western blot analysis was performed as described earlier (43). All of the primary antibodies, i.e., anti-PfRad51 (raised in rabbits), anti-actin, anti-ScActin, and anti-Hsp90 (all raised in mice), were used at 1:5,000 dilutions. HRP-conjugated secondary antibodies (anti-rabbit or anti-mouse) were used at 1:10,000 dilutions. An enhanced chemiluminescence (ECL) kit (Pierce) was used for the detection of the protein signal. Quantification of the band intensity was performed using Image J, software and the graph was plotted using GraphPad Prism 6 software.

MG132 treatment. Synchronous ring stage culture was treated with 133 nM MG132 for 12 h; then, culture was removed from MG132-containing medium and grown in complete medium until the late trophozoite/early schizont stage. Parasites were then harvested, and total protein was extracted and used for Western blot analysis.

MMS sensitivity assay. Synchronous ring stage parasites were treated with different concentrations of 17AAG (170 nM to 850 nM) or radicicol (1.5 μ M) and grown until the late trophozoite/early schizont stage. Pretreated parasites (1% parasitemia) were then subjected to MMS treatment (0.001%, 0.005%, and 0.1%) for 2 h. Further washing with RPMI medium was performed in order to remove the MMS. Then, the parasites were allowed to grow for 48 h in the presence of the respective concentrations of 17AAG or radicicol. Parasitemia was monitored by Giemsa-stained smear. The percent survivability was calculated using the following equation: % survivability = (% parasitemia in the absence of MMS/% parasitemia in the presence of MMS) \times 100.

PCR-based method to quantify DNA damage. Repair kinetics of damaged nuclear DNA were studied as previously described (27). Briefly, ring stage culture with a parasitemia of 6% was pretreated with 17AAG (1.7 μ M), with B02 (1 μ M), or with atovaquone (0.3 nM). Since treatment with 1.7 μ M 17-AAG resulted in a dramatic depletion of PfRad51 protein, this particular dose of 17-AAG was chosen for the DNA repair experiment. In a previous study, sublethal concentrations of B02 (1 μ M) and atovaquone (0.3 nM) were used as the positive control and negative control, respectively (27). DNA damage was induced at the early trophozoite stage through UV exposure at 100 J/m². Then, the cultures were maintained in the presence of the respective inhibitors for 24 h. The parasite was harvested for genomic DNA isolation before the damage (UT), just after the damage (0 h), at 12 h, and at 24 h. PCRs for long-range (7,200 bp) and short range (269 bp) fragments were performed from equal amounts of isolated genomic DNA for each time point, using the primer sets described earlier (27). Quantification of the PCR product was performed using SYBR green I dye, and the fluorescence readings of the long-range PCR products were normalized by the reading obtained from the short-range PCR product. The amount of damaged DNA at any given time point was deduced from the following equation: damaged DNA = 1-(fluores-fluorecence intensity of the long PCR product/fluorescence intensity of the short PCR product × 26.76), where the factor 26.76 represents the ratio of the sizes of the two amplicons. The amount of damaged DNA from the UV-untreated sample was considered to be 0% and the zero-hour sample was considered to be 100%. The amount of residual damaged DNA at each time point was plotted using GraphPad Prism 6

Fixed-ratio isobologram method for the determination of interaction between 17AAG and B02. Synchronous P. falciparum cultures of the late ring stage were used to determine the interactions between 17AAG and B02. For the determination of the IC_{50} of 17AAG, parasite cultures were incubated in the presence of various concentrations of 17AAG (0.1 nM to 1 mM) for 48 h, followed by parasite quantification using a SYBR green I-based method. The IC₅₀ value was determined from a semilogarithmic plot of percent inhibition versus concentrations of 17AAG using GraphPad Prism 6. Similarly, the IC₅₀ of B02 was also determined. For the drug interaction study, a fixed-ratio method was used as previously described (6). Briefly, in the combination assay, 17AAG and B02 were combined in four fixed ratios (4:1, 3:2, 2:3, and 1:4). Approximately 8-fold IC_{50} concentrations of each compound were taken as 100% so the IC_{so} of the individual compound fell in between the third and fourth of a 2-fold serial dilution. For each dilution, triplicate readings were taken. A SYBR green I-based evaluation of parasitemia was done to estimate percent inhibition. Semilogarithmic graphs were plotted using GraphPad Prism 6 software for each combination from three independent experiments to determine the IC_{50} values. The fractional inhibitory concentration (FIC) for each drug was determined by using the following equation: FIC = IC₅₀ of the drug in the mixture/ IC_{50} of the drug alone. The FIC values of both drugs were used to determine the interaction between 17AAG and B02 by using the following equation: \sum FIC = (IC $_{50}$ of 17AAG in the mixture/IC₅₀ of 17AAG alone) + (IC₅₀ of B02 in the mixture/IC₅₀ of B02 alone). An isobologram was plotted by using GraphPad Prism 6 software. An \sum FIC of 1 represents synergism, \sum FICs of \geq 1 and <2 represent additive interactions, and an \sum FIC of \geq 2 represents antagonism.

ACKNOWLEDGMENTS

This work was supported by grants from DST-SERB, Government of India (grant EMR/ 2017/001173), to S.B. and D.B.T. and the Government of India (grant BT/PR25858/GET/ 119/169/2017)2 to M.K.B. We acknowledge support from DST-FIST and UGC-SAP to the Department of Biochemistry and the Department of Biotechnology and Bioinformatics. W.T. and N.S. are supported by Senior Research Fellowships from the University Grants

Commission, Government of India. P.S. is supported by a Senior Research Fellowship from the Council for Scientific and Industrial Research, Government of India.

REFERENCES

- 1. Atamna H, Ginsburg H. 1993. Origin of reactive oxygen species in erythrocytes infected with *Plasmodium falciparum*. Mol Biochem Parasitol 61:231–241. https://doi.org/10.1016/0166-6851(93)90069-a.
- Lee AH, Symington LS, Fidock DA. 2014. DNA repair mechanisms and their biological roles in the malaria parasite *Plasmodium falciparum*. Microbiol Mol Biol Rev 78:469–486. https://doi.org/10.1128/MMBR.00059-13.
- Namsaraev E, Berg P. 1997. Characterization of strand exchange activity of yeast Rad51 protein. Mol Cell Biol 17:5359–5368. https://doi.org/10 .1128/MCB.17.9.5359.
- Bhattacharyya MK, Kumar N. 2003. Identification and molecular characterisation of DNA damaging agent induced expression of *Plasmodium falciparum* recombination protein PfRad51. Int J Parasitol 33:1385–1392. https://doi.org/10.1016/s0020-7519(03)00212-1.
- Bhattacharyya MK, Bhattacharyya Nee Deb S, Jayabalasingham B, Kumar N. 2005. Characterization of kinetics of DNA strand-exchange and ATP hydrolysis activities of recombinant PfRad51, a *Plasmodium falciparum* recombinase. Mol Biochem Parasitol 139:33–39. https://doi.org/10.1016/j.molbiopara.2004 .09.007.
- Vydyam P, Dutta D, Sutram N, Bhattacharyya S, Bhattacharyya MK. 2019. A small-molecule inhibitor of the DNA recombinase Rad51 from *Plasmodium fal*ciparum synergizes with the antimalarial drugs artemisinin and chloroquine. J Biol Chem 294:8171–8183. https://doi.org/10.1074/jbc.RA118.005009.
- Roy N, Bhattacharyya S, Chakrabarty S, Laskar S, Babu SM, Bhattacharyya MK. 2014. Dominant negative mutant of *Plasmodium* Rad51 causes reduced parasite burden in host by abrogating DNA double-strand break repair. Mol Microbiol 94:353–366. https://doi.org/10.1111/mmi.12762.
- Cadet J, Sage E, Douki T. 2005. Ultraviolet radiation-mediated damage to cellular DNA. Mutat Res 571:3–17. https://doi.org/10.1016/j.mrfmmm.2004.09.012.
- Wiseman H, Halliwell B. 1996. Damage to DNA by reactive oxygen and nitrogen species: role in inflammatory disease and progression to cancer. Biochem J 313:17–29. https://doi.org/10.1042/bj3130017.
- Constant JF, O'Connor TR, Lhomme J, Laval J. 1988. 9-[(10-(Aden-9-yl)-4,8-dia-zadecyl)amino]-6-chloro-2-methoxy-acridine incises DNA at apurinic sites. Nucleic Acids Res 16:2691–2703. https://doi.org/10.1093/nar/16.6.2691.
- Kaina B, Ochs K, Grösch S, Fritz G, Lips J, Tomicic M, Dunkern T, Christmann M. 2001. BER, MGMT, and MMR in defense against alkylationinduced genotoxicity and apoptosis. Prog Nucleic Acids Res Mol Biol 68:41–54. https://doi.org/10.1016/s0079-6603(01)68088-7.
- Nikolova T, Ensminger M, Löbrich M, Kaina B. 2010. Homologous recombination protects mammalian cells from replication-associated DNA double-strand breaks arising in response to methyl methanesulfonate. DNA Repair (Amst) 9:1050–1063. https://doi.org/10.1016/j.dnarep.2010.07.005.
- Tashiro S, Walter J, Shinohara A, Kamada N, Cremer T. 2000. Rad51 accumulation at sites of DNA damage and in postreplicative chromatin. J Cell Biol 150:283–291. https://doi.org/10.1083/jcb.150.2.283.
- Whitesell L, Lindquist SL. 2005. HSP90 and the chaperoning of cancer. Nat Rev Cancer 5:761–772. https://doi.org/10.1038/nrc1716.
- Biebl MM, Buchner J. 2019. Structure, function, and regulation of the Hsp90 machinery. Cold Spring Harb Perspect Biol 11:a034017. https://doi.org/10.1101/cshperspect.a034017.
- Grenert JP, Johnson BD, Toft DO. 1999. The importance of ATP binding and hydrolysis by hsp90 in formation and function of protein heterocomplexes. J Biol Chem 274:17525–17533. https://doi.org/10.1074/jbc.274.25 .17525.
- Stebbins CE, Russo AA, Schneider C, Rosen N, Hartl FU, Pavletich NP. 1997. Crystal structure of an Hsp90-geldanamycin complex: targeting of a protein chaperone by an antitumor agent. Cell 89:239–250. https://doi. org/10.1016/S0092-8674(00)80203-2.
- Roe SM, Prodromou C, O'Brien R, Ladbury JE, Piper PW, Pearl LH. 1999. Structural basis for inhibition of the Hsp90 molecular chaperone by the antitumor antibiotics radicicol and geldanamycin. J Med Chem 42:260–266. https://doi.org/10.1021/jm980403y.
- Murillo-Solano C, Dong C, Sanchez CG, Pizarro JC. 2017. Identification and characterization of the antiplasmodial activity of Hsp90 inhibitors. Malar J 16:292. https://doi.org/10.1186/s12936-017-1940-7.
- Posfai D, Eubanks AL, Keim Al, Lu KY, Wang GZ, Hughes PF, Kato N, Haystead TA, Derbyshire ER. 2018. Identification of Hsp90 inhibitors with

- anti-*Plasmodium* activity. Antimicrob Agents Chemother 62:e01799-17. https://doi.org/10.1128/AAC.01799-17.
- 21. Banumathy G, Singh V, Pavithra SR, Tatu U. 2003. Heat shock protein 90 function is essential for *Plasmodium falciparum* growth in human erythrocytes. J Biol Chem 278:18336–18345. https://doi.org/10.1074/jbc.M211309200.
- 22. Wider D, Péli-Gulli MP, Briand PA, Tatu U, Picard D. 2009. The complementation of yeast with human or *Plasmodium falciparum* Hsp90 confers differential inhibitor sensitivities. Mol Biochem Parasitol 164:147–152. https://doi.org/10.1016/j.molbiopara.2008.12.011.
- Bagatell R, Beliakoff J, David CL, Marron MT, Whitesell L. 2005. Hsp90 inhibitors deplete key anti-apoptotic proteins in pediatric solid tumor cells and demonstrate synergistic anticancer activity with cisplatin. Int J Cancer 113:179–188. https://doi.org/10.1002/ijc.20611.
- 24. Pennisi R, Ascenzi P, di Masi A. 2016. Correction: Pennisi, R., et al. Hsp90: a new player in DNA repair? Biomolecules 2015, 5, 2589-2618. Biomolecules 6:40. https://doi.org/10.3390/biom6040040.
- Suhane T, Laskar S, Advani S, Roy N, Varunan S, Bhattacharyya D, Bhattacharyya S, Bhattacharyya MK. 2015. Both the charged linker region and ATPase domain of Hsp90 are essential for Rad51-dependent DNA repair. Eukaryot Cell 14:64–77. https://doi.org/10.1128/EC.00159-14.
- Suhane T, Bindumadhavan V, Fangaria N, Nair AS, Tabassum W, Muley P, Bhattacharyya MK, Bhattacharyya S. 2019. Glu-108 in Saccharomyces cerevisiae Rad51 is critical for DNA damage-induced nuclear function. mSphere 4: e00082-19. https://doi.org/10.1128/mSphere.00082-19.
- Suthram N, Padhi S, Jha P, Bhattacharyya S, Bulusu G, Roy A, Bhattacharyya MK. 2020. Elucidation of DNA repair function of PfBlm and potentiation of artemisinin action by a small-molecule inhibitor of RecQ helicase. mSphere 5: e00956-20. https://doi.org/10.1128/mSphere.00956-20.
- Nathan DF, Lindquist S. 1995. Mutational analysis of Hsp90 function: interactions with a steroid receptor and a protein kinase. Mol Cell Biol 15:3917–3925. https://doi.org/10.1128/MCB.15.7.3917.
- Chalapareddy S, Bhattacharyya MK, Mishra S, Bhattacharyya S. 2014. Radicicol confers mid-schizont arrest by inhibiting mitochondrial replication in *Plasmodium falciparum*. Antimicrob Agents Chemother 58:4341–4352. https://doi.org/10.1128/AAC.02519-13.
- Pallavi R, Roy N, Nageshan RK, Talukdar P, Pavithra SR, Reddy R, Venketesh S, Kumar R, Gupta AK, Singh RK, Yadav SC, Tatu U. 2010. Heat shock protein 90 as a drug target against protozoan infections: biochemical characterization of HSP90 from *Plasmodium falciparum* and Trypanosoma evansi and evaluation of its inhibitor as a candidate drug. J Biol Chem 285:37964–37975. https://doi.org/10.1074/jbc.M110.155317.
- 31. Seraphim TV, Chakafana G, Shonhai A, Houry WA. 2019. *Plasmodium falciparum* R2TP complex: driver of parasite Hsp90 function. Biophys Rev 11:1007–1015. https://doi.org/10.1007/s12551-019-00605-3.
- Bayih AG, Pillai DR. 2014. Mouse studies on inhibitors of *Plasmodium fal-ciparum* Hsp90: progress and challenges. Parasitology 141:1216–1222. https://doi.org/10.1017/S0031182014000754.
- Chua CS, Low H, Sim TS. 2014. Co-chaperones of Hsp90 in *Plasmodium fal-ciparum* and their concerted roles in cellular regulation. Parasitology 141:1177–1191. https://doi.org/10.1017/S0031182013002084.
- 34. Ramdhave AS, Patel D, Ramya I, Nandave M, Kharkar PS. 2013. Targeting heat shock protein 90 for malaria. Mini Rev Med Chem 13:1903–1920. https://doi.org/10.2174/13895575113136660094.
- 35. Khurana N, Laskar S, Bhattacharyya MK, Bhattacharyya S. 2016. Hsp90 induces increased genomic instability toward DNA-damaging agents by tuning down RAD53 transcription. Mol Biol Cell 27:2463–2478. https://doi.org/10.1091/mbc.E15-12-0867.
- Haltiwanger BM, Matsumoto Y, Nicolas E, Dianov GL, Bohr VA, Taraschi TF. 2000. DNA base excision repair in human malaria parasites is predominantly by a long-patch pathway. Biochemistry 39:763–772. https://doi.org/10.1021/bi9923151.
- 37. Tajedin L, Anwar M, Gupta D, Tuteja R. 2015. Comparative insight into nucleotide excision repair components of *Plasmodium falciparum*. DNA Repair (Amst) 28:60–72. https://doi.org/10.1016/j.dnarep.2015.02 .009.

Downloaded from https://journals.asm.org/journal/aac on 17 August 2021 by 14.139.69.175.

- 38. Tarique M, Ahmad M, Chauhan M, Tuteja R. 2017. Genome wide in silico analysis of the mismatch repair components of Plasmodium falciparum and their comparison with human host. Front Microbiol 8:130. https://doi .org/10.3389/fmicb.2017.00130.
- 39. Tabassum W, Bhattacharyya S, Varunan SM, Bhattacharyya MK. 2021. Febrile temperature causes transcriptional downregulation of *Plasmodium* falciparum Sirtuins through Hsp90-dependent epigenetic modification. Mol Microbiol https://doi.org/10.1111/mmi.14692.
- 40. Trager W, Jensen JB. 1976. Human malaria parasites in continuous culture. Science 193:673-675. https://doi.org/10.1126/science.781840.
- 41. Williams B, Bhattacharyya MK, Lustig AJ. 2005. Mre11p nuclease activity is dispensable for telomeric rapid deletion. DNA Repair (Amst) 4:994-1005. https://doi.org/10.1016/j.dnarep.2005.04.016.
- 42. Jha P, Laskar S, Dubey S, Bhattacharyya MK, Bhattacharyya S. 2017. *Plasmodium* Hsp40 and human Hsp70: a potential cochaperone-chaperone complex. Mol Biochem Parasitol 214:10–13. https://doi.org/10.1016/j.molbiopara.2017.03.003.
- 43. Badugu SB, Nabi SA, Vaidyam P, Laskar S, Bhattacharyya S, Bhattacharyya MK. 2015. Identification of *Plasmodium falciparum* DNA repair protein Mre11 with an evolutionarily conserved nuclease function. PLoS One 10:e0125358. https:// doi.org/10.1371/journal.pone.0125358.

RESEARCH ARTICLE



Check for updates

Febrile temperature causes transcriptional downregulation of *Plasmodium falciparum* Sirtuins through Hsp90-dependent epigenetic modification

Wahida Tabassum ¹ | Sunanda Bhattacharyya ² | Shalu M. Varunan ¹ | Mrinal Kanti Bhattacharyya ¹

Correspondence

Mrinal Kanti Bhattacharyya, Department of Biochemistry, School of Life Sciences, University of Hyderabad, Hyderabad, TS, India.

Email: mkbsl@uohyd.ernet.in

Funding information

Science and Engineering Research Board, Grant/Award Number: DST-SERB/2015/000999

Abstract

Sirtuins (*PfSIR2A* and *PfSIR2B*) are implicated to play pivotal roles in the silencing of sub-telomeric genes and the maintenance of telomere length in *P. falciparum* 3D7 strain. Here, we identify the key factors that regulate the cellular abundance and activity of these two histone deacetylases. Our results demonstrate that *PfSIR2A* and *PfSIR2B* are transcriptionally downregulated at the mid-ring stage in response to febrile temperature. We found that the molecular chaperone PfHsp90 acts as a repressor of *PfSIR2A* & *B* transcription. By virtue of its presence in the *PfSIR2A* & *B* promoter proximal regions PfHsp90 helps recruiting H3K9me3, conferring heterochromatic state, and thereby leading to the downregulation of *PfSIR2A* & *B* transcription. Such transcriptional downregulation can be reversed by the addition of 17-(ally lamino)-17-demethoxygeldanamycin or Radicicol, two potent inhibitors of PfHsp90. The reduced occupancy of PfSir2 at sub-telomeric *var* promoters leads to the derepression of *var* genes. Thus, here we uncover how exposure to febrile temperature, a hallmark of malaria, enables the parasites to manipulate the expression of the two prominent epigenetic modifiers PfSir2A and PfSir2B.

KEYWORDS

antigenic variation, heat shock proteins, Sir2, telomere silencing, var gene

1 | INTRODUCTION

Malaria caused by the parasite *Plasmodium falciparum* continues to possess a serious threat to mankind due to failure in curbing the disease. Lack of an effective vaccine, development of resistant parasites to all the available antimalarial drugs, and emergence of insecticide-resistant mosquitos are the major impediments in controlling the disease. Thus, there is an urgent need to discover novel drug targets from the parasite biology. The developmental biology of *P. falciparum* is mainly controlled by the epigenetic regulations of gene transcriptions. Thus, characterizing the various epigenetic writers, readers, and erasers with a special emphasis on their regulation could discover novel druggable targets.

In *P. falciparum* two Sirtuin genes, namely *PfSIR2A* and *PfSIR2B* are characterized as epigenetic erasers (Tonkin et al., 2009). The PfSir2 proteins are NAD⁺-dependent histone deacetylases (Chakrabarty et al., 2008; Merrick & Duraisingh, 2007; Prusty et al., 2008). In model organisms the Sir2 proteins play important regulatory roles in several physiological processes, including mating-type silencing, rDNA silencing, prevention of ectopic recombination at rDNA loci, telomere position effect, DNA repair, replicative senescence, and caloric restriction (Guarente, 1999; Hasty, 2001). So far in malaria parasites PfSir2A/ PfSir2B have been implicated in heterochromatin silencing, telomere length maintenance, and antigenic variation (Tonkin et al., 2009). Although individual knockouts of both *PfSIR2A* and *PfSIR2B* genes have been generated (Tonkin et al., 2009), the

¹Department of Biochemistry, School of Life Sciences, University of Hyderabad, Hyderabad, India

²Department of Biotechnology and Bioinformatics, School of Life Sciences, University of Hyderabad, Hyderabad, India

double knockout has not been possible yet implying that the presence of at least one of these genes is essential for the parasite biology. Thus, it is of significant importance to study the mechanism of *PfSIR2* expression and regulation. As not many of the transcription factors are found in *Plasmodium* genome, epigenetic mode of gene regulation might play pivotal role in controlling *PfSIR2* gene expression (Hakimi & Deitsch, 2007; Iyer et al., 2008). In *P. falciparum* the known repressive marks are H3K9me3 and H3K36me2 (Chookajorn et al., 2007; Karmodiya et al., 2015; Lopez-Rubio et al., 2007). Keeping all these in mind, we hypothesize that the selective enrichment and cross talks of these epigenetic marks at *PfSIR2* promoter regions could dictate the transcriptional fate of *PfSIR2* genes.

Hsp90, initially discovered as a cytoplasmic chaperone, is found to play several functions at the nucleus of higher eukaryotes and in the budding yeast (Brown et al., 2015; Hamamoto et al., 2006; Laskar et al., 2011, 2015; Sawarkar & Paro, 2013; Sawarkar et al., 2012; Tariq et al., 2009). A number of transcription factors have been found to be the clients of Hsp90 in a variety of organisms (Khurana & Bhattacharyya, 2015). Additionally, Hsp90 has been found to be associated with the chromosomes at the promoter-proximal regions in higher organisms (Brown et al., 2015; Tariq et al., 2009). Till date the chromosomal occupancy of Hsp90 or its role in modulating chromatin dynamics has not been reported in any protozoan parasites. In *P. falciparum* four paralogs of the *HSP90* genes have been identified (Gardner et al., 2002). However, any direct or indirect roles of PfHsp90 in transcriptional regulation has not been established yet.

Antigenic variation is a strategy of the parasite by which they escape the host defense mechanism by exhibiting mono-allelic expression of var genes (Baruch et al., 1995; Scherf et al., 1998; Smith et al., 1995; Su et al., 1995). In natural isolates of P. falciparum the number var genes varies from 45 to 90 (Otto et al., 2018). In the reference genome of P. falciparum 3D7 strain there are at least 59 var gene present per haploid genome of the parasite, which are found to be distributed on 13 out of 14 chromosomes (Gardner et al., 2002). Majority of them are localized at sub-telomeric regions, whereas 24 of them are present at internal chromosomal loci (Gardner et al., 2002). The var genes have been classified into four subgroups based on the sequence similarity in their 5'promoter regions: Ups A, Ups B, Ups C, and Ups E (Kraemer et al., 2007). Among all of the 59 var genes, only one is found to be expressed at the protein level (PfEMP1) at trophozoite and schizont (intra erythrocytic) stages of the parasite while others remain silenced (Kraemer & Smith, 2006). Studies suggest that knockout of SIR2A leads to de-repression of var genes under the control of Ups A, Ups E, and Ups C, whereas var genes under the control of Ups B are found to be highly upregulated when SIR2B is disrupted (Tonkin et al., 2009).

Malaria parasites during the course of their complicated life cycle are subjected to various temperature variations: 37°C in the human host, 25°C-26°C in vector mosquito, and to higher febrile temperature above 40°C during malaria-induced fever in the host. It is well established in several organisms that changes in the environment lead to global changes in the transcriptome and at the mechanistic level they are governed by epigenetic modifications (Lobo, 2008;

Vinci, 2012). Studies aimed at investigating the transcriptome profiling upon exposure of parasite to febrile temperature have revealed that there is a tremendous impact of heat treatment on the transcriptome profile of the human malaria parasite P. falciparum (Oakley et al., 2007). In vitro transcriptome analysis done after subjecting these parasites to heat shock at 41°C for 2 hr revealed that there is upregulation in the expression of var genes (Oakley et al., 2007). Counter intuitively, it has also been observed that exposure of heat shock to asynchronous parasite leads to upregulation of SIR2A (Oakley et al., 2007). These findings were interesting, but puzzling. It remained unclear how upregulation of SIR2 and upregulation of var gene both happen upon heat shock where Sir2 is a known negative regulator of var expression, at least in the 3D7 strain. However, in other organism like yeast it has been observed that exposure of heat shock leads to downregulation of SIR2 with a concomitant derepression of sub-telomeric genes (Laskar et al., 2015). During the infection cycle of P. falciparum within the human host, the rupture of schizonts coincides with the malarial cyclical fever indicating that the ring stage of the parasite is subjected to high febrile temperature (Golgi, 1886). This prompted us to ask the following question: whether the effect of heat shock on the expression of PfSIR2 gene is stage-specific.

In this study, we have explored the mechanism of PfSIR2A and PfSIR2B gene in response to heat shock. Interestingly, we found that upon heat shock PfSIR2A and PfSIR2B are downregulated in a midring stage-specific manner and concomitantly majority of var genes are also de-repressed. Further our work shows that heat shock leads to increased occupancy of trimethylated-H3K9 at both $SIR2_{UAS}$ causing heterochromatinization of this locus. We have further established that such process is directly dependent on PfHsp90 activity at the promoter proximal region of PfSIR2A and PfSIR2B. Thus, this work depicts that an environmental cue, such as heat shock amends PfSIR2B and PfSIR2B gene expression via epigenetic modifications.

2 | RESULTS

2.1 | Brief exposure to elevated temperature results in downregulation of *PfSIR2A* and *PfSIR2B* expressions at the ring stage

Changes in the environment often leads to changes in gene transcription through epigenetic modifications of chromatins (Lobo, 2008; Vinci, 2012). Since the epigenetic erasers PfSir2A and PfSir2B have been implicated to play crucial roles in parasite physiology by virtue of regulating the virulence gene expression, we sought to explore whether the steady-state levels of these two proteins are altered due to exposure to febrile temperatures. To address this, we took synchronous parasite cultures of ring, trophozoite and schizont stages and divided each stage-specific culture in two parts: one part was subjected to heat shock at 41°C for 2 hr while the other part was grown at normal condition (37°C). Western blot analysis was performed with the total protein isolated from parasites grown under these conditions. To

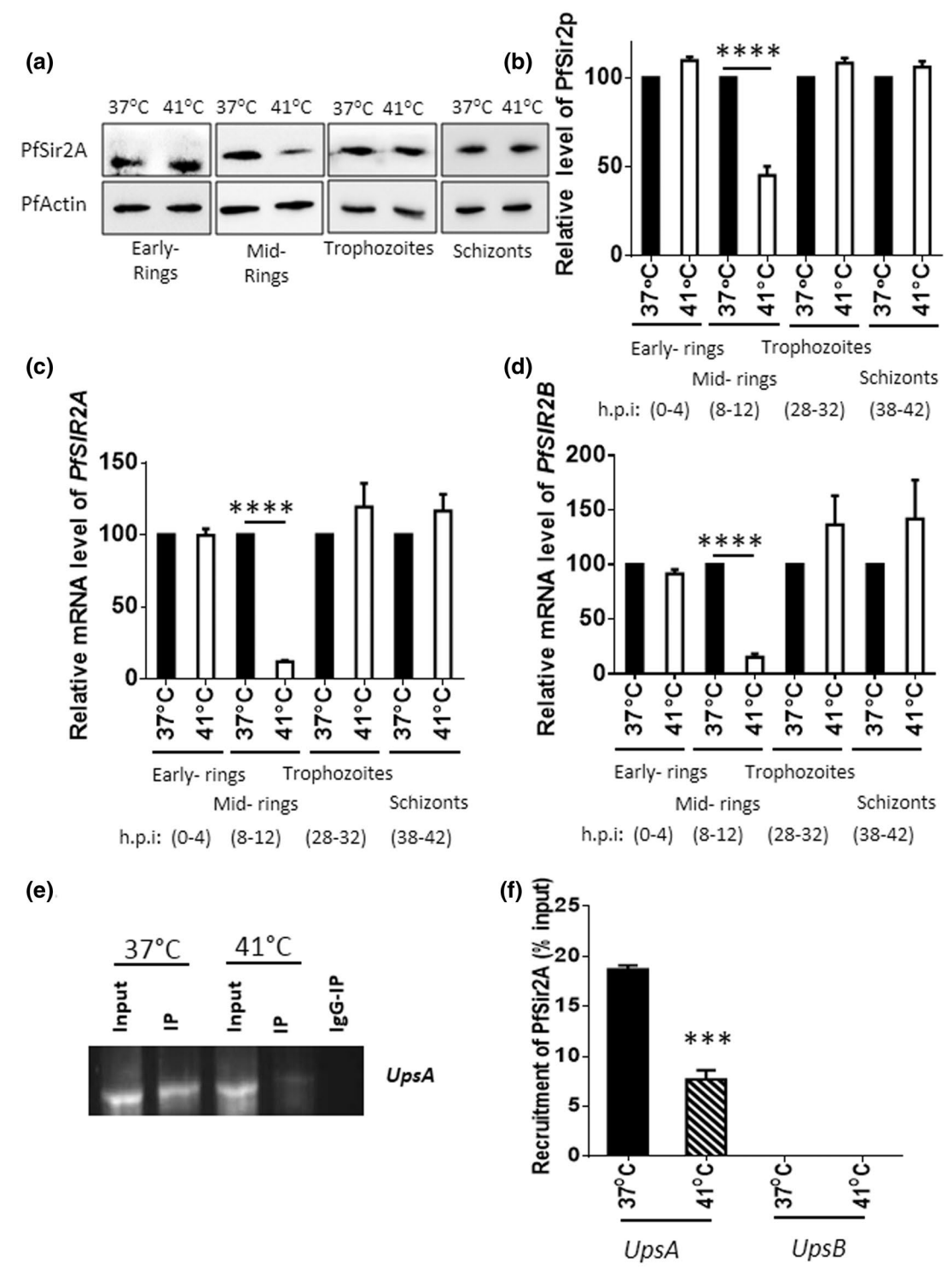


FIGURE 1 Heat-induced downregulation PfSir2A and PfSir2B expression are specific to the ring stage. (a) Western blot analysis of PfSir2A expression performed with total protein isolated from parasites of different stages grown under normal condition (37°C) and heat-treated condition (41°C). PfActin was used as a loading control. (b) Quantification of band intensities shows a lower abundance of PfSir2A upon heat shock at the mid-ring stage. Error bar indicates the SEM obtained from three individual experiments. (c) Real-time RT PCR analysis showing mRNA levels of PfSIR2A at the four different stages of parasites in control 37°C and heat-treated conditions. (d) Real-time RT PCR showing mRNA levels of PfSIR2B at four different stages of parasites in control and heat-treated conditions. The RT qPCR results are representative of three independent experiments, error bar indicates the SEM and SERYL-tRNA SYNTHETASE was used as the normalizing control. (e) ChIP assay was performed using mid-ring stage parasites grown under normal and heat-treated conditions. Anti PfSir2A antibody was used for precipitations. Input and immunoprecipitated DNA were amplified by PCR with primers specific to two Ups A sequences (PF3D7_0400400; PF3D7_1300300) and Ups B (PF3D7_10_v3:1650432.1650766). Gel picture depicts enrichment of PfSir2A at Ups A, lane1: Input (37°C), lane2: Sir2A IP (37°C), lane 3: Input (41°C), lane4: Sir2A IP (41°C), and lane5: IgG IP. (f) Graph was plotted from the value of band intensities obtained from three independent experiments with error bar indicating the SEM. Asterisks indicate values significantly different from the control, as follows: ****p <.0001, ****p <.0001

this end, we have raised an anti-PfSir2A antibody against recombinant PfSir2A protein that showed enzyme activity in an earlier study (Prusty et al., 2008). The specificity of the antibody was checked by Western blot analysis using parasite lysate. The antibody detected a specific band of molecular weight 30 kDa corresponding to PfSir2A but did not recognize PfSir2B protein (Figure S1). The specificity of this antibody was ascertained by the absence of a similar band on a blot probed with the pre-immune sera. PfSir2A antibody was used to detect the steadystate level of PfSir2A on Western blot, whereas PfActin was used as a loading control (Figure 1a). Due to the lack of a PfSir2B antibody we could not measure the steady-state level of this protein. We observed 2.2-fold reduction in the steady-state level of PfSir2A protein upon heat treatment at the mid-ring stage (Figure 1b). No such reduction of PfSir2A protein was observed if heat treatment was given at the earlyring, trophozoite, or schizont stages. In order to investigate whether the less abundance of PfSir2 protein is due to any downregulation at the transcriptional level, we performed real-time RT-PCR analysis with RNA isolated from control or heat-treated parasites and analyzed the expression of PfSIR2A and PfSIR2B. Rivetingly we observed that there is almost 8-fold downregulation in transcripts of both PfSIR2A and PfSIR2B upon heat shock (Figure 1c,d) and this downregulation is specific to the mid-ring stage (8-12 hr post invasion). In the case of trophozoite or schizont stages slight increase in the level of mRNA was observed in the heat-treated parasites. While we did not observe any change in the transcript level at the very early ring stage (0-4 hr post invasion). We were curious to investigate whether such downregulation in PfSIR2 expression is a sudden change that happens at only at 41°C or there is a trend of gradual downregulation with increasing temperature. To investigate this, synchronous mid-ring stage parasite culture was divided in five parts, one part was kept as control and grown at 37 °C, while others were subjected to heat stress at 38°C, 39°C, 40°C, and 41°C for 2 hr. Real-time RT-PCR analysis revealed that there is a gradual decrease in the transcript levels of PfSIR2A and PfSIR2B with increase in temperature and there was a significant reduction in transcription of both PfSIR2A and PfSIR2B upon heat shock even at 39°C (Figure S2).

We were interested in investigating whether lower abundance of PfSir2 under heat-treated condition results in lower occupancy of this protein at the var promoter leading to de-repression of var genes. To this end, we have performed chromatin immunoprecipitation (ChIP) experiment using anti-PfSir2A antibody and investigated the occupancy of PfSir2A at two var promoters: Ups A and Ups B. For amplification of Ups A we have used a primer set that would amplify two Ups A sequences. For Ups B amplification we have used a previously used primer set (Deshmukh et al., 2012). We observed that only Ups A is associated with PfSir2A protein (Figure 1e,f). The ChIP with IgG acted as a negative control. Lack of PfSir2A recruitment at the Ups B locus also acted as an internal negative control, emphasizing the specificity of the anti-PfSir2A antibody. This finding corroborates well with previous finding that PfSir2A regulates Ups A type var genes and PfSir2B regulates Ups B type var genes (Tonkin et al., 2009). As expected, we also observed that upon heat shock there is almost 3-fold reduced occupancy of PfSir2A at the Ups A loci (Figure 1f).

2.2 | Heat-induced recruitment of H3K9me3 is responsible for the repression of *PfSIR2* transcription

In order to get mechanistic insights into the heat-induced downregulation of PfSIR2A and PfSIR2B expression, we investigated the chromatin status of the upstream sequence of PfSIR2A (SIR2A_{LIPS}) and PfSIR2B ($SIR2B_{UPS}$) genes before and after heat treatment. Since the promoter or the transcription start site (TSS) is not defined for PfSIR2A or PfSIR2B we have taken about 300 bp sequence upstream of the translation start site (ATG) for both the genes for our analysis. To this end, we performed FAIRE (Formaldehyde Assisted Isolation of Regulatory Elements) technique, where the enrichment of FAIRE DNA represents the nucleosome-free state and the absence of FAIRE DNA represents the nucleosome-occupied state of the locus under investigation (Giresi & Lieb, 2009; Ponts et al., 2010). We observed that upon heat treatment there is a significant shift from the nucleosome-free state to the nucleosome-occupied state of both SIR2A_{UPS} and SIR2B_{UPS} loci (Figure 2a). The mitochondrial gene COX3 acted as a normalizing control as the mitochondrial genome is not associated with histones. Quantitative PCR analysis revealed 2.1-fold and 1.5-fold increase in the chromatin compaction at the $SIR2A_{UPS}$ locus and $SIR2B_{UPS}$ locus, respectively (Figure 2b). Thus, this result reveals that the heterochromatinization of the upstream regions of the PfSIR2 genes are responsible for the downregulation of PfSIR2 expression. As a negative control we have also analyzed the promoter region of PfARP gene as it is abundantly expressed at the ring stage. We observed that there was no change in the chromatin compaction before or after the heat treatment (Figure 2b). Thus, the promoter region of PfARP acted as a control for the FAIRE experiments emphasizing that the compaction of the PfSIR2A and PfSIR2B upstream regions are specific.

Furthermore, we wanted to decipher the epigenetic marks associated with such heterochromatinization of the PfSIR2A and PfSIR2B promoter proximal regions. To unravel this, we performed ChIP with synchronous mid-ring stage parasite cultures grown at 37°C (control sample) or at 41°C (heat-treated sample) using anti-H3K9me3, anti-H3K36me2, and pre-immune IgG antibodies. These antibodies are well established in detecting specific modifications on Plasmodium histones (Kafsack et al., 2014; Karmodiya et al., 2015). A dramatic increase in the recruitment of H3K9me3 was observed at both SIR2A_{UPS} and SIR2B_{UPS loci} (Figure 2c). We failed to detect any recruitment of H3K36me2 at the SIR2A_{UPS} or SIR2B_{UPS} loci before and after heat treatment (data not shown). The different recruitment patterns of the two repressor marks emphasize the specificity of the findings. ChIP experiment with IgG acted as a negative control. No recruitment was observed at the control locus ARP. As var-loci are known to be associated with H3K9me3, var-Ups A was used as a positive control for ChIP. Quantitative PCR analysis with ChIP DNA revealed that upon heat treatment there were almost 13-fold and 6-fold increased recruitment of H3K9me3 at the SIR2A_{LIPS} and SIR2B_{LIPS}, respectively (Figure 2d). These results suggest that the trimethylation of H3K9 is responsible for the heat-induced heterochromatinization of PfSIR2 promoter proximal region leading to the downregulation of

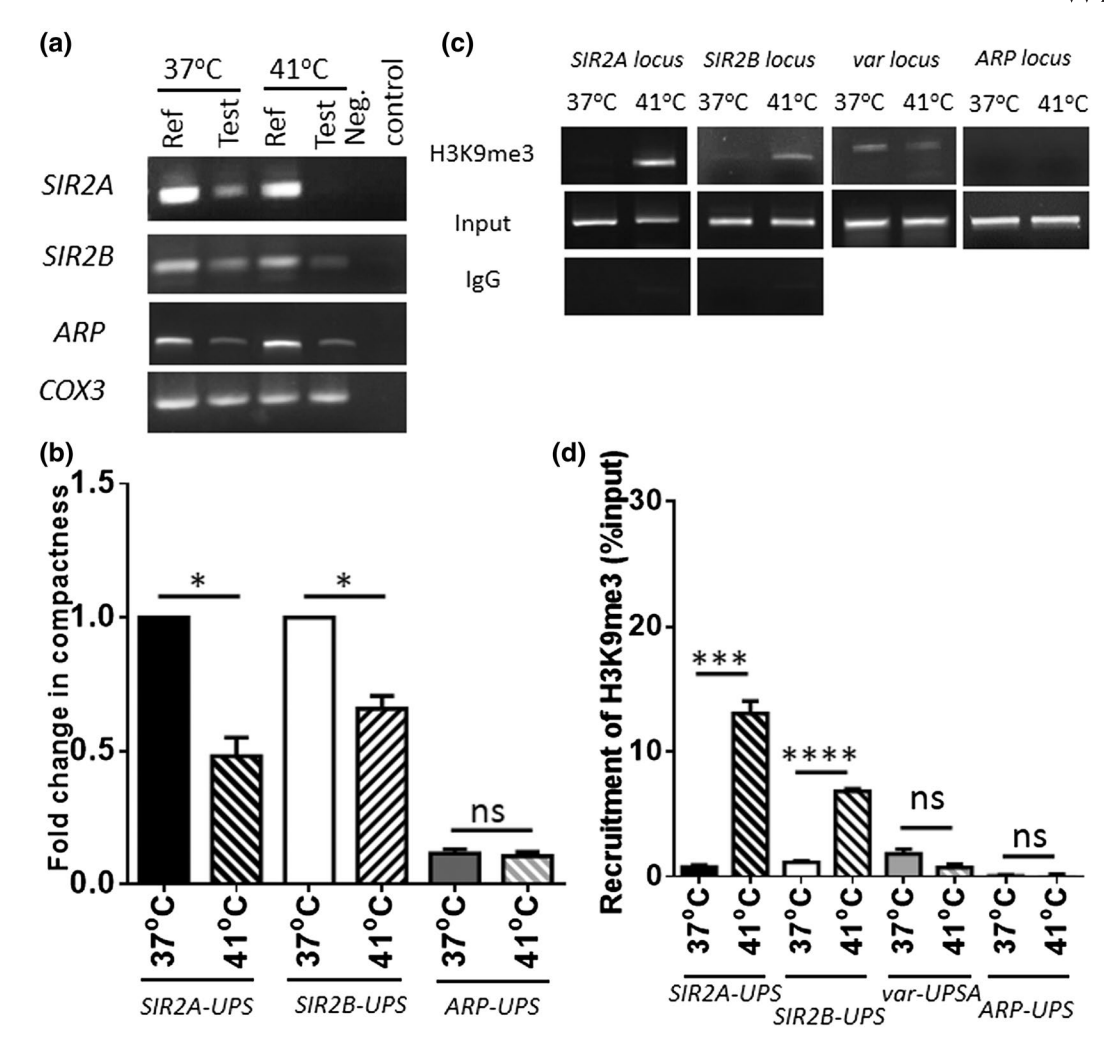


FIGURE 2 Heat-induced recruitment of H3K9me3 is responsible for the repression of PfSIR2A and PfSIR2B transcription. (a) FAIRE was performed using mid-ring stage parasites grown at normal condition and heat-treated condition to determine the change in chromatin compactness at $SIR2_{UPS}$ upon heat shock. Lane $1-37^{\circ}C$ reference, lane $2-37^{\circ}C$ test, lane $3-41^{\circ}C$ reference, lane $4-41^{\circ}C$ test, and lane 5- no template control. Semi-quantitative PCR was performed using DNA obtained through FAIRE and total DNA as reference DNA as templates. COX3 was used for normalization and ARP acted as a negative control for the assay. (b) Real-time PCR was performed to quantify the change in DNA abundance of nucleosome-free DNA upon heat shock. UPS stands for upstream sequences. The mean values $\pm SEM$ from three independent experiments are plotted (c) ChIP assay was performed using mid-ring stage parasites grown under normal condition (37°C) and parasite that were subjected to heat shock (41°C). Anti- H3K9me3 and IgG antibodies were used for immunoprecipitation. Input and immunoprecipitated DNA were amplified by PCR with primers specific to $SIR2A_{UPS}$ and $SIR2B_{UPS}$ and also of ARP_{UPS} which served as negative control and var_{UPS} that acted as the positive control. (d) Quantitative PCR from three different ChIP assay were performed and mean density $\pm SEM$ are plotted. Asterisks indicate values significantly different from the control, as follows: ****p < .0001, ***p < .0001, and *p < .005

PfSIR2 transcription. The recruitment of H3K9me3 at the *var*-UPS A loci was found to be little less upon heat treatment. However, such reduction was not statistically significant.

2.3 | Brief exposure to elevated temperature results in de-repression of multiple sub-telomeric *var* genes

In *P. falciparum* 3D7 strain PfSir2A and PfSir2B have been implicated as the negative regulators of sub-telomeric *var* gene expressions (Tonkin et al., 2009). However, for FCR3 or NF54 strains such strong negative correlation could not be established (Merrick et al., 2015). Thus,

we were interested in finding out whether heat shock-induced down-regulation of PfSir2A and PfSir2B correlates with the de-repression of sub-telomeric var genes in P. falciparum 3D7 strain. To investigate this, we have exposed synchronous parasites from the mid-ring stage of P. falciparum in vitro culture to heat treatment and analyzed the level of var transcripts by q-RT-PCR using the primer sets developed earlier (Salanti et al., 2003). These var genes belong to the different promoter types such as Ups A, Ups B, Ups C, and Ups E types and hybrid promoters Ups BA and Ups BC. In our study, we did not include any pseudovar or var-like sequences. We have performed our studies with in vitro grown parasite population that are expected to express the var genes randomly, instead of taking pan-selected or drug-selected parasites

where expression of a single *var* gene in the entire population is artificially induced. We observed that the majority of the *var* genes were upregulated irrespective of their chromosomal locations (Figure 3). Fourteen *var* genes exhibited more than 9-fold upregulation in their expression, 18 *var* genes were upregulated more than 3-fold but less than 9-fold, 12 *var* genes depicted less than 3-fold but more than 1.5-fold upregulation, and the remaining *var* genes showed less than 1.5-fold change in their expression upon heat shock (Table S1). These observations suggest that indeed environmental cue, such as temperature plays crucial role in governing the expression of *var* genes in *P. falciparum* 3D7 strain and such regulation is correlated well with the steady-state level of the prominent epigenetic modifier PfSir2 protein.

2.4 | Heat-induced downregulation of *PfSIR2* transcription is dependent on Hsp90 activity

As the molecular chaperon PfHsp90 is found to be induced when asynchronous cultures of *P. falciparum* are exposed to heat treatment (Oakley et al., 2007) and Hsp90 orthologs are known to play regulatory roles during transcription of several genes in a variety of

organisms (Khurana & Bhattacharyya, 2015; Sawarkar & Paro, 2013), we sought to investigate whether the stage-specific downregulations of PfSIR2A and PfSIR2B genes are mediated by PfHsp90. To address this, we first investigated whether PfHsp90 is induced in highly synchronous parasites belonging only to the ring stage. There are four paralogs of Hsp90 in P. falciparum genome having IDs as following: PF3D7 0708400; PF3D7 1222300; PF3D7 1118200; and PF3D7_1443900. Out of these, the gene product of PF3D7_0708400 (old ID: PF07_0029) is known to be recognized by the anti-Hsp90 antibody used in this study (Kumar et al., 2003). We observed that indeed there is 3-fold induction of PfHsp90 upon heat treatment (Figure 4a). PfActin was used as a loading control. We further observed that such induction is due to the transcriptional upregulation of PfHSP90 (Figure S3). Additionally, we observed that except for gene PF3D7_1443900 all other PfHSP90 genes are upregulated upon heat shock (Figure S3). In order to investigate whether PfHsp90 activity is required for transcriptional downregulation of PfSIR2A and PfSIR2B we used a potent chemical inhibitor of Hsp90, 17AAG. To this end we have treated in vitro cultures of P. falciparum with 170 nM 17AAG (1x) to inactivate PfHsp90 according to the previously established protocol (Chalapareddy et al., 2014).

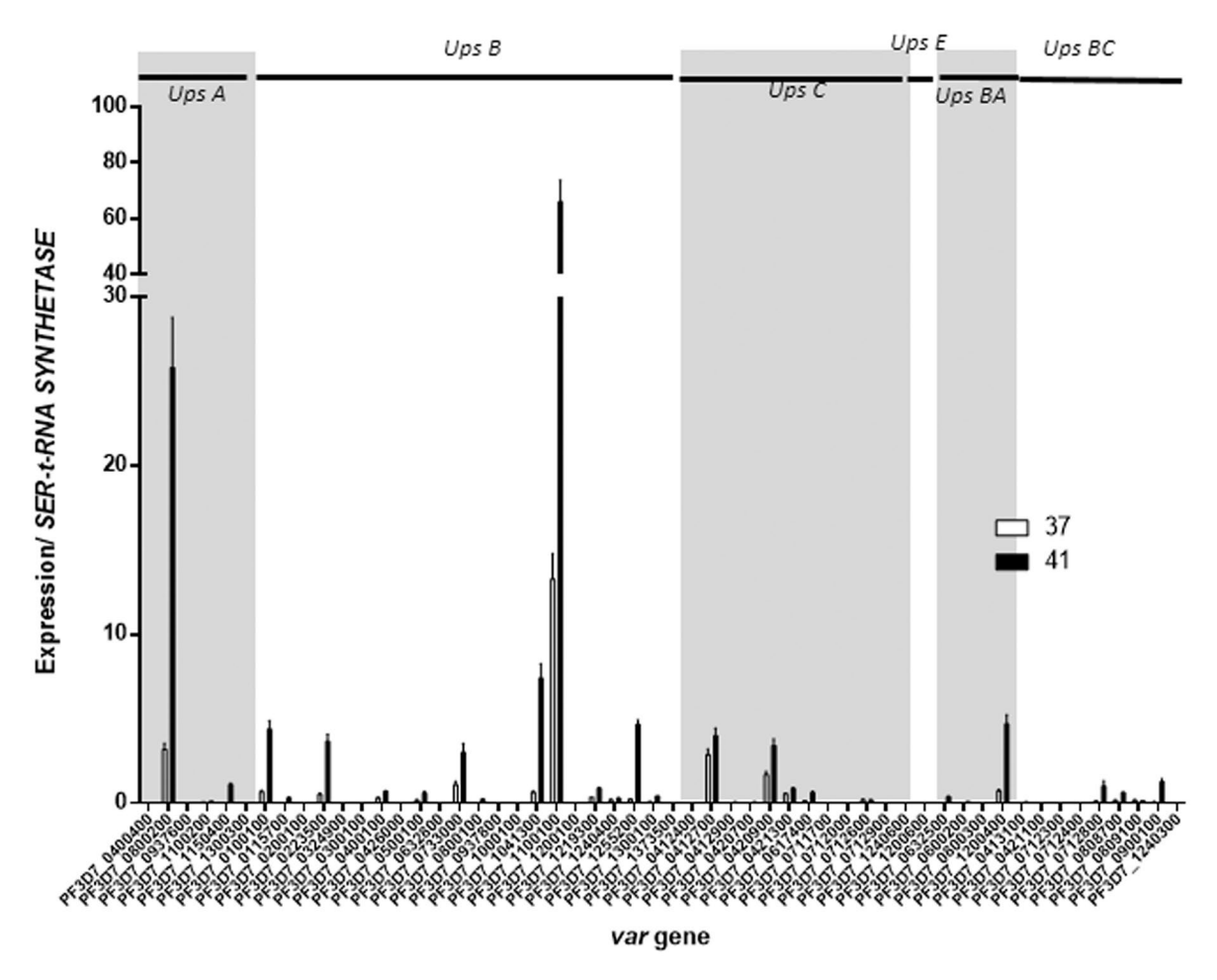


FIGURE 3 De-repression of *var* genes upon heat shock. The graph depicts the abundance of *var* transcripts with respect to *SERYL-tRNA SYNTHETASE* at normal condition (37°C) and upon heat shock at 41°C at mid-ring stage, quantified through real-time RT PCR. The qPCR results are representative of three independent experiments with data indicating the mean \pm *SEM*. The Gene ID of each *var* gene is written on the X-axis. The corresponding *UPS* type of each var gene is also marked

Synchronous parasite cultures of mid-ring stage were divided in four parts: two such cultures were grown at normal condition at 37°C with or without 17AAG treatment, while the other two cultures were subjected to heat treatment with and without 17AAG treatments. Real-time RT-PCR analysis on RNA isolated from the aforementioned four groups of parasites revealed that the heat-induced downregulation of *PfSIR2A* and *PfSIR2B* transcripts do not take place in cultures that were treated with 17AAG (Figure 4b). In order to ascertain the specificity of this finding that 17AAG-mediated inhibition

of PfHsp90 is responsible for the reversal of the heat-induced transcriptional downregulation of PfSIR2A and PfSIR2B genes we have performed a dose-dependent study: where in a parallel experiment we have treated the cultures with half the concentration of 17AAG (85 nM = 0.5x). We observed significant reversal of the phenotype, albeit to a lesser extent (Figure 4b). Additionally, we have performed an experiment where the parasite cultures were not pre-incubated with 17AAG and instead 17AAG (1x) was added at the onset of the 2-hr heat treatment. We observed a partial reversal of the phenotype,

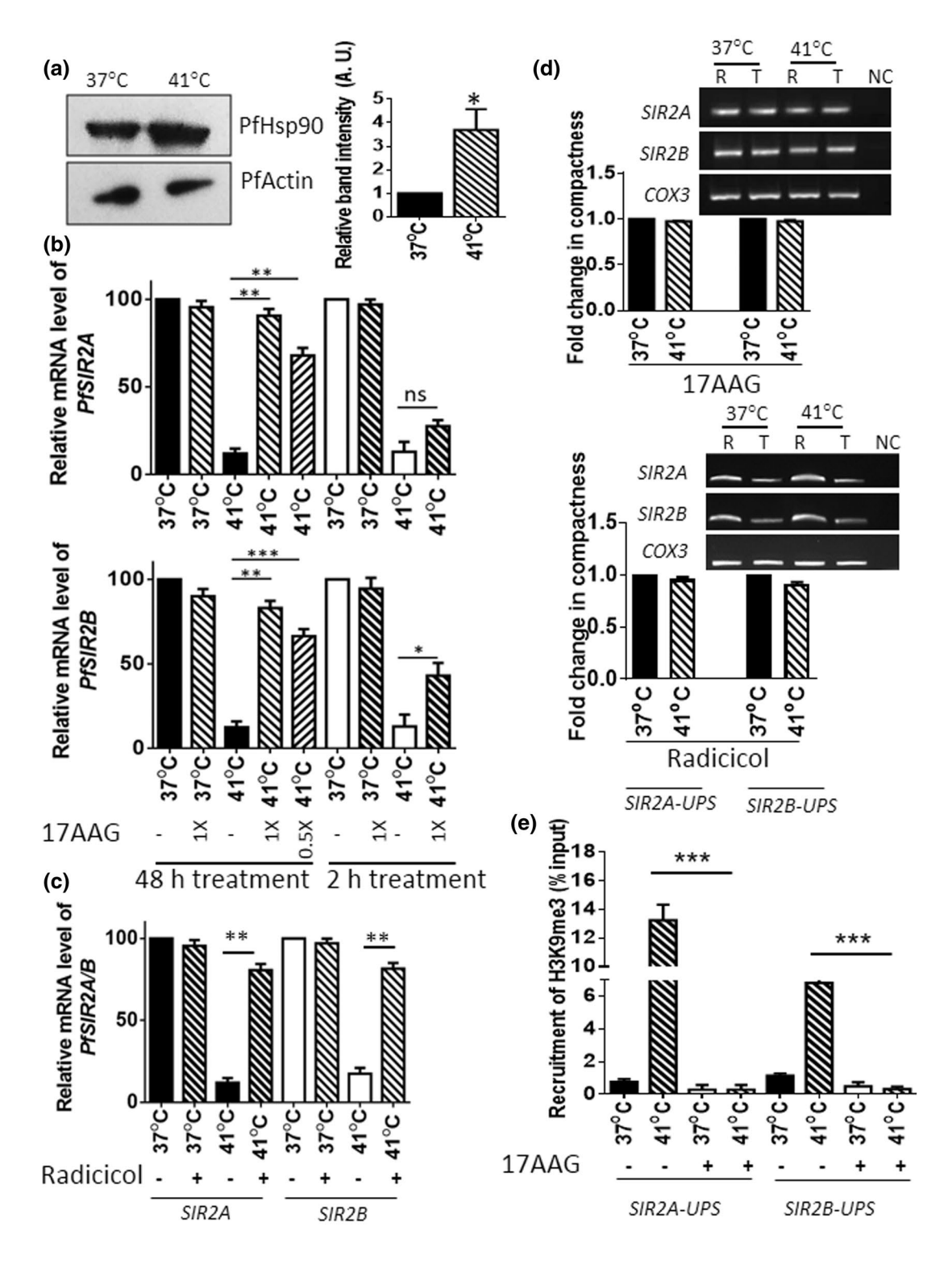


FIGURE 4 Heat-induced downregulation of PfSIR2A and PfSIR2B transcription is dependent on Hsp90 activity. (a) Western blot analysis to show PfHsp90 is over expressed in heat shock-treated ring stage parasites. Band intensity from three different experiments were quantified. Data were normalized against PfActin and mean density ± SEM were plotted. (b) Real-time RT-PCR were performed to quantify the relative abundance of PfSIR2A and PfSIR2B transcripts in 17AAG treated and untreated mid-ring stage parasites grown under normal and heat-treated conditions. Transcript levels were normalized by the housekeeping genes SERYL-tRNA SYNTHETASE transcript. The mean values ± SEM from three independent experiments are plotted. (c) Real-time RT-PCR were performed to quantify the relative abundance of PfSIR2A and PfSIR2B transcripts in Radicicol treated and untreated mid-ring stage parasites grown under normal and heat-treated conditions. Transcript levels were normalized by SERYL-tRNA SYNTHETASE transcript. The real-time plot is indicative of three independent experiments ± SEM. (d) FAIRE was performed to determine the chromatin compactness at PfSIR2A and PfSIR2B loci in 17AAG or Radicicoltreated mid-ring stage parasite grown at 37°C and at 41°C. Lane 1–37°C reference, lane 2–37°C test, lane 3–41°C reference, lane 4–41°C test, and lane 5- no template control. Semi-quantitative PCR was performed using DNA obtained through FAIRE and reference DNA as templates. COX3 was used for normalization. Quantitative PCR was performed to quantify the change in DNA abundance of nucleosomefree DNA. Mean value ± SEM were plotted. UPS stands for upstream sequences. (e) ChIP assay was performed with 17AAG-treated mid-ring parasites grown under normal and heat-treated conditions. The antibodies used are marked on the left side. Input and immunoprecipitated DNA were amplified by PCR with primers specific to SIR2A_{UPS}, SIR2B_{UPS}, and ARP_{UPS}, which served as a negative control. Quantitative PCR from three different ChIP experiments were performed and mean density \pm SEM are plotted. Asterisks indicate values significantly different from the control, as follows: ***p < .001, **p < .01, and *p < .05

which was significant for PfSIR2B but not for PfSIR2A (Figure 4b). Besides Geldanamycin and its derivatives, such as 17AAG, there is another unrelated chemical inhibitor, namely Radicicol, available that is found to be effective against PfHsp90 (Wider et al., 2009). We sought to investigate if treatment with Radicicol also can exert a similar effect on the heat-induced downregulation of PfSIR2A and PfSIR2B transcription. To this end, we have treated parasite cultures with 1.5 μM of Radicicol as it was observed earlier that higher concentrations of the drug results in the arrestation of the culture at the schizont stage (Chalapareddy et al., 2014). Parasites pre-treated with Radicicol were subjected to heat treatment for 2 hr at the midring stage and were evaluated for the level of PfSIR2A and PfSIR2B transcripts. Parallel cultures maintained at 37°C with or without Radicicol treatment were also evaluated. We observed that heatinduced transcriptional downregulation of both the genes do not take place if the cultures are treated with Radicicol (Figure 4c). These experiments clearly demonstrate that heat-induced downregulation of PfSIR2A and PfSIR2B expression is mediated by PfHsp90. As heatinduced transcriptional downregulation of PfSIR2 genes is associated with the heterochromatinization of PfSIR2_{UPS}, we wanted to find out whether treatment with 17AAG or Radicicol prevent the heatinduced compaction of the local chromatin. It was indeed observed that there is no reduction in the abundance of nucleosome-free DNA of PfSIR2A_{UPS} and PfSIR2B_{UPS} loci upon heat shock when the cultures were treated with 17AAG or Radicicol (Figure 4d). Primer specific to PfCOX3 was used as normalizing control. This suggests that Hsp90 activity is required for heat-induced heterochromatinization of PfSIR2A and PfSIR2B promoter proximal regions. In order to test that such failure in establishing the heterochromatic state is owing to a defect in the recruitment of H3K9me3 under Hsp90 inhibitory condition, we performed ChIP experiments with the control and heat-treated parasite cultures in the presence or absence of 17AAG. We observed a complete abolishment of H3K9me3 recruitment in 17AAG-treated samples (Figure 4e), suggesting that PfHsp90 activity is required for the epigenetic modification of the chromatin present at the PfSIR2A and PfSIR2B promoter proximal regions.

To investigate whether PfHsp90 plays any direct role in PfSIR2A and PfSIR2B downregulation, we performed ChIP experiment using anti-Hsp90 antibody to investigate its recruitment at PfSIR2_{UAS}. We have used five probes for each gene (PfSIR2A and PfSIR2B) to map the recruitment zones. Four probes were used to scan the upstream region (UPS) and one probe was within the gene (Figure 5a). Under heat-treated condition it was observed that, there is increased recruitment of PfHsp90 at immediate upstream sequences of PfSIR2 genes (A1/B1 regions). No recruitment was observed at control ARP locus (Figure 5b). Quantitative analysis of the ChIP DNA from the heat-treated samples revealed 2.8-fold and 2.2-fold more occupancy of PfHsp90 at PfSIR2A_{UPS} (A_1) and PfSIR2B_{UPS} (B_1) loci, respectively (Figure 5c). Further upstream regions (A_2 to A_4 or B_2 to B_4) were not associated with PfHsp90 protein and hence acted as internal negative controls for this experiment. PfHsp90 occupancy was not observed within the ORF of any of the genes (A₀ or B₀ regions). Thus, not only the recruitment of PfHsp90 at the immediately upstream region of PfSIR2 genes is very specific, but also its increased recruitment upon heat shock is very significant. The results from these experiments are suggestive of a direct role of PfHsp90 in modulating PfSIR2A and PfSIR2B transcription.

3 | DISCUSSION

Here, we report for the first time that the cellular abundance of PfSir2 is subjected to the change in temperature in a developmentally regulated manner. We report that a brief exposure to heat shock leads to the induction of PfHsp90 protein. Greater abundance of PfHsp90 results in greater chromosomal occupancy of this protein at the upstream regulatory regions of PfSIR2A and PfSIR2B genes, where PfHsp90 brings about changes in the associated chromatin structure: from the relatively nucleosome-free state to the heterochromatic state and thereby repressing the expression of PfSIR2A and PfSIR2B genes. As a result, the steady-state level of PfSir2 goes down, leading to the less occupancy at the corresponding *var*

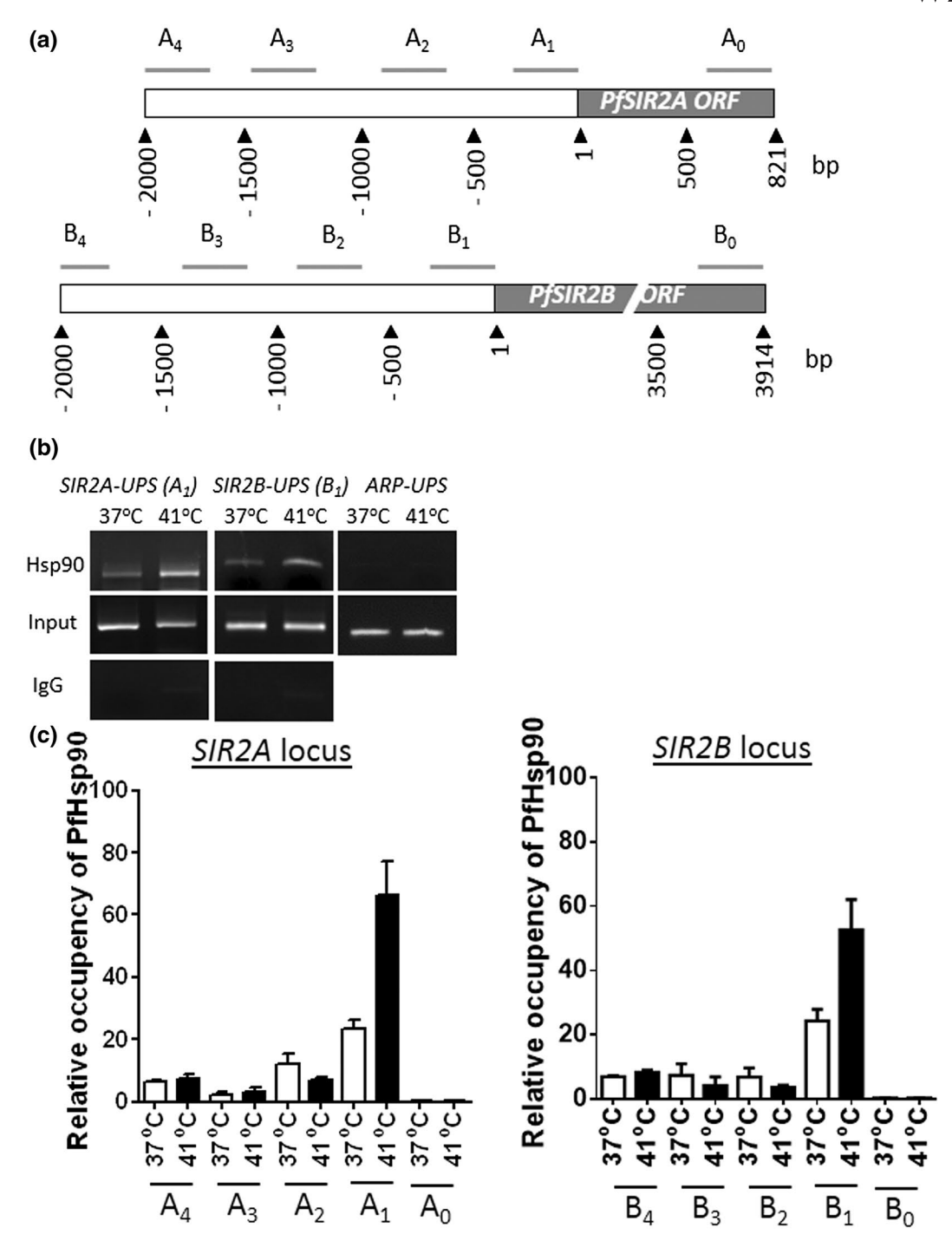


FIGURE 5 Occupancy of PfHsp90 at the upstream regions of PfSIR2A and PfSIR2B genes. (a) Schematic representation of PfSIR2A and PfSIR2B gene loci. Positions of PCR amplicons using ChIP DNA as template are marked as A_0 to A_4 and B_0 to B_4 . (b) ChIP assay was performed using parasites grown under normal or heat-treated conditions to determine the recruitment of PfHsp90 at PfSIR2A_{UPS} and PfSIR2B_{UPS}. Antibodies used are marked on the left side. Input and immunoprecipitated DNA were amplified by PCR with primers specific to A_1 region, B_1 region, and ARP_{UPS} , which served as a negative control. (c) Recruitment of PfHsp90 at different regions of the PfSIR2A and PfSIR2B gene loci. Quantitative PCR of three different ChIP experiments were performed and the mean density \pm SEM are plotted. Asterisks indicate values significantly different from the control, as follows *p <.05

promoters that eventually leads to the de-repression of *var* genes (Figure 6). Such loss of regulation is likely to impact antigenic variation and ultimately the pathophysiology of malaria infection. Interestingly, such downregulation of *PfSIR2* genes was found to be specific to the mid-ring stage. At this point it is noteworthy to

mention that during an in vivo infection in human host the ring stage parasites are exposed to febrile temperature.

In contrast to our finding on *PfSIR2A* and *PfSIR2B* downregulation, an earlier study reported upregulation of *PfSIR2A* transcription upon heat shock (Oakley et al., 2007). Although the heat treatment

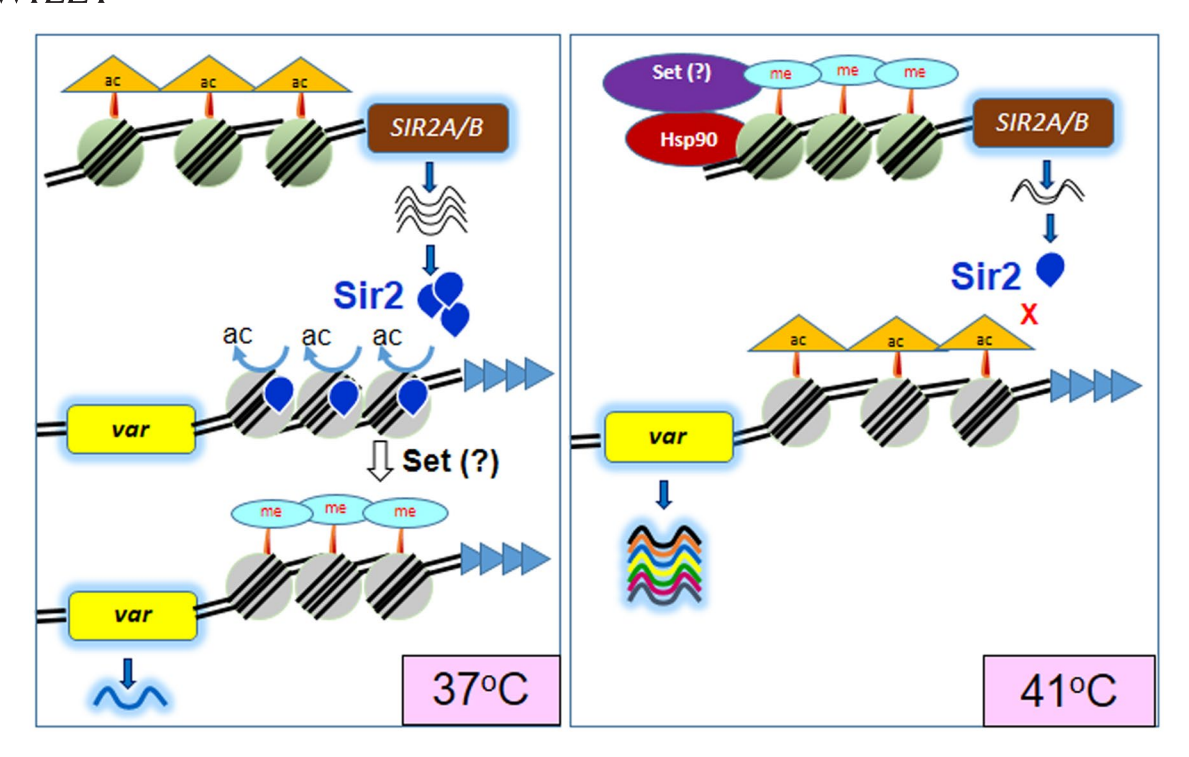


FIGURE 6 Model depicting transcriptional regulation of *PfSIR2A* and *PfSIR2B* and its consequence. At normal temperature (i.e., 37°C) the promoter region of *PfSIR2A* and *PfSIR2B* remains acetylated and in euchromatin form. Hence there are abundant *SIR2* transcript and protein, which deacetylate the *var UPS* regions that are further methylated by any of the histone methyl-transferases (SET domain-containing proteins) leading to silencing of *var* genes. At higher temperatures, that is, on exposure to heat shock of 41°C, PfHsp90 in coordination with a methyl transferase leads to methylation of *PfSIR2A* and *PfSIR2B* promoter and thereby results in the heterochromatinization of the promoter. As a result, there would be less abundance of *PfSIR2A* and *PfSIR2B* transcript and protein, which would fail to completely deacetylate the *var*_{IJPS} and would lead to de-repression of the majority of the *var* genes

protocols were the same between our study and the previous study, the difference was that we have used highly synchronous mid-ring stage culture for our experiment and in the previous study asynchronous parasite cultures were used. In order to investigate whether the difference stems from the use of cultures belonging to different developmental stages of the parasites, in our study we have tested the effect of heat shock on four different asexual stages of the parasite life cycle. We observed transcriptional downregulation of PfSIR2A and PfSIR2B transcripts at elevated temperatures only with highly synchronous mid-ring stage culture. Such downregulation was observed neither at more advanced stages nor at the very early ring stage of the in vitro cultures. Interestingly, at the trophozoite or schizont stages moderate upregulations of PfSIR2A and PfSIR2B were observed instead. This observation underscores the fact that heat-induced transcriptional downregulation of PfSIR2A and PfSIR2B is tightly controlled in a developmental stage-specific manner.

It is unlikely that the difference in the transcription profile between the treated and control cultures is due to any delay in the parasite development owing to the treatment, because in our study RNA was isolated from the cultures immediately after the brief exposure to heat stress while both the untreated and treated cultures were still in the mid-ring stage. Our findings also emphasize that the extent of downregulation of *PfSIR2A* and *PfSIR2B* transcription increases with the rise in temperature: while maximum effect was

observed at or beyond 41°C, no significant effect was found below 39°C. These findings corroborate with an earlier report demonstrating a slight increase in *PfSIR2A and PfSIR2B* transcripts from parasites isolated from patients with temperatures above 37.5°C. The same study also correlated *PfSIR2* expression with lactate levels in the patient and with severity of malaria (Merrick et al., 2012). Thus, the regulation of *PfSIR2* genes appears to be dependent on several environmental factors. Our study dissects out the contribution of one of the major factor, temperature.

We observed that the downregulation of *PfSIR2* upon heat shock is specific to the mid-ring stage, although PfHsp90 is not only present in all the asexual blood stages but also is upregulated upon heat treatment. Currently we do not know why PfHsp90-mediated transcription repression of *PfSIR2A* and *PfSIR2B* does not take place in all the stages. It could be possible that Hsp90 mediates transcriptional downregulation of *PfSIR2A* and *PfSIR2B* via one of the histone-methyl-transferase (HMT) proteins as our results reveal that there is more occupancy of H3K9me3 at the *PfSIR2A* and *PfSIR2B* upstream regions. In *P. falciparum* there are 10 HMT proteins (named as SET 1 to SET 10) (Chen et al., 2016). It is reasonable to propose that one or more of these SET proteins are engaged with PfHsp90 and such interaction could be ring stage-specific. It could also be possible that the expression or heat shock-induced upregulation of the client SET protein is

ring stage-specific. In mammalian cell it has been observed that a HMT protein (SMYD3) physically interacts with Hsp90 (Brown et al., 2015; Hamamoto et al., 2004). Future experimentation would be required to establish any such interaction in *P. falciparum*. In a previous study, it was established that in budding yeast *S. cerevisiae* Hsp90 indirectly regulates the expression of *ScSIR2* by modulating the stability of a transcription factor, Cup9 (Laskar et al., 2015). In fact, the stability of a number of transcription factors have been found to be maintained by Hsp90 in a variety of organisms (Khurana & Bhattacharyya, 2015). In *Plasmodium* not many TFs are identified and no association of any of the TFs with PfHsp90 has been established yet. However, the possibility of a ring stage-specific TF regulating *PfSIR2* expression upon heat stress cannot be ruled out.

It is widely accepted in the field that in *P. falciparum* gene regulation happens through epigenetic modifications on histones. The relative occupancy of the activation marks and repression marks coordinately brings out the heterochromatic or euchromatic states and thus control gene expression (Karmodiya et al., 2015). Thus it could be also possible that there may not be any transcription factor regulating *PfSIR2A* or *PfSIR2B* expression.

It is noteworthy that Hsp90 itself is not a DNA-binding protein. Thus its occupancy at various DNA elements is via interactions with other DNA-binding proteins. This is the first report that demonstrates the recruitment of PfHsp90 at the *PfSIR2* promoter-proximal region and its action as a transcriptional repressor. Other components of such repressor complex that along with PfHsp90 are involved in transcriptional repression are yet to be identified in this parasite.

This is the first study delineating some of the components involved in the transcriptional regulation *PfSIR2A* and *PfSIR2B* genes. Simultaneous downregulation of *PfSIR2A* and *PfSIR2B* transcripts and proteins in response to the overproduction of *PfHsp90* could provide us an experimental strategy to identify newer cellular functions of these two Sirtuins that remained elusive so far due to the absence of a parasite line carrying the double knockout of these two genes. Thus, understanding the molecular mechanism underlying *PfSIR2A* and *PfSIR2B* gene regulation might offer novel biological insights and hence newer intervention strategies for curbing malaria.

4 | EXPERIMENTAL PROCEDURES

4.1 | Parasite culture and synchronization

P. falciparum 3D7 cultures were maintained at 5% of hematocrit in RPMI 1640 medium supplemented with 1% albumax (Invitrogen, Carlsbad, CA, USA) and 0.005% of hypoxanthine by candle jar method at 37°C as described previously (Trager & Jensen, 1976). Parasite cultures were synchronized at the ring stage by treatment with 5% of sorbitol (Sigma, St. Louis, MO, USA).

4.2 | Heat shock

For heat shock treatment, cultures were subjected to higher temperature of 41°C for 2 hr.

4.3 | 17AAG and radicicol treatment

Synchronous ring stage parasite cultures were treated with 170 nM 17AAG (1x) or 85 nM (0.5x) (Sigma, St. Louis, MO, USA) for 48 hr as previously described (Chalapareddy et al., 2014). For Radicicol experiment 1.5 mM of Radicicol (Sigma, St. Louis, MO, USA) was used instead of 17AAG.

4.4 | RNA isolation

Synchronous asexual parasite stages such as ring, trophozoite, or schizonts were used. Total RNA was isolated following the protocol described elsewhere (Moll et al., 2013). Briefly, culture was gently spun and supernatant was removed, pre-warmed TRIzol (Sigma, St. Louis, MO, USA) was added to the pellet. For ring stage 10 pellet volume and for trophozoite and schizont 20 pellet volume of TRIzol was used. The sample was shaken to dissolve the clumps and then, incubated at 37°C for 5 min. A total of 0.2 TRIzol volume of chloroform was added to the sample to extract the aqueous layer. The aqueous layer containing RNA was precipitated by adding 0.5 TRIzol volume of 2-propanol and then, incubated at 4°C. Precipitated sample was then spun, obtained pellet was air-dried, and resuspended in nuclease-free water.

4.5 | Real-time PCR

The concentration of isolated RNA was measured by spectroscopic analysis using JASCO spectrophotometer EMC-709. Fifteen microgram of total RNA was subjected to DNase (Fermentas, Burlington, Ontario) treatment in order to remove the genomic DNA contamination. PCR analysis was performed without cDNA preparation (- RT) to confirm the complete removal of genomic DNA prior to cDNA synthesis. For cDNA synthesis, $1 \, \mu g$ of RNA was reverse transcribed with oligo dT primer (Sigma, St. Louis, MO, USA) using Omniscript reverse transcriptase (Qiagen, Hilden, Germany). The synthesized cDNA was further subjected to Real-time analysis using SYBR premix Ex taq (Takara Bio, Kusatsu, Shiga, Japan). Applied Biosystems 7500 fast real-time PCR machine was used for the real-time analysis. Primer used and real-time analysis for var genes were performed as described previously (Salanti et al., 2003). PCR cycling conditions for the analysis used was 95°C for 15 min followed by 40 cycles of 94°C for 30 s, 54°C for 40 s, and 72°C for 50 s with a final extension at 72°C for 10 min. The house keeping gene SERYL-tRNA SYNTHETASE was used as controls. As reported previously that SERYL-tRNA SYNTHETASE serves as best endogenous control for analysis of var genes expressions (Salanti et al., 2003), in this study also it was used to normalize and calculate the fold change in transcription of var gene upon heat shock using $\Delta\Delta$ CT method. For analyzing the effect of heat shock on transcription of PfSIR2A, PfSIR2B, and PfHSP90 genes, the primer used in the study has been listed in Table S2. All primers were obtained from IDT (Coralville, IA, USA). PCR cycling conditions used was 95°C for 15 min followed by 40 cycles of 94°C for 30 s, 57°C for 40 s, and 72°C for 50 s with a final extension at 72°C for 10 min. SERYL-tRNA SYNTHETASE was used for the normalization of the transcripts. The mean values (\pm SEM) from three independent experiments were plotted using GraphPad Prism 6 software.

4.6 | Chromatin immunoprecipitation

ChIP experiments were performed as described previously (Bozdech et al., 2013). Briefly cultures treated under different conditions were harvested and lysed by saponin treatment. The harvested parasites were then cross-linked with 0.5% of formaldehyde. The parasite plasma membrane was disrupted by applying 200 strokes in Dounce homogenizer and DNA was sheared using Elma water bath sonicator, sonication was done for six sessions (10 s burst and 5 min rest). For immunoprecipitation antibodies against H3K9me3 (Millipore Sigma, Burlington, MA, USA), H3K36me2 (Abcam, Cambridge, UK), Hsp90 (Sigma, St. Louis, MO, USA), and PfSir2A (generated in this study) were used. The primer sets used for amplifying various chromosomal loci using the precipitated DNA as template are listed in Table S2.

4.7 | FAIRE

The procedure for FAIRE was performed as previously described (Giresi & Lieb, 2009; Ponts et al., 2010). Briefly, P. falciparum in vitro cultures were harvested and resuspended in 1X PBS. For cross-linking culture was treated with 37% of formaldehyde (final concentration 1%) and incubated at room temperature on an orbital shaker at 80 RPM for 20 min. Formaldehyde was quenched by treatment with 2.5 M of glycine (final concentration 125 mM) and incubated at room temperature on an orbital shaker at the 80 RPM for 10 min. Further cultures were spun at 3,000 RPM for 10 min. Pellet obtained was washed with ice-cold PBS containing 2 mM of PMSF for three times. Washed pellet were frozen under liquid nitrogen. For reference sample, un-cross-linked cultures were frozen. Pellets were resuspended in lysis buffer (25 mM of Tris-HCl at pH7.8, 1 mM of EDTA, 0.25% of [v/v] IGEPAL CA-630, complete mini EDTA-free protease inhibitor cocktail (Roche, Basel, Switzerland), 20mM of Nethylmaleimide). One milliliter of lysis buffer was used per 0.4 g of pellet. The lysate was then sonicated for six sessions in Elma water bath sonicator (10 s burst and 5 min rest on ice) followed by centrifuging at 16,000 g for 20 min at 4°C. For isolation of DNA the supernatant was treated with equal volume of Phenol-Chloroform-Isoamyl alcohol (25:24:1) and DNA precipitation was performed from the aqueous layer.

4.8 | Western blot analysis

To check the effect of heat shock on expression of PfSir2A and PfHsp90 total parasite proteins were extracted from synchronous stages of the parasites. Further appropriate amount of protein was loaded and separated on 12% SDS polyacrylamide gel for western blot analysis as described earlier (Badugu et al., 2015). The primary antibody anti-PfSir2A raised in rabbit was used at 1:10,000 dilutions. Anti-Hsp90 and anti-Actin (Sigma, St. Louis, MO, USA) raised in mouse were used at 1:5,000 dilutions. HRP conjugated anti-rabbit and anti-mouse secondary antibodies (Promega, Madison, WI, USA) were used at 1:10,000 dilutions. The signal for the protein was detected by enhanced chemiluminescence kit (Pierce, Appleton, WI, USA). The band intensity was measured using ImageJ software and graphs were plotted using Graphpad prism 6 software.

ACKNOWLEDGMENTS

This work is supported by grants from DST-SERB, Government of India [DST-SERB/2015/000999] to MKB. Supports from DST-FIST and UGC-SAP to the Department of Biochemistry are acknowledged. WT is supported by the Senior Research Fellowship from the University Grants Commission, Government of India. The authors thank Prof. Suman Dhar, Jawaharlal Nehru University, New-Delhi, India for the plasmid construct containing *PfSIR2A* gene.

CONFLICT OF INTEREST

The authors certify that they have no conflict of interest with the content of this article.

AUTHOR CONTRIBUTIONS

MKB conceived the idea. MKB and SB designed the experiments. WT and SMV performed the experiments. MKB, SB, and WT analyzed the data. WT, SB, and MKB wrote the manuscript.

DATA AVAILABILITY STATEMENT

The data that support the findings of this study are available from the corresponding author upon reasonable request.

ORCID

Wahida Tabassum https://orcid.org/0000-0001-8202-4564
Mrinal Kanti Bhattacharyya https://orcid.
org/0000-0001-6640-4081

REFERENCES

Badugu, S.B., Nabi, S.A., Vaidyam, P., Laskar, S., Bhattacharyya, S. & Bhattacharyya, M.K. (2015) Identification of *Plasmodium falciparum* DNA repair protein Mre11 with an evolutionarily conserved nuclease

- function. PLoS One, 10, e0125358. https://doi.org/10.1371/journ al.pone.0125358
- Baruch, D.I., Pasloske, B.L., Singh, H.B., Bi, X., Ma, X.C., Feldman, M. et al. (1995) Cloning the P. falciparum gene encoding PfEMP1, a malarial variant antigen and adherence receptor on the surface of parasitized human erythrocytes. Cell, 82, 77–87. https://doi.org/10.1016/0092-8674(95)90054-3
- Bozdech, Z., Mok, S. & Gupta, A.P. (2013) DNA microarray-based genome-wide analyses of *Plasmodium* parasites. *Methods in Molecular Biology*, 923, 189–211.
- Brown, M.A., Foreman, K., Harriss, J., Das, C., Zhu, L., Edwards, M. et al. (2015) C-terminal domain of SMYD3 serves as a unique HSP90regulated motif in oncogenesis. Oncotarget, 6, 4005–4019. https:// doi.org/10.18632/oncotarget.2970
- Chakrabarty, S.P., Saikumari, Y.K., Bopanna, M.P. & Balaram, H. (2008) Biochemical characterization of *Plasmodium falciparum* Sir2, a NAD+-dependent deacetylase. *Molecular and Biochemical Parasitology*, 158, 139–151. https://doi.org/10.1016/j.molbiopara.2007.12.003
- Chalapareddy, S., Bhattacharyya, M.K., Mishra, S. & Bhattacharyya, S. (2014) Radicicol confers mid-schizont arrest by inhibiting mitochondrial replication in *Plasmodium falciparum*. Antimicrobial Agents and Chemotherapy, 58, 4341–4352. https://doi.org/10.1128/AAC.02519-13
- Chen, P.B., Ding, S., Zanghì, G., Soulard, V., DiMaggio, P.A., Fuchter, M.J. et al. (2016) Plasmodium falciparum PfSET7: Enzymatic characterization and cellular localization of a novel protein methyltransferase in sporozoite, liver and erythrocytic stage parasites. Scientific Reports, 6, 21802. https://doi.org/10.1038/srep21802
- Chookajorn, T., Dzikowski, R., Frank, M., Li, F., Jiwani, A.Z., Hartl, D.L. et al. (2007) Epigenetic memory at malaria virulence genes. Proceedings of the National Academy of Sciences of the United States of America, 104, 899–902.
- Deshmukh, A.S., Srivastava, S., Herrmann, S., Gupta, A., Mitra, P., Gilberger, T.W. et al. (2012) The role of N-terminus of Plasmodium falciparum ORC1 in telomeric localization and var gene silencing. Nucleic Acids Research, 40, 5313–5331. https://doi.org/10.1093/nar/gks202
- Gardner, M.J., Hall, N., Fung, E., White, O., Berriman, M., Hyman, R.W. et al. (2002) Genome sequence of the human malaria parasite Plasmodium falciparum. Nature, 419, 498–511. https://doi. org/10.1038/nature01097
- Giresi, P.G. & Lieb, J.D. (2009) Isolation of active regulatory elements from eukaryotic chromatin using FAIRE (Formaldehyde Assisted Isolation of Regulatory Elements). *Methods*, 48, 233–239.
- Golgi, C. (1886) Sull'infezione malarica. Archivio per le Scienze Mediche (Torino), 10, 109-134.
- Guarente, L. (1999) Diverse and dynamic functions of the Sir silencing complex. Nature Genetics, 23, 281–285. https://doi.org/10.1038/15458
- Hakimi, M.A. & Deitsch, K.W. (2007) Epigenetics in Apicomplexa: control of gene expression during cell cycle progression, differentiation and antigenic variation. *Current Opinion in Microbiology*, 10, 357–362. https://doi.org/10.1016/j.mib.2007.07.005
- Hamamoto, R., Furukawa, Y., Morita, M., Iimura, Y., Silva, F.P., Li, M. et al. (2004) SMYD3 encodes a histone methyltransferase involved in the proliferation of cancer cells. *Nature Cell Biology*, 6, 731–740. https://doi.org/10.1038/ncb1151
- Hamamoto, R., Silva, F.P., Tsuge, M., Nishidate, T., Katagiri, T., Nakamura, Y. et al. (2006) Enhanced SMYD3 expression is essential for the growth of breast cancer cells. Cancer Science, 97, 113–118. https://doi.org/10.1111/j.1349-7006.2006.00146.x
- Hasty, P. (2001) The impact energy metabolism and genome maintenance have on longevity and senescence: lessons from yeast to mammals.

- Mechanisms of Ageing and Development, 122, 1651–1662. https://doi.org/10.1016/S0047-6374(01)00294-9
- Iyer, L.M., Anantharaman, V., Wolf, M.Y. & Aravind, L. (2008) Comparative genomics of transcription factors and chromatin proteins in parasitic protists and other eukaryotes. *International Journal for Parasitology*, 38, 1–31. https://doi.org/10.1016/j.ijpara.2007.07.018
- Kafsack, B.F., Rovira-Graells, N., Clark, T.G., Bancells, C., Crowley, V.M., Campino, S.G. et al. (2014) A transcriptional switch underlies commitment to sexual development in malaria parasites. *Nature*, 507, 248– 252. https://doi.org/10.1038/nature12920
- Karmodiya, K., Pradhan, S.J., Joshi, B., Jangid, R., Reddy, P.C. & Galande, S. (2015) A comprehensive epigenome map of *Plasmodium falciparum* reveals unique mechanisms of transcriptional regulation and identifies H3K36me2 as a global mark of gene suppression. *Epigenetics & Chromatin*, 8, 32. https://doi.org/10.1186/s13072-015-0029-1
- Khurana, N. & Bhattacharyya, S. (2015) Hsp90, the concertmaster: tuning transcription. Frontiers in Oncology, 5, 100. https://doi.org/10.3389/ fonc.2015.00100
- Kraemer, S.M., Kyes, S.A., Aggarwal, G., Springer, A.L., Nelson, S.O., Christodoulou, Z. et al. (2007) Patterns of gene recombination shape var gene repertoires in *Plasmodium falciparum*: Comparisons of geographically diverse isolates. *BMC Genomics*, 8, 45. https://doi. org/10.1186/1471-2164-8-45
- Kraemer, S.M. & Smith, J.D. (2006) A family affair: var genes, PfEMP1 binding, and malaria disease. Current Opinion in Microbiology, 9, 374–380. https://doi.org/10.1016/j.mib.2006.06.006
- Kumar, R., Musiyenko, A. & Barik, S. (2003) The heat shock protein 90 of *Plasmodium falciparum* and antimalarial activity of its inhibitor, geldanamycin. *Malaria Journal*, 2, 30.
- Laskar, S., Bhattacharyya, M.K., Shankar, R. & Bhattacharyya, S. (2011) HSP90 controls SIR2 mediated gene silencing. *PLoS One*, 6, e23406. https://doi.org/10.1371/journal.pone.0023406
- Laskar, S., Sheeba, K., Bhattacharyya, M.K., Nair, A.S., Dhar, P. & Bhattacharyya, S. (2015) Heat stress-induced Cup9-dependent transcriptional regulation of SIR2. Molecular and Cellular Biology, 35, 437–450.
- Lobo, I. (2008) Environmental influences on gene expression. *Nature Education*, 1(1), 39.
- Lopez-Rubio, J.J., Gontijo, A.M., Nunes, M.C., Issar, N., Hernandez Rivas, R. & Scherf, A. (2007) 5' flanking region of var genes nucleate histone modification patterns linked to phenotypic inheritance of virulence traits in malaria parasites. *Molecular Microbiology*, 66, 1296–1305. https://doi.org/10.1111/j.1365-2958.2007.06009.x
- Merrick, C.J. & Duraisingh, M.T. (2007) Plasmodium falciparum Sir2: An unusual sirtuin with dual histone deacetylase and ADPribosyltransferase activity. Eukaryotic Cell, 6, 2081–2091. https://doi. org/10.1128/EC.00114-07
- Merrick, C.J., Huttenhower, C., Buckee, C., Amambua-Ngwa, A., Gomez-Escobar, N., Walther, M. et al. (2012) Epigenetic dysregulation of virulence gene expression in severe Plasmodium falciparum malaria. The Journal of Infectious Diseases, 205, 1593–1600. https://doi.org/10.1093/infdis/jis239
- Merrick, C.J., Jiang, R.H., Skillman, K.M., Samarakoon, U., Moore, R.M., Dzikowski, R. et al. (2015) Functional analysis of sirtuin genes in multiple Plasmodium falciparum strains. PLoS One, 10, e0118865.– https://doi.org/10.1371/journal.pone.0118865
- Moll, K., Kaneko, A., Scherf, A. & Wahlgren, M. (2013) Methods in malaria research.: EVIMalaR.
- Oakley, M.S., Kumar, S., Anantharaman, V., Zheng, H., Mahajan, B., Haynes, J.D. et al. (2007) Molecular factors and biochemical pathways induced by febrile temperature in intraerythrocytic Plasmodium falciparum parasites. Infection and Immunity, 75, 2012–2025. https:// doi.org/10.1128/IAI.01236-06
- Otto, T.D., Böhme, U., Sanders, M., Reid, A., Bruske, E.I., Duffy, C.W. et al. (2018) Long read assemblies of geographically dispersed *Plasmodium*

- falciparum isolates reveal highly structured subtelomeres. Wellcome Open Research, 3, 52. https://doi.org/10.12688/wellcomeopenres.14571.1
- Ponts, N., Harris, E.Y., Prudhomme, J., Wick, I., Eckhardt-Ludka, C., Hicks, G.R. *et al.* (2010) Nucleosome landscape and control of transcription in the human malaria parasite. *Genome Research*, 20, 228–238. https://doi.org/10.1101/gr.101063.109
- Prusty, D., Mehra, P., Srivastava, S., Shivange, A.V., Gupta, A., Roy, N. et al. (2008) Nicotinamide inhibits Plasmodium falciparum Sir2 activity in vitro and parasite growth. FEMS Microbiology Letters, 282, 266–272. https://doi.org/10.1111/j.1574-6968.2008.01135.x
- Salanti, A., Staalsoe, T., Lavstsen, T., Jensen, A.T., Sowa, M.P., Arnot, D.E. et al. (2003) Selective upregulation of a single distinctly structured var gene in chondroitin sulphate A-adhering Plasmodium falciparum involved in pregnancy-associated malaria. Molecular Microbiology, 49, 179–191. https://doi.org/10.1046/j.1365-2958.2003.03570.x
- Sawarkar, R. & Paro, R. (2013) Hsp90@chromatin.nucleus: an emerging hub of a networker. *Trends in Cell Biology*, 23, 193–201. https://doi.org/10.1016/j.tcb.2012.11.007
- Sawarkar, R., Sievers, C. & Paro, R. (2012) Hsp90 globally targets paused RNA polymerase to regulate gene expression in response to environmental stimuli. *Cell*, 149, 807–818. https://doi.org/10.1016/j. cell.2012.02.061
- Scherf, A., Hernandez-Rivas, R., Buffet, P., Bottius, E., Benatar, C., Pouvelle, B. *et al.* (1998) Antigenic variation in malaria: in situ switching, relaxed and mutually exclusive transcription of var genes during intra-erythrocytic development in *Plasmodium falciparum*. *The EMBO Journal*, 17, 5418–5426. https://doi.org/10.1093/emboj/17.18.5418
- Smith, J.D., Chitnis, C.E., Craig, A.G., Roberts, D.J., Hudson-Taylor, D.E., Peterson, D.S. et al. (1995) Switches in expression of Plasmodium falciparum var genes correlate with changes in antigenic and cytoadherent phenotypes of infected erythrocytes. Cell, 82, 101–110. https:// doi.org/10.1016/0092-8674(95)90056-X
- Su, X.Z., Heatwole, V.M., Wertheimer, S.P., Guinet, F., Herrfeldt, J.A., Peterson, D.S. *et al.* (1995) The large diverse gene family var encodes proteins involved in cytoadherence and antigenic variation

- of *Plasmodium falciparum*-infected erythrocytes. *Cell*, 82, 89–100. https://doi.org/10.1016/0092-8674(95)90055-1
- Tariq, M., Nussbaumer, U., Chen, Y., Beisel, C. & Paro, R. (2009) Trithorax requires Hsp90 for maintenance of active chromatin at sites of gene expression. *Proceedings of the National Academy of Sciences of the United States of America*, 106, 1157–1162.
- Tonkin, C.J., Carret, C.K., Duraisingh, M.T., Voss, T.S., Ralph, S.A., Hommel, M. *et al.* (2009) Sir2 paralogues cooperate to regulate virulence genes and antigenic variation in *Plasmodium falciparum*. *PLoS Biology*, 7, e84. https://doi.org/10.1371/journal.pbio.1000084
- Trager, W. & Jensen, J.B. (1976) Human malaria parasites in continuous culture. *Science*, 193, 673–675. https://doi.org/10.1126/science.781840
- Vinci, M.C. (2012) Sensing the environment: epigenetic regulation of gene expression. *Journal of Physical Chemistry & Biophysics*, S3-001. https://doi.org/10.4172/2161-0398.S3-001
- Wider, D., Péli-Gulli, M.P., Briand, P.A., Tatu, U. & Picard, D. (2009) The complementation of yeast with human or *Plasmodium falciparum* Hsp90 confers differential inhibitor sensitivities. *Molecular and Biochemical Parasitology*, 164, 147–152. https://doi.org/10.1016/j.molbiopara.2008.12.011

SUPPORTING INFORMATION

Additional Supporting Information may be found online in the Supporting Information section.

How to cite this article: Tabassum W, Bhattacharyya S, Varunan SM, Bhattacharyya MK. Febrile temperature causes transcriptional downregulation of *Plasmodium falciparum* Sirtuins through Hsp90-dependent epigenetic modification. *Mol Microbiol.* 2021;00:1–14. https://doi.org/10.1111/mmi.14692





Glu-108 in Saccharomyces cerevisiae Rad51 Is Critical for DNA **Damage-Induced Nuclear Function**

Tanvi Suhane, a Vijayalakshmi Bindumadhavan, b Nupur Fangaria, a Achuthsankar S. Nair, b Wahida Tabassum, c Poorvaja Muley, a Mrinal K. Bhattacharyya, c Sunanda Bhattacharyya

- ^aDepartment of Biotechnology and Bioinformatics, School of Life Sciences, University of Hyderabad, Hyderabad, India
- ^bDepartment of Computational Biology and Bioinformatics, University of Kerala, Thiruvanthapuram, India
- ^cDepartment of Biochemistry, School of Life Sciences, University of Hyderabad, Hyderabad, India

ABSTRACT DNA damage-induced Rad51 focus formation is the hallmark of homologous recombination-mediated DNA repair. Earlier, we reported that Rad51 physically interacts with Hsp90, and under the condition of Hsp90 inhibition, it undergoes proteasomal degradation. Here, we show that the dynamic interaction between Rad51 and Hsp90 is crucial for the DNA damage-induced nuclear function of Rad51. Guided by a bioinformatics study, we generated a single mutant of Rad51, which resides at the N-terminal domain, outside the ATPase core domain. The mutant with an E to L change at residue 108 (Rad51^{E108L}) was predicted to bind more strongly with Hsp90 than the wild-type (Rad51WT). A coimmunoprecipitation study demonstrated that there exists a distinct difference between the in vivo associations of Rad51WT-Hsp90 and of Rad51E108L-Hsp90. We found that upon DNA damage, the association between Rad51WT and Hsp90 was significantly reduced compared to that in the undamaged condition. However, the mutant Rad51^{E108L} remained tightly associated with Hsp90 even after DNA damage. Consequently, the recruitment of Rad51^{E108L} to the double-stranded broken ends was reduced significantly. The *E108L*rad51 strain manifested severe sensitivity toward methyl methanesulfonate (MMS) and a complete loss of gene conversion efficiency, a phenotype similar to that of the $\Delta rad51$ strain. Previously, some of the N-terminal domain mutants of Rad51 were identified in a screen for a Rad51 interaction-deficient mutant; however, our study shows that Rad51^{E108L} is not defective either in the self-interaction or its interaction with the members of the Rad52 epistatic group. Our study thus identifies a novel mutant of Rad51 which, owing to its greater association with Hsp90, exhibits a severe DNA repair defect.

IMPORTANCE Rad51-mediated homologous recombination is the major mechanism for repairing DNA double-strand break (DSB) repair in cancer cells. Thus, regulating Rad51 activity could be an attractive target. The sequential assembly and disassembly of Rad51 to the broken DNA ends depend on reversible protein-protein interactions. Here, we discovered that a dynamic interaction with molecular chaperone Hsp90 is one such regulatory event that governs the recruitment of Rad51 onto the damaged DNA. We uncovered that Rad51 associates with Hsp90, and upon DNA damage, this complex dissociates to facilitate the loading of Rad51 onto broken DNA. In a mutant where such dissociation is incomplete, the occupancy of Rad51 at the broken DNA is partial, which results in inefficient DNA repair. Thus, it is reasonable to propose that any small molecule that may alter the dynamics of the Rad51-Hsp90 interaction is likely to impact DSB repair in cancer cells.

KEYWORDS DNA repair, Hsp90, homologous recombination, Hsp90-Rad51 interaction, Rad51 recruitment to chromatin, molecular chaperone

Citation Suhane T, Bindumadhavan V, Fangaria N, Nair AS, Tabassum W, Muley P, Bhattacharyya MK, Bhattacharyya S. 2019. Glu-108 in Saccharomyces cerevisiae Rad51 is critical for DNA damage-induced nuclear function. mSphere 4:e00082-19. https://doi.org/10.1128/ mSphere.00082-19.

Editor Aaron P. Mitchell, Carnegie Mellon

Copyright © 2019 Suhane et al. This is an open-access article distributed under the terms of the Creative Commons Attribution 4.0 International license.

Address correspondence to Sunanda Bhattacharyya, sdeb70@gmail.com.

Received 1 February 2019 Accepted 28 February 2019 Published 20 March 2019





Thenever cells are exposed to DNA-damaging agents, the family of DNA repair proteins must relocate to the nucleus and be recruited to the damaged chromatins to elicit a DNA damage response and to ensure efficient repair of damaged DNA (1-3). These groups of proteins include DNA damage signaling proteins (Mre11, ATM, ATR, and DNA-PKcs), cell cycle checkpoint effectors (Chk1 and Chk2), and DNA processing enzymes (Mre11, Exol, Sae2, Rad51, Rad52, Rad54, BRCA1/2, BLM, Ku70/80, ligase IV, etc.) (4). The sequential assembly and disassembly of DNA repair proteins at DNA broken ends depend on reversible protein-protein interactions. Rad51, a central player of homology-directed double-strand break (DSB) repair, remains in the cytoplasm under normal conditions. DNA damage leads to the redistribution of Rad51 from the cytoplasm to the nucleus and its loading onto the broken ends of DNA. It is reasonable to propose that insufficient recruitment of Rad51 onto the chromatin is likely to have a severe impact on homologous recombination (HR) efficiency. Earlier reports demonstrated that in a human cell line, BRCA1 promotes the localization of BRCA2 to damage foci through the BRCA2 binding protein PALB2 (5-8). BRCA2 interacts with RAD51 and promotes RAD51 assembly onto single-stranded DNA (ssDNA) (9-11). However, BRCA2 is absent in lower eukaryotes, where HR is the predominant pathway for DNA repair. It is reported that in Saccharomyces cerevisiae, Rad52 promotes Rad51 filament assembly (12) by interacting with RPA. Rad52 is thought to replace RPA bound to ssDNA with Rad51 or provide a seeding site within the RPA-bound ssDNA for subsequent binding of Rad51 (13).

Our previous study revealed that Rad51 is a direct client of Hsp90 and is dependent upon Hsp90 for its maturity and activity (14). Apart from merely providing maturity to the client proteins, Hsp90 also assists in the translocation of proteins to different cellular compartments (15). Previous reports have established that the Hsp90 chaperone machinery not only escorts steroid hormone receptors (SHRs) to the nucleus but is also responsible for the recycling of the receptor on chromatin and stabilizing the DNA-binding properties of the receptor (16). Two cochaperones of Hsp90, p23 and Bag-1L, are found to modulate steroid hormone receptor function by controlling receptor binding to chromatin (16).

Our earlier study demonstrated that the charged linker deletion mutant of yHsp90 (Δ211-259hsp82) inhibits effective Rad51 focus formation in the nucleus upon DNA damage (14). This finding was positively correlated with severe methyl methanesulfonate (MMS) sensitivity (comparable to that for the Δrad51 strain) and with the complete loss of Rad51-dependent gene targeting function. We demonstrated that the charged linker deletion (Δ211-259hsp82) mutant strain is strikingly different than the wild-type strain in the distribution of Rad51 foci upon MMS treatment. Although there was only a 20% overall reduction in the Rad51 focus formation, the number of nuclei having multiple foci was drastically reduced in the mutant strain. This clearly indicates that in mutant nuclei, effective Rad51 levels may be low. Since the charged linker region is responsible for providing structural flexibility between amino and carboxyl-terminal domains of Hsp90 (17), an optimum interaction between Rad51 and Hsp90 may be compromised in the mutant. Hence, we hypothesize that effective Hsp90 and Rad51 interaction may be crucial for nuclear function of Rad51. To prove this, we utilized a bioinformatics approach to design a point mutant with an E to L change at residue 108 (Rad51^{E108L}), which has a stronger affinity toward Hsp90. Our data reveal that there exists a dynamic equilibrium between the association of wild-type Rad51 (Rad51WT) and Hsp90 under a normal condition and dissociation under DNA-damaging conditions. In the case of Rad51^{E108L}, due to tighter association, the interaction between Hsp90 and mutant Rad51 becomes irreversible; hence, even under DNA-damaging conditions, the mutant Rad51 protein does not proficiently dissociate from Hsp90. As a result, the mutant Rad51^{E108L} is not recruited to the broken DNA ends as efficiently as wild-type Rad51. Hence, the E108L-rad51 strain shows extreme sensitivity toward DNA-damaging agents and poor gene conversion activity. This study points out that the DNA damage-induced reversible protein-protein interaction between Rad51 and Hsp90 plays a critical role in Rad51 function.



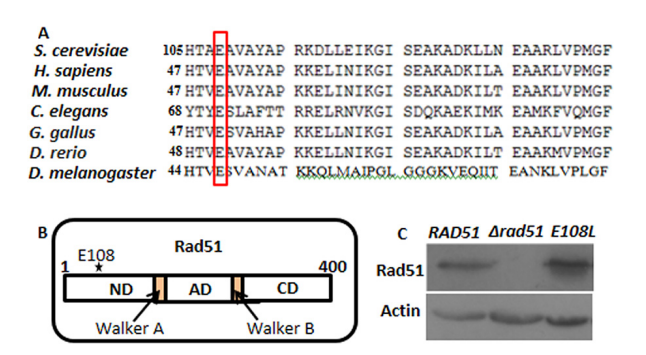


FIG 1 Generation of *RAD51* mutant strain. (A) Multiple sequence alignment of Rad51 (N-terminal domain) protein sequences of *S. cerevisiae* (yeast) with *Homo sapiens* (human), *Mus musculus* (mouse), *Gallus gallus* (bird), *Danio rerio* (zebrafish), *Caenorhabditis elegans* (nematode), and *Drosophila melanogaster* (fruit fly). The conserved glutamic acid residues among various organisms are represented by the red box. (B) Schematic representation of Rad51 domains demonstrating boundaries of N-terminal, ATPase (AD), and C-terminal domains along with the Walker A and Walker B motifs. The star depicts the approximate location of E108 in the N-terminal domain of Rad51. (C) Western blot was performed using protein extracts from wild-type, Δ*rad51*, and *E108L-rad51* strains. Actin was used as a loading control.

RESULTS

Generation of RAD51 mutant strain based on the molecular docking studies between yHsp90 and Rad51. Earlier studies in our lab demonstrated that yHsp90 and Rad51 can physically interact (14). Unlike other chaperones, there is no specific binding pocket present in Hsp90 through which it binds to the client proteins. Hence, in order to understand the point of contacts between yHsp90 and Rad51, we employed a bioinformatics approach. To that end, Rad51 proteins (PDB identifier [ID] 1SZP) having various combinations of monomers, dimers, and hexamers were allowed to dock with vHsp90 (PDB ID 2CG9) using the fully automated web-based program ClusPro 2.0 (18). which employs the improved fast Fourier transform (FFT)-based rigid docking program PIPER (19). Thirty models of the protein-protein complex for each type of interaction, namely, balanced, electrostatic favored, hydrophobic favored, and van der Waal's plus electrostatic, were generated for each docking. It was found that a hydrophobicfavored interaction showed the lowest energy scores; hence, the corresponding protein complex model with the largest cluster was chosen. The surface view of the threedimensional structure of Rad51 displays a characteristic pocket in each of the monomers into which the yHsp90 is found to dock. The docked complex models showed that the N-terminal residue of the Rad51 E chain, Glu 108 (1.88 Å), has the shortest bond distance with yHsp90 C-terminal residues. We conducted a multiple-sequence alignment of Rad51 (Fig. 1A) and found that E108, which is predicted to have the strongest association with Hsp90, is evolutionarily conserved. In Rad51, the amino acid residue E108 is present in the N-terminal domain of Rad51, which lies outside its catalytic domain (Fig. 1B). To explore whether the Hsp90 and Rad51 association mediates Rad51 nuclear function under DNA-damaging conditions, one approach may be the generation of a Rad51 mutant with a reduced affinity for Hsp90. However, as Rad51 is a client of Hsp90, we reasoned that any mutant of Rad51 that fails to interact with Hsp90 due to a low affinity would be unstable in the cell. Hence, we designed a strong-affinity mutant to establish our hypothesis. By in silico mutation, we created four single mutants of Rad51 where the glutamic acid at the 108th position was replaced by neutral residues (glycine, alanine, leucine, and isoleucine). Table 1 displays a comparison of the parameters of yHsp90 docking with the wild-type and mutant Rad51 based on ClusPro results. Our study shows that the mutant Rad51E108L and Hsp90 docked complex results in a maximum increase in cluster size of 139 compared to 71 for the wild type. This implies a greater probability of the receptor-ligand complex being found in that specific conformation. Furthermore, there is a decrease in the energy score from -1,407.2 to -1,512.6 between the wild-type and Rad51^{E108L} mutant, respectively, which points to an increased stability of the protein complex. The rad51 mutant was



TABLE 1 ClusPro results depicting cluster sizes and energy scores of yHsp90 (2CG9A) with wild-type and mutant Rad51

	Hydrophobic-favored	Hydrophobic-favored interaction	
Rad51 (1SZP ABCDEF) strain	Cluster size	Energy score	
Wild-type (E108)	71	-1,407.2	
E108G	117	-1,534.0	
E108A	117	-1,518.4	
E108I	113	-1,543.3	
E108L	139	-1,512.6	

subsequently cloned into a yeast 2μ expression vector pTA (20) having the GPD promoter. As the Rad51 and Hsp90 interaction is essential for the stability of Rad51, we determined the stability of Rad51 mutant proteins by Western blot analysis. For this, we generated yeast strains NRY1, NRY2, and TSY17 by transforming empty vector (pTA), pTA-RAD51, and pTA-E108L-rad51 vectors into a null rad51 yeast strain. The steady-state level of the mutant Rad51 was comparable to that of the wild type (Fig. 1C).

Rad51^{E108L} shows a stronger association with Hsp90 than the wild-type Rad51. To investigate the interaction between Rad51 and yHsp90, we performed coimmunoprecipitation experiments under normal as well as MMS treatment conditions. To capture a detectable association between yHsp90 and Rad51, we overexpressed both yHSP90 and RAD51 (or its mutant version) from two 2μ vectors, each having a GPD promoter. The yHsp90-Rad51 complex was coimmunoprecipitated from the whole-cell extract with an anti-Rad51 antibody, followed by detection on a Western blot using an anti-Hsp82 antibody (Fig. 2A and B). Under normal conditions, in the wild-type strain, a small fraction of Hsp90 was associated with Rad51, whereas, in the case of the mutant strain, a significantly larger fraction of Hsp90 was associated with Rad51. Quantification of the several experimental repeats showed that the relative association between Hsp90 and Rad51^{E108L} was almost double the association found between Hsp90 and Rad51WT. This signifies a stronger association of Hsp90 with Rad51E108L than with Rad51WT. In the presence of MMS, Hsp90 and Rad51 association was reduced in the wild-type strain. On the other hand, in the E108L-rad51 strain, even in the presence of MMS, there was no detectable reduction in the association between Hsp90 and

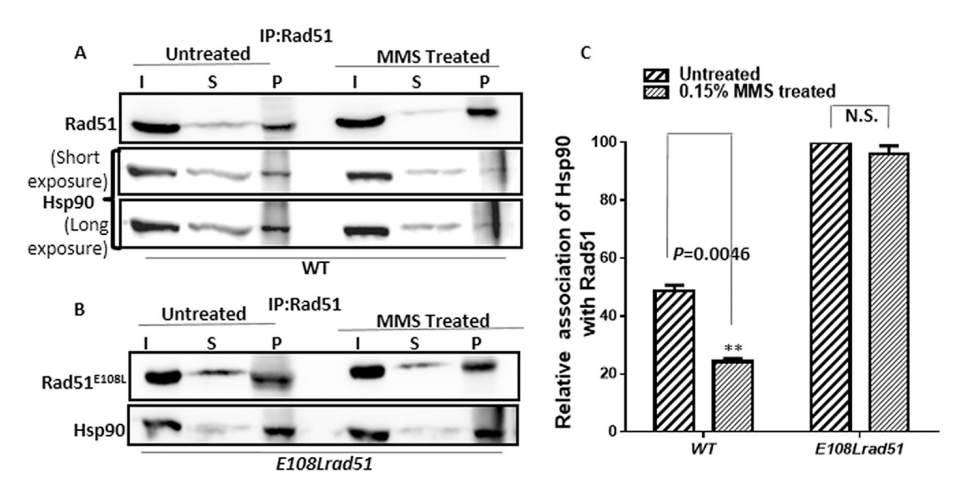


FIG 2 Rad51^{E108L} shows a stronger association with Hsp90 than the wild-type Rad51. (A) Western blot showing coimmunoprecipitation of Rad51 with Hsp90 from whole-cell extracts of wild-type strain and cells treated with 0.15% MMS for 2 h. I, input; S, supernatant; P, pellet. (B) Western blot showing coimmunoprecipitation of Rad51^{E108L} with Hsp90 from whole-cell extracts of E108L-rad51 mutant strain untreated and treated with 0.15% MMS for 2 h. Immunoprecipitation (IP) was performed using an anti-Rad51 antibody. An anti-Hsp90 antibody was used for Western blotting. (C) Relative association of Hsp90 with Rad51 was calculated from at least three independent experiments, and standard deviations are plotted for both wild-type and mutant strains. P values were calculated using the two-tailed Student's t test. **, P = 0.0046; N.S., not significant.



Rad51^{E108L}. We repeated this experiment three times and calculated the relative association of Hsp90 with Rad51 in the presence and absence of MMS. Our analysis shows that approximately 50% dissociation of the Rad51WT-Hsp90 complex occurs upon MMS treatment, whereas no significant dissociation of the Rad51^{E108L}-Hsp90 complex was observed under similar conditions (Fig. 2C). Thus, from this experiment, we conclude that there is a dynamic equilibrium between Rad51-Hsp90 complexes: in the presence of DNA damage, the equilibrium is shifted toward the dissociation of Rad51-Hsp90. However, this dynamic interaction is absent in the E108L-rad51 strain, and the complex remains in the associated form even in the presence of the DNAdamaging agent.

HO-induced Rad51 recruitment to the broken DNA ends is compromised in the E108L-rad51 strain. During homologous recombination-mediated DNA repair, Rad51 is recruited to the ssDNA overhangs. It searches for the homologous DNA and, once found, facilitates the repair by performing a strand exchange reaction. The recruitment of Rad51 to the broken ends is the hallmark of DNA repair. Our previous observations suggest that the E108L-rad51 mutant is defective in dissociating from Hsp90 upon DNA damage. This defect may cause inadequate recruitment of Rad51 mutants to the broken DNA. To study the recruitment of mutant Rad51 to the DSB, we employed chromatin immunoprecipitation (ChIP) assays. To that end, we used NA14 strains (21) harboring null rad51. We modified the NA14 strain and generated three strains, namely, TSY20, TSY21, and TSY22, where native RAD51 is knocked out, and into those backgrounds, the empty plasmid, wild-type RAD51, and the mutant rad51 were transformed, respectively. These strains have a cassette inserted in chromosome V with two copies of URA3, separated by 3 kb, of which one ura3 copy is inactivated by the insertion of an HO endonuclease restriction site (Fig. 3A). The KANMX gene is incorporated within the two URA3 genes. HO endonuclease is expressed in the strain by a galactose inducible promoter. A double-strand break (DSB) is generated in the ura3 gene upon induction of HO endonuclease. We pulled down the Rad51-bound DNA segments from uninduced and HO-induced samples and subsequently compared the recruitment of mutant Rad51 protein to the donor URA3 locus (22). This experiment was repeated three times, and representative data from one of these are presented (Fig. 3B). To ensure the specificity of Rad51 recruitment to the broken locus, we probed its recruitment at the ACT1 locus, which does not contain an HO cut site. We did not detect any band at the ACT1 locus. We quantified the extent of recruitment of Rad51 proteins by measuring the ratio of amplification in the pellet sample with respect to the amplification observed in the input. To confirm the specificity of Rad51 recruitment to the DSB, we performed ChIP with IgG, which does not result in any amplification with the precipitated sample (Fig. 3B). Although there was no recruitment of Rad51 in the HOuninduced condition, upon HO induction, the recruitment of Rad51^{E108L} was only 40% of that for the wild type (Fig. 3C). To ensure that the defect in the recruitment of the mutant Rad51 to the DSB was not due to the inefficiency of galactose-induced DSB, we probed the HO endonuclease recognition site in the presence and absence of HO induction. To that end, we amplified the HO site flanking the ura3 region using a forward primer, which is 20 bp upstream of the HO site, and a reverse primer, which is complementary to the middle part of KANMX gene. We observed the amplification of the target region in a galactose-untreated sample; however, after 1 h of galactose induction, the amplicon disappeared, indicating the successful generation of DSBs in all the strains (Fig. 3D). Overall, from these experiments, we conclude that the effective concentration of the Rad51^{E108L} mutant at broken DNA ends is less than that of the wild-type Rad51.

Mutation at the E108 position of Rad51 sensitizes the cells to MMS and renders them deficient in gene conversion. In S. cerevisiae, homologous recombination is the preferred pathway for repairing DSBs, in which Rad51 plays a central role. To understand the effect of rad51 mutation, we performed the return-to-growth assay upon DNA damage. This was conducted by exposing the strains to 0.03% MMS (methyl methanesulfonate) for 2 h. Subsequently, treated and untreated cells were serially



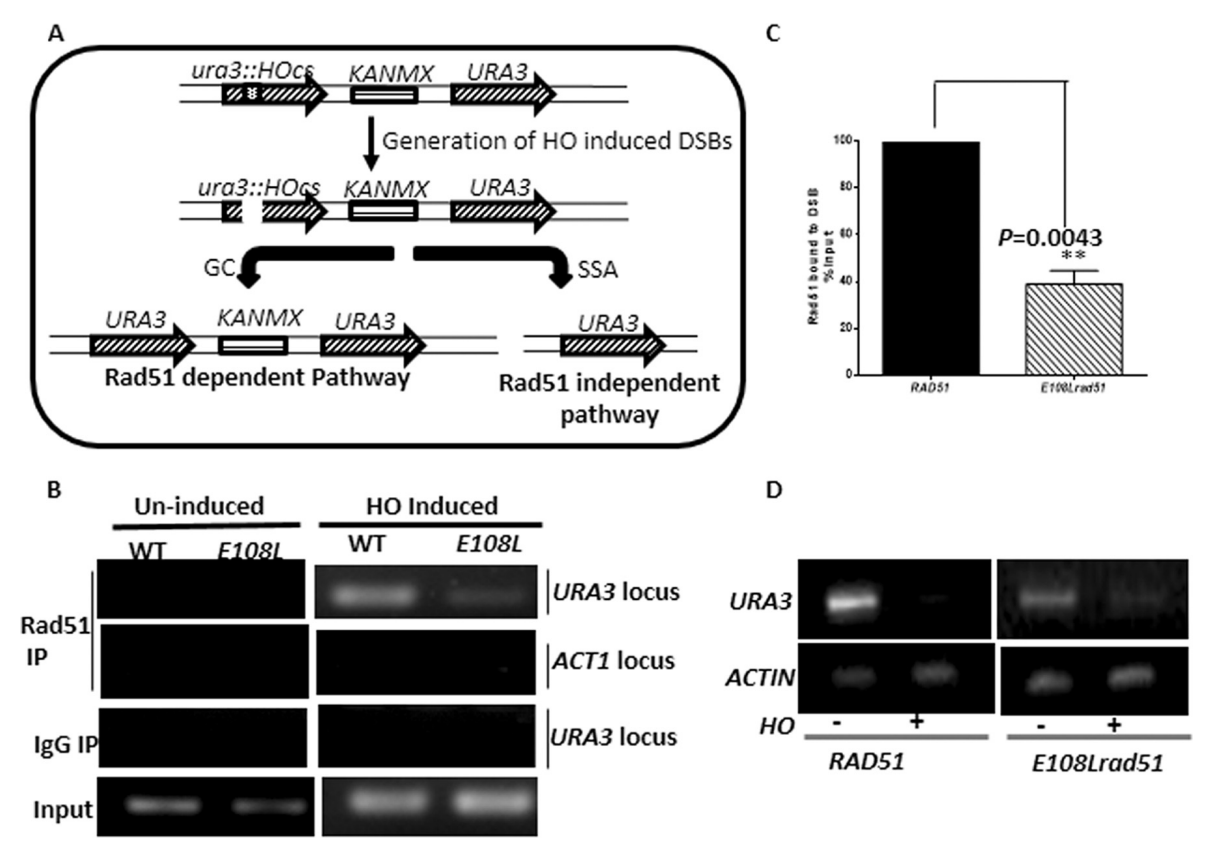


FIG 3 HO-induced Rad51 recruitment to the broken DNA ends is severely compromised in E108L-rad51 mutant. (A) Schematic diagram of a cassette incorporated in the strain used for studying gene conversion efficiency. It harbors two copies of URA3, one of which is mutated by the insertion of an HO endonuclease site. Induction with galactose creates single DSB in the mutated ura3, repair of which takes place in either a Rad51-dependent or Rad51-independent manner. KANMX cassette will be retained only if repair happens via the Rad51-dependent manner. (B) Chromatin immunoprecipitation (ChIP) of strains expressing wild-type Rad51 and E108L-rad51. Gel image showing one of the representative PCR products of input and precipitated samples using URA3 donor-specific primer and ACT1-specific primer. Immunoprecipitation was performed using anti-Rad51 and IgG antibodies. Input represents the total amount of DNA in the sample. (C) Each set was repeated three times, and the band intensities of the recruited samples upon HO induction were quantified using ImageJ software; comparative recruitment of Rad51 and Rad51^{E108L} is plotted with respect to the input. Error bars indicate standard deviations (SDs); n = 3 (P values were calculated using the two-tailed Student's t test). **, P < 0.01. (D) Semiquantitative reverse transcriptase PCR (RT-PCR), representing the amplification of DNA around the DSB site in ura3 before and after HO endonuclease induction. Lower intensity of band in HO-induced sample indicates the DSB generation in strains having wild-type Rad51 and E108L-rad51. Actin was used as a loading control.

diluted by 10-fold as presented in Fig. 4A and spotted on selective medium. We observed that the E108L-rad51 strain showed a slow growth phenotype compared to that of the wild type and $\Delta rad51$ strains. The survivability of the cells was positively correlated with the efficiency of DNA repair. We observed that E108L-rad51 cells were highly sensitive to MMS-induced DNA damage, similar to that observed in $\Delta rad51$ cells. The mechanism of homologous recombination involves repairing the DSBs by utilizing a homologous sequence from the genome. If the genome contains repetitive sequences and a double-strand break is created in any one of the repeats, it can be repaired by gene conversion, which is Rad51 dependent. We examined the gene conversion efficiency of the Rad51 mutant in the yeast strain NA14 (21). The DSB can be repaired by either of the two HR pathways (gene conversion or single strand annealing), and the repair products are easily distinguishable. If repaired by the Rad51-dependent gene conversion pathway, the strain behaves as G418 sulfate resistant; if it is repaired by the Rad51-independent single-strand annealing (SSA) pathway, the strain will be G418 sulfate sensitive (Fig. 3A) (21). The percent gene conversion was scored by growing cells on G418 sulfate-containing plates after galactose induction. Our experimental data indicate that there was no significant change in the gene conversion (GC) efficiency of the wild type (near 40%). However, the GC score for the



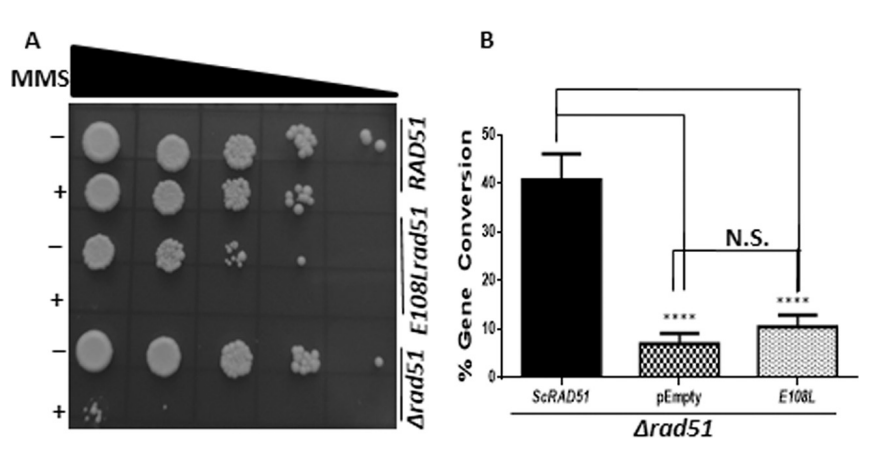


FIG 4 Mutation at E108 position of Rad51 sensitizes the cells to MMS and renders them deficient in gene conversion. (A) Pictorial representation of return-to-growth assay upon MMS treatment. Cells were spotted after serial dilution of treated and untreated cells for wild-type and mutant strains. First lane for each strain shows untreated and second lane shows treated cells. (B) Graph showing the percentages of gene conversion. Cells were spread on galactose-containing plates and subsequently obtained colonies were patched on G418 sulfate plates. Percentage was determined by calculating the number of colonies grown on G418 sulfate plate versus number of colonies obtained on galactose plate. Error bars indicate SDs; n = 3; P values were calculated using the two-tailed Student's t test. *****, P < 0.0001; N.S., not significant.

E108L-rad51 mutant (10.5%) was comparable to that of the Δ rad51 strain (7%) (Fig. 4B). Overall, we conclude from our experimental data that the E108L-rad51 mutant behaved as a complete loss-of-function mutant of Rad51 in our assav.

Rad51^{E108L} can form homodimers and interacts efficiently with the Rad52 epistasis group of proteins. It has been established that to execute the nuclear function, Rad51 interacts with itself. Also, Rad52 and Rad54 modulate the catalytic activity of Rad51 via direct physical interaction. We wanted to test whether Rad51^{E108L} has any defect in self-association or association with Rad52 and Rad54. To that end, we used a yeast two-hybrid assay to measure the protein-protein interaction between Rad51E108L and the Rad52 epistasis group. Figure 5 (top) shows the results with wild-type Rad51, which acts as a positive control in our study. The bottom of Fig. 5 shows that Rad51^{E108L}

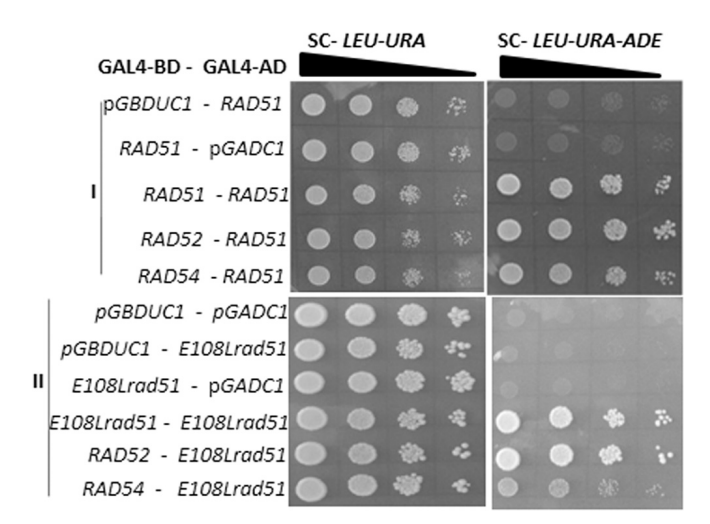


FIG 5 Rad51^{E108L} can form homodimers and bind efficiently to the Rad52 epistasis group of proteins. Yeast two-hybrid analysis depicting the interaction of RAD51/rad51 mutants with Rad52 epistasis group. Various strains harboring bait and prey vectors are represented on the left. Cells of each strain were grown to an ${\rm OD}_{600}$ of 0.5 and serially diluted before spotting. To monitor the interaction between proteins, diluted cells were spotted on medium lacking Leu and Ura (left panel) as well as on medium lacking Leu, Ura, and Ade. Homodimerization as well as interaction of Rad51 (positive control) (I) and Rad51^{E108L} (II) with Rad52 and Rad54 was unaltered.



interacted efficiently with itself as well as with Rad52 and Rad54. We verified that Rad52 and Rad54 do not cause self-activation of a reporter gene (data not shown). No growth in a triple-drop-out plate for the strains PMY11 and PMY14 indicated that there was no self-activation for the indicative strains.

DISCUSSION

Rad51 protein, which facilitates homologous strand exchange, is the central player for HR in mammalian cells. Disruption of this gene is associated with embryonic lethality in mice (23). It is reported that haploinsufficiency of this gene is linked with defects in human neurodevelopment (24, 25). The Rad51 focus formation in response to DNA damage is one of the regulatory events in HR.

Previously, we established that besides providing stability to the Rad51 protein, Hsp90 also controls its nuclear function, i.e., DNA damage-induced focus formation. Taking that study further, we show that the dynamic interaction between Hsp90 and Rad51 can influence the nuclear function of Rad51. We are reporting for the first time that DNA damage triggers the dissociation of Rad51 and Hsp90, which could be a prerequisite for the nuclear function of Rad51. Due to a stronger association with Hsp90, the Rad51^{E108L} protein probably remains locked with Hsp90; hence, the recruitment of Rad51^{E108L} to the broken DNA ends, even at a very high MMS concentration (0.15%), is considerably defective. This is evident by 10.5% GC efficiency and complete loss of cell survivability in the E108L-rad51 mutant cells under DNA-damaging conditions. Thus, our study shows that there is a positive correlation between the extent of Hsp90-Rad51 dissociation after DNA damage and Rad51 nuclear activity. It appears that in the case of E108L-rad51, a major portion of the Hsp90 pool is associated with Rad51, which might result in an insufficient availability of free Hsp90 for other cellular functions. This is supported by our observation that the E108L-rad51 mutant strain showed a slow growth phenotype compared to that of the wild-type strain. However, it is possible that the constitutive form of yHsp90, namely, Hsc82, might be sufficient for the essential cellular function of Hsp90, ensuring the survivability of the mutant strain.

A defect in recruitment to the damaged DNA may result from a defect in DNA binding or defects in its interactions with other nuclear proteins. An earlier report showed that glycine at the 103rd position of Rad51 is crucial for DNA binding (26). Another report showed that valine at 328, proline at 339, and isoleucine at 345 are also involved in DNA binding (27). Although there is no report available regarding the DNA binding capacity of the mutant used in our study, we do not anticipate any defect in DNA binding, as the mutant was recruited to the chromatin DNA albeit at lesser extent, probably due to the lesser availability of free Rad51^{E108L} proteins. In the case of the Rad51^{E108L} mutant, despite its apparent defect in reversible dissociation from Hsp90 under DNA-damaging conditions, its 40% recruitment confirms that it is not defective in DNA binding.

In our study, we expressed *RAD51* and *E108L-rad51* from episomal plasmids in a $\Delta rad51$ background and compared their phenotypes. Thus, it is important to ensure that the observed phenotypes were not due to overexpression. In an earlier study, it was observed that overexpression of Rad51 does not have any effect on MMS sensitivity or repair of a single DSB in wild-type cells. However, it sensitizes $\Delta srs2$ and $\Delta ku70$ strains toward MMS (28). It was also observed that a high level of Rad51 reduces the frequency of but does not eliminate HR (28). In our study, the steady-state levels of Rad51^{WT} and Rad51^{E108L} were comparable. Thus, the severe DNA repair defects observed in the *E108L-rad51* strain compared to that in *RAD51* cells are not due to overexpression but rather to the point mutation.

It did not escape our notice that nearly 50% less recruitment of Rad51 in the *E108L-rad51* strain had a profound effect on DNA repair. It is not unexpected, as our earlier study demonstrated that an only 20% reduction of Rad51 focus formation in the $\Delta 211-259hsp82$ strain led to severe sensitivity to MMS and UV treatment (14). These



findings prompted us to conclude that 20% to 50% less occupancy of Rad51 at the broken DNA ends is sufficient to perturb DSB repair.

The E108 residue of Rad51 that is in close proximity to Hsp90 resides outside the ATPase domain of Rad51 and is evolutionary conserved. The N-terminal domain of Rad51 is implicated in the monomer-monomer interaction as well as the interactions with the members of the Rad52 epistasis group (27, 29). Although the mutation is present in the N-terminal domain, it was not previously identified in Rad51 interactiondeficient mutants (30). The yeast two-hybrid assay confirms that the ability of Rad51^{E108L} for self-association as well as for associations with Rad52 and Rad54 are comparable to that of wild-type Rad51. As Rad51 recruitment to the broken DNA ends is an upstream event, the defect will be dominant over any other defects. Thus, the drastic phenotype found in the E108L-rad51 strain is likely to be one of the primary causes for the loss-of-function phenotype in the mutant strain.

It is known that Hsp90 shows a variable degree of association with its clients. Hsp90 clients such as kinases are primarily associated with Hsp90 through transient interactions, and once chaperoned, they are readily released from Hsp90 as functional proteins. On the other hand, clients such as steroid hormone receptors remain associated with Hsp90 to maintain their functional forms. Also, the extent of association between Hsp90 and its client can alter the cellular function of its client. For example, the single point mutations in the epidermal growth factor receptor (EGFR^{L858R}) and B-Raf kinase (B-Raf^{V600E}) promote tumor formation. It was observed that these point mutants have enhanced levels of association with Hsp90 compared to those of their wild-type counterparts (31, 32). While binding with its clients, Hsp90 exhibits specificity toward the hydrophobic residues of proteins (33). The incorporation of leucine at the 108th position of Rad51 increases the hydrophobic stretch on Rad51 (107 to 113 amino acids). We speculate that such an increase in hydrophobicity might result in a tighter binding between Hsp90 and mutant Rad51 protein.

Collectively, our work establishes the importance of Hsp90 in the HR pathway, where it appears to regulate the stability and functions of Rad51. Increasing lines of evidence suggest that the functions of several DNA repair proteins, such as BRCA1, BRCA2, Chk1, DNA-PKcs, FANCA, and the Mre11/Rad50/NBS, are likely to be dependent on Hsp90 (34). A recent report showed that overexpression of Hsp90 leads to genomic instability through a negative regulation of the checkpoint kinase RAD53 (22). Our work along with these reports embarks on the relationship of Hsp90 with DNA repair. Currently, DNA repair along with the Hsp90 inhibitor is being targeted in many cancer studies. Understanding the detailed regulation of HR will be beneficial for further knowledge in the field.

There are many reports which show that in response to various signals, Hsp90/ Hsp82 gets posttranslational modifications (PTMs), and such PTMs help the release of the client protein (35–37). Currently, it is not known whether such PTM of Hsp90 occurs due to MMS treatment and that causes the decrease in association between Rad51WT and Hsp90. It is also unclear how the stronger association between Rad51E108L and Hsp90 was not overcome during the DNA damage response (DDR). These questions are interesting but beyond the scope of this report, and future studies might unravel the mechanism underlying the dissociation of Rad51 from Hsp90 upon DNA damage.

MATERIALS AND METHODS

Plasmids. The sequences of all the primers used in this paper are tabulated in Table 2. The RAD51 mutant (E108L-rad51) was cloned in 2μ yeast expression vector pTA (20) between the BamH1 and Pst1 restriction sites to generate the pTA-E108L-rad51 plasmid. pTA-RAD51 was used as a positive control in our study (20). Full-length RAD51 and E108L-rad51 were subcloned into prey vector pGADC1 and bait vector pGBDUC1 from pTA-RAD51 and pTA-E108L-rad51, respectively. Thus, the plasmids pGADC1/ RAD51, pGBDUC1/RAD51, pGADC1/E108L-rad51, and pGBDUC1/E108L-rad51 were generated. Full-length RAD52 was amplified using the OSB330/OSB331 primer set and cloned into pGBDUC1 vector between EcoRI and Sall restriction sites to create the pGBDUC1/RAD52 plasmid. To generate the pGBDUC1/RAD54 plasmid, RAD54 was amplified using the OSB332/OSB333 primer set and cloned into pGBDUC1 vector between EcoRI and SalI restriction sites.



TABLE 2 Primer list

Primer	Sequence (5'→3')	Purpose
OMKB90	GGATCCATGTCTCAAGTTCAAGAAC	Forward primer to amplify full-length RAD51
OMKB88	CTGCAGCTACTCGTCTTCTCC	Reverse primer to amplify full-length RAD51
OMKB149	GTCGACCTCGTCTTCTTCTGG	Reverse primer used to clone E108L-rad51 into pET22b vecto
OSB305	CTCGGATCCATGTCTCAAGTTCAAGAACAAC	Forward primer used to amplify full-length rad51 mutants
OSB293	GTCGTCGACCTCGTCTTCTTCTGGGG	Reverse primer used to amplify full-length rad51 mutants
OSB315	AGTGGGCTTCACACTGCTTTGGCGGTAGCA	Forward primer to create rad51 E108L mutation
OSB314	TCTGGGAGCATATGCTACCGCCAAAGCAGTG	Reverse primer to create rad51 E108L mutation
OSB278	CATGCAAGGGCTCCCTAGC	Forward primer used to amplify URA3 region for ChIP
OSB279	CAACCAATCGTAACCTTCATCT	Reverse primer used to amplify URA3 region for ChIP
OSB289	GTTAGTTGAAGCATTAGGTCC	Forward primer used to confirm HO digestion
KanB1	TGTACGGGCGACAGTCACAT	Reverse primer used to confirm HO digestion
OSB21	GACGGATCCATGGCTAGTGAAACTTTTGAATTTC	Forward primer to amplify full-length hsp82
OSB22	CGGGTCGACCTAATCTACCTCTTCCATTTCGG	Reverse primer to amplify full-length hsp82
OSB16	TGACCAAACTACTTACAACTCC	Forward primer to amplify 307 bp of 3' end of ACT1
OSB14	TTAGAAACACTTGTGGTGAACG	Reverse primer to amplify ACT1
OSB330	CATGAATTCATGAATGAAATTATGGATATCGATG	Forward primer to amplify RAD52
OSB331	CATGTCGACTCAAGTAGGCTTGCGTGCATG	Reverse primer to amplify RAD52
OSB332	CATGAATTCATGGCAAGACGCAGATTACC	Forward primer to amplify RAD54
OSB333	CATGTCGACTCAATGTGAAATATATTGAAATGC	Reverse primer to amplify RAD54

Site-directed mutagenesis. Point mutations were introduced in RAD51 by using the splice overlap extension (SOE) PCR technique. A primer set was designed to incorporate the required mutation in RAD51 at the desired location. Yeast genomic DNA was used as a template, and the full-length gene was amplified in two segments in order to insert the point mutation. For amplifying the first and second segments to generate the E108L-rad51 mutation, primer sets OSB305/OSB314 and OSB315/OSB293 were used, respectively. Full-length RAD51 containing the E108L mutation was then amplified by using the first two segments along with primer set OMKB90/OMKB88. The rad51 mutant was then cloned into the pTA 2μ yeast expression vector using the sites BamH1 and Pstl. After successful cloning, the pTA-E108L-rad51 construct was sequenced to confirm the desired mutation. To create the E108L-rad51 mutant, we changed the codon GAA to TTG.

Yeast strains. The strains used in this study are tabulated in Table 3. LS402 $\Delta rad51$ was transformed with empty vector (pTA), pTA-RAD51, and pTA-E108L-rad51 to generate NRY1, NRY2, and TSY17, respectively. For the gene conversion assay, pTA-RAD51 and pTA-E108L-rad51 were transformed into NA14 $\Delta rad51$ (21) to generate TSY21 and TSY22. For a negative control, the NA14 $\Delta rad51$ strain was transformed with pTA empty vector to generate TSY20. To perform the yeast two-hybrid analysis, empty pGADC1 and pGBDUC1 vectors were transformed into a pJ694a parent strain to generate the PMY3 yeast strain. To study the interaction of wild-type Rad51 with itself and with Rad52 and Rad54 proteins, PMY8, PMY9, and PMY10 were created by transforming prey-RAD51 plus bait-RAD51, prey-RAD51 plus bait-RAD52, and prey-RAD51 plus bait-RAD54 constructs, respectively, into the pJ694a strain. Similarly, to study the interaction of Rad51^{E108L} with itself and with Rad52 and Rad54, strains TSY10, PMY12, and PMY13 were generated by transforming prey-E108L-rad51 plus bait-E108L-rad51, prey-E108L-rad51 plus bait-RAD52, and prey-E108L-rad51 plus bait-RAD54 constructs, respectively. Strains PMY4, PMY7, PMY14, and PMY11 were utilized as controls. These strains were generated by transforming empty prey plus bait-RAD51, prey-RAD51 plus empty bait, empty prey plus bait-E108L-rad51, and prey-E108L-rad51 plus empty bait vectors, respectively, into the pJ694a strain.

Yeast two-hybrid analysis. Yeast two hybrid analysis was performed as described earlier (20). The strains PMY3, PMY8, PMY9, PMY10, TSY10, PMY12, PMY13, PMY4, PMY7, PMY14, and PMY11 were grown in SC-Ura-Leu medium until logarithmic phase. They were then diluted serially as shown in Fig. 5 and spotted on SC-uracil (Ura)-Leu and SC-Ura-Leu-adenine (Ade) medium. The plates were kept at 30°C for 3 to 4 days. The strain PMY3 was used as the negative control in our study.

MMS sensitivity assay. NRY1, NRY2, and TSY17 were tested for DNA damage sensitivity. All strains were grown in tryptophan dropout synthetic medium overnight at 30°C. The next day, a secondary culture was grown to an optical density at 600 nm (OD_{600}) of 0.5 at 30°C. The culture was then divided into two sets. One set of cells was treated with 0.03% (vol/vol) of methyl methanesulfonate (MMS) (Sigma-Aldrich) and grown at 30°C for 2 h, and the other set was continuously grown at 30°C for 2 h without MMS. After that, the cells were serially diluted as mentioned, spotted on selective medium, and incubated at 30°C for 2 to 3 days.

Gene conversion assay. TSY20, TSY21, and TSY22 strains were generated by transforming pTA (empty vector), pTA-RAD51 and pTA-E108L-rad51, respectively, into the NA14 Δrad51 strain. The transformed cells were initially patched on a plate containing glycerol as a sole carbon source. Next, equal numbers of cells were counted and spread on two different plates, one containing glycerol and other containing galactose as a carbon source, and incubated at 30°C for 3 to 5 days. Cells which survived on galactose plates were then patched on another plate containing G418 sulfate and incubated at 30°C for 36 h in order to determine the percentage gene conversion. Cells grown on G418 sulfate-containing plates utilize the Rad51-mediated gene conversion pathway for repair as they retain KANMX6. The ratio of the number of cells grown on the G418 sulfate plate to the number of cells grown on the galactose



SI
raji
t st
east
×ِ
쁘
ø
₹

Strain Genotype Source or ra NRY1 M47a leu2-3,112 tp1-1 can1-100 ura3-1 ade2-1 his3-11,15 [phi ⁺] RAD51:::EU2 pTA-RAD51 20 NRY2 M47a leu2-3,112 tp1-1 can1-100 ura3-1 ade2-1 his3-11,15 [phi ⁺] RAD51:::EU2 pTA-RAD51 20 TSY17 M47a leu2-3,112 tp1-1 can1-100 ura3-1 ade2-1 his3-11,15 [phi ⁺] RAD51:::EU2 pTA-RAD51 This study TSY17 M47a leu2-3,112 tp1-1 can1-100 ura3-1 ade2-1 his3-11,15 [phi ⁺] RAD51:::EU2 pTA-RAD51 This study TSY17 M47a inc ura3-HOcs lys2::ura3-HOcs-inc ade3::GALHO ade2-1 leu2-3,112 his3-11,15 tp1-1 can1-100 RAD51:::EU2 pTA-RAD51 This study TSY21 M47a inc ura3-HOcs lys2::ura3-HOcs-inc ade3::GALHO ade2-1 leu2-3,112 his3-11,15 tp1-1 can1-100 RAD51:::EU2 pTA-RAD51 This study PMY3 M47a inc ura3-HOcs lys2::ura3-HOcs-inc ade3::GALHO ade2-1 leu2-3,112 his3-11,15 tp1-1 can1-100 RAD51:::EU2 pTA-RAD51 This study PMY3 M47a inc ura3-HOcs lys2::ura3-HOcs-inc ade3::GALHO ade2-1 leu2-3,112 his3-11,15 tp1-1 can1-100 RAD51 pGBDUC1/RAD51 This study PMY3 M47a inc ura3-HOcs lys2::ura3-HOcs-inc ade3::GALHO ade2-1 leu2-3,112 his3-11,15 tp1-1 can1-100 RAD51 pGBDUC1/RAD52 This study PMY9 M47a irp-901 leu2-3,112 ura3-52 his3-200 ga14A ga180A LYS2::GALHIS3 GAL2-ADE2 met2::GAL7-lac2 pGADC1/ROB54 This study PMY1 M47a irp-901 leu2-	ייייי בייייייייייייייייייייייייייייייי	מסר סגומוויס	
MATa leu2-3,112 trp1-1 can1-100 ura3-1 ade2-1 his3-11,15 [phi+] RAD51::LEU2 pTA-RAD51 MATa leu2-3,112 trp1-1 can1-100 ura3-1 ade2-1 his3-11,15 [phi+] RAD51::LEU2 pTA-RAD51 MATa leu2-3,112 trp1-1 can1-100 ura3-1 ade2-1 his3-11,15 [phi+] RAD51::LEU2 pTA-F108L-rad51 MATa inc ura3-HOcs ys2:ura3-HOcs ys2:ura3-HOcs-inc ade3::GALHO ade2-1 leu2-3,112 his3-11,15 trp1-1 can1-100 RAD51::LEU2 pTA-RAD51 MATa inc ura3-HOcs ys2:ura3-HOcs-inc ade3::GALHO ade2-1 leu2-3,112 his3-11,15 trp1-1 can1-100 RAD51::LEU2 pTA-RAD51 MATa inc ura3-HOcs ys2:ura3-HOcs-inc ade3::GALHO ade2-1 leu2-3,112 his3-11,15 trp1-1 can1-100 RAD51::LEU2 pTA-RAD51 MATa inc ura3-HOcs ys2:ura3-HOcs-inc ade3::GALHO ade2-1 leu2-3,112 his3-11,15 trp1-1 can1-100 RAD51::LEU2 pTA-RAD51 MATa trp1-901 leu2-3,112 ura3-52 his3-200 ga14Δ ga180Δ LYS2::GALH-HIS3 GAL2-ADE2 met2::GAL7-lac2 pGADC1/RAD51 pGBDUC1/RAD52 MATa trp1-901 leu2-3,112 ura3-52 his3-200 ga14Δ ga180Δ LYS2::GALH-HIS3 GAL2-ADE2 met2::GAL7-lac2 pGADC1/ScRAD51 pGBDUC1/RAD54 MATa trp1-901 leu2-3,112 ura3-52 his3-200 ga14Δ ga180Δ LYS2::GALH-HIS3 GAL2-ADE2 met2::GAL7-lac2 pGADC1/ScRAD51 pGBDUC1/RAD54 MATa trp1-901 leu2-3,112 ura3-52 his3-200 ga14Δ ga180Δ LYS2::GALH-HIS3 GAL2-ADE2 met2::GAL7-lac2 pGADC1/RAD51 MATa trp1-901 leu2-3,112 ura3-52 his3-200 ga14Δ ga180Δ LYS2::GALH-HIS3 GAL2-ADE2 met2::GAL7-lac2 pGADC1/RAD51 MATa trp1-901 leu2-3,112 ura3-52 his3-200 ga14Δ ga180Δ LYS2::GALH-HIS3 GAL2-ADE2 met2::GAL7-lac2 pGADC1/RAD51 MATa trp1-901 leu2-3,112 ura3-52 his3-200 ga14Δ ga180Δ LYS2::GALH-HIS3 GAL2-ADE2 met2::GAL7-lac2 pGADC1/E108L-ad51 pGBDUC1/RAD54 MATa trp1-901 leu2-3,112 ura3-52 his3-200 ga14Δ ga180Δ LYS2::GALH-HIS3 GAL2-ADE2 met2::GAL7-lac2 pGADC1/E108L-ad51 pGBDUC1/RAD54 MATa trp1-901 leu2-3,112 ura3-52 his3-200 ga14Δ ga180Δ LYS2::GALH-HIS3 GAL2-ADE2 met2::GAL7-lac2 pGADC1/E108L-ad51 pGBDUC1/E108L-ad51 pGBDUC1/E	Strain	Genotype	Source or reference
MATa leu2-3,112 trp1-1 can1-100 ura3-1 ade2-1 his3-11,15 [phi+*] RAD51::LEU2 pTA-FAD51 MATa leu2-3,112 trp1-1 can1-100 ura3-1 ade2-1 his3-11,15 [phi+*] RAD51::LEU2 pTA-F108L-rad51 MATa leu2-3,112 trp1-1 can1-100 ura3-1 ade2-1 his3-11,15 [phi+*] RAD51::LEU2 pTA-F108L-rad51 MATa inc ura3-HOcs lys2::ura3-HOcs-inc ade3::GALHO ade2-1 leu2-3,112 his3-11,15 trp1-1 can1-100 RAD51::LEU2 pTA-F108L-rad51 MATa inc ura3-HOcs lys2::ura3-HOcs-inc ade3::GALHO ade2-1 leu2-3,112 his3-11,15 trp1-1 can1-100 RAD51::LEU2 pTA-F108L-rad51 MATa trp1-901 leu2-3,112 ura3-52 his3-200 ga14A ga180A LYS2::GALI-HIS3 GAL2-ADE2 met2::GAL7-lac2 pGADC1/RAD51 pGBDUC1/RAD52 MATa trp1-901 leu2-3,112 ura3-52 his3-200 ga14A ga180A LYS2::GALI-HIS3 GAL2-ADE2 met2::GAL7-lac2 pGADC1/RAD51 pGBDUC1/RAD54 MATa trp1-901 leu2-3,112 ura3-52 his3-200 ga14A ga180A LYS2::GALI-HIS3 GAL2-ADE2 met2::GAL7-lac2 pGADC1/RAD51 pGBDUC1/RAD54 MATa trp1-901 leu2-3,112 ura3-52 his3-200 ga14A ga180A LYS2::GALI-HIS3 GAL2-ADE2 met2::GAL7-lac2 pGADC1/RAD51 pGBDUC1/RAD54 MATa trp1-901 leu2-3,112 ura3-52 his3-200 ga14A ga180A LYS2::GALI-HIS3 GAL2-ADE2 met2::GAL7-lac2 pGADC1/R108L-rad51 pGBDUC1/RAD54 MATa trp1-901 leu2-3,112 ura3-52 his3-200 ga14A ga180A LYS2::GALI-HIS3 GAL2-ADE2 met2::GAL7-lac2 pGADC1/R108L-rad51 pGBDUC1/RAD54 MATa trp1-901 leu2-3,112 ura3-52 his3-200 ga14A ga180A LYS2::GALI-HIS3 GAL2-ADE2 met2::GAL7-lac2 pGADC1/R108L-rad51 pGBDUC1/R108L-rad51 pGBDUC1/R108L-rad51 pGBDUC1/R108L-rad51 pGBDUC1/R108L-rad51 pGBDUC1/R108L-rad51 pGBDUC1/R108L-rad51 pGBDUC1/R108L-rad51 pGBDUC1/R108L-rad51 pGBDUC1/R108L-rad51 pGBDUC1/R108-rad51 pGBDUC1/R108L-rad51 pGB	NRY1	MATa leuz-3,112 trp1-1 can1-100 ura3-1 ade2-1 his3-11,15 [phi+†] RAD51::LEU2 pTA	20
MATa leu2-3,112 ttp1-1 can1-100 ura3-1 ade2-1 his3-11,15 [phi ⁺] RAD51::LEU2 pTA-E108L-rad51 MATa inc ura3-HOcs lys2::ura3-HOcs-inc ade3::GALHO ade2-1 leu2-3,112 his3-11,15 trp1-1 can1-100 RAD51::LEU2 pTA-RAD51 MATa inc ura3-HOcs lys2::ura3-HOcs-inc ade3::GALHO ade2-1 leu2-3,112 his3-11,15 trp1-1 can1-100 RAD51::LEU2 pTA-RAD51 MATa inc ura3-HOcs lys2::ura3-HOcs-inc ade3::GALHO ade2-1 leu2-3,112 his3-11,15 trp1-1 can1-100 RAD51::LEU2 pTA-E108L-rad51 MATa trp1-901 leu2-3,112 ura3-52 his3-200 ga14Δ ga180Δ LYS2::GAL1-HIS3 GAL2-ADE2 met2::GAL7-lac2 pGADC1/RAD51 pGBDUC1/RAD52 MATa trp1-901 leu2-3,112 ura3-52 his3-200 ga14Δ ga180Δ LYS2::GAL1-HIS3 GAL2-ADE2 met2::GAL7-lac2 pGADC1/RAD51 pGBDUC1/RAD52 MATa trp1-901 leu2-3,112 ura3-52 his3-200 ga14Δ ga180Δ LYS2::GAL1-HIS3 GAL2-ADE2 met2::GAL7-lac2 pGADC1/E108L-rad51 pGBDUC1/RAD52 MATa trp1-901 leu2-3,112 ura3-52 his3-200 ga14Δ ga180Δ LYS2::GAL1-HIS3 GAL2-ADE2 met2::GAL7-lac2 pGADC1/E108L-rad51 pGBDUC1/RAD54 MATa trp1-901 leu2-3,112 ura3-52 his3-200 ga14Δ ga180Δ LYS2::GAL1-HIS3 GAL2-ADE2 met2::GAL7-lac2 pGADC1/E108L-rad51 pGBDUC1/RAD54 MATa trp1-901 leu2-3,112 ura3-52 his3-200 ga14Δ ga180Δ LYS2::GAL1-HIS3 GAL2-ADE2 met2::GAL7-lac2 pGADC1 pGBDUC1/RAD51 MATa trp1-901 leu2-3,112 ura3-52 his3-200 ga14Δ ga180Δ LYS2::GAL1-HIS3 GAL2-ADE2 met2::GAL7-lac2 pGADC1 pGBDUC1/RAD51 MATa trp1-901 leu2-3,112 ura3-52 his3-200 ga14Δ ga180Δ LYS2::GAL1-HIS3 GAL2-ADE2 met2::GAL7-lac2 pGADC1 pGBDUC1/R08L-rad51 MATa trp1-901 leu2-3,112 ura3-52 his3-200 ga14Δ ga180Δ LYS2::GAL1-HIS3 GAL2-ADE2 met2::GAL7-lac2 pGADC1 pGBDUC1/R08L-rad51 MATa trp1-901 leu2-3,112 ura3-52 his3-200 ga14Δ ga180Δ LYS2::GAL1-HIS3 GAL2-ADE2 met2::GAL7-lac2 pGADC1 pGBDUC1/R08L-rad51 MATa trp1-901 leu2-3,112 ura3-52 his3-200 ga14Δ ga180Δ LYS2::GAL1-HIS3 GAL2-ADE2 met2::GAL7-lac2 pGADC1/R02-gal2-rad51 pGBDUC1/R02-gal2-rad51 pGBDUC1/R02-gal2-rad51 pGBDUC1/R02-gal2-rad51 pGBDUC1/R02-gal2-rad51 pGBDUC1/R02-gal2-rad51 pGBDUC1/R02-gal2-rad51 pGBDUC1/R02-gal2-rad51 pGBDUC1/R02-gal2-gal2-rad51 pGBDUC1/R02-gal2-gal2-rad2	NRY2	MATa leu2-3,112 trp1-1 can1-100 ura3-1 ade2-1 his3-11,15 [phi+†] RAD51::LEU2 pTA-RAD51	20
MATa inc ura3-HOcs lys2::ura3-HOcs-inc ade3::GALHO ade2-1 leu2-3,112 his3-11,15 trp1-1 can1-100 RAD51::LEU2 pTA-RAD51 MATa inc ura3-HOcs lys2::ura3-HOcs-inc ade3::GALHO ade2-1 leu2-3,112 his3-11,15 trp1-1 can1-100 RAD51::LEU2 pTA-F108L-rad51 MATa inc ura3-HOcs lys2::ura3-HOcs-inc ade3::GALHO ade2-1 leu2-3,112 his3-11,15 trp1-1 can1-100 RAD51::LEU2 pTA-F108L-rad51 MATa trp1-901 leu2-3,112 ura3-52 his3-200 ga14D ga180D LYS2::GAL1-HIS3 GAL2-ADE2 met2::GAL7-lacZ pGADC1/RAD51 pGBDUC1/RAD51 MATa trp1-901 leu2-3,112 ura3-52 his3-200 ga14D ga180D LYS2::GAL1-HIS3 GAL2-ADE2 met2::GAL7-lacZ pGADC1/RAD51 pGBDUC1/RAD52 MATa trp1-901 leu2-3,112 ura3-52 his3-200 ga14D ga180D LYS2::GAL1-HIS3 GAL2-ADE2 met2::GAL7-lacZ pGADC1/RAD51 pGBDUC1/RAD52 MATa trp1-901 leu2-3,112 ura3-52 his3-200 ga14D ga180D LYS2::GAL1-HIS3 GAL2-ADE2 met2::GAL7-lacZ pGADC1/RAD51 pGBDUC1/RAD54 MATa trp1-901 leu2-3,112 ura3-52 his3-200 ga14D ga180D LYS2::GAL1-HIS3 GAL2-ADE2 met2::GAL7-lacZ pGADC1/RAD51 pGBDUC1/RAD54 MATa trp1-901 leu2-3,112 ura3-52 his3-200 ga14D ga180D LYS2::GAL1-HIS3 GAL2-ADE2 met2::GAL7-lacZ pGADC1/RAD51 pGBDUC1/RAD51 MATa trp1-901 leu2-3,112 ura3-52 his3-200 ga14D ga180D LYS2::GAL1-HIS3 GAL2-ADE2 met2::GAL7-lacZ pGADC1 pGBDUC1 MATa trp1-901 leu2-3,112 ura3-52 his3-200 ga14D ga180D LYS2::GAL1-HIS3 GAL2-ADE2 met2::GAL7-lacZ pGADC1 pGBDUC1 MATa trp1-901 leu2-3,112 ura3-52 his3-200 ga14D ga180D LYS2::GAL1-HIS3 GAL2-ADE2 met2::GAL7-lacZ pGADC1 pGBDUC1 MATa trp1-901 leu2-3,112 ura3-52 his3-200 ga14D ga18D0 LYS2::GAL1-HIS3 GAL2-ADE2 met2::GAL7-lacZ pGADC1 pGBDUC1 MATa trp1-901 leu2-3,112 ura3-52 his3-200 ga14D ga18D0 LYS2::GAL1-HIS3 GAL2-ADE2 met2::GAL7-lacZ pGADC1 pGBDUC1	TSY17	MATa leuz-3,112 trp1-1 can1-100 ura3-1 ade2-1 his3-11,15 [phi+†] RAD51::LEU2 pTA-E108L-rad51	This study
MATa inc ura3-HOcs lys2:ura3-HOcs-inc ade3::GALHO ade2-1 leu2-3,112 his3-11,15 trp1-1 can1-100 RAD51::LEU2 pTA-RAD51 MATa inc ura3-HOcs lys2:ura3-HOcs-inc ade3::GALHO ade2-1 leu2-3,112 his3-11,15 trp1-1 can1-100 RAD51::LEU2 pTA-E108L-rad51 MATa trp1-901 leu2-3,112 ura3-52 his3-200 ga14Δ ga180Δ LYS2::GAL1-HIS3 GAL2-ADE2 met2::GAL7-lacZ pGADC1/RAD51 pGBDUC1/RAD51 MATa trp1-901 leu2-3,112 ura3-52 his3-200 ga14Δ ga180Δ LYS2::GAL1-HIS3 GAL2-ADE2 met2::GAL7-lacZ pGADC1/RAD51 pGBDUC1/RAD52 MATa trp1-901 leu2-3,112 ura3-52 his3-200 ga14Δ ga180Δ LYS2::GAL1-HIS3 GAL2-ADE2 met2::GAL7-lacZ pGADC1/E108L-rad51 pGBDUC1/RAD52 MATa trp1-901 leu2-3,112 ura3-52 his3-200 ga14Δ ga180Δ LYS2::GAL1-HIS3 GAL2-ADE2 met2::GAL7-lacZ pGADC1/E108L-rad51 pGBDUC1/RAD52 MATa trp1-901 leu2-3,112 ura3-52 his3-200 ga14Δ ga180Δ LYS2::GAL1-HIS3 GAL2-ADE2 met2::GAL7-lacZ pGADC1/F108L-rad51 pGBDUC1/RAD54 MATa trp1-901 leu2-3,112 ura3-52 his3-200 ga14Δ ga180Δ LYS2::GAL1-HIS3 GAL2-ADE2 met2::GAL7-lacZ pGADC1/RAD51 pGBDUC1/RAD54 MATa trp1-901 leu2-3,112 ura3-52 his3-200 ga14Δ ga180Δ LYS2::GAL1-HIS3 GAL2-ADE2 met2::GAL7-lacZ pGADC1/E108L-rad51 pGBDUC1/E108L-rad51 MATa trp1-901 leu2-3,112 ura3-52 his3-200 ga14Δ ga180Δ LYS2::GAL1-HIS3 GAL2-ADE2 met2::GAL7-lacZ pGADC1/E108L-rad51 pGBDUC1 MATa trp1-901 leu2-3,112 ura3-52 his3-200 ga14Δ ga180Δ LYS2::GAL1-HIS3 GAL2-ADE2 met2::GAL7-lacZ pGADC1/E108L-rad51 pGBDUC1 MATa trp1-901 leu2-3,112 ura3-52 his3-200 ga14Δ ga180Δ LYS2::GAL1-HIS3 GAL2-ADE2 met2::GAL7-lacZ pGADC1/E108L-rad51 pGBDUC1 MATa trp1-901 leu2-3,112 ura3-52 his3-200 ga14Δ ga180Δ LYS2::GAL1-HIS3 GAL2-ADE2 met2::GAL7-lacZ pGADC1/E108L-rad51 pGBDUC1	TSY20	MATa inc ura3-HOcs lys2::ura3-HOcs-inc ade3::GALHO ade2-1 leu2-3,112 his3-11,15 trp1-1 can1-100 RAD51::LEU2 pTA	This study
MATa inc ura3-HOcs lys2:ura3-HOcs-linc ade3::GALHO ade2-1 leu2-3,112 his3-11,15 trp1-1 can1-100 RAD51::LEU2 pTA-E108L-rad51 MATa trpl-901 leu2-3,112 ura3-52 his3-200 ga14Δ ga180Δ LYS2::GALI-HIS3 GAL2-ADE2 met2::GAL7-lac2 pGADC1/RAD51 pGBDUC1/RAD51 MATa trpl-901 leu2-3,112 ura3-52 his3-200 ga14Δ ga180Δ LYS2::GALI-HIS3 GAL2-ADE2 met2::GAL7-lac2 pGADC1/RAD51 pGBDUC1/RAD52 MATa trpl-901 leu2-3,112 ura3-52 his3-200 ga14Δ ga180Δ LYS2::GALI-HIS3 GAL2-ADE2 met2::GAL7-lac2 pGADC1/RAD51 pGBDUC1/RAD52 MATa trpl-901 leu2-3,112 ura3-52 his3-200 ga14Δ ga180Δ LYS2::GALI-HIS3 GAL2-ADE2 met2::GAL7-lac2 pGADC1/E108L-rad51 pGBDUC1/RAD52 MATa trpl-901 leu2-3,112 ura3-52 his3-200 ga14Δ ga180Δ LYS2::GALI-HIS3 GAL2-ADE2 met2::GAL7-lac2 pGADC1/F108L-rad51 pGBDUC1/RAD54 MATa trpl-901 leu2-3,112 ura3-52 his3-200 ga14Δ ga180Δ LYS2::GALI-HIS3 GAL2-ADE2 met2::GAL7-lac2 pGADC1/RAD51 pGBDUC1/RAD54 MATa trpl-901 leu2-3,112 ura3-52 his3-200 ga14Δ ga180Δ LYS2::GALI-HIS3 GAL2-ADE2 met2::GAL7-lac2 pGADC1/RAD51 pGBDUC1 MATa trpl-901 leu2-3,112 ura3-52 his3-200 ga14Δ ga180Δ LYS2::GALI-HIS3 GAL2-ADE2 met2::GAL7-lac2 pGADC1/E108L-rad51 MATa trpl-901 leu2-3,112 ura3-52 his3-200 ga14Δ ga180Δ LYS2::GALI-HIS3 GAL2-ADE2 met2::GAL7-lac2 pGADC1/E108L-rad51 MATa trpl-901 leu2-3,112 ura3-52 his3-200 ga14Δ ga180Δ LYS2::GALI-HIS3 GAL2-ADE2 met2::GAL7-lac2 pGADC1/E108L-rad51 MATa trpl-901 leu2-3,112 ura3-52 his3-200 ga14Δ ga180Δ LYS2::GALI-HIS3 GAL2-ADE2 met2::GAL7-lac2 pGADC1/E108L-rad51 MATa trpl-901 leu2-3,112 ura3-52 his3-200 ga14Δ ga180Δ LYS2::GALI-HIS3 GAL2-ADE2 met2::GAL7-lac2 pGADC1/E108L-rad51 MATa trpl-901 leu2-3,112 ura3-52 his3-200 ga14Δ ga180Δ LYS2::GALI-HIS3 GAL2-ADE2 met2::GAL7-lac2 pGADC1/E108L-rad51	TSY21	MATa inc ura3-HOcs lys2::ura3-HOcs-inc ade3::GALHO ade2-1 leu2-3,112 his3-11,15 trp1-1 can1-100 RAD51::LEU2 pTA-RAD51	This study
MATa trpl-901 leu2-3,112 ura3-52 his3-200 ga14∆ ga180∆ LYS2::GALI-HIS3 GAL2-ADE2 met2::GAL7-lacZ pGADC1/RAD51 pGBDUC1/RAD51 MATa trpl-901 leu2-3,112 ura3-52 his3-200 ga14∆ ga180∆ LYS2::GAL1-HIS3 GAL2-ADE2 met2::GAL7-lacZ pGADC1/RAD51 pGBDUC1/RAD52 MATa trpl-901 leu2-3,112 ura3-52 his3-200 ga14∆ ga180∆ LYS2::GAL1-HIS3 GAL2-ADE2 met2::GAL7-lacZ pGADC1/RAD51 pGBDUC1/RAD54 MATa trpl-901 leu2-3,112 ura3-52 his3-200 ga14∆ ga180∆ LYS2::GAL1-HIS3 GAL2-ADE2 met2::GAL7-lacZ pGADC1/E108L-rad51 pGBDUC1/RAD54 MATa trpl-901 leu2-3,112 ura3-52 his3-200 ga14∆ ga180∆ LYS2::GAL1-HIS3 GAL2-ADE2 met2::GAL7-lacZ pGADC1/E108L-rad51 pGBDUC1/RAD54 MATa trpl-901 leu2-3,112 ura3-52 his3-200 ga14∆ ga180∆ LYS2::GAL1-HIS3 GAL2-ADE2 met2::GAL7-lacZ pGADC1/E108L-rad51 pGBDUC1/RAD54 MATa trpl-901 leu2-3,112 ura3-52 his3-200 ga14∆ ga180∆ LYS2::GAL1-HIS3 GAL2-ADE2 met2::GAL7-lacZ pGADC1/RAD51 MATa trpl-901 leu2-3,112 ura3-52 his3-200 ga14∆ ga180∆ LYS2::GAL1-HIS3 GAL2-ADE2 met2::GAL7-lacZ pGADC1/RAD51 pGBDUC1 MATa trpl-901 leu2-3,112 ura3-52 his3-200 ga14∆ ga180∆ LYS2::GAL1-HIS3 GAL2-ADE2 met2::GAL7-lacZ pGADC1/E108L-rad51 pGBDUC1 MATa trpl-901 leu2-3,112 ura3-52 his3-200 ga14∆ ga180∆ LYS2::GAL1-HIS3 GAL2-ADE2 met2::GAL7-lacZ pGADC1/E108L-rad51 pGBDUC1 MATa trpl-901 leu2-3,112 ura3-52 his3-200 ga14∆ ga180∆ LYS2::GAL1-HIS3 GAL2-ADE2 met2::GAL7-lacZ pGADC1/E108L-rad51 pGBDUC1	TSY22	MATa inc ura3-HOcs lys2::ura3-HOcs-inc ade3::GALHO ade2-1 leu2-3,112 his3-11,15 trp1-1 can1-100 RAD51::LEU2 pTA-E108L-rad51	This study
MATa trpl-901 leu2-3,112 ura3-52 his3-200 ga14Δ ga180Δ LYS2::GALI-HIS3 GAL2-ADE2 met2::GAL7-lacZ pGADC1/RAD51 pGBDUC1/RAD52 MATa trpl-901 leu2-3,112 ura3-52 his3-200 ga14Δ ga180Δ LYS2::GAL1-HIS3 GAL2-ADE2 met2::GAL7-lacZ pGADC1/RAD51 pGBDUC1/RAD52 MATa trpl-901 leu2-3,112 ura3-52 his3-200 ga14Δ ga180Δ LYS2::GAL1-HIS3 GAL2-ADE2 met2::GAL7-lacZ pGADC1/E108L-rad51 pGBDUC1/RAD54 MATa trpl-901 leu2-3,112 ura3-52 his3-200 ga14Δ ga180Δ LYS2::GAL1-HIS3 GAL2-ADE2 met2::GAL7-lacZ pGADC1/E108L-rad51 pGBDUC1/RAD52 MATa trpl-901 leu2-3,112 ura3-52 his3-200 ga14Δ ga180Δ LYS2::GAL1-HIS3 GAL2-ADE2 met2::GAL7-lacZ pGADC1/E108L-rad51 pGBDUC1/RAD54 MATa trpl-901 leu2-3,112 ura3-52 his3-200 ga14Δ ga180Δ LYS2::GAL1-HIS3 GAL2-ADE2 met2::GAL7-lacZ pGADC1/RAD51 MATa trpl-901 leu2-3,112 ura3-52 his3-200 ga14Δ ga180Δ LYS2::GAL1-HIS3 GAL2-ADE2 met2::GAL7-lacZ pGADC1/RAD51 pGBDUC1 MATa trpl-901 leu2-3,112 ura3-52 his3-200 ga14Δ ga180Δ LYS2::GAL1-HIS3 GAL2-ADE2 met2::GAL7-lacZ pGADC1/E108L-rad51 pGBDUC1 MATa trpl-901 leu2-3,112 ura3-52 his3-200 ga14Δ ga180Δ LYS2::GAL1-HIS3 GAL2-ADE2 met2::GAL7-lacZ pGADC1/E108L-rad51 pGBDUC1 MATa trpl-901 leu2-3,112 ura3-52 his3-200 ga14Δ ga180Δ LYS2::GAL1-HIS3 GAL2-ADE2 met2::GAL7-lacZ pGADC1/E108L-rad51 pGBDUC1	PMY3	MATa trpl-901 leu2-3,112 ura3-52 his3-200 ga14Δ ga180Δ LYS2::GALI-HIS3 GAL2-ADE2 met2::GAL7-lac2 pGADC1 pGBDUC1	This study
MATa trpl-901 leu2-3,112 ura3-52 his3-200 ga14Δ ga180Δ LYS2::GALI-HIS3 GAL2-ADE2 met2::GAL7-lac2 pGADC1/RAD51 pGBDUC1/RAD52 MATa trpl-901 leu2-3,112 ura3-52 his3-200 ga14Δ ga180Δ LYS2::GAL1-HIS3 GAL2-ADE2 met2::GAL7-lac2 pGADC1/Er08L-rad51 pGBDUC1/RAD54 MATa trpl-901 leu2-3,112 ura3-52 his3-200 ga14Δ ga180Δ LYS2::GAL1-HIS3 GAL2-ADE2 met2::GAL7-lac2 pGADC1/Er08L-rad51 pGBDUC1/RAD52 MATa trpl-901 leu2-3,112 ura3-52 his3-200 ga14Δ ga180Δ LYS2::GAL1-HIS3 GAL2-ADE2 met2::GAL7-lac2 pGADC1/Er08L-rad51 pGBDUC1/RAD54 MATa trpl-901 leu2-3,112 ura3-52 his3-200 ga14Δ ga180Δ LYS2::GAL1-HIS3 GAL2-ADE2 met2::GAL7-lac2 pGADC1/RAD51 MATa trpl-901 leu2-3,112 ura3-52 his3-200 ga14Δ ga180Δ LYS2::GAL1-HIS3 GAL2-ADE2 met2::GAL7-lac2 pGADC1/RAD51 pGBDUC1 MATa trpl-901 leu2-3,112 ura3-52 his3-200 ga14Δ ga180Δ LYS2::GAL1-HIS3 GAL2-ADE2 met2::GAL7-lac2 pGADC1/Er08L-rad51 pGBDUC1 MATa trpl-901 leu2-3,112 ura3-52 his3-200 ga14Δ ga180Δ LYS2::GAL1-HIS3 GAL2-ADE2 met2::GAL7-lac2 pGADC1/Er08L-rad51 pGBDUC1 MATa trpl-901 leu2-3,112 ura3-52 his3-200 ga14Δ ga180Δ LYS2::GAL1-HIS3 GAL2-ADE2 met2::GAL7-lac2 pGADC1/Er08L-rad51 pGBDUC1	PMY8	MATa trpl-901 leu2-3,112 ura3-52 his3-200 ga14Δ ga180Δ LYS2::GALI-HIS3 GAL2-ADE2 met2::GAL7-lacZ pGADC1/RAD51 pGBDUC1/RAD51	This study
MATa trpl-901 leu2-3,112 ura3-52 his3-200 ga14Δ ga180Δ LYS2::GALI-HIS3 GAL2-ADE2 met2::GAL7-lacZ pGADC1/5cRAD51 pGBDUC1/RAD54 MATa trpl-901 leu2-3,112 ura3-52 his3-200 ga14Δ ga180Δ LYS2::GAL1-HIS3 GAL2-ADE2 met2::GAL7-lacZ pGADC1/E108L-rad51 pGBDUC1/E108L-rad51 MATa trpl-901 leu2-3,112 ura3-52 his3-200 ga14Δ ga180Δ LYS2::GAL1-HIS3 GAL2-ADE2 met2::GAL7-lacZ pGADC1/E108L-rad51 pGBDUC1/RAD54 MATa trpl-901 leu2-3,112 ura3-52 his3-200 ga14Δ ga180Δ LYS2::GAL1-HIS3 GAL2-ADE2 met2::GAL7-lacZ pGADC1/E108L-rad51 pGBDUC1/RAD54 MATa trpl-901 leu2-3,112 ura3-52 his3-200 ga14Δ ga180Δ LYS2::GAL1-HIS3 GAL2-ADE2 met2::GAL7-lacZ pGADC1/RAD51 pGBDUC1 MATa trpl-901 leu2-3,112 ura3-52 his3-200 ga14Δ ga180Δ LYS2::GAL1-HIS3 GAL2-ADE2 met2::GAL7-lacZ pGADC1/E108L-rad51 MATa trpl-901 leu2-3,112 ura3-52 his3-200 ga14Δ ga180Δ LYS2::GAL1-HIS3 GAL2-ADE2 met2::GAL7-lacZ pGADC1/E108L-rad51 pGBDUC1	PMY9	MATa trpl-901 leu2-3,112 ura3-52 his3-200 ga14Δ ga180Δ LYS2::GALI-HIS3 GAL2-ADE2 met2::GAL7-lacZ pGADC1/RAD51 pGBDUC1/RAD52	This study
 MATa trpl-901 leu2-3,112 ura3-52 his3-200 ga14Δ ga180Δ LYS2::GALI-HIS3 GAL2-ADE2 met2::GAL7-lacZ pGADC1/E108L-rad51 pGBDUC1/E108L-rad51 MATa trpl-901 leu2-3,112 ura3-52 his3-200 ga14Δ ga180Δ LYS2::GAL1-HIS3 GAL2-ADE2 met2::GAL7-lacZ pGADC1/E108L-rad51 pGBDUC1/RAD52 MATa trpl-901 leu2-3,112 ura3-52 his3-200 ga14Δ ga180Δ LYS2::GAL1-HIS3 GAL2-ADE2 met2::GAL7-lacZ pGADC1/E108L-rad51 pGBDUC1/RAD54 MATa trpl-901 leu2-3,112 ura3-52 his3-200 ga14Δ ga180Δ LYS2::GAL1-HIS3 GAL2-ADE2 met2::GAL7-lacZ pGADC1/RAD51 pGBDUC1 MATa trpl-901 leu2-3,112 ura3-52 his3-200 ga14Δ ga180Δ LYS2::GAL1-HIS3 GAL2-ADE2 met2::GAL7-lacZ pGADC1/E108L-rad51 MATa trpl-901 leu2-3,112 ura3-52 his3-200 ga14Δ ga180Δ LYS2::GAL1-HIS3 GAL2-ADE2 met2::GAL7-lacZ pGADC1/E108L-rad51 pGBDUC1 MATa trpl-901 leu2-3,112 ura3-52 his3-200 ga14Δ ga180Δ LYS2::GAL1-HIS3 GAL2-ADE2 met2::GAL7-lacZ pGADC1/E108L-rad51 pGBDUC1 	PMY10	MATa trpl-901 leu2-3,112 ura3-52 his3-200 ga14Δ ga180Δ LYS2::GALI-HIS3 GAL2-ADE2 met2::GAL7-lacZ pGADC1/ScRAD51 pGBDUC1/RAD54	This study
 MATa trpl-901 leu2-3,112 ura3-52 his3-200 ga14Δ ga180Δ LYS2::GALI-HIS3 GAL2-ADE2 met2::GAL7-lacZ pGADC1/E108L-rad51 pGBDUC1/RAD52 MATa trpl-901 leu2-3,112 ura3-52 his3-200 ga14Δ ga180Δ LYS2::GAL1-HIS3 GAL2-ADE2 met2::GAL7-lacZ pGADC1/E108L-rad51 pGBDUC1/RAD54 MATa trpl-901 leu2-3,112 ura3-52 his3-200 ga14Δ ga180Δ LYS2::GAL1-HIS3 GAL2-ADE2 met2::GAL7-lacZ pGADC1/RAD51 pGBDUC1 MATa trpl-901 leu2-3,112 ura3-52 his3-200 ga14Δ ga180Δ LYS2::GAL1-HIS3 GAL2-ADE2 met2::GAL7-lacZ pGADC1/RAD51 pGBDUC1 MATa trpl-901 leu2-3,112 ura3-52 his3-200 ga14Δ ga180Δ LYS2::GAL1-HIS3 GAL2-ADE2 met2::GAL7-lacZ pGADC1/E108L-rad51 pGBDUC1 MATa trpl-901 leu2-3,112 ura3-52 his3-200 ga14Δ ga180Δ LYS2::GAL1-HIS3 GAL2-ADE2 met2::GAL7-lacZ pGADC1/E108L-rad51 pGBDUC1 	TSY10	MATa trpl-901 leu2-3,112 ura3-52 his3-200 ga14Δ ga180Δ LYS2::GALI-HIS3 GAL2-ADE2 met2::GAL7-lacZ pGADC1/E108L-rad51 pGBDUC1/E108L-rad51	This study
 MATa trpl-901 leu2-3,112 ura3-52 his3-200 ga14Δ ga180Δ LYS2::GALI-HIS3 GAL2-ADE2 met2::GAL7-lacZ pGADC1/E108L-rad51 pGBDUC1/RAD54 MATa trpl-901 leu2-3,112 ura3-52 his3-200 ga14Δ ga180Δ LYS2::GAL1-HIS3 GAL2-ADE2 met2::GAL7-lacZ pGADC1/RAD51 pGBDUC1 MATa trpl-901 leu2-3,112 ura3-52 his3-200 ga14Δ ga180Δ LYS2::GAL1-HIS3 GAL2-ADE2 met2::GAL7-lacZ pGADC1/RAD51 pGBDUC1 MATa trpl-901 leu2-3,112 ura3-52 his3-200 ga14Δ ga180Δ LYS2::GAL1-HIS3 GAL2-ADE2 met2::GAL7-lacZ pGADC1/E108L-rad51 pGBDUC1 MATa trpl-901 leu2-3,112 ura3-52 his3-200 ga14Δ ga180Δ LYS2::GAL1-HIS3 GAL2-ADE2 met2::GAL7-lacZ pGADC1/E108L-rad51 pGBDUC1 	PMY12	MATa trpl-901 leu2-3,112 ura3-52 his3-200 ga14Δ ga180Δ LYS2::GALI-HIS3 GAL2-ADE2 met2::GAL7-lacZ pGADC1/E108L-rad51 pGBDUC1/RAD52	This study
MATa trpl-901 leu2-3,112 ura3-52 his3-200 ga14Δ ga180Δ LYS2::GALI-HIS3 GAL2-ADE2 met2::GAL7-lacZ pGADC1 pGBDUC1/RAD51 MATa trpl-901 leu2-3,112 ura3-52 his3-200 ga14Δ ga180Δ LYS2::GALI-HIS3 GAL2-ADE2 met2::GAL7-lacZ pGADC1/RAD51 pGBDUC1 MATa trpl-901 leu2-3,112 ura3-52 his3-200 ga14Δ ga180Δ LYS2::GALI-HIS3 GAL2-ADE2 met2::GAL7-lacZ pGADC1 pGBDUC1/E108L-rad51 MATa trpl-901 leu2-3,112 ura3-52 his3-200 ga14Δ ga180Δ LYS2::GALI-HIS3 GAL2-ADE2 met2::GAL7-lacZ pGADC1/E108L-rad51 pGBDUC1	PMY13	MATa trpl-901 leu2-3,112 ura3-52 his3-200 ga14Δ ga180Δ LYS2::GALI-HIS3 GAL2-ADE2 met2::GAL7-lacZ pGADC1/E108L-rad51 pGBDUC1/RAD54	This study
MATa trpl-901 leu2-3,112 ura3-52 his3-200 ga14Δ ga180Δ LYS2::GALI-HIS3 GAL2-ADE2 met2::GAL7-lacZ pGADC1/R4D51 pGBDUC1 MATa trpl-901 leu2-3,112 ura3-52 his3-200 ga14Δ ga180Δ LYS2::GALI-HIS3 GAL2-ADE2 met2::GAL7-lacZ pGADC1 pGBDUC1/E108L-rad51 MATa trpl-901 leu2-3,112 ura3-52 his3-200 ga14Δ ga180Δ LYS2::GAL1-HIS3 GAL2-ADE2 met2::GAL7-lacZ pGADC1/E108L-rad51 pGBDUC1	PMY4	MATa trpl-901 leu2-3,112 ura3-52 his3-200 ga14Δ ga180Δ LYS2::GALI-HIS3 GAL2-ADE2 met2::GAL7-lacZ pGADC1 pGBDUC1/RAD51	This study
MATa trpl-901 leu2-3,112 ura3-52 his3-200 ga14Δ ga180Δ LYS2::GALI-HIS3 GAL2-ADE2 met2::GAL7-lacZ pGADC1 pGBDUC1/E108L-rad51 MATa trpl-901 leu2-3,112 ura3-52 his3-200 ga14Δ ga180Δ LYS2::GAL1-HIS3 GAL2-ADE2 met2::GAL7-lacZ pGADC1/E108L-rad51 pGBDUC1	PMY7	MATa trpl-901 leu2-3,112 ura3-52 his3-200 ga14Δ ga180Δ LYS2::GALI-HIS3 GAL2-ADE2 met2::GAL7-lacZ pGADC1/RAD51 pGBDUC1	This study
MATa trpl-901 leu2-3,112 ura3-52 his3-200 ga14∆ ga180∆ LYS2::GAL1-HIS3 GAL2-ADE2 met2::GAL7-lac2 pGADC1/E108L-rad51 pGBDUC1	PMY14	MATa trpl-901 leu2-3,112 ura3-52 his3-200 ga14Δ ga180Δ LYS2::GALI-HIS3 GAL2-ADE2 met2::GAL7-lacZ pGADC1 pGBDUC1/E108L-rad51	This study
	PMY11	MATa trpl-901 leu2-3,112 ura3-52 his3-200 ga14Q ga180\ LYS2::GALI-HIS3 GAL2-ADE2 met2::GAL7-lac2 pGADC1/E108L-rad51 pGBDUC1	This study



plate was calculated to determine the percent gene conversion. The assay was performed more than 3 times, and the mean values were plotted using GraphPad Prism.

Chromatin immunoprecipitation. TSY21 and TSY22 were grown in the selective medium to an OD $_{600}$ of 0.3 in the presence of 3% glycerol. Half of the batch of cells was then treated with 3% galactose for 3 h, and other half continued to grow in glycerol medium. The ChIP assay was performed as described earlier (38). One microgram anti-Rad51 antibody was added to the sample to precipitate Rad51-bound DNA fragments. Recruitment of Rad51 was then monitored by PCR with 30 cycles using primer set OSB278/OSB279 in a reaction mixture volume of 50 μ l using the immunoprecipitate and input DNA samples. Samples were subjected to electrophoresis on 2% agarose. For control, ChIP was performed with rabbit IgG antibody. To verify whether a double-stranded break (DSB) was generated by HO digestion in the assay strain, we used OSB289 as a forward primer, which is complementary to the 20 bp upstream of HO cut site (HOcs), and a reverse primer (KanB1) which is complementary to the *KANMX* gene. We amplified full-length *ACT1* using OSB14 and OSB16 as a normalization control.

Western blotting. Western blottin was performed to check Rad51 levels in NRY1, NRY2, and TSY17 strains. Protein samples were loaded on an SDS polyacrylamide gel. A polyvinylidene difluoride (PVDF) membrane was used for the transfer as described earlier (39). The primary antibodies used were mouse anti-Act1 (Abcam), rabbit anti-Rad51 (Santa Cruz), and mouse anti-Hsp82 (Calbiochem) at 1:5,000 dilutions. For subcellular fractionation, we used anti-Pgk1 antibody (Novus Biologicals) and mouse anti-Nsp1 antibody (Abcam) at 1:3,000 and 1:5,000 dilutions, respectively. For secondary antibodies, horseradish peroxide-conjugated anti-rabbit antibody (Promega) and anti-mouse antibody (Santa Cruz Biotechnology Inc., CA, USA) were used at 1:10,000 dilutions. The Western blots were developed using a chemiluminescent detection system (Pierce). Every experiment was repeated at least 3 times, and band intensities were quantified by using Image J software. Mean relative densities were plotted using GraphPad prism.

Protein-protein docking. The protein sequence of Rad51 with entry P25454 and the ATP-dependent molecular chaperone yHsp90 (Hsp82) with entry P02829 of Saccharomyces cerevisiae (strain ATCC 204508/S288c) are publicly available from the central repository of protein sequence and function, UniProt (Universal Protein Resource). The three-dimensional (3D) structures of Rad51 (PDB ID 1SZP) and yHsp90 (PDB ID 2CG9) were retrieved from the RCSB protein data bank. Protein-protein docking was conducted using a fully automated web-based program ClusPro 2.0, which employs an improved fast Fourier transform (FFT)-based rigid docking program PIPER. The program output is a short list of putative complexes ranked according to their clustering properties (18). Biovia Discovery Studio Visualizer is utilized for visualization and analysis of protein complexes. For mutation studies, the sequence of Rad51 protein retrieved from PDB (1SZP ABCDEF) was viewed in the sequence viewer of Biovia Discovery Studio software. The critical amino acids to be mutated were selected in all six chains and replaced. The sulfate ions were removed, and the structure of the protein generated was subjected to clean geometry and energy minimization before using for protein-protein docking. The amino acid Glu108 (E108) was mutated with four different amino acids, namely, leucine (E108L), alanine (E108A), glycine (E108G), and isoleucine (E108I), in chains A, B, C, D, E, and F to generate single mutant hexamers. The mutated Rad51 proteins were again subjected to protein-protein interaction with yHsp90 2CG9A. Protein-protein docking similar to that of the wild type was repeated with the mutant protein against Hsp90 using the online tool ClusPro

Coimmunoprecipitation. Wild-type and E108L-rad51 cells harboring yHsp90 overexpression plasmid (under GPD promoter; 2μ vector) were grown to an ${\rm OD_{600}}$ of 0.5. Ten milliliters of each culture was harvested, resuspended in 1 ml spheroplast buffer (50 mM Tris-HCl [pH 8], 25 mM HEPES [pH 7.4], 0.2% Casamino Acids, 0.2% yeast nitrogen base [YNB], 1% glucose, 18.2% sorbitol) containing dithiothreitol (DTT) and lyticase, and incubated at 30°C for 90 min. Subsequently, glass beads were added and the cells were intermittently vortexed and incubated on ice six times for a period of 30 s each. An anti-Rad51 antibody was added to the supernatant for overnight incubation at 4°C. Protein A agarose (25%; Calbiochem) was added, and the mixture was incubated for 2 h at room temperature. The beads were then spun down for 15 s at 1,000 rpm, and the pellet was washed 3 times with NETNS buffer (20 mM Tris-HCl [pH 8], 1 mM EDTA, 1 M NaCl, 0.5% [vol/vol] NP-40 with protease inhibitor) and twice with NETN buffer (20 mM Tris-HCl [pH 8], 1 mM EDTA, 100 mM NaCl, 0.5% [vol/vol] NP-40 with protease inhibitor). The bound protein was eluted with 4× Laemmli buffer by boiling for 10 min and was further spun down, and the supernatant was collected and used for Western blotting. The proteins in the supernatant were precipitated using 20% trichloroacetic acid, eluted using 4 × SDS loading dye containing dithiothreitol (DTT) and Tris (pH 8.8), and boiled for 10 min. The sample was spun down and the proteins in the supernatant were used for Western blotting. After the coimmunoprecipitation, the relative association of Hsp90 with Rad51 was calculated for each experiment using the following formula: relative association of Hsp90 with Rad51 = (Hsp90 in the pellet/Hsp90 in the input) ÷ (Rad51 in the pellet/Rad51 in the input).

ACKNOWLEDGMENTS

The work was supported by the Council of Scientific and Industrial Research (India), [37(1669)/16/EMR-II] to S.B. T.S. and W.T. were supported by senior research fellowships from the University Grants Commission, India, and N.F. was supported by a junior research fellowship from the Council for Scientific and Industrial Research (CSIR), India. P.M. was supported by an MSc thesis grant, Department of Biotechnology, India.

We declare no conflict of interest.



REFERENCES

- Polo SE, Jackson SP. 2011. Dynamics of DNA damage response proteins at DNA breaks: a focus on protein modifications. Genes Dev 25:409 – 433. https://doi.org/10.1101/gad.2021311.
- Tembe V, Henderson BR. 2007. Protein trafficking in response to DNA damage. Cell Signal 19:1113–1120. https://doi.org/10.1016/j.cellsig.2007 .03.001.
- 3. Reynolds P, Botchway SW, Parker AW, O'Neill P. 2013. Spatiotemporal dynamics of DNA repair proteins following laser microbeam induced DNA damage—when is a DSB not a DSB? Mutat Res 756:14–20. https://doi.org/10.1016/j.mrgentox.2013.05.006.
- Ciccia A, Elledge SJ. 2010. The DNA damage response: making it safe to play with knives. Mol Cell 40:179–204. https://doi.org/10.1016/j.molcel .2010.09.019.
- Xia B, Sheng Q, Nakanishi K, Ohashi A, Wu J, Christ N, Liu X, Jasin M, Couch FJ, Livingston DM. 2006. Control of BRCA2 cellular and clinical functions by a nuclear partner, PALB2. Mol Cell 22:719–729. https://doi .org/10.1016/j.molcel.2006.05.022.
- Sy SMH, Huen MSY, Chen J. 2009. PALB2 is an integral component of the BRCA complex required for homologous recombination repair. Proc Natl Acad Sci U S A 106:7155–7160. https://doi.org/10.1073/pnas .0811159106.
- 7. Zhang F, Ma J, Wu J, Ye L, Cai H, Xia B, Yu X. 2009. PALB2 links BRCA1 and BRCA2 in the DNA-damage response. Curr Biol 19:524–529. https://doi.org/10.1016/j.cub.2009.02.018.
- Zhang F, Fan Q, Ren K, Andreassen PR. 2009. PALB2 functionally connects the breast cancer susceptibility proteins BRCA1 and BRCA2. Mol Cancer Res 7:1110–1118. https://doi.org/10.1158/1541-7786.MCR-09-0123.
- Jensen RB, Carreira A, Kowalczykowski SC. 2010. Purified human BRCA2 stimulates RAD51-mediated recombination. Nature 467:678–683. https://doi.org/10.1038/nature09399.
- Liu J, Doty T, Gibson B, Heyer WD. 2010. Human BRCA2 protein promotes RAD51 filament formation on RPA-covered single-stranded DNA. Nat Struct Mol Biol 17:1260–1262. https://doi.org/10.1038/nsmb.1904.
- Thorslund T, McIlwraith MJ, Compton SA, Lekomtsev S, Petronczki M, Griffith JD, West SC. 2010. The breast cancer tumor suppressor BRCA2 promotes the specific targeting of RAD51 to single-stranded DNA. Nat Struct Mol Biol 17:1263–1265. https://doi.org/10.1038/nsmb.1905.
- 12. Shinohara A, Ogawa T. 1998. Stimulation by Rad52 of yeast Rad51-mediated recombination. Nature 391:404–407. https://doi.org/10.1038/34943.
- Song B, Sung P. 2000. Functional interactions among yeast Rad51 recombinase, Rad52 mediator, and replication protein A in DNA strand exchange. J Biol Chem 275:15895–15904. https://doi.org/10.1074/jbc .M910244199.
- Suhane T, Laskar S, Advani S, Roy N, Varunan S, Bhattacharyya D, Bhattacharyya S, Bhattacharyya MK. 2015. Both charged linker region and ATPase domain of Hsp90 are essential for Rad51-dependent DNA repair. Eukaryot Cell 14:64–77. https://doi.org/10.1128/EC.00159-14.
- Pratt WB, Toft DO. 2003. Regulation of signaling protein function and trafficking by the hsp90/hsp70-based chaperone machinery 1. Exp Biol Med (Maywood) 228:111–133. https://doi.org/10.1177/153537020322800201.
- Cato L, Neeb A, Brown M, Cato AC. 2014. Control of steroid receptor dynamics and function by genomic actions of the cochaperones p23 and Bag-1L. Nucl Recept Signal 12:e005. https://doi.org/10.1621/nrs.12005.
- Jahn M, Rehn A, Pelz B, Hellenkamp B, Richter K, Rief M, Buchner J, Hugel T. 2014. The charged linker of the molecular chaperone Hsp90 modulates domain contacts and biological function. Proc Natl Acad Sci U S A 111:17881–17886. https://doi.org/10.1073/pnas.1414073111.
- Comeau SR, Gatchell DW, Vajda S, Camacho CJ. 2004. ClusPro: a fully automated algorithm for protein–protein docking. Nucleic Acids Res 32:W96–W99. https://doi.org/10.1093/nar/gkh354.
- Kozakov D, Brenke R, Comeau SR, Vajda S. 2006. PIPER: an FFT-based protein docking program with pairwise potentials. Proteins 65:392–406. https://doi.org/10.1002/prot.21117.
- Roy N, Bhattacharyya S, Chakrabarty S, Laskar S, Babu SM, Bhattacharyya MK. 2014. Dominant negative mutant of Plasmodium Rad51 causes reduced parasite burden in host by abrogating DNA double-strand break repair. Mol Microbiol 94:353–366. https://doi.org/10.1111/mmi.12762.
- Agmon N, Pur S, Liefshitz B, Kupiec M. 2009. Analysis of repair mechanism choice during homologous recombination. Nucleic Acids Res 37: 5081–5092. https://doi.org/10.1093/nar/gkp495.

- Khurana N, Laskar S, Bhattacharyya MK, Bhattacharyya S. 2016. Hsp90 induces increased genomic instability toward DNA-damaging agents by tuning down RAD53 transcription. Mol Biol Cell 27:2463–2478. https://doi.org/10.1091/mbc.E15-12-0867.
- 23. Tsuzuki T, Fujii Y, Sakumi K, Tominaga Y, Nakao K, Sekiguchi M, Matsushiro A, Yoshimura Y, Morita T. 1996. Targeted disruption of the Rad51 gene leads to lethality in embryonic mice. Proc Natl Acad Sci U S A 93:6236–6240. https://doi.org/10.1073/pnas.93.13.6236.
- Depienne C, Bouteiller D, Méneret A, Billot S, Groppa S, Klebe S, Charbonnier-Beaupel F, Corvol JC, Saraiva JP, Brueggemann N, Bhatia K, Cincotta M, Brochard V, Flamand-Roze C, Carpentier W, Meunier S, Marie Y, Gaussen M, Stevanin G, Wehrle R, Vidailhet M, Klein C, Dusart I, Brice A, Roze E. 2012. RAD51 haploinsufficiency causes congenital mirror movements in humans. Am J Hum Genet 90:301–307. https://doi.org/10.1016/j.ajhg.2011.12.002.
- Gallea C, Popa T, Hubsch C, Valabregue R, Brochard V, Kundu P, Schmitt B, Bardinet E, Bertasi E, Flamand-Roze C, Alexandre N, Delmaire C, Méneret A, Depienne C, Poupon C, Hertz-Pannier L, Cincotta M, Vidailhet M, Lehericy S, Meunier S, Roze E. 2013. RAD51 deficiency disrupts the corticospinal lateralization of motor control. Brain 136:3333–3346. https://doi.org/10.1093/ brain/awt258.
- Zhang XP, Lee KI, Solinger JA, Kiianitsa K, Heyer WD. 2005. Gly-103 in the N-terminal domain of *Saccharomyces cerevisiae* Rad51 protein is critical for DNA binding. J Biol Chem 280:26303–26311. https://doi.org/10.1074/ ibc.M503244200.
- Fortin GS, Symington LS. 2002. Mutations in yeast Rad51 that partially bypass the requirement for Rad55 and Rad57 in DNA repair by increasing the stability of Rad51-DNA complexes. EMBO J 21:3160–3170. https://doi.org/10.1093/emboj/cdf293.
- Paffett KS, Clikeman JA, Palmer S, Nickoloff JA. 2005. Overexpression of Rad51 inhibits double-strand break-induced homologous recombination but does not affect gene conversion tract lengths. DNA Repair (Amst) 4:687–698. https://doi.org/10.1016/j.dnarep.2005.03.003.
- Donovan JW, Milne GT, Weaver DT. 1994. Homotypic and heterotypic protein associations control Rad51 function in double-strand break repair. Genes Dev 8:2552–2562. https://doi.org/10.1101/gad.8.21.2552.
- Krejci L, Damborsky J, Thomsen B, Duno M, Bendixen C. 2001. Molecular dissection of interactions between Rad51 and members of the recombination-repair group. Mol Cell Biol 21:966–976. https://doi.org/ 10.1128/MCB.21.3.966-976.2001.
- Grbovic OM, Basso AD, Sawai A, Ye Q, Friedlander P, Solit D, Rosen N. 2006. V600E B-Raf requires the Hsp90 chaperone for stability and is degraded in response to Hsp90 inhibitors. Proc Natl Acad Sci U S A 103:57–62. https://doi.org/10.1073/pnas.0609973103.
- Shimamura T, Lowell AM, Engelman JA, Shapiro Gl. 2005. Epidermal growth factor receptors harboring kinase domain mutations associate with the heat shock protein 90 chaperone and are destabilized following exposure to geldanamycins. Cancer Res 65:6401–6408. https://doi.org/ 10.1158/0008-5472.CAN-05-0933.
- 33. Karagöz GE, Rüdiger SG. 2015. Hsp90 interaction with clients. Trends Biochem Sci 40:117–125. https://doi.org/10.1016/j.tibs.2014.12.002.
- 34. Pennisi R, Ascenzi P, di Masi A. 2015. Hsp90: a new player in DNA repair? Biomolecules 5:2589–2618. https://doi.org/10.3390/biom5042589.
- Kekatpure VD, Dannenberg AJ, Subbaramaiah K. 2009. HDAC6 modulates Hsp90 chaperone activity and regulates activation of aryl hydrocarbon receptor signaling. J Biol Chem 284:7436–7445. https://doi.org/10.1074/jbc.M808999200.
- Kovacs JJ, Murphy PJ, Gaillard S, Zhao X, Wu JT, Nicchitta CV, Yoshida M, Toft DO, Pratt WB, Yao TP. 2005. HDAC6 regulates Hsp90 acetylation and chaperone-dependent activation of glucocorticoid receptor. Mol Cell 18:601–607. https://doi.org/10.1016/j.molcel.2005.04.021.
- Robbins N, Leach MD, Cowen LE. 2012. Lysine deacetylases Hda1 and Rpd3 regulate Hsp90 function thereby governing fungal drug resistance. Cell Rep 2:878–888. https://doi.org/10.1016/j.celrep.2012.08.035.
- Laskar S, Sheeba K, Bhattacharyya MK, Nair AS, Dhar P, Bhattacharyya S.
 2015. Heat stress-induced Cup9-dependent transcriptional regulation of SIR2. Mol Cell Biol 35:437–450. https://doi.org/10.1128/MCB.01046-14.
- Laskar S, Bhattacharyya MK, Shankar R, Bhattacharyya S. 2011. HSP90 controls SIR2 mediated gene silencing. PLoS One 6:e23406. https://doi.org/10.1371/journal.pone.0023406.





Hsp90 Is Essential for Chl1-Mediated Chromosome Segregation and Sister Chromatid Cohesion

Nidhi Khurana,a Sayan Bakshi,b Wahida Tabassum,b Mrinal K. Bhattacharyya,b Sunanda Bhattacharyya

^aDepartment of Biotechnology and Bioinformatics, School of Life Sciences, University of Hyderabad, Hvderabad, India

ABSTRACT Recent studies have demonstrated that aberrant sister chromatid cohesion causes genomic instability and hence is responsible for the development of a tumor. The Chl1 (chromosome loss 1) protein (homolog of human ChlRl/DDX11 helicase) plays an essential role in the proper segregation of chromosomes during mitosis. The helicase activity of Chl1 is critical for sister chromatid cohesion. Our study demonstrates that Hsp90 interacts with Chl1 and is necessary for its stability. We observe that the Hsp90 nonfunctional condition (temperature-sensitive iG170Dhsp82 strain at restrictive temperature) induces proteasomal degradation of Chl1. We have mapped the domains of Chl1 and identified that the presence of domains II, III, and IV is essential for efficient interaction with Hsp90. We have demonstrated that Hsp90 inhibitor 17-AAG (17-allylamino-geldenamycin) causes destabilization of Chl1 protein and enhances significant disruption of sister chromatid cohesion, which is comparable to that observed under the $\Delta chl1$ condition. Our study also revealed that 17-AAG treatment causes an increased frequency of chromosome loss to a similar extent as that of the $\Delta chl1$ cells. Hsp90 functional loss has been earlier linked to aneuploidy with very poor mechanistic insight. Our result identifies Chl1 as a novel client of Hsp90, which could be further explored to gain mechanistic insight into aneuploidy.

IMPORTANCE Recently, Hsp90 functional loss has been linked to aneuploidy; however, until now none of the components of sister chromatid cohesion (SCC) have been demonstrated as the putative clients of Hsp90. In this study, we have established that Chl1, the protein which is involved in maintaining sister chromatid cohesion as well as in preventing chromosome loss, is a direct client of Hsp90. Thus, with understanding of the molecular mechanism, how Hsp90 controls the cohesion machinery might reveal new insights which can be exploited further for attenuation of tumorigenesis.

KEYWORDS Chl1, Hsp90, chromosome segregation, sister chromatid cohesion

enome stability is of paramount significance, and the failure to maintain it is lacksquare associated with genetic diseases, abnormal immune responses, and susceptibility to cancer (1). The role of heat shock protein 90 (Hsp90) in maintaining genomic stability is well appreciated, as considerable progress has been made to understand the molecular mechanism that illustrates how Hsp90 inhibition synergizes with the radiation sensitivity of the cancer cell. Molecular insight into varied potential mechanisms through which Hsp90 orchestrates the DNA repair pathway unveils several major proteins of DNA break repair machinery as the clients of Hsp90 (2-5). In lower eukaryotes, it has been demonstrated that Hsp90 function is indispensable for homologous recombination (HR) and the stability of the Rad51 protein, which is a key player in searching for the homologous templates (6). Owing to the ability of Hsp90 to

Received 23 April 2018 Accepted 7 May 2018 **Published** 6 June 2018

Citation Khurana N, Bakshi S, Tabassum W, Bhattacharyya MK, Bhattacharyya S. 2018. Hsp90 is essential for Chl1-mediated chromosome segregation and sister chromatid cohesion. mSphere 3:e00225-18. https://doi .org/10.1128/mSphere.00225-18.

Editor Michael Lorenz, University of Texas Health Science Center

Copyright © 2018 Khurana et al. This is an open-access article distributed under the terms of the Creative Commons Attribution 4.0 International license.

Address correspondence to Sunanda Bhattacharyya, sdeb70@gmail.com.

^bDepartment of Biochemistry, School of Life Sciences, University of Hyderabad, Hyderabad, India



regulate gene expression, one of the previous works has established a link between Hsp90 abundance and genomic instability (7). Following various lines of evidence, Hsp90 has been shown to negatively regulate *RAD53* (DNA damage signaling kinase) transcription and thereby attenuate the DNA damage response pathway (7).

However, genome integrity is measured not only by the capability of the cells to repair broken DNA. A crucial factor which decides the fate of genome integrity is sister chromatid cohesion (SCC). A mutation in the family of genes that controls sister chromatid cohesion can cause various human diseases, and in all these cases, the patients suffer from increased genomic instability (8). Errors in the proper functioning of SCC lead to frequent improper segregation of chromosomes which eventually results in aneuploidy (9). Evidence suggests indirect implications of Hsp90 inhibition for sister chromatid cohesion. It has been found that the Hsp90-Sgt1 chaperone-cochaperone complex modulates the kinetochore assembly by providing stability to the Mis12 complex (10). However, Mis12 is a bona fide kinetochore protein and is not involved in sister chromatid cohesion. A recent study has shown that Hsp90 functional loss is linked to aneuploidy (11), but whether the effect of Hsp90 inhibition on chromosome segregation is because of instability of any component of the SCC machinery has not been studied until now.

A genome-wide screen by Zhao et al. in 2005 has revealed several interactors with Hsp90 (12); however, interaction with Chl1 could not be detected. Interestingly, in another screen with the N-terminal domain of Hsp90, Chl1 protein was found to interact. Earlier, it has been demonstrated that the chl1 mutation induces mitotic chromosome loss and is responsible for increased frequency of spontaneous mitotic recombination (13). Chl1 has been found to function as an establishment factor in the cohesin complex responsible for efficient SCC (14). Its significant role in chromosome segregation is evident from the studies which show that loss of Chl1p leads to reduced retention of cohesin complex subunit (Scc1p) at centromeres, and $\Delta chl1$ mutants lose sister centromere cohesion in both S phase and G₂ phase (15). In mammals, ChIR1 is found to be crucial for embryonic development and in preventing aneuploidy, as it is required for binding of the cohesin complex to the centromere as well as the chromosome arms (16). ChIR1 in humans is unique in its ability to resolve the DNA triplex helix (17) and two-stranded antiparallel G quadruplex DNA (18) and thereby protects the cells from genomic instability. Biallelic mutations in the CHLR1 gene in humans have been associated with the occurrence of the neurological disease termed Warsaw breakage syndrome (WABS) (19). Another family of WABS was identified with a mutation in the Fe-S domain (R263Q) of the chlr1 gene which drastically reduces the DNA-dependent ATP hydrolysis activity of ChIR1, and hence, its helicase activity is significantly impaired (20). ATP binding mutants of both Chl1 (yeast) and ChlR1 (human) have been found to be compromised in their ability to perform the catalytic function in chromosome segregation (19-22). Interestingly, recent studies have claimed that under genotoxic stress conditions, the helicase activity of Chl1 is essential for its recruitment to the replisome but is dispensable for its function in SCC (23). A wide range of functions performed by this protein makes it an important target of study regarding its activity and regulation.

Sister chromatid cohesion is a crucial determinant of genome integrity as it facilitates the accurate flow of genetic material to daughter cells via faithful segregation of chromosomes and thereby provides the homologous template for DNA repair to occur. Among the cohesion establishment factors, Chl1 acts at the interface between DNA repair and sister chromatid cohesion. Its participation in DNA repair was reported in 2006 (24), where $\Delta chl1$ mutants displayed hypersensitivity toward DNA-damaging agents. A study also suggests a more direct role of Chl1 and Ctf4 in homologous recombination (HR) repair, which is not directed via the establishment of SCC (25). ChlR1 depletion leads to the accumulation of DNA damage, and the defects are observed in the repair of DNA double-strand breaks during DNA replication (26).

Keeping in view the role of Hsp90 in the maintenance of genome integrity and the vital role of Chl1 and ChlR1 in efficient DNA repair, we intended to ask whether Hsp90



is essential for Chl1 stability and in mediating chromosome segregation and sister chromatid cohesion. To this end, we have used Saccharomyces cerevisiae as a model organism. We were able to show that Hsp90 and Chl1 physically interact, and using a yeast two-hybrid assay, we have determined the domains of Chl1 which are required for maintaining such interaction. Our study demonstrates that Hsp90 inhibition leads to the degradation of Chl1 and hence causes the abrogation of Chl1-dependent sister chromatid association and alters faithful segregation of chromosomes.

RESULTS Inhibition of Hsp90 function causes destabilization of Chl1 and promotes its proteasomal degradation. In order to understand the role of Hsp90 in Chl1-mediated proper segregation of chromosomes, we first set out to determine whether yeast Hsp90 (yHsp90) is required for Chl1 stability. Yeast has two paralogs of Hsp90: Hsp82, which is the inducible form, and Hsc82, which is the constitutively expressed form. Hence, to figure out the effect of yHsp90 on Chl1p, the steady-state level of Chl1p was studied under single-knockout conditions as $\Delta hsp82$ and $\Delta hsc82$ mutants. Western blot analysis was performed to investigate the steady-state level of Chl1 (Fig. 1A). The quantification of band intensities in Fig. 1B shows that under single-knockout conditions, i.e., $\Delta hsp82$ and $\Delta hsc82$ mutants, the levels of Chl1p remain unaffected. This observation can be attributed to the functional redundancy observed between the two isoforms of Hsc82 and Hsp82. To overcome the obstacle of functional redundancy of Hsp82 and Hsc82, we treated the cells with 40 μ M 17-AAG for 18 h to inactivate both the isoforms. The Western blot analysis of 17-AAG-treated cells is compared with that of the untreated cells, and Fig. 1C shows that Chl1 levels are significantly reduced in treated cells. The quantification of band intensities in Fig. 1D reveals that the steady-state level of Chl1p is reduced by 3-fold under the condition where the yHsp90 function is lost. However, there is no reduction in the CHL1 transcript under such a condition (Fig. 1E). It was earlier established that inhibition of Hsp90 induces proteasomal degradation of the proteins that are Hsp90 clients (27). So, we monitored Chl1 protein level in the presence and absence of proteasome degradation pathway inhibitor MG132 (Fig. 1F). For this experiment, we have used a temperature-sensitive strain, iG170Dhsp82 (28), which is a double knockout for endogenous Hsc82 and Hsp82 and harbors a TS (temperaturesensitive) mutant of hsp82 at the HIS3 gene locus under the noninducible GPD (glyceraldehyde-3-phosphate dehydrogenase) promoter. This copy bears an alteration of glycine to aspartic acid at a conformationally restrictive position which leads to an improper folding of Hsp82 at a high temperature such as 37°C. Consequently, the function of Hsp82 is compromised at 37°C; however, at a lower temperature such as 25°C, the strain behaves as wild type, keeping the Hsp82 function intact. We incubated the strain at 37°C with a potent proteasome inhibitor, MG132, at the concentration of 50 μ M. The protein extract was isolated from the cells growing under three conditions—at 25°C (wild-type condition), 37°C (Hsp90 loss-of-function condition), and 37°C with MG132 supplementation in the medium (proteasome inhibition along with Hsp90 functional loss). Hsp90 level was used as a loading control, because in this strain Hsp90 is expressed from a plasmid under the control of the constitutively expressed GPD promoter. Thus, its level should not change at a different temperature or with MG132 treatment. Upon analyzing the Western blot, we have found that MG132 treatment resulted in the accumulation of Chl1, which supports the idea that the proteasome pathway is involved in regulating basal levels of Chl1 (Fig. 1F). To confirm the efficiency of treatment by MG132, Rad51 (client of Hsp90) levels were monitored under the same conditions, and we observed that Rad51 levels are also accumulated upon MG132 treatment, which accords with our previous finding (6). Taken together, these data suggest that Hsp90 chaperone activity is required to maintain the endogenous level of Chl1 and that inhibition of Hsp90 function induces the proteasomal degradation of Chl1. We did not, however, observe any reduction in the CHL1 transcript in the iG170Dhsp82 strain while it was grown at the restrictive and permissive temperature



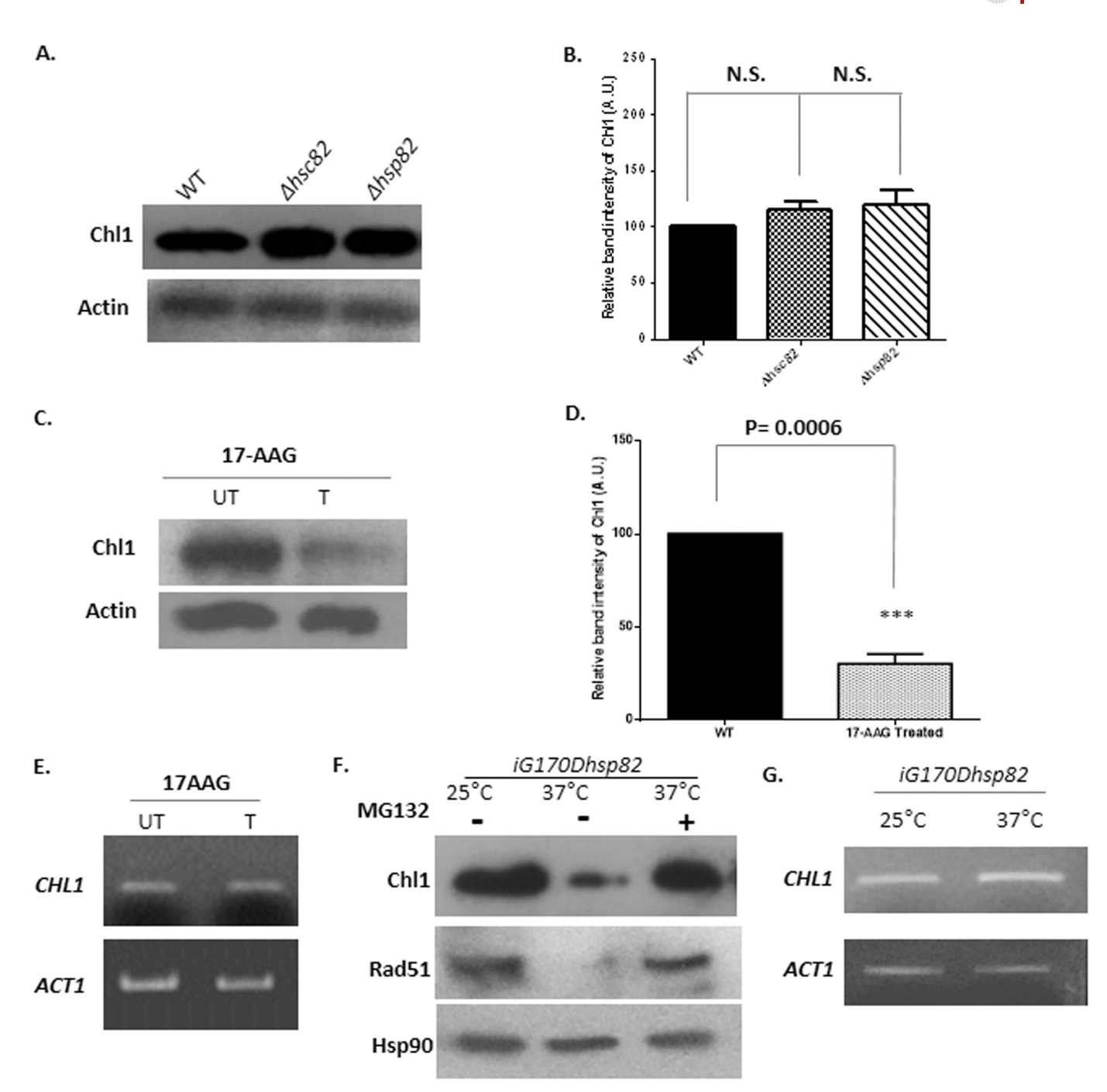


FIG 1 Inhibition of Hsp90 function causes destabilization of Chl1 and promotes its proteasomal degradation. (A) Western blot analysis shows the steady-state levels of Chl1 under single-knockout conditions of either form of yHsp90. Actin acts as a loading control. WT, wild type. (B) Quantification of the band intensities shows that Chl1 level remains unchanged under the conditions mentioned above. The band intensities in each lane are normalized against actin, and mean densities ± SDs are plotted. N.S., not significant. (C) Western blots revealing the effect of 17-AAG on the stability of Chl1 compared to the untreated condition. UT, untreated; T, treated. (D) Quantification of the band intensities from three different experiments displays 3-fold reductions in the level of Chl1 upon loss of function of Hsp90. The band intensities are normalized against actin, and mean densities ± SDs are plotted. (E) Semiquantitative reverse transcription-PCR analysis showing no effect on CHL1 transcript levels under 17-AAG-treated condition normalized against ACTIN. (F) Western blot analysis showing the reaccumulation of Chl1 upon the inhibition of the proteasome degradation pathway when Hsp90 is nonfunctional. The experiment was carried out in a temperature-sensitive strain at permissive and restrictive temperatures. Levels of Hsp90 remain unaffected owing to its regulation under the noninducible GPD promoter. (G) Semiquantitative reverse transcription-PCR analysis showing no effect on CHL1 transcript levels under permissive and restrictive temperatures normalized against ACTIN.

(Fig. 1G). Thus, it suggests that destabilization of Chl1 is likely the major mechanism for Chl1 loss under the Hsp90-inactivated condition.

Hsp90 physically interacts with Chl1. In view of being a client of Hsp90, the protein must physically interact with Hsp90. To study whether Chl1 exhibits physical



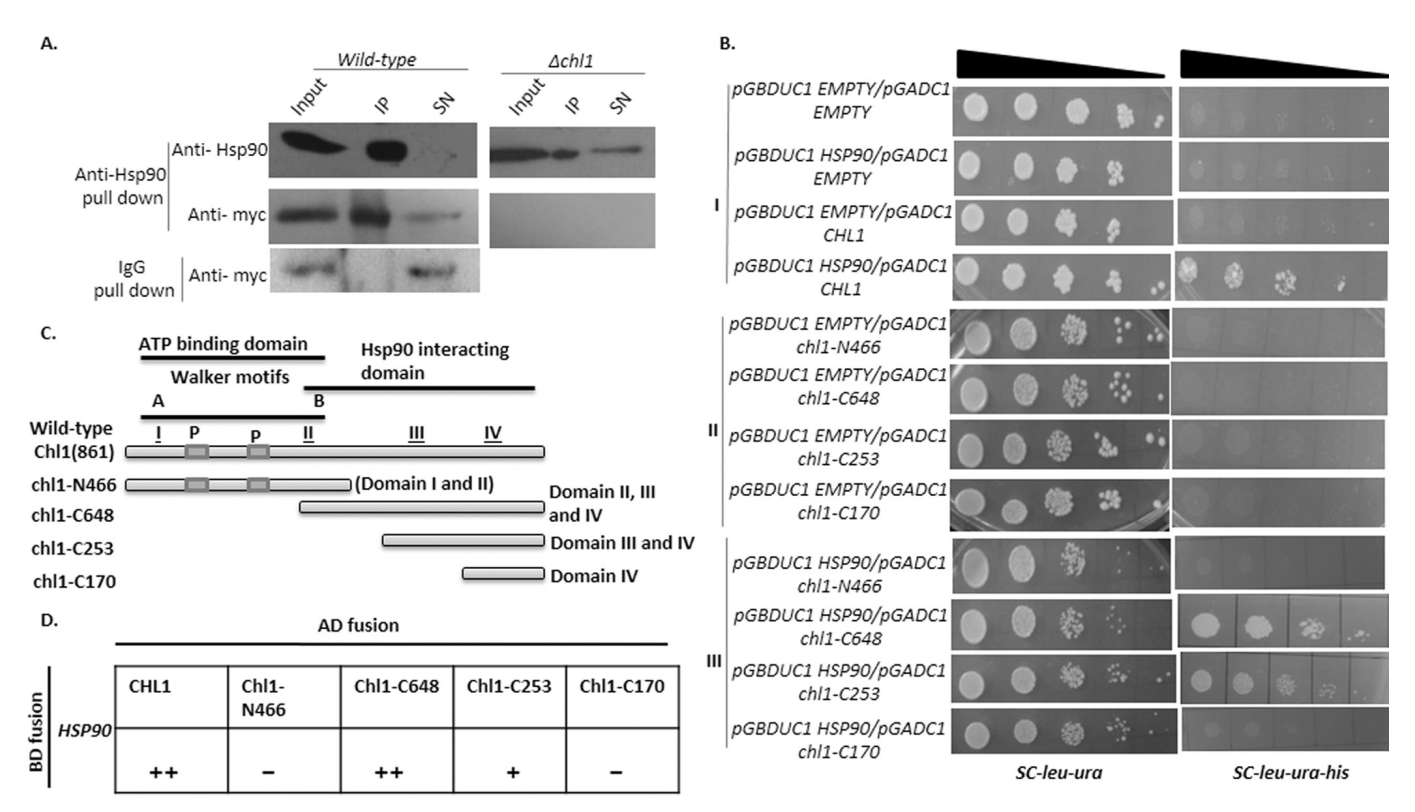


FIG 2 Hsp90 physically interacts with Chl1. (A) Coimmunoprecipitation data showing the interaction of Hsp90 with Chl1. The pulldown assay was performed with anti-Hsp90 antibody as well as with preimmune sera, and the assay mixture was immunoblotted with anti-Myc antibody to probe Chl1. IP, immunoprecipitate; SN, supernatant. (B) The right panels show yeast two-hybrid analysis exhibiting the extent of the interaction between Hsp90 and different constructs of Chl1. To study the protein-protein interaction, equal numbers of cells were serially diluted and spotted on medium lacking uracil, leucine, and histidine. The left panels show various combinations of bait and prey vectors. They show that all the strains are viable under normal conditions. In the right panels, growth is displayed only by the strains harboring Hsp90-bait vector and Chl1-prey vector, which indicates that interaction exists between these proteins. (C) Schematic representation of the domain organization of full-length Chl1 and different truncated versions created for interaction analysis with Hsp90. P, PEST sequences. (D) Interaction evaluated according to growth in triple dropout medium: strong (++), weak (+), or no (-) interaction.

interaction with Hsp90, we performed a coimmunoprecipitation (Co-IP) assay. The result demonstrated that a significant amount of Chl1 protein is associated with Hsp90. However, the control strain lacking Chl1 showed no detectable background, although a significant proportion of Hsp90 was immunoprecipitated from cellular extract (Fig. 2A). The interaction between Hsp90 and Chl1 was further validated using yeast two-hybrid (Y2H) analysis. Full-length CHL1 was cloned into a prey vector (pGADC1), and full-length HSP90 was cloned in a bait vector (pGBDUC1). After transformation of these plasmids into the PJ69-4A strain, the transformants were scored for interaction on synthetic medium plates lacking histidine (for HIS3 reporter gene activity). The results indicate that Chl1 interacts with Hsp90 (Fig. 2B, panel I). To map the domains of Chl1 which are crucial for interaction with Hsp90, we cloned four truncated regions of CHL1 in the pGADC1 vector. The schematic representation is given in Fig. 2C. The first construct comprises the N-terminal 466 amino acids of Chl1 (N-466) (29). This will express domain I (Walker A motif) and domain II (Walker B motif) of the Chl1 protein, which contain its ATP binding domain. Between domain I and domain II, there are two PEST sequences (P1 and P2), the presence of which reduces the stability of a protein. The second construct comprises 648 amino acids of Chl1 (C-648) that express domains II, III, and IV of Chl1 protein. Thus, it lacks the Walker A motif along with two PEST sequences. The third construct contains domain III and domain IV of Chl1. The fourth construct comprises the last 160 amino acids containing the C-terminal domain, which expresses domain IV. We transformed four different constructs of chl1-fused prey vectors to PJ69-4A cells harboring pGBDUC1/HSP90, and they were plated in synthetic medium lacking histidine (Fig. 2B, panel III). We observed substantial interaction when domains II, III, and IV were present. We also found feeble interaction when domains III



and IV were present. However, the presence of domains I and II together was not sufficient to ensure interaction. Similarly, domain IV alone did not show any interaction. The extent of interaction between various truncated forms of Chl1 and Hsp90 is schematically represented (Fig. 2C). From our experiments, it can be concluded that there are several contact points between Chl1 and Hsp90 which span domains II, III, and IV of Chl1. Deletion of any part of this region eliminates the strong interaction between Chl1 and Hsp90.

Inhibition of Hsp90 function exhibits a defect in chromosome segregation to the same extent as that of the chl1 deletion mutant. Chl1 prevents chromosome loss from the cells, and Hsp90 has been associated with the chromosome loss phenotype earlier (11). However, we wanted to determine whether the extent of chromosome loss under the 17-AAG treatment condition is similar to what would occur under the $\Delta chl1$ condition. To that end, we used an assay strain where one nonessential chromosome was inserted which carries a SUP11 gene that suppresses ade2 mutation of the assay strain (30). Retention of the extra chromosome (the 17th chromosome) allows the cell to bypass the ade2 null phenotype, and the cells grow as a white colony. However, the loss of the extra chromosome (the total number of chromosomes is 16) produces a red-pigmented phenotype like that of the $\Delta ade2$ mutant, implying loss of SUP11. This strain was made $\Delta chl1$ to score for the frequency of chromosome loss under such conditions. The PDR5 gene was knocked out to ensure the uptake of 17-AAG. The frequency of first-division chromosome loss was evaluated for this experiment. Figure 3A shows the schematic representation of chromosome loss assay with the possible outcome of the different-color colonies. Figure 3B represents the images of the kinds of colonies obtained under different conditions, i.e., wild-type cells, 17-AAG-treated cells, and $\Delta chl1$ cells. The first two panels show more than or at least 50% red colonies, which implies first-division chromosome loss, and these were the kinds of colonies taken into account. The third and fourth images correspond to the colonies which were excluded from the analysis as they were either a completely red colony or less than 50% red sectored, implying that the chromosome loss happened either before plating or later than first division. Upon analysis, we found that the frequency of first-division chromosome loss obtained for the $\Delta chl1$ and Hsp90 inhibition conditions was 4- and 5-fold higher than the wild type, respectively, but similar to each other (Fig. 3C). Next, we wanted to determine whether the interaction between Chl1 and Hsp90 is crucial for the chromosome segregation function of Chl1. Earlier, it had been demonstrated that the ATP binding site of Chl1 is essential for chromosome segregation (31). However, it is not known whether other domains of Chl1 are required for chromosome segregation. To decipher that, we expressed truncated Chl1 (domain I and II) in the $\Delta chl1$ strain and performed a chromosome loss assay. We generated isogenic positive and negative controls by expressing full-length Chl1 and empty vector in the $\Delta chl1$ strain. Our result shows that the absence of the Hsp90-interacting region of Chl1 causes a 4-fold increase in chromosome loss compared to the full-length Chl1 (Fig. 3D). Thus, the presence of the ATPase domain (domains I and II) alone is not sufficient to prevent chromosome loss. The presence of the entire Hsp90-interacting domain (domains II to IV) is also required.

Inhibition of Hsp90 is associated with a reduction in sister chromatid cohesion. Since the stability of Chl1 depends upon Hsp90, we wanted to investigate whether the loss-of-function mutation of Hsp90 would affect Chl1 function in sister chromatid cohesion. Chl1 is known to promote the loading of Scc2 and cohesion proteins on DNA and thereby plays a critical role in sister chromatid cohesion (32). The strain lacking *chl1* exhibits severe chromosome segregation and cohesion defects (13, 14). We intended to assess sister chromatid dissociation upon Hsp90 inhibition. For this purpose, we used a strain, NKY4, where *TET* operator sites are integrated at the *URA3* location at chromosome V. Expression of red fluorescent protein (RFP)-tagged Tet repressor protein (RFP-TetR) allows the visualization of the sister chromatids. The illustration of the principle behind this assay is shown in Fig. 4A. We have tagged the Myc epitope at the chromosomal locus of *PDS1* so that we can use indirect immunofluorescence to



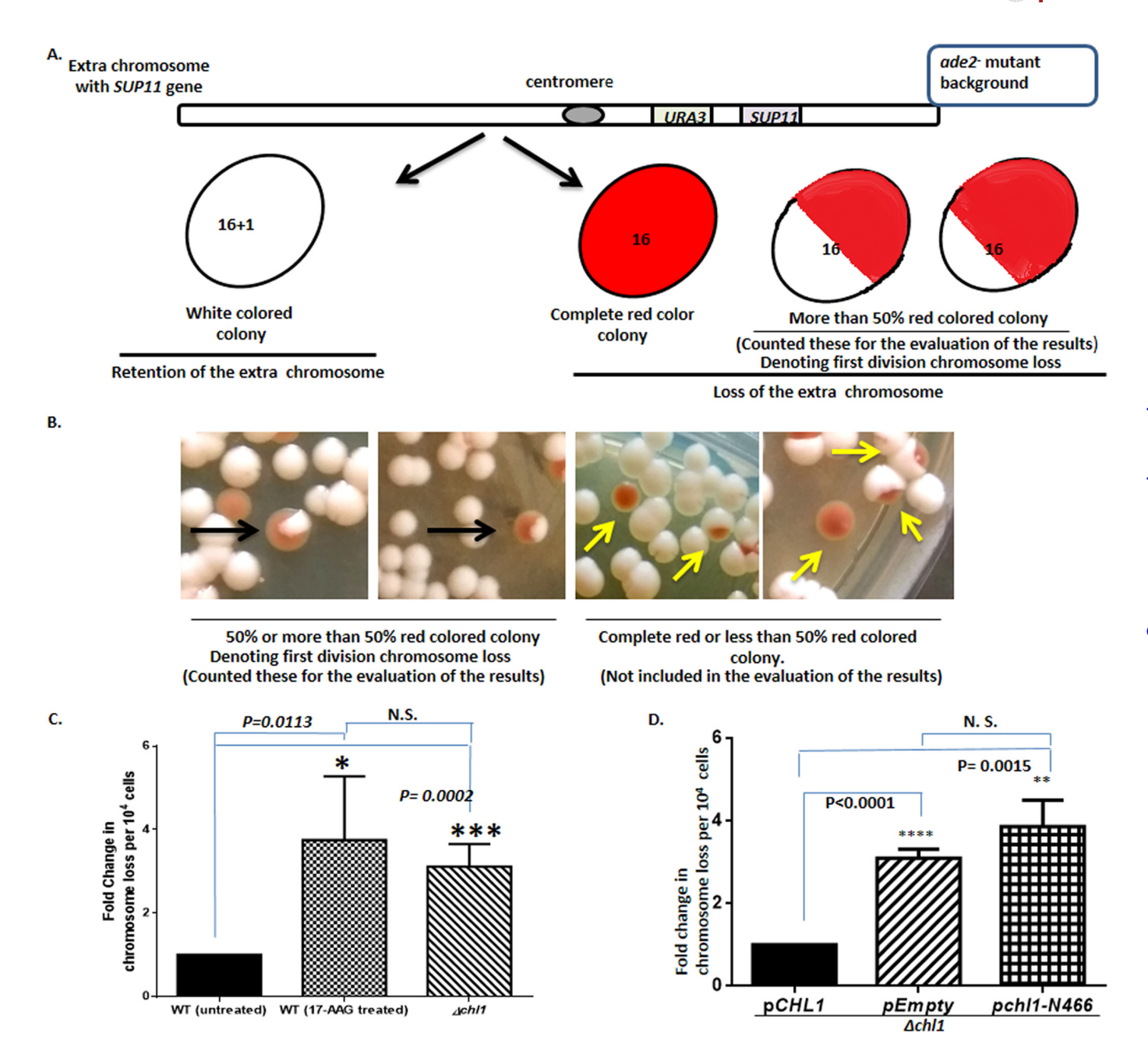


FIG 3 Inhibition of Hsp90 function exhibits a defect in chromosome segregation to the same extent as that of the *chl1* deletion mutant. (A) Schematic representation of the chromosome loss assay, indicating the possible outcome of different-color colonies. (B) Representative images of the colonies obtained. The black arrows indicate the colony with first-division chromosome loss; the yellow arrows show the colonies that are not considered for the analysis, as a fully red colony denotes chromosome loss before plating and a colony less than 50% red denotes chromosome loss later than the first division. (C) Bar graph showing fold change in chromosome loss frequency exhibited by the wild-type strain, Hsp90-inhibited strain, and $\Delta chl1$ strain. (D) Bar graph showing fold changes in chromosome loss frequency exhibited by the null *chl1* strain harboring the truncated Chl1 (N-466) that blocks the interaction with Hsp90. The experiment was done in the presence of an isogenic positive control (null *chl1* strain harboring full-length *CHL1*) and a negative control (the same strain harboring empty plasmid). The number of colonies showing first-division chromosome loss for each condition was obtained from three different sets of experiments. Error bars indicate SDs (n = 3). P values were calculated using the two-tailed Student t test; NS, not significant.

visualize Pds1 expression as a marker for preanaphase cells. We knocked out *chl1* from the assay strain, which was used as the negative control in our assay. To determine the effect of Hsp90 inhibition on sister chromatid cohesion, we treated the assay strain with 17-AAG. In order to achieve maximum uptake of 17-AAG, *PDR5* was knocked out in the assay strain. To assay for the cohesion defect, we used the nocodazole-arrested wild-type strain, the 17-AAG (Hsp90 inhibitor)-treated strain, and the $\Delta chl1$ strain. To verify that cells were arrested at the preanaphase stage, we monitored cell morphology



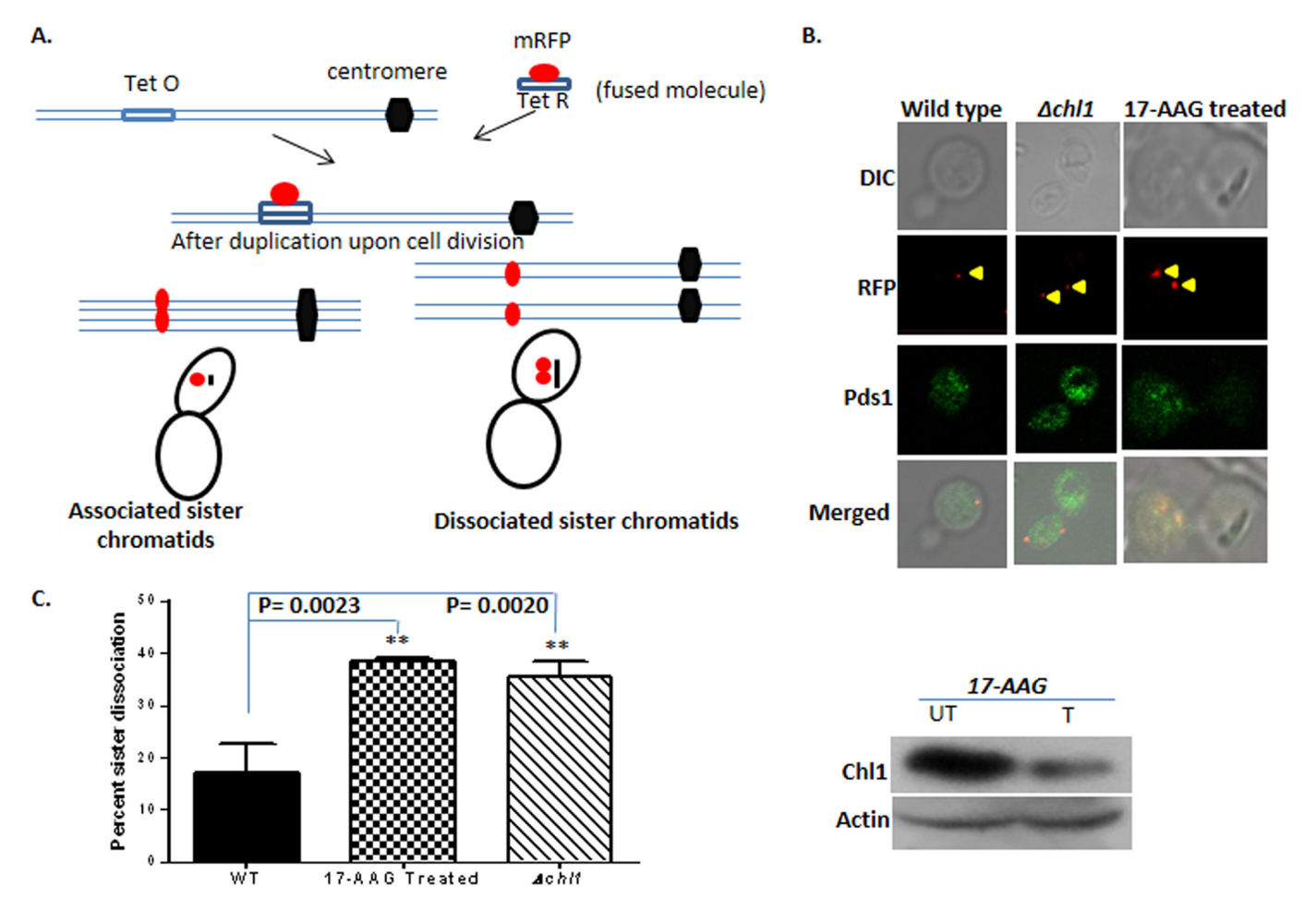


FIG 4 Inhibition of Hsp90 is associated with a reduction in sister chromatid cohesion. (A) Illustration of the principle behind the assay. The mRFP (monomeric red fluorescent protein) molecule fused with the Tet repressor indirectly labels the chromosome, which can be visualized under the confocal microscope. The cells are arrested with nocodazole at preanaphase. After duplication of chromosomes, if the sister chromatids are associated, then that will appear as one red focus, and if they are dissociated, then that will appear as either two distinct foci or one diffused focus. (B) Representative images for different strains (wild type, $\Delta chl1$, and 17-AAG treated) are shown. The top panel shows the cells in bright field. The second panel depicts the associated/dissociated sister chromatids marked by red foci which are indicated by yellow arrowheads in a single cell. The third panel shows the expression of Pds1p as marked by green fluorescence. The bottom panel shows the merged image. DIC, differential interference contrast. (C) Graph showing average percentage of cells displaying dissociated sister chromatids from three different sets of experiments. For each strain, at least 1,000 cells were counted. The error bars represent standard deviations. The Western blot panel at right confirms that Chl1 protein levels are diminished upon Hsp90 inhibition by 17-AAG treatment. UT, untreated; T, treated.

and Pds1 expression. Pds1-positive cells were monitored for RFP-tagged chromosomal loci. The wild-type cells predominantly produced single red dots, indicating that sister chromatids are tightly associated. On the other hand, $\Delta chl1$ cells mostly showed two closely spaced dots, indicating that the sister chromatids are dissociated (Fig. 4B). Our study showed that in wild-type cells only 17% of sister chromatids are dissociated, whereas the $\Delta chl1$ strain showed 35% sister chromatid dissociation. These results strongly corroborate previous reports (14), suggesting that the assay system is reproducible. Once the assay was established, we wanted to investigate the effect of Hsp90 inhibition on sister chromatid cohesion. We observed that 17-AAG treatment causes a significant increase in the amount of sister chromatid dissociation (about 38%) (Fig. 4C), which is comparable to that found in the case of $\Delta chl1$ strains. The accompanying Western blot in this figure confirms that Chl1 is significantly destabilized upon 17-AAG treatment. These data put forward the critical role of Hsp90 in preventing missegregation of chromatids among daughter cells under normal conditions.

DISCUSSION

In recent years, several studies have established the important role of Hsp90 in maintaining genome integrity. Multiple components of DNA double-strand break repair



pathways have been demonstrated to be the direct client of Hsp90 (5). In this work, we have established for the first time that Chl1, one of the major components of sister chromatid cohesion machinery, serves as a bona fide client of Hsp90. Genome-wide yeast hybrid screens identified that the N-terminal domain of yHsp90 (1 to 220 amino acids) interacts with Chl1, but such studies failed to detect any interaction with the full-length Hsp90 (12). Our study demonstrates that the full-length Hsp90 could also associate itself with Chl1. We have also confirmed the physical association between Chl1 and Hsp90 using coimmunoprecipitation. Hsp90 shows a variable degree of association with its clients. Some of the clients like heat shock factor, steroid hormone receptors, Rad51, etc., remain associated with Hsp90 to maintain their functional form. However, Hsp90 kinase clients are primarily associated with Hsp90 through transient interaction, and once chaperoned, they are readily released from Hsp90 as a functional protein. As a result, they are not detectable in coimmunoprecipitation (33). In the case of Chl1, we found that a significant proportion of Chl1 remains associated with Hsp90 as detected in coimmunoprecipitation. This indicates that Chl1 requires continuous association with Hsp90 to main its stability.

The exquisite importance of Chl1 in cohesion establishment came into light when it was shown to play a role in the Eco1-independent cohesion stabilizing pathway. Chl1 and Ctf4 (cohesion establishment factors) contribute to cohesion establishment in a way distinct from the mere cohesin stabilization on the chromosomes (34). This study describes the importance of the contribution of Chl1 in sister chromatid cohesion. Our results for the first time demonstrate that the stability of Chl1 depends on Hsp90 and inhibition of Hsp90 leads to sister chromatid dissociation. We do not rule out the possibility that 17-AAG-mediated increased percent sister chromatid dissociation may occur due to the inactivation of additional clients of Hsp90 in the cohesion family. However, the fact that Hsp90 inhibition also results in a defect in chromosome segregation strongly suggests that Chl1 is one of the main clients of Hsp90 that controls aneuploidy, as the mutation of Chl1 has been shown to produce defects in both chromosome segregation and sister chromatid cohesion. To establish specificity toward Hsp90 inhibition and Chl1 stability, we tried to overexpress Chl1 under the Hsp90-inactivated condition and look for the reversal of phenotype. However, our work showed that the overexpression of Chl1 manifests a dominant negative effect (data not shown). It may be possible that a higher abundance of Chl1 may have detrimental effects on the cell. This may be explained by the presence of two PEST sequences at the amino-terminal domain of Chl1 which destabilize the protein. Our study also shows that the interaction between Hsp90 and Chl1 is essential for Chl1-dependent chromosome segregation. This conclusion is derived from our finding that in cells harboring truncated Chl1, where Hsp90-interacting domains are absent, the chromosome loss frequency is comparable to that of cells devoid of Chl1, and it is enhanced by 4-fold compared to the cells harboring wild-type Chl1. However, we cannot formally rule out the possibility that the truncated version of the Chl1 protein might lack other important but unidentified domains which might be required for Chl1-mediated chromosome segregation.

Earlier studies have shown that CHL1-deficient cells are more sensitive to DNAdamaging agents such as methyl methanesulfonate (MMS) and UV radiation than are the wild-type cells (35). Thus, any condition that destabilizes Chl1 should also reduce cell survivability under DNA-damaging conditions. Previously, we have also observed that the HSP90-inactivated condition causes sensitivity toward DNA-damaging agents in S. cerevisiae (6), and our work established that the important proteins of homologous recombination such as Rad51 and Rad52 are destabilized under such conditions. As the establishment of sister chromatid cohesion is essential for HR, destabilization of Chl1 may also be responsible for inefficient HR and decreased survivability under DNAdamaging conditions. Since Hsp90 may have several clients involved in the DNA repair pathway, we have monitored specialized functions of Chl1 under the Hsp90-inactivated condition. The increased frequency of chromosome loss, as well as increased frequency



of sister chromatid dissociation, pinpoints that Chl1 function is lost specifically under the Hsp90-inhibitory condition.

The deregulated activity of Chl1/ChlR1 has been associated with cancer. The deregulated expression of ChIR1 leads to its amplification in a variety of tumors like melanomas, breast cancer, ovarian cancer, and pancreatic and lung cancer. Our study has important implications for cancer therapy as recent studies have shown that inhibition of sister chromatid cohesion along with anaphase-promoting complex (APC/c) leads to the fetal mitotic arrest in several cancer cell lines (36). Thus, understanding the molecular mechanism of how Hsp90 controls the cohesion machinery might reveal new target molecules within the cohesion family, which can be explored further to understand the molecular mechanism of formation/development of tumors in humans.

MATERIALS AND METHODS

Plasmids. The plasmids used for yeast two-hybrid assays were pGBDUC1 as the bait vector and pGADC1 as the prey vector (37). We have amplified the full-length HSP82 using the primer pairs OSB 21 and OSB 22 and cloned it into the bait vector. Similarly, the full-length CHL1 and truncated versions of chl1 were amplified using the primer pairs OSB 90-OSB 91, OSB 90-OSB 381 (which amplifies bp 1 to 1398 of chl1), OSB 382-OSB 91 (which amplifies bp 640 to 2586 of chl1), OSB 383-OSB 91 (which amplifies bp 1825 to 2586 of chl1), and OSB 384-OSB 91 (which amplifies bp 2074 to 2586 of chl1), generating full-length CHL1, chl1-N466, chl1-C648, chl1-C253, and chl1-C170 (as presented in Fig. 2C), respectively, and cloned into the prev vector. Full-length CHL1 and chl1-N466 were subcloned into 2 u veast expression vector pLA, which expresses CHL1 under the control of the GPD promoter. The C-terminal MYC tagging of CHL1 at the chromosomal locus was done by using pFA6a-13MYC-KANMX and pFA6a-13MYC-TRP vectors (38) as a template. The primers used for MYC tagging of CHL1 and confirmation of the tag were OSB 78, OSB 79, and OSB 80, respectively. The knockout of CHL1 was achieved by using pFA6a-TRP and pFA6a-HIS vectors as the templates and primers OSB 107 and OSB 108 (38). To confirm the generation of the $\Delta chl1$ knockout strain, OSB 109 and OSB 108 were used. To knock out PDR5, the knockout cassette pFA6a-TRP (38) was amplified using the primer pairs OMKB 411 and OMKB 412. The $\Delta pdr5$ knockout strain was confirmed using the primer pair OMB 413 and OSB 290. Another strategy taken up to knock out PDR5 in NKY2 was the amplification of the knockout cassette at the PDR5 locus from the SLY89 strain using the primers OSB 318 and OSB 319. For the amplification of CHL1 cDNA, we have used the OSB 160 and OSB 91 primer pair, and for the amplification of ACTIN cDNA, the primer pair OSB 16 and OSB 14 was used. Sequences of all the primers used in this paper are shown in Table 1.

Yeast strains. The strains used in this study are listed in Table 2. For monitoring the level of Chl1, we incorporated the MYC tag at the C-terminal end of CHL1 in isogenic wild-type, $\Delta hsc82$, and $\Delta hsp82$ strains and in the temperature-sensitive iG170Dhsp82 strain to generate NKY2, NKY39, NKY40, NKY41, and NKY45 strains. To determine the level of Chl1 in the presence of 17-AAG, we knocked out PDR5 from the NKY2 strain to generate NKY43, so that maximum uptake of 17-AAG is ensured. For the sister chromatid cohesion assay, we used NKY4 as a parental strain. To visualize the expression of PDS1 under our assay condition, we MYC tagged PDS1 in NKY4 to generate NKY9. To perform the sister chromatid cohesion assay in the presence of 17-AAG, PDR5 was knocked out in NKY9 to generate NKY61. Also, to perform the same in the absence of CHL1, CHL1 was knocked out from NKY9 to generate NKY62. The parental strain used for chromosome loss assay is YMH58a. CHL1 and PDR5 knockouts were created in this background to generate NKY46 and NKY47, respectively. We have transformed truncated Chl1 (pLAchl1-N466), full-length Chl1, and empty vector individually to the NKY46 strain to create SBY1, SBY2, and SBY3 strains, respectively. To perform yeast two-hybrid analysis, the PJ69-4A strain was employed (37). We have transformed pGBDUC1/HSP82 and pGADC1/CHL1 into the PJ69-4A strain to generate NKY49. The transformants were selected in medium lacking uracil and leucine. In order to check for self-activation of bait and prey fusion products, NKY48, NKY50, and NKY51 were created. To map the domains of Chl1 that are responsible for interaction with Hsp90, we have transformed four truncated chl1-prey vectors, pGADC1chl1-N466, pGADC1chl1-C648, pGADC1chl1-C253, and pGADC1chl1-C170, to the pGBDUC1HSP90containing strain to generate NKY56, NKY57, NKY58, and NKY59, respectively. For checking self-activation of the truncated chl1-prey vectors, NKY52, NKY53, NKY54, and NKY55 strains were generated.

Treatment with inhibitors. For treatment with 17-AAG, the cells were grown until they reached an optical density at 600 nm (OD₆₀₀) of 0.3 at 30°C. Next, we added 17-AAG at the working concentration of 40 μM and cells were allowed to grow overnight. In the case of experiments which required mid-log-phase cells, a secondary inoculum was given the next day in the presence of 17-AAG, and the cells were grown until the required OD₆₀₀ was reached. For treatment with MG132, the NKY45 strain was grown at 37°C overnight in the presence of MG132 at the working concentration of 50 μ M.

Western blotting. For protein extraction, exponentially growing cells of the strains NKY2 and NKY43 were taken. To achieve the functional loss of Hsp82 in NKY45 strains, one batch of cells was grown at 37°C overnight, and the other batch of cells was allowed to grow at 25°C. Equal amounts of cells were finally harvested, and protein was isolated from them by the trichloroacetic acid (TCA) method and subsequently followed for Western blotting (39). The antibodies used were mouse anti-Act1 antibody (Abcam) and mouse anti-Hsp82 antibody (Calbiochem) at 1:5,000 dilutions. Rabbit anti-Myc antibody (Abcam) was used at 1:8,000 dilutions. For secondary antibodies, horseradish peroxide-conjugated



TABLE 1 Primers used in this study

Primer name	Sequence	Purpose
OSB 90	5' CTG TGG ATC CAT GGA CAA AAA GGA ATA TTC 3'	Forward primer used to amplify full-length CHL1
OSB 91	5' CGA TGT CGA CTT AGC GTG AAT TCA GGC TGC 3'	Reverse primer used to amplify full-length CHL1
OSB 78	5' AAC ACG GAA GTT TTT TTC AAT GCG CAG CCT GAA	Forward primer used to generate MYC tag
	TTC ACG CCG GAT CCC CGG GTT AAT TAA 3'	at the C-terminal end of CHL1 at the chromosomal locus
OSB 79	5' ATA TAG TAG TAA TCA CAG TAT ACA CGT AAA CGT	Reverse primer used to generate MYC tag
	ATT CCT TGA ATT CGA GCT CGT TTA AAC 3'	at the C-terminal end of CHL1 at the chromosomal locus
OSB 80	5' CGG CAT GCA AAT GAT TAC GC 3'	Forward primer used to confirm MYC tagging of CHL1
OSB107	5' GTA GAA AAC CAG GCT AAA AAC AGT CAC ACT	Forward primer used for CHL1 knockout
	AGT CCA AAA ACG GAT CCC CGG GTT AAT TAA 3'	
OSB 108	5' ATA TAG TAG TAA TCA CAG TAT ACA CGT AAA CGT	Reverse primer used for CHL1 knockout
	ATT CCT TGA ATT CGA GCT CGT TTA AAC 3'	·
OSB 109	5' CGT AAC CAC AGA GTT GAG GTA G 3'	Forward primer used for CHL1 knockout confirmation
OMKB 411	5' AAG TTT TCG TAT CCG CTC GTT CGA AAG ACT TTA	Forward primer used for <i>PDR5</i> knockout
	GAC AAA ACG GAT CCC CGG GTT AAT TAA 3'	using pFA6a-TRP plasmid
OMKB 412	5' TCT TGG TAA GTT TCT TTT CTT AAC CAA ATT CAA	Reverse primer used for PDR5 knockout
	AAT TCT AGA ATT CGA GCT CGT TTA AAC 3'	using pFA6a-TRP plasmid
OMKB 413	5' AAG TCA CGC AAA GTT GCA AAC 3'	Forward primer used for confirmation of <i>PDR5</i> knockout
OSB 290	5' CCG TAA TCA TTG ACC AGA GCC 3'	Reverse primer used for confirmation
		of <i>PDR5</i> knockout using pFA6a-TRP plasmid
OSB 318	5' CTG TTG AAC GTA ATC TGA GC 3'	Forward primer used for PDR5 knockout from SLY89 strain
OSB 319	5' TTC TCG GAA TTC TTT CGG AC 3'	Reverse primer used for <i>PDR5</i> knockout from SLY89 strain
OSB 160	5' GGA AGA GGA AGC TTC ACG AG 3'	Forward primer used to amplify CHL1 for semiquantitative PCR
OSB 91	5' TTA GCG TGA ATT CAG GCT GC 3'	Reverse primer used to amplify CHL1 for semiquantitative PCR
OSB 16	5' TGA CCA AAC TAC TTA CAA CTC C 3'	Forward primer used to amplify ACT1 for semiquantitative PCR
OSB 14	5' TTA GAA ACA CTT GTG GTG AAC G 3'	Reverse primer used to amplify ACT1 for semiquantitative PCR
OSB 381	5' TAT TTC TTG TCC TAT CTT C 3'	Reverse primer used to amplify N-466 of chl1
OSB 382	5' TCG AGA GAT CCA AAC AAT GGC 3'	Forward primer used to amplify C-648 of chl1
OSB 383	5' TCG TGC AAT CAT GTT ATA CCG 3'	Forward primer used to amplify C-253 of chl1
OSB 384	5' GTG AGG AAA ATA TTC TAT GAA GC 3'	Forward primer used to amplify C-170 of chl1

anti-rabbit antibody (Promega) and anti-mouse antibody (Santa Cruz Biotechnology Inc., CA, USA) were used at 1:10,000 dilutions. The Western blots were developed using a chemiluminescent detection system (Pierce). The bands on the blots were quantified using ImageJ software, and the relative densities thus obtained were plotted using GraphPad Prism 6 software. The mean values from three independent experiments were plotted (± standard deviation [SD]).

RNA isolation and semiquantitative PCR. RNA isolation and cDNA preparation from two batches of NKY1 strains were performed by growing the strain at 25°C and 37°C overnight, respectively. The cells corresponding to an OD_{600} of 10 were harvested, and total RNA was then isolated by using the acid phenol method as described previously (39). The cDNA was synthesized in the same way as depicted in the above reference and then subjected to PCR amplification (27 cycles) with gene-specific primers to score for CHL1 transcription by amplifying 262 bp at the 3' end of the transcript. As a normalization control, the ACT1 transcript was amplified, corresponding to 307 bp.

Co-IP assay. Wild-type and $\Delta chl1$ cells were grown until mid-logarithmic phase in 10 ml medium. We performed the coimmunoprecipitation (Co-IP) assay using the protocol described previously (6). The anti-Hsp82 antibody was used to immunoprecipitate Hsp82. Western blotting was then performed with the immunoprecipitate obtained along with the supernatant and total cellular protein of the cell serving as input. The membrane was probed with anti-Myc antibody to witness the physical interaction between Hsp90 and Chl1. The control antibody used for Co-IP was rabbit IgG.

Yeast two-hybrid analysis. For yeast two-hybrid analysis, HIS3 reporter gene expression was monitored as the readout of protein-protein interactions. The cells were grown to an OD_{600} of 0.5 and then subjected to serial dilutions. The diluted cells were then spotted simultaneously on two plates: one lacking uracil and leucine and the other lacking uracil, leucine, and histidine. Growth on these plates was scored after 5 days of incubation at 30°C. The self-activation was scored for baits in PJ69-4A, and the lack of growth ensured that the bait fusions did not lead to self-activation.

Sister chromatid cohesion assay. The percentage of sister chromatid cohesion was determined by indirect immunofluorescence. The NKY61 and NKY62 strains were grown until reaching an OD₆₀₀ of 0.2 in an appropriate selective medium. Nocodazole was then added at the final concentration of 15 μ g/ml, and the cells were allowed to grow for 1.5 h to 2 h to achieve a high number of budding cells, which was confirmed by observing them under the microscope. After the complete arrest of a maximum number of cells, 10⁷ to 10⁸ cells from each strain were harvested by centrifugation. The spheroplasts were fixed on a slide with poly-L-lysine (Sigma) and incubated with anti-RFP as primary antibody at a dilution of 1:200 (Allied Scientific) overnight at 4°C. This step was followed by washing the slide five times with buffer W.T. (1% nonfat dry milk, 200 mM NaCl, 50 mM HEPES-KOH, pH 7.5, 1 mM NaN₃, 0.1% Tween 20). Incubation with anti-goat-Alexa Fluor 594 (Invitrogen catalog no. A-11032) at 1:200 dilutions was carried out for 90 min in the dark. The samples were then washed with buffer W.T. five times. Slides were covered



TABLE 2 Yeast strains used in this study

Strain	Genotype	Source or reference
W303α	MATα 15ade2-1 ura3-1,112 his3-11 trp1 leu2-3	This study
NKY39	MAT a 15ade2-1 ura3-1,112 his3-11 trp1 leu2-3 VIIL::ADE2 CHL1-13MYC::TRP	This study
NKY40	MATa 15ade2-1 ura3-1,112 his3-11 trp1 leu2-3 VIIL::ADE2 HSC82::KAN CHL1-13MYC::TRP	This study
NKY41	MATa 15ade2-1 ura3-1,112 his3-11 trp1 leu2-3 VIIL::ADE2 HSP82::KAN CHL1-13MYC::TRP	This study
NKY43	MAT α 15ade2-1 ura3-1,112 his3-11 trp1 leu2-3 CHL1-13MYC::TRP Δpdr::loxP-leu2-loxP	This study
VKY2	MATα 15ade2-1 ura3-1,112 his3-11 trp1 leu2-3 CHL1-13MYC::TRP	This study
NKY3	MATα 15ade2-1 ura3-1,112 his3-11 trp1 leu2-3 chl1::TRP	This study
SLY89	Δhsc82::kanMX4Δhsp82::kanMX4/piHGpd-G170Dhsp82-HIS Δpdr::loxP-leu2-loxP	This study
32103	$trp1-289 \ leu2-3,112 \ his3-\Delta 200URA \ 3-52 \ ade2-101\Delta c \ lys2-801 \ am$	Tills Study
NKY45	Δhsc82::kanMX4Δhsp82::kanMX4/piHGpd-G170Dhsp82-HIS Δpdr::loxP-leu2-loxP trp1-289	This study
INICIAS		Tills study
7D 144T-	leu2-3,112 his3-Δ200URA 3-52 ade2-101Δc lys2-801 am CHL1-13MYC::TRP	Gift from Santanu K. Ghosh
7D MAT a	7D MATa SPC29-CFP::KAN mRFP-TETR URA3::TETO	GITT from Santanu K. Gnosr
	GFP-LACI::LEU2 YCPlac112GAL CEN LACO-TRP1	
NKY4	7D MATa SPC29-CFP::KAN mRFP-TETR URA3::TETO GFP-LACI::LEU2 YCPlac112GAL	This study
NKY9	7D MATa SPC29-CFP::KAN mRFP-TETR URA3::TETO	This study
	GFP-LACI::LEU2 YCPlac112GAL PDS1-13MYC::TRP	
NKY61	7D MATa SPC29-CFP::KAN mRFP-TETR URA3::TETO	This study
	GFP-LACI::LEU2 YCPlac112GAL PDS1-13MYC::TRP pdr5::HIS3	
NKY62	7D MATa SPC29-CFP::KAN mRFP-TETR URA3::TETO	This study
	GFP-LACI::LEU2 YCPlac112GAL chl1::HIS3 PDS1-13MYC::TRP	•
YMH58a	MAT a 15ade2-1 ura3-1,112 his3-11 trp1-1 leu2-3 CFIII (CEN3.L.YMH58) URA3 SUP11	Gift from Akash Gunjan
NKY46	MAT a 15ade2-1 ura3-1,112 his3-11 trp1-1 leu2-3 CFIII (CEN3.L.YMH58) URA3 SUP11 chl1::TRP	This study
NKY47	MATa 15ade2-1 ura3-1,112 his3-11 trp1-1 leu2-3 CFIII (CEN3.L.YMH58) URA3 SUP11 pdr5::TRP	This study
SBY1	MATa 15ade2-1 ura3-1,112 his3-11 trp1-1 leu2-3	This study
3011	CFIII (CEN3.L.YMH58) URA3 SUP11 chl1::TRP pLAchl1-N-466	Tills study
CDVa	•	This about
SBY2	MAT a 15ade2-1 ura3-1,112 his3-11 trp1-1 leu2-3	This study
CD\/0	CFIII (CEN3.L.YMH58) URA3 SUP11 chl1::TRP pLACHL1	- 1.
SBY3	MAT a 15ade2-1 ura3-1,112 his3-11 trp1-1 leu2-3	This study
	CFIII (CEN3.L.YMH58) URA3 SUP11 chl1::TRP pLA	
PJ69-4A	MAT $f a$ trpl-901 leu2-3,112 ura3-52 his3-200 ga14 Δ	37
	ga180Δ LYS2:: GAL1-HIS3 GAL2-ADE2 met2::GAL7-lacZ	
NKY48	MATa trpl-901 leu2-3,112 ura3-52 his3-200 ga14∆ ga180∆ LYS2:: GAL1-HIS3 GAL2-ADE2	This study
	met2::GAL7-lacZ pGBDUC1 pGADC1	
NKY49	MAT a trpl-901 leu2-3,112 ura3-52 his3-200 ga14Δ ga180Δ LYS2:: GAL1-HIS3 GAL2-ADE2	This study
	met2::GAL7-lacZ pGBDUC1/HSP82 pGADC1/CHL1	ŕ
NKY50	MAT a trpl-901 leu2-3,112 ura3-52 his3-200 ga14Δ ga180Δ LYS2:: GAL1-HIS3 GAL2-ADE2	This study
	met2::GAL7-lacZ pGBDUC1/HSP82 pGADC1	
NKY51	MAT a trpl-901 leu2-3,112 ura3-52 his3-200 ga14Δ ga180Δ LYS2::GAL1-HIS3 GAL2-ADE2	This study
INICISI	met2::GAL7-lacZ pGBDUC1 pGADC1/CHL1	This study
NKY52	·	This study
INNTOZ	MATa trpl-901 leu2-3,112 ura3-52 his3-200 ga14Δ ga180Δ LYS2:: GAL1-HIS3 GAL2-ADE2	This study
NUC/50	met2::GAL7-lacZ pGBDUC1 pGADC1/chl1-N466	-1
NKY53	MAT a trpl-901 leu2-3,112 ura3-52 his3-200 ga14Δ ga180Δ LYS2:: GAL1-HIS3 GAL2-ADE2	This study
	met2::GAL7-lacZ pGBDUC1 pGADC1/chl1-C648	
NKY54	MAT a trpl-901 leu2-3,112 ura3-52 his3-200 ga14∆ ga180∆ LYS2:: GAL1-HIS3 GAL2-ADE2	This study
	met2::GAL7-lacZ pGBDUC1 pGADC1/chl1-C253	
NKY55	MATa trpl-901 leu2-3,112 ura3-52 his3-200 ga14∆ ga180∆ LYS2:: GAL1-HIS3 GAL2-ADE2	This study
	met2::GAL7-lacZ pGBDUC1 pGADC1/chl1-C170	
NKY56	MATa trpl-901 leu2-3,112 ura3-52 his3-200 ga14Δ ga180Δ LYS2:: GAL1-HIS3 GAL2-ADE2	This study
	met2::GAL7-lacZ pGBDUC1/HSP82 pGADC1/chl1-N466	•
NKY57	MAT a trpl-901 leu2-3,112 ura3-52 his3-200 ga14Δ ga180Δ LYS2:: GAL1-HIS3 GAL2-ADE2	This study
141(13)	met2::GAL7-lacZ pGBDUC1/HSP82 pGADC1/chl1-C648	Tins study
NKY58	MAT a trpl-901 leu2-3,112 ura3-52 his3-200 ga14Δ ga180Δ LYS2:: GAL1-HIS3 GAL2-ADE2	This study
OC L/IVI		This study
NUCYEO	met2::GAL7-lacZ pGBDUC1/HSP82 pGADC1/chl1-C253	This should
NKY59	MATa trpl-901 leu2-3,112 ura3-52 his3-200 ga14Δ ga180Δ LYS2:: GAL1-HIS3 GAL2-ADE2	This study
	met2::GAL7-lacZ pGBDUC1/HSP82 pGADC1/chl1-C170	

with a mounting solution and observed under a confocal fluorescence microscope (Zeiss LSM 510 Meta). The mean values (±SDs) from three independent experiments were plotted using GraphPad Prism 6 software.

Chromosome loss assay. Strains NKY46 and NKY47 were grown overnight in synthetic complete (SC)-Ura medium. Similarly, SBY1, SBY2, and SBY3 were grown in the SC-Ura-Leu medium. The next day, the secondary inoculum was given such that the starting OD_{600} was 0.1. The cells were allowed to grow until reaching an OD₆₀₀ of 0.3 to 0.4. Cells to the number of 10⁴ were then spread from each culture on the yeast extract-peptone-dextrose (YPD) plates. After the colonies were obtained, the plates were kept at 4°C for 5 to 6 days for color development. For determining first-division chromosome loss, only the



sectored colonies showing at least 50% but not 100% red color were taken into account. We calculated the number of at least 50% red colonies in wild-type cells as well as the *chl1* null strain or the 17-AAG treatment condition. Fold change in the chromosome loss frequencies was plotted. The mean values (±SDs) from three independent experiments were plotted using GraphPad Prism 6 software.

ACKNOWLEDGMENTS

The research is funded by the Department of Biotechnology, Government of India (BT/PR5739/BRB/10/1101/2012) to S.B. N.K. is supported by the Senior Research Fellowship from CSIR (Council of Science and Industrial Research), Government of India.

We thank Akash Gunjan, Florida State University, for providing the strain for chromosome loss assay. We also thank Santanu Kumar Ghosh, IIT, Mumbai, for providing the strain for sister chromatid cohesion.

REFERENCES

- Jackson SP, Bartek J. 2009. The DNA-damage response in human biology and disease. Nature 461:1071–1078. https://doi.org/10.1038/ pature 08467
- Dote H, Burgan WE, Camphausen K, Tofilon PJ. 2006. Inhibition of hsp90 compromises the DNA damage response to radiation. Cancer Res 66: 9211–9220. https://doi.org/10.1158/0008-5472.CAN-06-2181.
- Arlander SJ, Eapen AK, Vroman BT, McDonald RJ, Toft DO, Karnitz LM. 2003. Hsp90 inhibition depletes Chk1 and sensitizes tumor cells to replication stress. J Biol Chem 278:52572–52577. https://doi.org/10 .1074/jbc.M309054200.
- Stecklein SR, Kumaraswamy E, Behbod F, Wang W, Chaguturu V, Harlan-Williams LM, Jensen RA. 2012. BRCA1 and HSP90 cooperate in homologous and non-homologous DNA double-strand-break repair and G2/M checkpoint activation. Proc Natl Acad Sci U S A 109:13650–13655. https://doi.org/10.1073/pnas.1203326109.
- Pennisi R, Ascenzi P, di Masi A. 2015. Hsp90: a new player in DNA repair? Biomolecules 5:2589–2618. https://doi.org/10.3390/biom5042589.
- Suhane T, Laskar S, Advani S, Roy N, Varunan S, Bhattacharyya D, Bhattacharyya S, Bhattacharyya MK. 2015. Both charged linker region and ATPase domain of Hsp90 are essential for Rad51 dependent DNA repair. Eukaryot Cell 14:64–77. https://doi.org/10.1128/EC.00159-14.
- Khurana N, Laskar S, Bhattacharyya MK, Bhattacharyya S. 2016. Hsp90 induces increased genomic instability toward DNA-damaging agents by tuning down RAD53 transcription. Mol Biol Cell 27:2463–2478. https:// doi.org/10.1091/mbc.E15-12-0867.
- Mannini L, Menga S, Musio A. 2010. The expanding universe of cohesin functions: a new genome stability caretaker involved in human disease and cancer. Hum Mutat 31:623–630. https://doi.org/10.1002/humu .21252.
- Barbero JL. 2011. Sister chromatid cohesion control and aneuploidy. Cytogenet Genome Res 133:223–233. https://doi.org/10.1159/000323507.
- Davies AE, Kaplan KB. 2010. Hsp90-Sgt1 and Skp1 target human Mis12 complexes to ensure efficient formation of kinetochore-microtubule binding sites. J Cell Biol 189:261–274. https://doi.org/10.1083/jcb.200910036.
- Chen G, Bradford WD, Seidel CW, Li R. 2012. Hsp90 stress potentiates rapid cellular adaptation through induction of aneuploidy. Nature 482: 246–250. https://doi.org/10.1038/nature10795.
- Zhao R, Davey M, Hsu YC, Kaplanek P, Tong A, Parsons AB, Krogan N, Cagney G, Mai D, Greenblatt J, Boone C, Emili A, Houry WA. 2005. Navigating the chaperone network: an integrative map of physical and genetic interactions mediated by the hsp90 chaperone. Cell 120: 715–727. https://doi.org/10.1016/j.cell.2004.12.024.
- Liras P, McCusker J, Mascioli S, Haber JE. 1978. Characterization of a mutation in yeast causing nonrandom chromosome loss during mitosis. Genetics 88:651–671.
- Skibbens RV. 2004. Chl1p, a DNA helicase-like protein in budding yeast, functions in sister-chromatid cohesion. Genetics 166:33–42. https://doi.org/10.1534/genetics.166.1.33.
- Laha S, Das SP, Hajra S, Sanyal K, Sinha P. 2011. Functional characterization of the Saccharomyces cerevisiae protein Chl1 reveals the role of sister chromatid cohesion in the maintenance of spindle length during S-phase arrest. BMC Genet 12:83. https://doi.org/10.1186/1471-2156-12-83.
- Inoue A, Li T, Roby SK, Valentine MB, Inoue M, Boyd K, Kidd VJ, Lahti JM.
 2007. Loss of ChIR1 helicase in mouse causes lethality due to the

- accumulation of aneuploid cells generated by cohesion defects and placental malformation. Cell Cycle 6:1646–1654. https://doi.org/10.4161/cc.6.13.4411.
- Guo M, Hundseth K, Ding H, Vidhyasagar V, Inoue A, Nguyen CH, Zain R, Lee JS, Wu Y. 2015. A distinct triplex DNA unwinding activity of ChlR1 helicase. J Biol Chem 290:5174–5189. https://doi.org/10.1074/jbc.M114 634923
- Wu Y, Sommers JA, Khan I, de Winter JP, Brosh RM. 2012. Biochemical characterization of Warsaw breakage syndrome helicase. J Biol Chem 287:1007–1021. https://doi.org/10.1074/jbc.M111.276022.
- van der Lelij P, Chrzanowska KH, Godthelp BC, Rooimans MA, Oostra AB, Stumm M, Zdzienicka MZ, Joenje H, de Winter JP. 2010. Warsaw breakage syndrome, a cohesinopathy associated with mutations in the XPD helicase family member DDX11/ChlR1. Am J Hum Genet 86:262–266. https://doi.org/10.1016/j.ajhg.2010.01.008.
- Capo-Chichi JM, Bharti SK, Sommers JA, Yammine T, Chouery E, Patry L, Rouleau GA, Samuels ME, Hamdan FF, Michaud JL, Brosh RM, Jr., Mégarbane A, Kibar Z. 2013. Identification and biochemical characterization of a novel mutation in DDX11 causing Warsaw breakage syndrome. Hum Mutat 34:103–107. https://doi.org/10.1002/humu.22226.
- Hirota Y, Lahti JM. 2000. Characterization of the enzymatic activity of hChIR1, a novel human DNA helicase. Nucleic Acids Res 28:917–924. https://doi.org/10.1093/nar/28.4.917.
- 22. Wu Y. 2012. Unwinding and rewinding: double faces of helicase? J Nucleic Acids 2012:140601. https://doi.org/10.1155/2012/140601.
- Samora CP, Saksouk J, Goswami P, Wade BO, Singleton MR, Bates PA, Lengronne A, Costa A, Uhlmann F. 2016. Ctf4 links DNA replication with sister chromatid cohesion establishment by recruiting the Chl1 helicase to the replisome. Mol Cell 63:371–384. https://doi.org/10.1016/j.molcel .2016.05.036.
- 24. Laha S, Das SP, Hajra S, Sau S, Sinha P. 2006. The budding yeast protein Chl1p is required to preserve genome integrity upon DNA damage in S-phase. Nucleic Acids Res 34:5880–5891. https://doi.org/10.1093/nar/gkl749.
- Ogiwara H, Ui A, Lai MS, Enomoto T, Seki M. 2007. Chl1 and Ctf4 are required for damage-induced recombinations. Biochem Biophys Res Commun 354:222–226. https://doi.org/10.1016/j.bbrc.2006.12.185.
- Shah N, Inoue A, Woo Lee S, Beishline K, Lahti JM, Noguchi E. 2013. Roles of ChIR1 DNA helicase in replication recovery from DNA damage. Exp Cell Res 319:2244–2253. https://doi.org/10.1016/j.yexcr.2013.06.005.
- 27. Blagg BS, Kerr TD. 2006. Hsp90 inhibitors: small molecules that transform the Hsp90 protein folding machinery into a catalyst for protein degradation. Med Res Rev 26:310–338. https://doi.org/10.1002/med.20052.
- Nathan DF, Vos MH, Lindquist S. 1997. In vivo functions of the Saccharomyces cerevisiae Hsp90 chaperone. Proc Natl Acad Sci U S A 94: 12949–12956. https://doi.org/10.1073/pnas.94.24.12949.
- Gerring SL, Spencer F, Hieter P. 1990. The CHL1 (CTF1) gene product of Saccharomyces cerevisiae is important for chromosome transmission and normal cell cycle progression in G2/M. EMBO J 9:4347–4358.
- Gunjan A, Verreault A. 2003. A Rad53 kinase-dependent surveillance mechanism that regulates histone protein levels in S. cerevisiae. Cell 115:537–549. https://doi.org/10.1016/S0092-8674(03)00896-1.
- 31. Holloway SL. 2000. *CHL1* is a nuclear protein with an essential ATP binding site that exhibits a size-dependent effect on chromosome seg-



- regation. Nucleic Acids Res 28:3056-3064. https://doi.org/10.1093/nar/ 28.16.3056.
- 32. Rudra S, Skibbens RV. 2013. Chl1 DNA helicase regulates Scc2 deposition specifically during DNA-replication in Saccharomyces cerevisiae. PLoS One 8:e75435. https://doi.org/10.1371/journal.pone.0075435.
- 33. Arlander SJ, Felts SJ, Wagner JM, Stensgard B, Toft DO, Karnitz LM. 2006. Chaperoning checkpoint kinase 1 (Chk1), an Hsp90 client, with purified chaperones. J Biol Chem 281:2989-2998. https://doi.org/10.1074/jbc M508687200.
- 34. Borges V, Smith DJ, Whitehouse I, Uhlmann F. 2013. An Eco1-independent sister chromatid cohesion establishment pathway in S. cerevisiae. Chromosoma 122:121-134. https://doi.org/10.1007/s00412-013-0396-y.
- 35. Das SP, Sinha P. 2005. The budding yeast protein Chl1p has a role in transcriptional silencing, rDNA recombination, and aging. Biochem Biophys Res Commun 337:167-172. https://doi.org/10.1016/j.bbrc.2005.09
- 36. De Lange J, Faramarz A, Oostra AB, de Menezes RX, van der Meulen IH, Rooimans MA, Rockx DA, Brakenhoff RH, van Beusechem VW, King RW, de Winter JP, Wolthuis RM. 2015. Defective sister chromatid cohesion is synthetically lethal with impaired APC/C function. Nat Commun 6:8399. https://doi.org/10.1038/ncomms9399.
- 37. James P, Halladay J, Craig EA. 1996. Genomic libraries and a host strain designed for highly efficient two-hybrid selection in yeast. Genetics 144:1425-1436.
- 38. Longtine MS, McKenzie A, III, Demarini DJ, Shah NG, Wach A, Brachat A, Philippsen P, Pringle JR. 1998. Additional modules for versatile and economical PCR-based gene deletion and modification in Saccharomyces cerevisiae. Yeast 14:953-961. https://doi.org/10.1002/(SICI)1097 -0061(199807)14:10<953::AID-YEA293>3.0.CO;2-U.
- 39. Laskar S, Bhattacharyya MK, Shankar R, Bhattacharyya S. 2011. HSP90 controls SIR2 mediated gene silencing. PLoS One 6:e23406. https://doi .org/10.1371/journal.pone.0023406.

Cite This: Org. Lett. 2019, 21, 9040-9044

Benzimidazolinone-Free Peptide o-Aminoanilides for Chemical **Protein Synthesis**

Jamsad Mannuthodikayil, †, § Sameer Singh, †, § Anamika Biswas, † Abhisek Kar, † Wahida Tabassum, ‡, § Pratap Vydyam,^{‡,§} Mrinal Kanti Bhattacharyya,[‡] and Kalyaneswar Mandal^{*,†}®

[†]TIFR Centre for Interdisciplinary Sciences, Tata Institute of Fundamental Research Hyderabad, 36/p Gopanpally, Hyderabad, Telangana 500107, India

[‡]Department of Biochemistry, School of Life Sciences, University of Hyderabad, Gachibowli, Hyderabad, Telangana 500046, India

Supporting Information

ABSTRACT: The thioester surrogate 3,4-diaminobenzoic acid (Dbz) facilitates the efficient synthesis of peptide thioesters by Fmoc chemistry solid phase peptide synthesis and the optional attachment of a solubility tag at the C-terminus. The protection of the partially deactivated orthoamine of Dbz is necessary to obtain contamination-free peptide synthesis. The reported carbamate protecting groups promote a serious side reaction, benzimidazolinone formation. Herein we introduce the Boc-protected Dbz that prevents the benzimidazolinone formation, leading to clean peptide o-aminoanilides suitable for the total chemical synthesis of proteins.

Native chemical ligation (NCL) is a well-established protocol for the condensation of unprotected peptide segments in aqueous media. 1 NCL has been routinely used for the total synthesis of a wide variety of protein molecules over the past two and half decades.² In recent times, membraneassociated proteins have also become frequent targets for total chemical protein synthesis using NCL. The NCL polypeptide condensation reaction requires effective syntheses, handling, purification, and characterization of peptide thioester segments. Among the several methods reported to date,³ the two most common strategies used to prepare the peptide thioester surrogate by Fmoc chemistry solid phase peptide synthesis (SPPS) involve the utilization of a 3,4-diaminobenzoic acid (Dbz) (1, Figure 1A) derivative (Dawson linker)^{3a} and a hydrazide^{3b} linker, respectively. Both of these linkers can be converted to a peptide thioester by NaNO2-mediated oxidation under aqueous conditions. 3b,c

The majority of the functional proteins contain a hydrophobic patch in their polypeptide sequence. Hydrophobic peptide segments are sometimes difficult to purify, even after their successful synthesis using advanced SPPS methods, mainly due to their restricted solubility in the solvent systems generally used for purification by high-performance liquid chromatography (HPLC). The limited solubility of such peptides in ligation buffer can also contribute to difficulty in the NCL reaction. This poor solubility can be overcome by adding a "solubility tag", consisting of multiple Arg residues, at the C-terminus of the thioester or thioester surrogate peptide. 5,3c The polyarginine "solubility tag" assists peptide purification and enhances peptide solubility in aqueous buffer in NCL reaction but does not end up in the ligation product. The hydrazide linker, however, does not allow the incorporation of a solubility tag at the peptide C-terminus. Therefore, the use of a Dbz linker is the method of choice for attaching a polyarginine tag when making peptide o-aminoanilides as a thioester surrogate.3c

One of the difficulties in making peptide o-aminoanilides as thioester surrogates is the overacylation of the deactivated ortho-amine group of the Dbz linker. Substantial research efforts by several research groups around the world have been devoted to circumventing the overacylation issue (Figure 1A). These include the utilization of 4-amino-3-nitrobenzoic acid (2; Figure 1A) as an alternative thioester surrogate, 6a and the orthogonal carbamate protection of the deactivated amine group of Dbz by Alloc (3; Figure 1A), 6b Proc (4; Figure 1A), 6c or 2-ClZ (5; Figure 1A, designed specifically for Boc chemistry SPPS).6d However, these strategies suffered from either racemization at the C-terminal residue, restricting the applicability to the synthesis of peptides having a Gly residue only at the C-terminus, 6a or the need for an additional step, as in case of Alloc or Proc, that involves palladium catalyst treatment^{6b,c} for the removal of the protecting groups.

Nowadays, high-temperature Fmoc SPPS is very common. It is widely believed that peptide synthesis at an elevated temperature results in more efficient chain assembly by Fmoc chemistry SPPS. However, for the synthesis of peptide

Received: September 28, 2019 Published: October 30, 2019

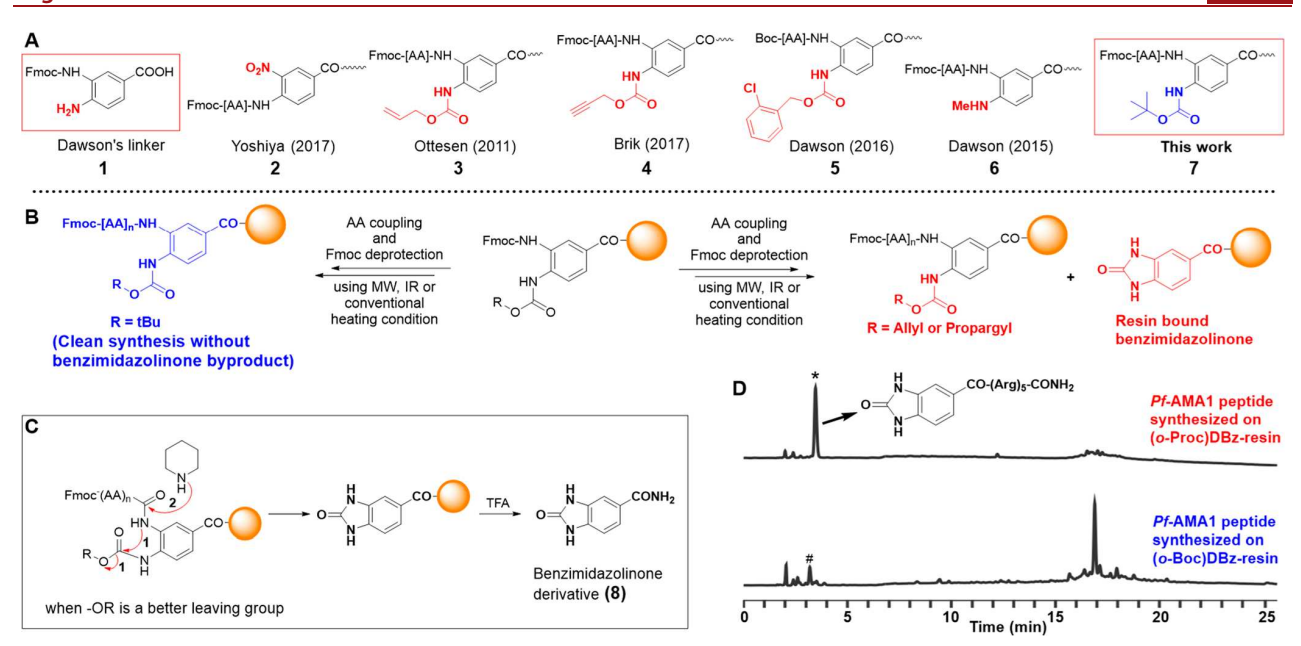


Figure 1. (A) Various 3,4-diaminobenzoic acid derivatives used as thioester surrogates over the years. (B) Benzimidazolinone byproduct (8) observed during Fmoc chemistry SPPS at elevated temperature when Alloc- or Proc-protected Dbz was used. The (*o*-Boc)Dbz linker gives clean synthesis without any peptide chain loss or benzimidazolinone formation. (C) Possible mechanism of the formation of 8.^{6a} Step 1: Peptide benzimidazolinone forms under basic conditions. Step 2: Nucleophilic attack by piperidine results in chain loss. (D) HPLC chromatogram of the crude Pf-AMA1(Cys149–Phe183) peptide having an (Arg)₅ tag at the C-terminus synthesized on Proc-protected Dbz-resin (top) and Boc-protected Dbz-resin (bottom). * indicates the benzimidazolinone-Arg₅-CONH₂ byproduct. # indicates the acetylated Dbz-Arg₅-CONH₂ obtained from the acetylation in the capping step after first residue coupling on (*o*-Boc)Dbz.

o-aminoanilides at elevated temperatures, a serious drawback of both Alloc and Proc protection has been the formation of a significant amount of benzimidazolinone byproduct (8; Figure 1B,C) in every Fmoc deprotection step during Fmoc chemistry SPPS. ^{6a,g} Interestingly, the most efficient strategy to date to prevent overacylation was reported by Dawson's group by the methylation of the deactivated amine of the DBz linker (MeDBz, 6; Figure 1A) that delivered a benzimidazolinone-free peptide using Fmoc deprotection even at 90 °C under microwave irradiation conditions. ^{6e} However, MeDbz is resistant to NaNO₂-mediated oxidation. Hence, on-resin activation was obligatory for the peptides synthesized using the MeDBz linker.

Here we sought to introduce the tert-butyloxycarbonyl (Boc) group as a very simple, acid-labile, and efficient protecting group for the deactivated amine of Dbz. The Boc group has several advantages. It can be introduced easily by either on-resin or off-resin treatment of Fmoc-Dbz with Bocanhydride in 20% water in dimethylformamide (DMF). Unlike Proc or Alloc, the Boc group can be removed by trifluoroacetic acid (TFA) during the global deprotection of the peptide from resin without the need for an additional step. Boc deprotection also avoids the usage of a Pd catalyst, thus preventing the possibility of the contamination of chemically synthesized peptides with toxic heavy-metal impurities. Most importantly, being a poor leaving group, the sterically crowded tert-butyloxy group abrogates acylbenzimidazolinone formation during Fmoc chemistry SPPS under heating conditions, preventing undesired peptide chain loss during every Fmoc deprotection cycle and improving the purity and yield of the peptides.

The protection of the deactivated *ortho*-amine group of Dbz with a Boc group was readily performed either in solution or on a solid support. Solution phase synthesis of the building

block Fmoc-(o-Boc)Dbz-OH was straightforward (Scheme 1A; Supporting Information (SI) Section 2.2). The Boc protection of Fmoc-Dbz-OH with (Boc)₂O in the presence of 20% water in DMF furnished Fmoc-(o-Boc)Dbz-OH with quantitative conversion (based on the UV intensity in the RP-HPLC chromatogram). The presence of a polar protic solvent (in this case, 20% water) in the reaction mixture has been found to reduce the unwanted side products drastically. The Fmoc-(o-Boc)Dbz-OH was then successfully coupled to the Rink Amide aminomethyl resin and used for further peptide chain assembly. We have also shown that the Boc protection can be carried out using the same reaction conditions on a solid support, if preferred (Scheme 1B, SI Section 2.5). However, because of the difficulty associated with the on-resin monitoring of Boc protection (see SI Section 2.5), we recommend using the solution phase synthesis of Fmoc-(o-Boc)Dbz-OH.

 $^a({\rm A})$ Off-resin chemical synthesis and coupling of Fmoc-(o-Boc)Dbz linker on to the resin. (B) On-resin Boc protection of Fmoc-Dbz-resin. (C) Solution-phase coupling of Fmoc-Arg(Pbf)-COOH on Dbz, followed by Boc protection.

Boc protection of one of the amines was expected to reduce the reactivity of the remaining amine on (o-Boc)Dbz after Fmoc deprotection. Therefore, it was imperative to check the efficiency of the first amino acid coupling on the Boc-protected Dbz linker. We selected 10 representative amino acids to study the coupling efficiency onto (o-Boc)Dbz-resin (Table S1; see SI Section 3.1) using high-temperature coupling conditions. DIC/Oxyma (0.1 equiv N,N-diisopropylethylamine (DIEA)) activation with 0.5 M amino acid provided near-quantitative conversion for most of the amino acids in a single coupling cycle at 75 °C (Figure S5). To avoid racemization, His and Cys were coupled at room temperature (Figure S6). Attempts to couple Fmoc-Arg(Pbf)-OH at 75 °C gave very poor (<20%) conversion. It is well known that during the activation and coupling step, the nucleophilic side chain of arginine is susceptible to δ -lactam formation. 8a This side reaction is known to be favored at elevated temperatures^{8b} and effectively reduces the activated arginine concentration during hightemperature coupling. In contrast, room-temperature coupling of arginine does not lead to significant δ -lactam formation because the rate of coupling to form a peptide bond would be higher than the δ -lactam formation. DIC/Oxyma (0.1 equiv DIEA) activation with 0.5 M Fmoc-Arg(Pbf)-OH at roomtemperature triple coupling resulted in ~90% conversion

To avoid multiple coupling cycles for Arg residues on-resin, we preferred the coupling of a preformed Fmoc-Arg(Pbf)Dbz(o-Boc)-OH. We prepared the Fmoc-Arg(Pbf)Dbz(o-Boc)-OH in only two simple steps by coupling Fmoc-Arg(Pbf)-OH to commercially available DBz, followed by the protection of the deactivated amine by a Boc group using the same protocol as previously discussed (Scheme 1C; SI Section 3.2). Thus our result represents an opportunity to choose either an on-resin or an off-resin route for the efficient coupling of any amino acid on the Boc-protected Dbz linker.

To demonstrate the feasibility of the synthesis of a large peptide segment on Fmoc-(o-Boc)Dbz-(Arg(Pbf))5-Rink-Amide aminomethyl resin, we carried out the synthesis of a 35-residue hydrophobic peptide segment, (Cys149-Phe183), associated with Plasmodium falciparum protein apical membrane antigen 1 (Pf-AMA1 (3D7 strain)), with a poly-Arg tag at the C-terminus, which had defied our repeated synthesis attempts with a Proc-protected Dbz derivative under heating conditions. The high-temperature peptide chain assembly (coupling at 60 $^{\circ}\text{C}$ and Fmoc deprotection at 50 $^{\circ}\text{C})$ on Fmoc-(o-Proc)Dbz-(Arg(Pbf))₅-Rink-Amide aminomethyl resin resulted in significant peptide chain loss during every Fmoc deprotection cycle, leaving virtually no desired target peptide (o-Proc)aminoanilide (Figure 1D, top). The mechanism of the peptide chain loss most likely involves the formation of peptide-benzimidazolinone in basic medium under thermal conditions and the subsequent cleavage of the peptide-benzimidazolinone by the nucleophilic attack of piperidine used for Fmoc deprotection (Figure 1C). 6a,g The formation of benzimidazolinone is reminiscent of the aspartimide formation often observed during Fmoc chemistry SPPS. Because of the very early retention time shift in the standard HPLC gradient, the byproduct 8 usually remains unnoticed and is frequently ignored. In contrast, peptide synthesis at an elevated temperature using Fmoc-(o-Boc)Dbz-(Arg(Pbf))₅-Rink-Amide aminomethyl resin produced a clean synthesis of the crude peptide without the formation of "branched" byproducts and benzimidazolinone derivatives,

demonstrating the extremely high thermal stability of the Boc group compared with the Proc group (Figure 1D, bottom; see SI Section 4).

Finally, we demonstrated the general utility of Fmoc-(o-Boc)Dbz chemistry by the total chemical synthesis of two proteins, ubiquitin and the extra cellular domain of the membrane protein "rhoptry neck protein 2" (RON2), a key protein associated with the human red blood cell invasion by malaria parasites.

Ubiquitin is an important protein marker that is covalently conjugated with other proteins and modulates their biochemical properties, triggering unique cellular functions, such as proteasomal degradation, the regulation of the chromatin structure, and protein localization. Several researchers have chemically synthesized the ubiquitin protein to investigate its biochemical and biophysical properties. The nonaromatic hydrophobic cluster located at the N-terminus of ubiquitin makes the segment spanning the first two beta strands sparingly soluble in aqueous solvent and may require a solubility tag for the easy handling and purification; hence we selected ubiquitin as a suitable protein target to demonstrate the applicability of Fmoc-(o-Boc)Dbz-linker.

Human ubiquitin contains a 76-residue polypeptide chain having no cysteines (Figure 2A). We prepared ubiquitin from three unprotected peptide segments using two consecutive N-to-C ligation reactions, followed by desulfurization (Figure 2B). We synthesized the N-terminal hydrophobic peptide segment, Met1-Lys27-Dbz-(Arg)₄-CONH₂ (12), with a poly-

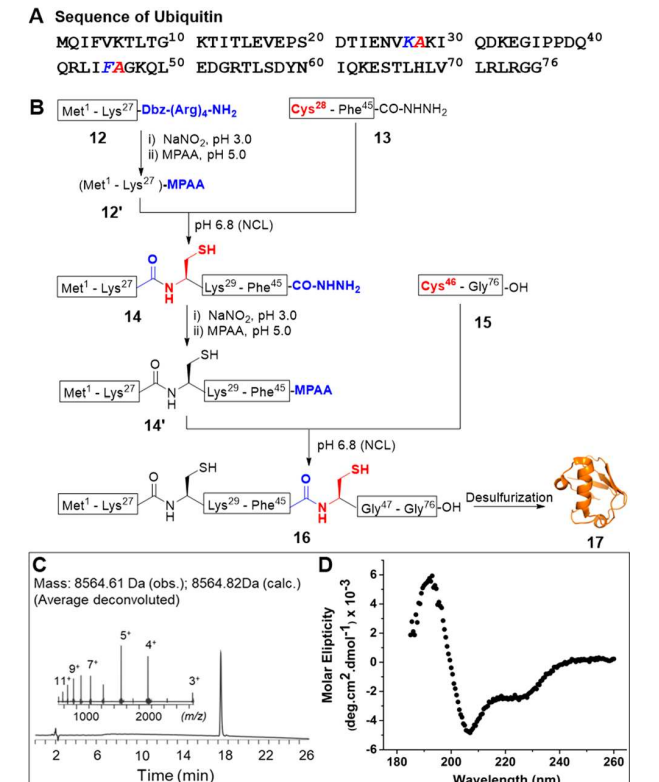


Figure 2. Total chemical synthesis of ubiquitin. (A) Sequence and (B) synthetic strategy. The cartoon representation of 17 was taken from PDB ID 1YIW. (C) LC–MS data of purified ubiquitin and (D) CD of the folded ubiquitin.

Arg tag at the C-terminus on Fmoc-(o-Boc)Dbz-(Arg(Pbf))₄-Rink-Amide aminomethyl resin with excellent crude purity (Figure S16). As described in the synthetic strategy, the Nterminal peptide segment was first activated at low temperature with NaNO2 (20 mM) and thioesterified with 4-mercaptophenylacetic acid (MPAA) (100 mM), giving the peptide- C^{α} -MPAA-thioester (12'), which upon reaction with the second segment Cys28-Phe45-CONHNH₂ (13) at pH 6.8 gave the NCL product Met1-Phe45-CONHNH₂ (14) within 15 h. The purified polypeptide 14 (64% based on the limiting peptide 12) was then further activated by NaNO2 and exchanged with MPAA to give peptide C^{α} -MPAA-thioester (14'). The Cterminus segment Cys1-Gly76 (15) was then added, and the pH was adjusted to 6.8. Within 3 h, the NCL was complete, furnishing the target full-length polypeptide Met1-Gly76 (16) in 79.4% isolated yield (based on the limiting peptide 14).

The radical mediated desulfurization ¹⁰ of **16** in the presence of VA044 (100 mM), 150 mM tris(2-carboxyethyl)phosphine (TCEP), and MESNa (75 mM) at 42 °C produced the native ubiquitin polypeptide. The purified ubiquitin had the desired mass (Figure 2C) and was obtained in very good yield (5.5 mg, 60% based on **16**). Circular dichroism (CD) data in phosphate buffer revealed the presence of the characteristic secondary structural elements of the folded ubiquitin protein molecule (Figure 2D).

As a part of our ongoing research using phage display to design protein inhibitors to interfere with the *P. falciparum* parasite invasion of human red blood cells, we undertook the total chemical synthesis of a biotinylated analogue of the membrane-associated extracellular domain of the parasite protein rhoptry neck protein 2 (here designated as *Pf*-RON2ed). We selected RON2ed as our target protein because the sequence is highly conserved among all of the available strains of *P. falciparum*. The sequence of *Pf*-RON2ed is shown in Figure 3A. We attached a biotin tag at the N-terminus, keeping a 38-atom spacer and a Gly residue to facilitate the immobilization of the target protein for phage screening in the future. The chemical structure of the biotin tag is shown in Figure 3B.

We synthesized *Pf*-RON2ed by the NCL of two unprotected peptide segments, followed by folding under air oxidation conditions, as shown in the synthetic strategy (Figure 3C). Because the N-terminus segment was found to be poorly soluble in aqueous solvents, we synthesized the N-terminus segment with an Arg₄ tag attached at the C-terminus preceding the (o-Boc)Dbz linker. The Arg₄-tagged peptide was obtained in very high crude purity, as evidenced from the chromatogram shown in Figure S24. The low-temperature activation of the purified N-terminal segment 19 by NaNO2 at pH 3.0, followed by MPAA exchange gave the corresponding thioester 19', which upon reaction with the Cys peptide 20 at pH 6.8 furnished the desired biotin-tagged full-length polypeptide 21 in 35% yield. The purified full-length polypeptide was then folded under air oxidation conditions with the concomitant formation of the disulfide bond. The folded and purified protein had a mass of 4949.4 Da (Figure 3D). The chemically synthesized biotin-tagged RON2ed inhibited the growth of the P. falciparum (3D7) parasite in the growth inhibition activity (GIA) assay in vitro (Figure 3E).

In summary, we have demonstrated the use of the Boc group as a very simple and efficient protection strategy for the deactivated *ortho*-amine of the Dbz thioester equivalent used in Fmoc chemistry SPPS. The Boc-proteced Dbz derivative, A Sequence of extracellular domain of *P. falciparum* membrane protein RON2

DITQQAKDIG²⁰³⁰ AGPVA*SC*TTT²⁰⁴⁰ RMSPPQQICL²⁰⁵⁰ NSVVNTALS²⁰⁵⁹

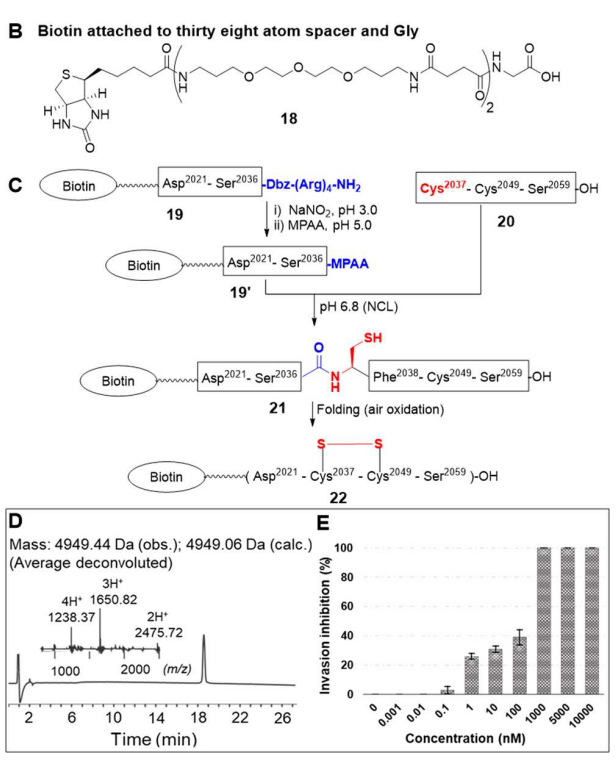


Figure 3. Total chemical synthesis of the biotinylated analogue of the extracellular domain of *Pf*-RON2. (A) Sequence, (B) chemical structure of the biotin tag with spacer, (C) synthetic strategy, (D) LC–MS data of the purified chemically synthesized biotinylated ectodomain of RON2, and (E) in vitro parasite growth inhibition activity (GIA) of the chemically synthesized biotinylated analogue of the extracellular domain of *Pf*-RON2 protein (3D7 strain).

Fmoc-(o-Boc)Dbz-OH, can be utilized as an effective linker for attaching a solubility tag at the C-terminus when synthesizing peptide o-aminoanilides as thioester surrogates using Fmoc chemistry SPPS under heating conditions. The protection of the Fmoc-Dbz ortho-amine by the Boc group has been found to be superior to other reported protecting groups, such as Alloc and Proc. Boc protection precludes the possibility of the formation of an undesired benzimidazolinone byproduct under standard high-temperature Fmoc chemistry SPPS. The Boc group removal does not need any additional step and is removed using TFA during the global deprotection of the peptide. Boc deprotection also avoids the usage of toxic heavymetal catalysts frequently used for Alloc or Proc group removal. Therefore, we believe that the (o-Boc)Dbz linker will find many applications in the field of chemical protein synthesis.

ASSOCIATED CONTENT

S Supporting Information

The Supporting Information is available free of charge on the ACS Publications website at DOI: 10.1021/acs.orglett.9b03440.

Protocols for the synthesis and purification of Dbz derivatives and peptides; HPLC, LC-MS, ¹H NMR, and ¹³C NMR data; protocols for the chemical synthesis of

ubiquitin and RON2ed; and protocols for parasite growth inhibition assay (PDF)

AUTHOR INFORMATION

Corresponding Author

*E-mail: kmandal@tifrh.res.in.

ORCID ®

Kalyaneswar Mandal: 0000-0002-3194-1378

Author Contributions

 \S J.M. and S.S. contributed equally. W.T. and P.V. contributed equally.

Notes

The authors declare no competing financial interest.

ACKNOWLEDGMENTS

This work was supported by TIFR and the Wellcome Trust/DBT India Alliance Grant (grant no. IA/I/15/1/501847) awarded to K.M. We acknowledge the biophysics core facility (for the CD instrument), TIFR Hyderabad.

REFERENCES

- (1) Dawson, P. E.; Muir, T. W.; Clark-Lewis, I.; Kent, S. B. Science 1994, 266, 776-9.
- (2) (a) Kent, S. B. H. Protein Sci. 2019, 28, 313–328. (b) Kent, S. B. H. Bioorg. Med. Chem. 2017, 25, 4926–4937.
- (3) (a) Blanco-Canosa, J. B.; Dawson, P. E. Angew. Chem., Int. Ed. 2008, 47, 6851–5. (b) Fang, G. M.; Li, Y. M.; Shen, F.; Huang, Y. C.; Li, J. B.; Lin, Y.; Cui, H. K.; Liu, L. Angew. Chem., Int. Ed. 2011, 50, 7645–9. (c) Wang, J. X.; Fang, G. M.; He, Y.; Qu, D. L.; Yu, M.; Hong, Z. Y.; Liu, L. Angew. Chem., Int. Ed. 2015, 54, 2194–2198. (d) Li, H. X.; Dong, S. W. Sci. China: Chem. 2017, 60, 201–213. (e) Agouridas, V.; El Mahdi, O.; Diemer, V.; Cargoet, M.; Monbaliu, J. C. M.; Melnyk, O. Chem. Rev. 2019, 119, 7328–7443.
- (4) (a) Merrifield, R. B. J. Am. Chem. Soc. 1963, 85, 2149–2154. (b) Schnolzer, M.; Alewood, P.; Jones, A.; Alewood, D.; Kent, S. B. H. Int. J. Pept. Res. Ther. 2007, 13, 31–44. (c) Mijalis, A. J.; Thomas, D. A.; Simon, M. D.; Adamo, A.; Beaumont, R.; Jensen, K. F.; Pentelute, B. L. Nat. Chem. Biol. 2017, 13, 464–466.
- (5) Johnson, E. C.; Kent, S. B. Tetrahedron Lett. 2007, 48, 1795–1799.
- (6) (a) Tsuda, S.; Uemura, T.; Mochizuki, M.; Nishio, H.; Yoshiya, T. Synlett 2017, 28, 1956—1960. (b) Mahto, S. K.; Howard, C. J.; Shimko, J. C.; Ottesen, J. J. ChemBioChem 2011, 12, 2488—94. (c) Bondalapati, S.; Eid, E.; Mali, S. M.; Wolberger, C.; Brik, A. Chem. Sci. 2017, 8, 4027—4034. (d) Weidmann, J.; Dimitrijevic, E.; Hoheisel, J. D.; Dawson, P. E. Org. Lett. 2016, 18, 164—167. (e) Blanco-Canosa, J. B.; Nardone, B.; Albericio, F.; Dawson, P. E. J. Am. Chem. Soc. 2015, 137, 7197—7209. (f) Pala-Pujadas, J.; Albericio, F.; Blanco-Canosa, J. B. Angew. Chem., Int. Ed. 2018, 57, 16120—16125. (g) Hong, Z. Z.; Yu, R. R.; Zhang, X.; Webb, A. M.; Burge, N. L.; Poirier, M. G.; Ottesen, J. J. bioRxiv 2019.
- (7) (a) Liu, T. Z.; Lee, S. D.; Bhatnagar, R. S. *Toxicol. Lett.* **1979**, *4*, 469–473. (b) Liu, T. Z.; Khayambashi, H.; Bhatnagar, R. S. *Clin. Chem.* **1977**, 23, 1119–1119a. (c) Chen, M. L.; Chen, S. X.; Du, M.; Tang, S. H.; Chen, M.; Wang, W.; Yang, H.; Chen, Q. Y.; Chen, J. M. *Aquat. Toxicol.* **2015**, 159, 208–216.
- (8) (a) Cezari, M. H.; Juliano, L. Pept. Res. 1996, 9, 88–91. (b) White, P.; Collins, J.; Cox, Z. J. Comparative Study of Conventional and Microwave-Assisted Synthesis. In 19th American Peptide Symposium, San Diego, CA, 2005.
- (9) (a) Debelouchina, G. T.; Gerecht, K.; Muir, T. W. Nat. Chem. Biol. 2017, 13, 105–110. (b) Komander, D.; Rape, M. Annu. Rev. Biochem. 2012, 81, 203–229. (c) Bang, D.; Makhatadze, G. I.; Tereshko, V.; Kossiakoff, A. A.; Kent, S. B. Angew. Chem., Int. Ed.

2005, 44, 3852—3856. (d) Pan, M.; Gao, S.; Zheng, Y.; Tan, X. D.; Lan, H.; Tan, X. L.; Sun, D. M.; Lu, L. N.; Wang, T.; Zheng, Q. Y.; Huang, Y. C.; Wang, J. W.; Liu, L. J. Am. Chem. Soc. 2016, 138, 7429—7435. (e) Kumar, K. S. A.; Bavikar, S. N.; Spasser, L.; Moyal, T.; Ohayon, S.; Brik, A. Angew. Chem. Int. Ed. 2011, 50, 6137—6141. (f) Riemen, A. J.; Waters, M. L. Biopolymers 2008, 90, 394—398. (g) We encountered extreme difficulty in solubilizing a synthetic peptide segment containing the first 17 residues of ubiquitin in aqueous solution (data not shown).

(10) Wan, Q.; Danishefsky, S. J. Angew. Chem., Int. Ed. 2007, 46, 9248-52.

Brief Communication

Functional Studies of *Plasmodium falciparum's* Prohibitin1 and Prohibitin 2 in Yeast

Savitha Chellappan¹, Subarna Roy¹, Jyoti M. Nagmoti², Wahida Tabassum³, S. L. Hoti¹, Mrinal Kanti Bhattacharyya³, Praveen Balabaskaran Nina^{1,4}

¹Indian Council of Medical Research - National Institute of Traditional Medicine, ²Department of Microbiology, K.L.E. University, Belagavi, Karnataka, ³Department of Biochemistry, School of Life Sciences, University of Hyderabad, Hyderabad, Telangana, ⁴Department of Epidemiology and Public Health, Central University of Tamil Nadu, Thiruvarur, Tamil Nadu, India

Abstract

Prohibitins (PHBs) are evolutionarily conserved mitochondrial integral membrane proteins, shown to regulate mitochondrial structure and function, and can be classified into PHB1 and PHB2. PHB1 and PHB2 have been shown to interact with each other, and form heterodimers in mitochondrial inner membrane. *Plasmodium falciparum* has orthologues of PHB1 and PHB2 in its genome, and their role is unclear. Here, by homology modelling and yeast two-hybrid analysis, we show that putative *Plasmodium* PHBs (PfPHB1 and PfPHB2) interact with each other, which suggests that they could form supercomplexes of heterodimers in *Plasmodium*, the functional form required for optimum mitochondrial function.

Keywords: Mitochondria, *Plasmodium falciparum*, prohibitins, supercomplex, yeast two-hybrid analysis

Introduction

Prohibitins (PHBs) cluster into PHB1 and PHB2, and these proteins share >50% similarity, and are evolutionarily conserved across all phyla.[1] PHBs, along with stomatin, flotillin and HflK/C, belong to the SPFH family.^[2] Alternating blocks of PHB1 and PHB2 form high-molecular-weight complexes (~1.2 MDa) in the mitochondrial inner membrane. [3] PHBs are made up of an N-terminal transmembrane domain, a conserved PHB domain and a C-terminal coiled-coil domain through which the two PHBs interact with each other.^[4] Even though PHBs are considered to be pleiotropic proteins with diverse cellular functions, their role in mitochondrial function has been of considerable interest.^[1,5] In mitochondria, PHBs maintain the copy number and organisation of mitochondrial DNA, support mitochondrial protein synthesis, act as membrane-bound chaperones in assisting respiratory complex assembly, maintain structural integrity, regulate respiratory complex assembly and respiration and are thought to serve as protein and lipid scaffolds in mitochondria.[1,5]

Mitochondrial electron transport chain (mtETC) in *Plasmodium* falciparum (Pf) is an established drug target. [6] Atovaquone, an inhibitor of the bc1 complex of the mtETC, is already in clinical

Access this article online

Quick Response Code:

Website:
www.ijmm.org

DOI:
10.4103/ijmm.IJMM_20_28

use, and drug discovery efforts have led to the advancement of ELQ-300, a mtETC inhibitor as a pre-clinical drug candidate. ^[7] Given the importance of mtETC as an attractive drug target, it is a high priority that we understand the structure and functional importance of the mitochondrial membrane proteins in *Plasmodium*. *Pf* contains two PHBs: *PfPHB1* and *PfPHB2*. In addition, stomatin-like protein and unusual PHB-like protein are also present in the *Plasmodium* genome. PHB1 and PHB2 of *Plasmodium berghei* (Pb) localise to the mitochondria, and are suggested to be essential. ^[8] Here, based on homology modelling, and yeast two-hybrid studies, we show that *PfPHB1* and *PfPHB2* are structurally similar to other PHBs, and physically interact with each other, presumably to form heterodimers, required for regulating the structure and function of mitochondria.

Address for correspondence: Dr. Praveen Balabaskaran Nina, Department of Epidemiology and Public Health, Central University of Tamil Nadu, Thiruvarur - 610 005, Tamil Nadu, India. E-mail: praveen@cutn.ac.in

 Received: 23-01-2020
 Revised: 23-05-2020

 Accepted: 21-07-2020
 Published Online: 29-08-2020

This is an open access journal, and articles are distributed under the terms of the Creative Commons Attribution-NonCommercial-ShareAlike 4.0 License, which allows others to remix, tweak, and build upon the work non-commercially, as long as appropriate credit is given and the new creations are licensed under the identical terms.

For reprints contact: reprints@medknow.com

How to cite this article: Chellappan S, Roy S, Nagmoti JM, Tabassum W, Hoti SL, Bhattacharyya MK, et al. Functional studies of *Plasmodium falciparum*'s prohibitin 1 and prohibitin 2 in yeast. Indian J Med Microbiol 2020:38:213-5

METHODS

Homology modelling

Phyre2 (Protein Homology/Analog Y Recognition Engine)^[9] server was used to predict the protein structure of PfPHB1 and PfPHB2 (http://www.sbg.bio.ic.ac.uk/phyre2). The output of Phyre2 was analysed using RasMol as shown in Figure 1. After Phyre2 prediction, PfPHB1 and PfPHB2 were modelled based on the crystal structure of a core stomatin domain (chain c) of c3bk6c from *Pyrococcus horikoshii*. The confidence rate of prediction is >99.9%, with 57% and 51% sequence coverage for PfPHB1 and PfPHB2, respectively.

Interacting sites in PfPHB1 and PfPHB2 modelled protein structures were determined in the Phyre2 web portal for protein modelling, prediction and analysis, [9] and the interacting residues are shown in red for PfPHB1 and PfPHB2 [Figure 1c and d]. Two continuous interface regions are seen in PfPHB1 and PfPHB2, and the sequences are FQTPYIY-IK/HLSYGK-A and FERSIIY-VR/HLSFSN-E, respectively. These amino acids could facilitate interaction with one another and with other proteins.

Yeast two-hybrid analysis

Yeast two-hybrid experiments were carried out to identify the interaction between PfPHB1 and PfPHB2. Yeast two-hybrid assay was done as described by James *et al.*[10] using the pGADC1 and pGBDUC1 plasmids encoding GAL4 activation domain and DNA-binding domain, respectively.

The constructs, pGADC1:PfPHB1 and pGBDUC1:PfPHB2, were transformed into PJ69-4A yeast cells using the lithium acetate method.[11] The cells transformed with empty pGADC1 and pGBDUC1 were used as negative control. Two-hybrid interactions were tested with the yeast strain PJ69-4A which has the ADE2 reporter gene. The transformed strains were grown in SC-Ura-Leu medium till log phase at 30°C. Tenfold serial dilutions were prepared starting with an equal optical density of 0.5 OD ml⁻¹ and spotted on the control plate (Sc-Ura-Leu) and experimental plate (Sc-Ura-Leu-Ade) to test the strength of the protein-protein interaction. The plates were incubated at 30°C for 72 h. The colonies on the control plate were observed from the 2^{nd} day of incubation. The colonies in the experimental plate (Sc-Ura-Leu-Ade) were observed after 3 days, and their growth was slow compared to that of the control plate (Sc-Ura-Leu). Growth was measured in liquid media, and the number of cells in the media was equalised before spotting. Transformation efficiency and expression of URA3 and LEU2 genes in the plasmids were assessed by the growth of colonies in the SC-Ura-Leu plates. Two random clones were taken to test the strength of protein-protein interaction, and both the clones responded equally. Both the clones grew till the third dilution (10⁻³) on SC-Ura-Leu-Ade plates, which suggests a strong interaction between PfPHB1 and PfPHB2, as shown in Figure 1e.

RESULTS AND DISCUSSION

PHB1 and PHB2 have been found to be integral membrane

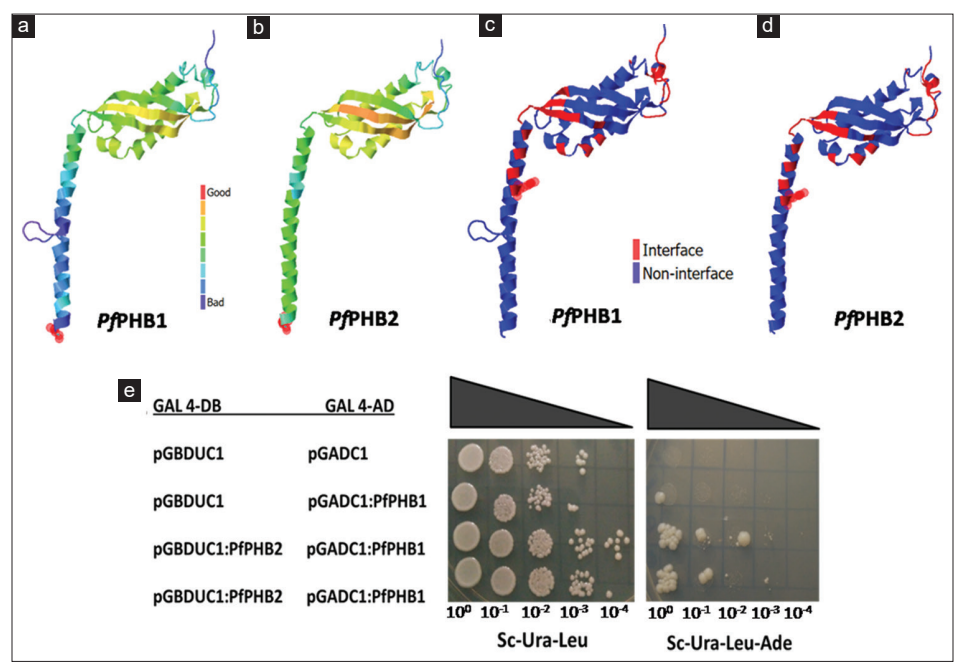


Figure 1: Phyre2 predicted structures of PfPHB1 (a) and PfPHB2 (b). The colour bars represent the quality of prediction. ProQ2 quality assessment algorithm was used to predict the local and global quality of the protein model. The quality (bad to good) of PfPHB1 and PfPHB2 models is represented by the colour scale (a and b). Protein—protein interface residues of PfPHB1 (c) and PfPHB2 (d) interface (red) and non-interface (blue) residues are represented in different colours. (e) Yeast two-hybrid analysis of PfPHB1 and PfPHB2. pGDBUC1 and pGADC1 represent empty plasmids. pGADC1:PfPHB1 represents full-length PfPHB1 in pGADC1 plasmid. pGDBUC1:PfPHB2 indicates full-length PfPHB2 in pGDBUC1 plasmid. The control plate: Sc-Ura-Leu and experimental plate: Sc-Ura-Leu-Ade shows spots with increasing order of dilution

proteins of the mitochondrial inner membrane.^[3] PHB1 and PHB2 physically interact, and the PHB complex is considered to be the physiologically active form as loss of one subunit leads to the degradation of the other.^[12] Yeast has been shown to be an excellent heterologous model system to study the function of *Plasmodium* proteins.^[13] Homology modelling predicts the presence of putative interacting sites in *PfPHBs*. Yeast two-hybrid experiments show that *PfPHB1* and *PfPHB2* strongly interact with each other. These experiments strongly suggest that *PfPHBs* could make similar physiological interactions in the *Plasmodium* mitochondrion. Native page experiments on isolated *Plasmodium* mitochondria will help us identify the size of the PHB complex.

Knockdown of PHBs in other organisms has been shown to disrupt the mitochondrial morphology. [14,15] Processes regulating mitochondrial morphology and mitochondrial DNA organisation and maintaining copy number in *Plasmodium* are poorly understood, and PfPHBs may play an important role. Attempts to knockout PHB1 and PHB2 in Pb have been unsuccessful. [8] Whole-genome saturation screen in *Pf* suggests that PHB2 is non-mutable in the coding sequence. [16] Overall, we provide an important mechanical insight into the functioning of *PfPHB1* and *PfPHB2* by showing that they physically interact with each other. Future studies should focus on understanding the role of *PHB1* and *PHB2* in *Pf* biology.

Acknowledgement for financial support

We thank Department of Science and Technology (DST) for financial support.

Financial support and sponsorship

This study was financially supported by DST through DSTWOS A funds to Ms.Savitha Chellappan and Inspire faculty research funds to Dr. Praveen Balabaskaran Nina.

Conflicts of interest

There are no conflicts of interest.

REFERENCES

1. Osman C, Merkwirth C, Langer T. Prohibitins and the functional

- compartmentalization of mitochondrial membranes. J Cell Sci 2009;122:3823-30.
- Browman DT, Hoegg MB, Robbins SM. The SPFH domain-containing proteins: More than lipid raft markers. Trends Cell Biol 2007;17:394-402.
- Tatsuta T, Model K, Langer T. Formation of membrane-bound ring complexes by prohibitins in mitochondria. Mol Biol Cell 2005;16:248-59.
- Winter A, Kämäräinen O, Hofmann A. Molecular modeling of prohibitin domains. Proteins 2007;68:353-62.
- Thuaud F, Ribeiro N, Nebigil CG, Désaubry L. Prohibitin ligands in cell death and survival: Mode of action and therapeutic potential. Chem Biol 2013;20:316-31
- Sheiner L, Vaidya AB, McFadden GI. The metabolic roles of the endosymbiotic organelles of Toxoplasma and Plasmodium spp. Curr Opin Microbiol 2013;16:452-8.
- Frueh L, Li Y, Mather MW, Li Q, Pou S, Nilsen A, et al. Alkoxycarbonate ester prodrugs of preclinical drug candidate ELQ-300 for prophylaxis and treatment of malaria. ACS Infect Dis 2017;3:728-35.
- Matz JM, Goosmann C, Matuschewski K, Kooij TW. An unusual prohibitin regulates malaria parasite mitochondrial membrane potential. Cell Rep 2018;23:756-67.
- Kelley LA, Mezulis S, Yates CM, Wass MN, Sternberg MJ. The Phyre2 web portal for protein modeling, prediction and analysis. Nat Protoc 2015;10:845-58.
- James P, Halladay J, Craig EA. Genomic libraries and a host strain designed for highly efficient two-hybrid selection in yeast. Genetics 1996;144:1425-36.
- Ito H, Fukuda Y, Murata K, Kimura A. Transformation of intact yeast cells treated with alkali cations. J Bacteriol 1983;153:163-8.
- 12. Coates PJ, Nenutil R, McGregor A, Picksley SM, Crouch DH, Hall PA, et al. Mammalian prohibitin proteins respond to mitochondrial stress and decrease during cellular senescence. Exp Cell Res 2001;265:262-73.
- Bergman LW, Kaiser K, Fujioka H, Coppens I, Daly TM, Fox S, et al. Myosin A tail domain interacting protein (MTIP) localizes to the inner membrane complex of Plasmodium sporozoites. J Cell Sci 2003;116:39-49.
- Artal-Sanz M, Tsang WY, Willems EM, Grivell LA, Lemire BD, van der Spek H, et al. The mitochondrial prohibitin complex is essential for embryonic viability and germline function in Caenorhabditis elegans. J Biol Chem 2003;278:32091-9.
- Osman C, Haag M, Potting C, Rodenfels J, Dip PV, Wieland FT, et al. The genetic interactome of prohibitins: Coordinated control of cardiolipin and phosphatidylethanolamine by conserved regulators in mitochondria. J Cell Biol 2009;184:583-96.
- Zhang M, Wang C, Otto TD, Oberstaller J, Liao X, Adapa SR, et al. Uncovering the essential genes of the human malaria parasite Plasmodium falciparum by saturation mutagenesis. Science 2018;360:eaap7847.

J Vector Borne Dis 57, December 2020, pp. 325–330

Functional studies of *Plasmodium falciparum* putative SURF1 in *Saccharomyces cerevisiae*

Savitha Chellappan¹, Subarna Roy¹, Jyoti M Nagmoti², Wahida Tabassum³, Raja Vukanti⁴, SL Hoti¹, Mrinal Kanti Bhattacharyya³, Praveen Balabaskaran Nina^{1, 5}

¹Indian Council of Medical Research-National Institute of Traditional Medicine, Belagavi, Karnataka, India; ²Department of Microbiology, KLE Academy for higher education, Jawaharlal Nehru Medical college, Belagavi, Karnataka, India; ³Department of Biochemistry, School of Life Sciences, University of Hyderabad, Hyderabad, Telangana State, India; ⁴Department of Microbiology, Central University of Tamil Nadu, Thiruvarur, Tamil Nadu, India; ⁵Department of Epidemiology and Public Health, Central University of Tamil Nadu, Thiruvarur, Tamil Nadu, India

ABSTRACT

Background and objectives: The mitochondrial electron transport chain (mtETC) of Plasmodium falciparum is an important drug target. Identification and functional validation of putative mitochondrial proteins of the mtETC is critical for drug development. Many of the regulatory subunits and assembly factors of cytochrome c oxidase readily identifiable in humans and yeast are missing in P. falciparum. Here, we describe our efforts to identify and validate the function of putative Pfsurf1, a key assembly factor of complex IV of the mtETC.

Methods: Multiple sequence alignment of SURF 1/Shy 1 was carried out in Clustal X 2.1. Phylogenetic tree was constructed using "Draw tree" option in Clustal X, and was analyzed using interactive Tree of Life software. To identify the conserved sequences, domain search was done using Jalview version 2.8.2 (BLOSUM 62 scoring). The haploid Saccharomyces cerevisiae strain (BY4741) containing the null allele shy1 (Orf: YGR112w) (shy1::Kan) was complemented with putative Pfsurf1 to study its ability to rescue the growth defect.

Results: Similarity searches of PfSURF1-like protein in the Pfam shows statistically significant E=4.7e-10 match to SURF1 family. Sequence alignment of PfSURF1 with other SURF1-like proteins reveals the conservation of transmembrane domains, α -helices and β -pleated sheets. Phylogenetic analysis clusters putative PfSURF1 with apicomplexan SURF1-like proteins. Yeast complementation studies show that Pfsurf1 can partially rescue the yeast shy1 mutant, YGR112w.

Interpretation & conclusion: Bioinformatics and complementation studies in yeast show that *P. falciparum*'s SURF1 is the functional ortholog of human SURF1 and yeast Shy1.

Key words Plasmodium falciparum, SURF1, Yeast complementation

INTRODUCTION

Cytochrome c oxidase (COX) or complex IV is a multisubunit catalytic enzyme of the electron transport chain that participates in energy conservation under aerobic conditions. COX is located in the inner mitochondrial membrane and is made up of 14 structural subunits in human and 11 in yeast¹⁻³. The core subunits: COX1, COX2 and COX3 are mitochondrially encoded and are highly conserved across organisms, while the rest of the subunits are encoded in the nucleus and are imported from the cytosol⁴. COX1 and COX2 are mechanistically important subunits that contain CuB (two haem molecules and a copper ion) and CuA (two copper ions) sites respectively; these sites along with the haem a_3 molecule form the active centre of the enzyme¹.

COX being a multi-protein and multi-cofactor enzyme, requires many assembly factors to help in its as-

sembly. In Saccharomyces cerevisiae, more than 25 assembly factors that help in Cox maturation have been described⁴⁻⁶. Human COX does not have all the yeast homologs, but more than 15 proteins involved in COX biogenesis have been identified^{4,7–8}. One of the well-studied assembly factors in Saccharomyces cerevisiae Cox is Shy1. Disruption of Shy1 leads to drastic reduction of Cox and mutants show growth defect in non-fermentable carbon sources9. Biochemical and genetic studies of Shy1 have helped identify several key proteins (Coa1- Coa4) involved in Cox assembly¹⁰⁻¹⁴. Surfeit locus protein1 (SURF1), the human homologue of Shy1, was used as the starting bait to identify other assembly factors such as MITRAC12, TIM21, MITRAC15 and CMC17. Shy1 and its homologues have been suggested to play an important role in the maturation of Cox1 by direct incorporation of haem a3 or by acting as a chaperone^{12,15–17}. Shy1 has been suggested to play a role in the release of Mss51 from Cox1

assembly intermediate^{11–12,15}. Mutations in SURF1 lead to COX deficiency and patients exhibit the phenotype of the Leigh syndrome^{18–19}.

The 6 kb mitochondrial genome of *Plasmodium* encodes just 3 proteins – Cytochrome *b*, COX1 and COX3²⁰. Intriguingly, COX2 is split into COX2a and COX2b, and are coded in the nucleus²¹. In addition to these core subunits, *Plasmodium* database PlasmoDB (*http://www.plasmodb.org/*) has yeast and human orthologs of COX4, COX5B, COX6B and COX7A. Many of the putative assembly factors (COX10, COX11, COX14, COX15, COX17, COX19, SCO1, OXA1, PET117, PET191, and SURF1-domain containing protein) of COX have been annotated in PlasmoDB.

The role of assembly factors in *Plasmodium* COX biogenesis has not been investigated so far. This study details the bioinformatics analysis and functional complementation of putative *Pfsurf1* in a yeast *shyl* mutant.

MATERIAL AND METHODS

Multiple sequence alignment and domain analysis

The Shy1 and SURF1 protein sequences were retrieved from NCBI (https://www.ncbi.nlm.nih.gov/protein) and used in multiple sequence alignment and domain analysis. The protein sequences include: Homo sapiens SURF1 (Swiss-Prot: Q15526.1), Drosophila melanogaster Surfeit 1 (NCBI reference sequence: NP 524758), Caenorhabditis elegans SURF1-like protein (GenBank: CCD72250.1), Monosiga brevicollis MX1 predicted protein (GenBank: EDQ90553.1), Saccharomyces cerevisiae Shy1 (GenBank: KZV11341.1), Schizosaccharomyces pombe SURF-family protein Shy1 (predicted) (GenBank: CAB50922.1), Arabidopsis thaliana Surfeit locus 1 cytochrome c oxidase biogenesis protein (NCBI reference sequence: NP 566592.1), Dictyostelium discoideum SURF1 family protein (NCBI reference sequence: XP 644359.2), Chlamydomonas reinhardtii cytochrome c oxidase assembly protein (NCBI reference sequence: XP 001701449), Babesia microti SURF1 family (NCBI reference sequence: XP 012648526), Toxoplasma gondii SURF1 family protein (GenBank: KFH02210.1), Trypanosoma brucei gambiense DAL972 hypothetical protein, conserved (NCBI reference sequence: XP 011779678.1), Plasmodium falciparum conserved Plasmodium protein with unknown function (NCBI reference sequence: XP 001351864.1). Multiple sequence analysis was performed in Clustal X 2.1 using complete sequences from the selected prokaryotic and eukaryotic species²². Phylogenetic tree was constructed using "Draw tree" option in Clustal X using NeighbourJoining algorithm with default settings (Gap opening:10, Gap extension:0.2, bootstrap number:1000), and the output PHYLIP file was analyzed using interactive Tree of Life (iTOL) software for scientific representation²³. Domain search was done to identify the conserved sequences in the selected sequences using Jalview version 2.8.2 (BLOSUM 62 scoring)²⁴.

Plasmids

Full length gene of *Pfsurf1* (2127 bp) and *Sc-SHY1*(1167 bp) were cloned in the pBMFH plasmid between BamHI and SalI sites, and is under the control of the bi-directional GPD promoter. The plasmids were sequence verified before transformation. The pBMFH plasmid is a fusion plasmid containing the GPD promoter from pBEVY-T, and selection marker (HIS3) and tag from pESC-His plasmid (Stratagene, La Jolla, USA).

Yeast transformation and complementation studies

Ahaploid Saccharomyces cerevisiae strain (BY4741) containing the null allele shyl (Orf: YGR112w) (shy1::Kan) was purchased from European Saccharomyces cerevisiae Archive For Functional Analysis (EU-ROSCARF); referred to as YGR112w. YGR112w was transformed with either full length Pfsurf1 or ScSHY1 genes using lithium acetate procedure²⁵. Transformants were selected by their growth in synthetic medium lacking histidine and containing glucose as carbon source. Approximately 10⁵ yeast cells, and their subsequent 10 fold serial dilutions were spotted on yeast extract, peptone (YEP) plates containing either 2% glucose or 2% glycerol as carbon source. With glucose as carbon source, plates were incubated at 30 °C for three days and with glycerol as carbon source, plates were incubated at 30 °C for five days.

Fluctuation assay

To estimate the phenotypic complementation rate, fluctuation assay²⁶ was performed for YGR112w+pBM-FH*ScSHY1*, YGR112w+pBMFH*Pfsurf1* and YGR112w-pBMFH. A single clone of each transformant was grown overnight to saturation in a synthetic medium lacking histidine with glucose as carbon source. The cells were grown till uniform cell density was reached. Equal number of cells (~500 cells) were spread on YEP (2% glycerol) plates at 30 °C, and individual colonies were counted after 3–4 days of incubation, and their growth is shown as percentage survival. The percentage complementation of *Pf*SURF1 and *ScSHY1* in YGR112w was calculated by Rosche and Foster method²⁷.

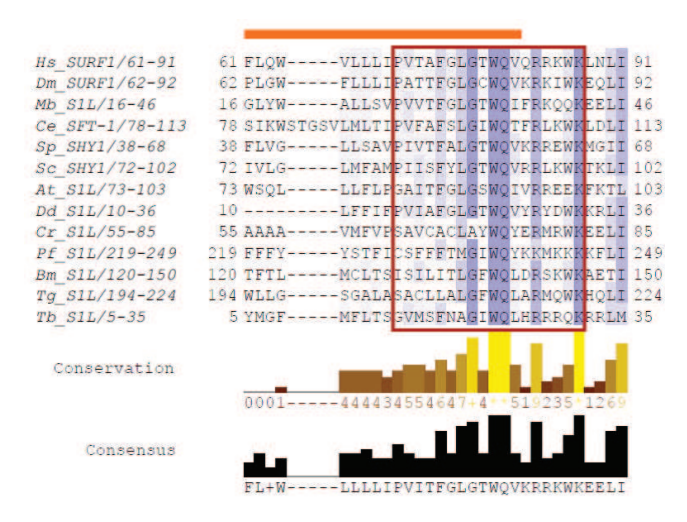


Fig. 1:(a) Bioinformatics analysis of PfSURF1. Conserved domain in SURF1/Shy1 proteins from different organisms using Jalview as listed below (numbers represent the amino acid residues of domains coverage in each organism). Conservation bars represents the degree of conservation in the amino acid residues in numbers.

RESULTS

Multiple sequence alignment and phylogenetic analysis of PfSURF1

PfSURF1 is listed as a putative SURF1 domain containing protein (PF3D7_0531000) in PlasmoDB, and has not been characterized yet. SURF1-like proteins are conserved and are seen in evolutionarily disparate groups such as mammals and bacteria. Multiple sequence alignment (Fig. 1a) shows that the putative PfSURF1 shares both the conserved transmembrane domains with SURF1-like proteins from evolutionarily disparate spp. Fig. 1a shows

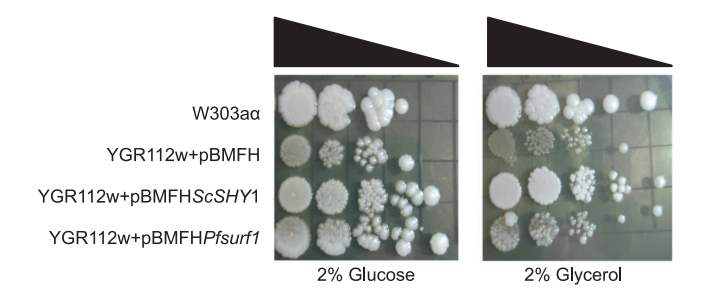


Fig. 2:(a) Growth of different yeast strains on YEP agar plates containing either 2% glucose or 2% glycerol. Changes in the amount of growth among different yeast strains after their spot inoculation with equal number of cells on YEP agar containing 2% glycerol. Different yeast strains were: wild type (W303a); YGR112w+pBMFH (mutant with Shy1 deletion and the empty plasmid [pBMFH]); YGR112w+pBMFHScShy1 (mutant complemented with ScShy1); YGR112w+pBMFHPfsurf1 (mutant complemented with Pfsurf1). Sc = Saccharomyces cerevisiae. Pf = Plasmodium falciparum.

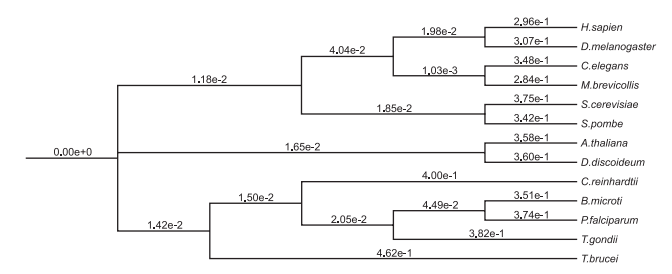


Fig. 1:(b) Phylogenetic analysis of putative PfSURF1. H. sapien:
Homo sapien; D. melanogaster: Drosophila melanogaster,
C. elegans: Caenorhabditis elegans; M. brevicollis: Monosiga brevicollis; S. cerevisiae: Saccharomyces cerevisiae; S.
pombe: Schizosaccharomyces pombe; A. thaliana: Arabidopsis thaliana; D. discoideum: Dictyostelium discoideum; C.
reinhardtii: Chlamydomonas reinhardtii; B. microti: Babesia microti; P. falciparum: Plasmodium falciparum; T. gondii:
Toxoplasma gondii; T. brucei: Trypanosoma brucei. *Apicomplexans are highlighted in grey.

the conservation of one of the transmembrane domains across all aligned SURF1-like proteins. The α -helices and β -sheets of PfSURF1 align at a similar conserved region of other SURF-1 like proteins (Supplementary Fig. 1, Supplementary Table 1). Similarity searches of PfSURF1-like protein in the Pfam shows statistically significant E=4.7e-10 match to SURF1 family. In NCBI CD databases, it is a E=8.82e-09 match to CDD cd06662 SURF1 superfamily. Phylogenetic analysis of putative PfSURF1 indicates that it clusters with SURF-1 like proteins of other apicomplexans (Fig. 1b).

Yeast complementation studies

To assess the extent of growth of the colony, wild type and transformed yeasts were uniformly spotted on YEP plates containing 2% glucose or 2% glycerol as carbon source. The inoculated plates were grown at three different temperatures-30 °C, 25 °C and 19 °C. As the growth of YGR112w with empty plasmid pBMFH was very slow at 25 °C and 19 °C (data not shown), growth was compared at 30 °C. With glucose as carbon sugar, growth (morphology of the colony) of wild type yeast (W303a), transformed yeasts (YGR112w+pBMFH, YGR112w+pBMFHScShy1, YGR112w+pBMFH*Pfsurf1*) similar (Fig. 2a). With glycerol as carbon source, the growth of YGR112w+pBMFH is slower and lesser when compared to either W303a or YGR112w+pBMFHScShy1 (Fig. 2a). However, the growth of YGR112w+pBMFHPfsurf1 is more than the growth of YGR112w+pBMFH and lesser than W303a. To better understand the growth phenotype, a fluctuation assay was performed. While 57±1% cells of YGR112w+pBMFH seeded cells

formed colonies, 68±0.7% and 68±0.1% cells, respectively of YGR112w+pBMFHScShy1 and YGR112w+pBMFHPfsurf1, survived and formed colonies (Fig. 2b). The number of survived cells were significantly higher for YGR112w+pBMFHScShy1 and YGR112w+pBMFHPfsurf1, when compared to those of YGR112w+pBMFH (p < 0.001). The difference in % survival between YGR112w+pBMFHScShy1 and YGR112w+pBMFHPfsurf1 was not significant.

DISCUSSION

The SURF1 proteins are evolutionarily conserved across eukaryotes and prokaryotes²⁸. Sequence alignment shows that PfSURF1 contains the two conserved hydrophobic transmembrane domains found in all SURF1 sequences. The α -helices and β -sheets of the putative PfSURF1 align at the similar predicted location of SURF1-like proteins. Phylogenetic analysis clusters putative PfSURF1 with apicomplexan SURF1-like proteins. Bioinformatics analysis strongly suggest that the PfSURF1 is the ortholog of human SURF1 and yeast Shv1.

Saccharomyces cerevisiae is an excellent model organism to understand the mechanism of cellular and biochemical maintenance of respiration. In yeast, even under aerobic conditions, ATPs are primarily generated by fermentation and glycolysis²⁹. Yeast cells grown on non-fermentable carbon sources like glycerol or ethanol

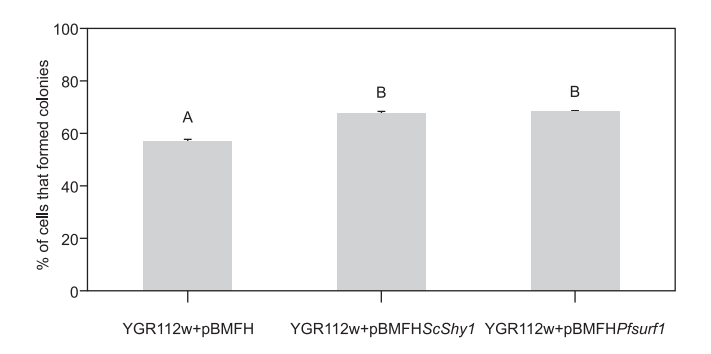


Fig. 2:(b) Fluctuation assay was done by inoculating 500 cells of three yeast strains (YGR112w+ pBMFH, YGR112w+ pBMFHScShy1, and YGR112w+ pBMFHPfsurf1) onto the YEP agar containing 2% glycerol and counting the colonies after 3 days at 30 °C. Values (% of cells that formed colonies) are means (n = 3) along with ±1 standard error of the mean. The bars connected by different letters are significantly different (F = 85.55; P < 0.001). The bars connected by the same letter are not statistically different (one-way ANOVA along with Tukey's post hoc tests for multiple comparisons; [SPSS v20; IBM Inc.]).

require fully active and functional mitochondria for respiration³⁰. The *shy1* Δ mutants are defective in oxidative capacity; their size is smaller and their doubling time is much longer than the wild type³¹. A similar slow growth rate and small colonies were observed when the $shyl\Delta$ mutant was grown in glycerol, and when complemented with Pfsurf1 or ScSHY1, the growth rate and colony morphology could be partially restored to that of the wild type. The fluctuation assay showed a significant difference in the number of colonies between the YGR112w ($shy1\Delta$) and YGR112w complemented with *Pfsurf1* or *ScSHY1*, strongly indicating a growth defect in the YGR112w mutant that is rescued by complementing with *Pfsurf1* or *Sc*-SHY1. Rescue of YGR112w was more efficient with Sc-SHY1 when compared to Pfsurf1, and this is not surprising as the tertiary structure of PfSURF1 may not be the same as that of Shy1, and the slight differences in conformation could affect protein function.

The minimalistic mitochondrion of *Plasmodium* is essential for the parasite survival, and hosts several pathways involved in the production of molecules essential for nucleic acid metabolism, DNA transcription, replication and other key processes^{20, 32}. A recent saturation mutagenesis study in *P. falciparum* has shown that many proteins and assembly factors of the mtETC are essential for parasite survival³³. The mutagenesis index score and mutant fitness score based on the saturation mutagenesis study are 0.12 and -3.156 respectively for *Pfsurf1*, indicating that it is highly essential for the parasite lifecycle³³. Similarly, a CRISPR screen in the related apicomplexan Toxoplasma gondii shows the putative Tgsurf1 to be indispensable for its life cycle³⁴. The mitochondrial electron transport chain of *P. falciparum* is an established target, and several drug molecules targeting the mtETC are constantly being evaluated by the drug development programs³⁵. Validation of the function of *Pfsurf1* is an important first step for future studies that could use *Pf*SURF1 as a bait to pull down Complex IV, as done in humans and yeast^{12, 36}, and characterize the novel subunits of PfCOX complex, some of them could be attractive drug targets.

CONCLUSION

Bioinformatics and complementation studies in yeast show that *P. falciparum*'s SURF1 is the functional ortholog of human SURF1 and yeast Shy1. In yeast and humans, using Shy1/SURF1, many of the assembly factors and assembly intermediates of Complex IV have been characterized. Efforts have been initiated to pull down the *Pf*COX complex using *Pf*SURF1 as the bait.

Conflict of Interest: None

ACKNOWLEDGEMENTS

The authors thank the Department of Science and Technology, Government of India (Inspire Faculty Award, DST-CRG/2018/002803 and WOS-A) for funding. The authors thank Dr. Michael W. Mather (Drexel University) for his valuable input and help in bioinformatics analysis. The authors thank the ICMR-NITM, Belagavi, India and Department of Biochemistry, University of Hyderabad, India for the instrumentation facility to conduct the study. This manuscript was approved by the publication committee of ICMR - NITM and bears Library Accession No.009 dated 20.6.2018.

REFERENCES

- Tsukihara T, Aoyama H, Yamashita E, Tomizaki T, Yamaguchi H, Shinzawa-Itoh K, et al. The whole structure of the 13-sub-unit oxidized cytochrome c oxidase at 2.8 A. Science 1996; 272(5265): 1136–1144.
- Balsa E, Marco R, Perales-Clemente E, Szklarczyk R, Calvo E, Landazuri MO, et al. NDUFA4 is a subunit of complex IV of the mammalian electron transport chain. Cell Metab 2012; 16(3): 378–386.
- Pitceathly RD, Rahman S, Wedatilake Y, Polke JM, Cirak S, Foley AR, et al. NDUFA4 mutations underlie dysfunction of a cytochrome c oxidase subunit linked to human neurological disease. Cell Rep 2013; 3(6): 1795–1805.
- Mick DU, Fox TD, Rehling P. Inventory control: cytochrome c oxidase assembly regulates mitochondrial translation. *Nat Rev Mol Cell Biol* 2011; *12*(1): 14–20.
- Barrientos A, Gouget K, Horn D, Soto IC, Fontanesi F. Suppression mechanisms of COX assembly defects in yeast and human: insights into the COX assembly process. *Biochim Biophys Acta* 2009; 1793(1): 97–107.
- Kim HJ, Khalimonchuk O, Smith PM, Winge DR. Structure, function, and assembly of heme centers in mitochondrial respiratory complexes. *Biochim Biophys Acta* 2012; 1823(9): 1604–1616
- Mick DU, Dennerlein S, Wiese H, Reinhold R, Pacheu-Grau D, Lorenzi I, et al. MITRAC links mitochondrial protein translocation to respiratory-chain assembly and translational regulation. Cell 2012; 151(7): 1528–1541.
- 8. Dennerlein S, Oeljeklaus S, Jans D, Hellwig C, Bareth B, Jakobs S, *et al.* MITRAC7 Acts as a COX1-Specific Chaperone and Reveals a Checkpoint during Cytochrome c Oxidase Assembly. *Cell Rep* 2015; *12*(10): 1644–1655.
- 9. Mashkevich G, Repetto B, Glerum DM, Jin C, Tzagoloff A. SHY1, the yeast homolog of the mammalian SURF-1 gene, encodes a mitochondrial protein required for respiration. *J Biol Chem* 1997; 272(22): 14356–14364.
- Pierrel F, Khalimonchuk O, Cobine PA, Bestwick M, Winge DR. Coa2 is an assembly factor for yeast cytochrome c oxidase biogenesis that facilitates the maturation of Cox1. *Mol Cell Biol* 2008; 28(16): 4927–4939.
- 11. Pierrel F, Bestwick ML, Cobine PA, Khalimonchuk O, Cricco

- JA, Winge DR. Coal links the Mss51 post-translational function to Cox1 cofactor insertion in cytochrome c oxidase assembly. *EMBO J* 2007; *26*(20): 4335–4346.
- Mick DU, Wagner K, van der Laan M, Frazier AE, Perschil I, Pawlas M, et al. Shy1 couples Cox1 translational regulation to cytochrome c oxidase assembly. EMBO J 2007; 26(20): 4347– 4358.
- Bestwick M, Jeong MY, Khalimonchuk O, Kim H, Winge DR. Analysis of Leigh syndrome mutations in the yeast SURF1 homolog reveals a new member of the cytochrome oxidase assembly factor family. *Mol Cell Biol* 2010; 30(18): 4480–4491.
- 14. Mick DU, Vukotic M, Piechura H, Meyer HE, Warscheid B, Deckers M, *et al.* Coa3 and Cox14 are essential for negative feedback regulation of COX1 translation in mitochondria. *J Cell Biol* 2010; *191*(1): 141–154.
- Khalimonchuk O, Bestwick M, Meunier B, Watts TC, Winge DR. Formation of the redox cofactor centers during Cox1 maturation in yeast cytochrome oxidase. *Mol Cell Biol* 2010; 30(4): 1004–1017.
- Bundschuh FA, Hannappel A, Anderka O, Ludwig B. Surfl, associated with Leigh syndrome in humans, is a heme-binding protein in bacterial oxidase biogenesis. *J Biol Chem* 2009; 284(38): 25735–25741.
- 17. Smith D, Gray J, Mitchell L, Antholine WE, Hosler JP. Assembly of cytochrome-c oxidase in the absence of assembly protein Surflp leads to loss of the active site heme. *J Biol Chem* 2005; 280(18): 17652–17656.
- Zhu Z, Yao J, Johns T, Fu K, De Bie I, Macmillan C, et al. SURF1, encoding a factor involved in the biogenesis of cytochrome c oxidase, is mutated in Leigh syndrome. Nat Genet 1998; 20(4): 337–343.
- Tiranti V, Hoertnagel K, Carrozzo R, Galimberti C, Munaro M, Granatiero M, et al. Mutations of SURF-1 in Leigh disease associated with cytochrome c oxidase deficiency. Am J Hum Genet 1998; 63(6): 1609–1621.
- Vaidya AB, Mather MW. Mitochondrial evolution and functions in malaria parasites. *Annu Rev Microbiol* 2009; 63: 249–267.
- Funes S, Davidson E, Reyes-Prieto A, Magallon S, Herion P, King MP, et al. A green algal apicoplast ancestor. Science 2002; 298(5601): 2155.
- Larkin MA, Blackshields G, Brown NP, Chenna R, McGettigan PA, McWilliam H, et al. Clustal W and Clustal X version 2.0. Bioinformatics 2007; 23(21): 2947–2948.
- Letunic I, Bork P. Interactive tree of life (iTOL) v3: an online tool for the display and annotation of phylogenetic and other trees. *Nucleic Acids Res* 2016; 44(W1): W242–245.
- Waterhouse AM, Procter JB, Martin DM, Clamp M, Barton GJ. Jalview Version 2–a multiple sequence alignment editor and analysis workbench. *Bioinformatics* 2009; 25(9): 1189–1191.
- Gietz RD, Woods RA. Transformation of yeast by lithium acetate/single-stranded carrier DNA/polyethylene glycol method. *Methods Enzymol* 2002; 350: 87–96.
- 26. Luria SE, Delbruck M. Mutations of Bacteria from Virus Sensitivity to Virus Resistance. *Genetics* 1943; 28(6): 491–511.
- 27. Rosche WA, Foster PL. Determining mutation rates in bacterial populations. *Methods* 2000; 20(1): 4–17.
- Poyau A, Buchet K, Godinot C. Sequence conservation from human to prokaryotes of Surf1, a protein involved in cytochrome c oxidase assembly, deficient in Leigh syndrome. *FEBS Lett* 1999; 462(3): 416–420.
- 29. Gancedo JM. Yeast carbon catabolite repression. *Microbiol Mol Biol Rev* 1998; *62*(2): 334–361.

- Altmann K, Durr M, Westermann B. Saccharomyces cerevisiae as a model organism to study mitochondrial biology: general considerations and basic procedures. *Methods Mol Biol* 2007; 372: 81–90.
- 31. Barrientos A, Korr D, Tzagoloff A. Shylp is necessary for full expression of mitochondrial COX1 in the yeast model of Leigh's syndrome. *EMBO J* 2002; 21(1-2): 43–52.
- 32. Sheiner L, Vaidya AB, McFadden GI. The metabolic roles of the endosymbiotic organelles of Toxoplasma and Plasmodium spp. *Curr Opin Microbiol* 2013; *16*(4): 452–458.
- 33. Zhang M, Wang C, Otto TD, Oberstaller J, Liao X, Adapa SR, *et al.* Uncovering the essential genes of the human malaria parasite Plasmodium falciparum by saturation mutagenesis. *Science* 2018; *360*(6388): eaap7847.
- 34. Sidik SM, Huet D, Ganesan SM, Huynh MH, Wang T, Nasamu AS, *et al.* A Genome-wide CRISPR Screen in Toxoplasma Identifies Essential Apicomplexan Genes. *Cell* 2016; *166*(6): 1423–35 e12.
- 35. Nixon GL, Pidathala C, Shone AE, Antoine T, Fisher N, O'Neill PM, *et al.* Targeting the mitochondrial electron transport chain of Plasmodium falciparum: new strategies towards the development of improved antimalarials for the elimination era. *Future Med Chem* 2013, *5*(13): 1573–1591.
- 36. Fontanesi F, Clemente P, Barrientos A. Cox25 teams up with Mss51, Ssc1, and Cox14 to regulate mitochondrial cytochrome c oxidase subunit 1 expression and assembly in Saccharomyces cerevisiae. *J Biol Chem* 2011, 286(1): 555–566.

Correspondence to: Dr Praveen Balabaskaran Nina, Assistant Professor, Department of Epidemiology and Public Health, CLC II building, Kankalancherry Thiruvarur, India.

E-mail: praveen@cutn.ac.in

Received: 12 July 2018 Accepted in revised form: 06 May 2019

Studying the canonical and noncanonical functions of Hsp90 in Plasmodium falciparum chromatin biology

by Wahida Tabassum

Submission date: 13-Dec-2021 10:24AM (UTC+0530)

Submission ID: 1728795394

File name: WAHIDA TABASSUM.pdf (2.33M)

Word count: 25639 Character count: 129154 This is to certify that two of the publications of Ms. wanida Tabassum constitute the major part of her thesis, and hence those scores (numbers 1,2,3, and 5 = 33%) should be deducted from the total score.

Studying the canonical and non-canonical functions of Hsp90 in Plasmodium falciparum chromatin biology

ORIGINALITY REPORT

43% SIMILARITY INDEX

11%

INTERNET SOURCES

38%

PUBLICATIONS

8%

STUDENT PAPERS

PRIMARY SOURCES

Wahida Tabassum, Sunanda Bhattacharyya, Shalu M. Varunan, Mrinal Kanti Bhattacharyya. "Febrile temperature causes transcriptional down - regulation of Sirtuins through Hsp90 dependent epigenetic modification ", Molecular Microbiology, 2021

18%

Wahida Tabassum, Priyanka Singh, Niranjan Suthram, Sunanda Bhattacharyya, Mrinal Kanti Bhattacharyya. "Elevated DNA damage sensitivity in malaria parasite induced by the synergistic action between PfHsp90 inhibitor and PfRad51 inhibitor", Antimicrobial Agents and Chemotherapy, 2021

Publication

8%

Wahida Tabassum, Priyanka Singh, Niranjan Suthram, Sunanda Bhattacharyya, Mrinal Kanti Bhattacharyya. "Synergistic Action between PfHsp90 Inhibitor and PfRad51 Inhibitor Induces Elevated DNA Damage Sensitivity in the Malaria Parasite",

5%

Antimicrobial Agents and Chemotherapy, 2021

Publication

	Tabilitation	
4	Submitted to University of Hyderabad, Hyderabad Student Paper	5%
5	Wahida Tabassum, Sunanda Bhattacharyya, Shalu M. Varunan, Mrinal Kanti Bhattacharyya. "Febrile temperature causes transcriptional downregulation of Sirtuins through Hsp90 - dependent epigenetic modification ", Molecular Microbiology, 2021 Publication	2%
6	www.ncbi.nlm.nih.gov Internet Source	<1%
7	baadalsg.inflibnet.ac.in Internet Source	<1%
8	hdl.handle.net Internet Source	<1%
9	orca.cf.ac.uk Internet Source	<1%
10	zombiedoc.com Internet Source	<1%
11	Submitted to Jawaharlal Nehru University (JNU) Student Paper	<1%

Date of Registration: 03/7/2015
Date of Expiry : 31/12/22

UNIVERSITY OF HYDERABAD SCHOOL OF LIFE SCIENCES DEPARTMENT OF BIOCHEMISTRY

PROFORMA FOR SUBMISSION OF THESIS/DISSERTATION

1.	Name of the Candidate	: Wahida Tabassum
2.	Roll No.	: 15 LB PHO6
3.	Year of Registration	2015
4.	Topic	Studying the canonical & noncanonical
5,	Supervisor(s) and affiliations	Studying the canonical & non canonical felctions of 45p40 in Pleumodus foliopersum finds Prof M. K. Bhattachayya, Professor
6.	Whether extension/re-registration (Specify below)	granted: NA
7.	Date of submission	13.12.21
8.	Last class attended on (M.Phil/Pro	e-Ph.D): Pre PhD Seminar on 22/6/21
9.	Whether tuition fee for the current	t period Paid: Receipt No.& Dt: NA
10.	Whether thesis submission fee pai	d: Receipt No & Dt: 211213110679714 13/12/21
11.	Whether hostel dues cleared	: Receipt No & Dt: NO clues Cleared through ϵ gov.
12.	Whether a summary of the disserta	
Supervi Signatur Dean, o	PARTMENT OF BY DERABAD SCHOOL OF MESSAGE CES SCHOOL OF MESSAGE CES SULVERSITY OF HYDERABAD TYDERABAD-500046 MDIA. THE SCHOOL OF MY DERABAD THE	Signature of the Head of the HEAD Department. Dept. of Biochemistry SCHOOL OF LIFE SCIENCES UNIVERSITY OF HYDERABAD HYDERABAD-500 046.
Hy	derabad	